Testing for Exhaust Emissions of Diesel Powered Off-Road Engines

Project Reference Number: ARB Contract Number 98-317

Final Project Report
May 29, 2002

Prepared for the California Air Resources Board and the California Environmental Protection Agency

P.O. Box 2815

Sacramento   CA   95812

Submitted by:

Department of Mechanical and Aerospace Engineering

P.O. Box 6106

West Virginia University

Morgantown, West Virginia   26506

Federal or Entity Identification Number: 550665758

Mridul Gautam, Ph.D. (Principal Investigator)
Professor
Voice: (304) 293-3111 ext. 2312
Fax: (304) 293-6689
Email: mgautam@mail.wvu.edu

Daniel K. Carder
Nigel N. Clark, Ph.D.
Donald W. Lyons, Ph.D.

Disclaimer

The statements and conclusions in this Report are those of the contractor and not necessarily those of the California Air Resources Board. The mention of commercial products, their source, or their use in connection with material reported herein is not to be construed as actual or implied endorsement of such products.

Acknowledgements

Table of Contents

List of Tables

List of Figures

Abstract

Emissions databases from off-road diesel-powered equipment suffer immensely from insufficient real-world activity data. Moreover, there is little information available regarding the validity of standardized dynamometer engine test cycles that are currently used for emissions certification. The present study was initiated in order to fill the current void in the off-road equipment testing cycles and the consequent lack of "real-world" emissions data that is needed for accurately modeling emissions inventories.

For this study, onboard engine data was logged from four off-road vehicles in order to generate transient test cycles that could be used to simulate real-world operating conditions for exhaust emissions research. The off-road diesel-powered equipment targeted for this study was selected to be representative of the major off-road diesel emissions contributors in California. Specifically, these vehicles were: an Elgin Pelican street sweeper (51-120 hp), a John Deere 444 rubber-tired loader (121-250 hp), a Komatsu PC400LC3 excavator (251-500 hp), and a Caterpillar D-11RCD bulldozer (>500 hp). The engines were removed from the street sweeper, rubber-tired front-end loader, and the excavator and operated according to the transient test cycles developed from the recorded in-field data, as well as the standard steady-state 8-mode test cycle, prescribed by ISO 8178-6.3 Test Cycles type C, which is used for certification of off-road diesel engines. Regulated gaseous emissions and gravimetric PM emissions were collected according to procedures recommended by the Code of Federal Regulations (CFR) 40, Part 86, Subpart N. In addition, size-selective PM mass emissions, and particle sizing data were collected. Exhaust emissions from the Caterpillar D-11R CD track-type tractor were measured in the field as the dozer performed its normal operating activities. This on-board testing was performed using West Virginia University's Mobile Emissions Measurement System (MEMS) for gaseous exhaust components, and a Real-time Particulate Mass Monitor (RPM 100) developed by the Mid-Atlantic Research Institute (MARI).

Results indicate that the current steady-state, ISO 8178, 8-mode test cycle does not adequately represent the actual emissions produced by off-road, diesel-powered equipment during day-to-day operations. Furthermore, the exhaust emissions produced by a vehicle are highly vehicle and task-specific.

Executive Summary

Background

Exhaust emissions from heavy-duty diesel engines (both off- and on-highway) are a major contributor of both oxides of nitrogen (NO_x) and particulate matter (PM) to emissions inventories. In addition to a range of respiratory problems, high levels of NO_x emissions from diesel vehicles react with hydrocarbons to form tropospheric (ground level) ozone. In-use exhaust emissions from not only truck and bus diesel engines but also from off-road diesel-powered equipment are of grave concern because long term exposure to particulate matter has been associated with excess lung cancer in experimental animals. It is well established that emission inventories have grossly underestimated the emissions from mobile sources, especially from diesel-powered equipment.

During the last decade, emissions standards have tightened for the off-road diesel engine industry. Developing transient test cycles and generating real-world mass emissions rates from off-road vehicles is now imperative in light of the urgent need for California to develop State Implementation Plans (SIP) to meet the stringent emissions standards by 2010. This study was initiated to provide CARB with high quality vehicle activity estimates and real-world emissions data developed from off-road equipment using transient cycles developed from in-use logged activity data. Based on the results of the current study, CARB would be in a position to modify its emission inventory models and implement appropriate pollution control policies that will help California achieve attainment by 2010 and stay in compliance with the new fine PM standards. The study focused on collecting real-world activity data, from the off-road vehicles, and measuring exhaust mass emissions rates from these vehicles. The collected in-field activity data was used to generate transient engine dynamometer cycles that would characterize the duty cycles performed by such vehicles during everyday operation. In addition, the engines were tested according to the currently used, steady-state, ISO 8178 8-mode test cycle (similar to the Federal 8-mode cycle).

Methods

Four off-road vehicles were identified for testing based upon engine power output and CARB vehicle inventory estimates. An Elgin Pelican street sweeper (51-120 hp), a John Deere 444 rubber-tired loader (121-250 hp), a Komatsu PC400LC3 excavator (251-500 hp), and a Caterpillar D-11RCD bulldozer (>500 hp) were all instrumented for in-field evaluation.

For the street sweeper, the rubber-tired loader, and the excavator, engine speed and raw exhaust emissions data were recorded as the vehicles were operated in-field under real-world conditions. The engines were then removed and installed on engine dynamometer test beds. Brake-specific raw CO_2 maps were generated while operating the engines on the dynamometer test beds. By doing so, in-field engine power was then inferred from the sampled raw carbon dioxide (CO_2) concentration and engine speed data. This estimated power was then used to derive speed-load set points which were used to exercise the engine on the dynamometer while raw exhaust CO_2 concentration

levels were recorded using the same multi-gas analyzer setup that was used for the in-field testing. The collected data from the dynamometer test cycle was then compared to the in-field data taken previously, and the engine load set points were adjusted to facilitate convergence of the laboratory CO_2 trace with that of the in-field CO_2 data. Once an acceptable level of correlation was obtained, regulated gaseous emissions and gravimetric PM emissions were collected according to procedures recommended by the Code of Federal Regulations (CFR) 40, Part 86, Subpart N. In addition, size-selective PM mass emissions and particle sizing data were collected. In order to provide a benchmark for the transient test cycle data, ISO-8178 Cycle C1 steady-state tests were also conducted on the street sweeper, the rubber-tired loader, and the excavator engines.

Emissions test results and vehicle activity data for the dozer were collected using WVU's Mobile Emissions Measurement System (MEMS) and Mid-Atlantic Research Institute's Real-time Particulate Mass Monitor (RPM 100). The MEMS utilizes an NDIR detector for the determination of CO_2, a zirconium-oxide sensor for measurement of NO_x, and an Annubar™ averaging pitot-static device for the measurement of engine exhaust flow rates. The RPM100 comprises of a portable, compact (103mm H x 175mm Dx 317 mm W; 4 kg), high performance dilution system and a quartz crystal microbalance (same size). The unit is capable of diluting a raw exhaust slip-stream and providing real-time PM mass information as well as provide for optional filter-based PM information.

It should be noted that the MEMS is capable of logging engine control unit data streams for the inference of engine torque, but the necessary engine load data stream was not publicly broadcast by the Caterpillar D11RCD engine control unit. Therefore, a representative from Caterpillar logged engine speed and estimated load, using a proprietary Caterpillar engine control unit (ECU) interface. The correlation of the MEMS with a full-flow CFV-CVS system operating according to CFR 40, Part 86, Subpart N was established before the unit was installed and tested on the Caterpillar D11RCD dozer. The dozer was operated by Buffalo Coal Corporation under typical operating conditions.

Results

In-field test results indicate that each vehicle has very distinct modes of operation relevant to engine loading. These modes most normally involve transport, idle, and work performance, which can have task specific characteristics. In the derivation of the cycles used for dynamometer testing, particular attention was given to distinct modes that seemed to occur frequently. The derived test cycle was weighted such that the overall percentage of time spent operating in each distinct mode was representative of the original data collected.

Data collected from laboratory instruments indicate that emissions rates for these engines vary widely with the nature of the test cycle. Of particular interest is the difference between transient and steady state test emissions. Weighted emissions rates for the ISO 8178 8-Mode test are much higher than those recorded during transient operation of the engines. For the loader, the weighted brake specific 8-Mode results were 100 to 550 percent higher than the transient results for HC, CO, CO_2, NO_x, and PM. For the Street Sweeper, the differences ranged from 75 to 300 percent higher in value

between steady state and transient operation. However, comparisons of different transient cycles and even the loader cycle returned much closer brake specific results with the largest percent difference being 93 percent between CO emissions measured with the John Deere 4039T engine operating on the sweeper and loader cycle. Emissions data for the excavator showed the same trend with 8-Mode results being 10 to 70 percent higher than those recorded during transient tests. Due to this, an investigation was performed to see if different weighting factors would bring 8-mode results closer to transient results. By discretizing the transient cycle to determine the operational characteristics of the engine, the percentage of time the engine operated in a speed range and the percentage of time spent in a load range, an approximate weighting factor can be determined. These new weighting factors brought the sweeper results to within 10 to 50 percent between 8-Mode and transient test results.

Correlation results of engine speed and CO_2 traces recorded during field operation of the engine and dynamometer testing showed that the dynamometer test cycle represented the in-field cycle within the limitations of cycle to cycle repeatability of the same test cycle as recorded by the instruments used.

Data collected from in-field testing of the dozer indicates that the duty cycle is very repetitive in nature. Due to the lack of fueling data from the engine, reporting of emissions from this testing is limited to mass emission rates, however, with the fueling maps used by the engine, one could determine approximate fuel specific emissions rates and engine loading factors from the engine speed and gaseous emissions data collected.

Conclusions

The research reported herein suggests that the inference of in-field torque through raw exhaust CO_2 measurements is an effective means of determining the engine load information of off-road vehicles. These cycles can then be used to develop standardized off-road cycles that can be used for emissions certification as well as emissions inventory purposes. The current certification standard, based upon the ISO 8178, steady-state 8-mode test cycle, does provide a universally accepted method of testing these engines, but the mass emissions rates may not be representative of actual in-field emissions production from off-road diesel-powered vehicles. Furthermore, the results presented from the in-field-derived transient test cycles suggest that the exhaust emissions produced by off-road vehicles are very vehicle- and task-specific in nature.

The in-field emissions data collected for this study is believed to be representative of typical operating conditions for the vehicles tested, and therefore should be ideally suited for emissions inventory purposes, using these test vehicles as "average" values. However the results generated by this project have indicated that exhaust emissions vary widely with the operating cycle, which is very dependent on vehicle type. Therefore to provide the most representative data for emissions inventory purposes, a wide variety of vehicle types should be tested. Similar vehicles of different model years should also be compared over the same cycle, considering the amount of advancement has been made in electronic diesel engine control technology during the last decade. A large percentage of in-use off-road vehicles are mechanically controlled and the emissions of HC and CO may be several times higher than their modern electronically controlled counterparts.

Moreover, the lack of feedback control of these engines causes increased variability in the emissions production levels.

Testing for Exhaust Emissions of Diesel Powered Off-Road Engines

1 Introduction

Development of transient test cycles for off-road vehicles in order to provide improved quantification of real-world mass emissions rates is now imperative in light of the urgent need for California to develop State Implementation Plans (SIP) to meet the stringent emissions standards of 2010. West Virginia University was commissioned to provide CARB with high quality vehicle activity estimates and real-world emissions data from off-road equipment, using transient cycles developed from in-field vehicle activity records. The results of the this study will provide CARB with additional information in order to modify its emission inventory models and implement appropriate pollution control policies that will help California achieve attainment by 2010 and stay in compliance with the new fine-PM standards.

Emissions inventories have often grossly underestimated the emissions from mobile sources, especially from diesel-powered equipment. Emissions databases from off-road diesel powered equipment suffer immensely from insufficient real-world activity data and, more so, from the fact that emissions standards regulating such equipment have only been in existence since 1996. The focus of this study was to fill the current void in off-road equipment testing cycles and the consequent lack of "real-world" emissions data that is needed to accurately model emissions inventories. The currently used steady-state ISO 8-mode tests (similar to the Federal 8-mode cycle) do provide a universally accepted method of testing these engines, but the mass emissions rates may not be representative of that particular equipment's usage. It is therefore difficult to use such test results for the development of accurate emissions inventories. This study focused on collecting real-world activity data from four off-road vehicles that were identified as being representative of major off-road diesel emissions contributors in California. In-field vehicle activity data from these four vehicles was collected and the engines were removed and installed on dynamometer test beds. From the collected in-field data, transient dynamometer test cycles were generated, and the engines were operated according to the derived transient cycles while engine exhaust emissions were recorded. For the emissions testing, measurements of currently regulated exhaust species were made as well as exhaust particulate matter size distributions and concentrations. For comparative purposes, a standard certification test cycle (ISO 8178 steady-state 8-mode cycle) was also performed.

The following section includes a brief background pertaining to emissions testing of diesel vehicles. The study objectives and a summary of relevant published literature and commercially available on-board emissions measurement systems conclude this introductory section.

1.1   Background

Exhaust emissions from heavy-duty diesel engines (both off- and on-highway) are a major contributor of both oxides of nitrogen (NO_x) and particulate matter (PM). In addition to a range of respiratory problems, the high levels of NO_x emissions from diesel vehicles react with hydrocarbons to form tropospheric (ground level) ozone. In-use

exhaust emissions from not only truck and bus diesel engines but also from off-road diesel-powered equipment are of grave concern, because long term exposure to particulate matter has been associated with excess lung cancer in experimental animals. During the past few decades, the Environmental Protection Agency (EPA) and the California Air Resources Board (CARB) have introduced increasingly tighter standards regarding the permissible amount of pollution released into the environment from various sources. An area of particular concern is the pollution created by diesel-engine powered vehicles that operate both on- and off-road.

The current exhaust emissions regulations for diesel engines concentrate on the four major components HC, total particulate matter (TPM), CO, and NO_x. In addition, the production of CO_2 is becoming more closely scrutinized globally, as talks continue between nations regarding the development of world-wide green-house gas policies. The regulation of diesel exhaust gas emissions is aimed at limiting the serious health effects caused by diesel exhaust gas constituents. When inhaled, NO_x and CO readily bond to the hemoglobin in blood and reduce the oxygen carrying capacity to cells. If exposure levels are high enough, death from suffocation may result. NO_x has also been found to play a role in the formation of photochemical smog, which is an unsightly and unhealthy problem for many cities [18]. The semi-volatile and heavier HC components of diesel exhaust, which adsorb and condense onto the PM, are of great concern since these compounds have been shown to exhibit carcinogenic or mutagenic properties in biological testing at the cellular level [18]. PM found in the exhaust stream can be inhaled deeply into the lung and may cause severe respiratory problems. Significant reductions in particulate mass in diesel-powered engines have occurred in the past twenty years through intercooling, high boost pressures, centralized injector nozzle positioning, much higher injection pressures, lower combustion chamber swirl, and piston bowl refinement measures. However, it was determined in a study [35] that while overall particulate emissions have been reduced to only 10% of the prevalent levels of 15 to 20 years ago, the very fine nano-particle count was actually increased by these technologies at all load points, sometimes by as much as a factor of six. It is known, that older individuals suffering from chronic respiratory and cardiac diseases are at greatest risk and that fine PM has a greater effect than do the larger size fractions. Of particular concern are the ultrafine particles that may not contribute to the mass concentration, but may pose the greatest health risk because of the higher number count. The health concerns regarding direct human exposure to these exhaust emissions are heightened for many of the off-road diesel applications due to poorly ventilated work areas and direct exhaust plume exposure to the equipment operator and immediate co-workers.

Traditionally, diesel engines have served as the power source for the majority of heavy-duty off-road equipment. Yet, emissions research activities aimed solely at the off-road arena has been minimal, largely overshadowed by the extensive efforts directed toward the on-highway sector. However, current trends indicate that the performance of these off-road vehicles will become increasingly more scrutinized by federal regulatory agencies due to their substantial contribution toward the total emissions inventory. On a national scale, off-road engines are estimated to emit nearly 20% of all NO_x (Oxides of Nitrogen) and about half of all fine PM (particulate matter) pollution from mobile sources. Current projections indicate that the NO_x emissions from non-road engines will surpass those of on-road engines by the year 2005 [1].

A considerable amount of diesel engine emissions research involving on-highway vehicles has been directed toward the development of standardized transient testing cycles that accurately represent real-world operating conditions for these vehicles. This cycle development process provides a performance benchmark to assist in developing standardized emissions regulations and an evolutionary approach to cleaner, more efficient engine designs. With increasing attention being focused on the reduction of emissions from off-road sources, the development of representative testing cycles for these vehicles is of utmost importance. Similarly, improved protocols need to be developed that address the manner in which emissions from off-road diesel engines are measured. Since the off-road sector encompasses a multitude of applications in which the diesel engine is implemented, a better understanding of the correlation, or lack thereof, between current engine certification tests cycles and actual in-field operating conditions needs to be afforded. The development of standardized test cycles would be a daunting task indeed, and the validity of such cycles could only be evaluated by comparing them with actual in-field emissions production. A powerful tool that would assist in these efforts would be the development of on-board emissions measurement systems and test protocols for on-board exhaust emissions measurements.

In the past, exhaust emissions testing has been performed predominantly on an engine dynamometer test bed or on a vehicle chassis dynamometer. Engine tests on an engine dynamometer test bed are time consuming and labor intensive. The engine must be removed from the vehicle and installed on the dynamometer test bed with all the related engine subsystems (intake, exhaust, cooling, fuel, electrical) implemented so as to most accurately mimic the operating conditions of the test vehicle. Chassis dynamometer testing of engines provides a more realistic test of the integrated engine-vehicle system, but is also associated with unique problems. The vehicle operator is required to read and accurately follow a cycle that is broadcast to a computer screen, which can introduce human error into the testing process. In addition, the operating style of the driver (level of natural aggression) can have a significant impact on the emissions measurements. It is difficult to compensate for such inconsistencies. For instance, repeatability mandates that the same test driver be used in subsequent tests, but driver performance becomes variant due to improvements made as a result of cycle repetitions.

Exhaust emissions testing of off-road engines has heretofore been exclusively performed on an engine dynamometer test bed. Vehicle design generally prohibits a chassis dynamometer configuration from properly loading the test vehicle, since hydraulic systems and specialized drive attachments are often integrated into off-road vehicles. To accurately test these vehicles, chassis dynamometer test beds would have to be customized for each test vehicle, and, if the hydraulic and unique power attachments could be accommodated, the fact remains that there are no widely accepted, representative chassis cycles available. Therefore, an obvious alternative is on-board vehicle exhaust emissions testing. For such testing, engine exhaust samples can be measured on a continuous basis, or integrated exhaust gas samples can also be collected in special Tedlar bags and analyzed as a post-test process. While the integrated bag approach provides for the simplification of the on-board measurement component of the system, it can only be used to determine an average of the emissions produced during a particular operation or cycle. Use of the bags makes it very difficult for the researcher to determine the effects of transient conditions on emission rates and makes cycle

development work nearly impossible. Conversely, a continuous on-board emissions measurement system provides detailed information on transient vehicle response, and data that is crucial for the accurate recreation of representative engine dynamometer test cycles.

Portable, relatively compact on-board emissions testing equipment is currently available that can be integrated to make raw exhaust gas sampling possible during actual in-field operation of the equipment being studied. Engine speed can be readily determined from the alternator or inductive-pickup devices, such as Hall-effect sensors. Intake and exhaust temperatures can easily be measured with thermocouples and pressure data can be obtained with miniaturized pressure transducers. The most difficult parameter to measure in field is engine load. Although emissions test data can be reported in a variety of ways, data presentation standards have typically favored a brake-specific format. While this format provides for a more direct emissions comparison for engines with different power output levels, it requires a very accurate determination of engine work - which is inherently difficult measure while the engine is installed in the vehicle. An alternative presentation would be a fuel-specific basis, which would be a near equivalent to the brake-specific approach, since fueling and power output is so closely related. Critics of this method note that higher fueling rates could provide misleading results that would lower fuel-specific exhaust emissions test results. However, such a practice would be highly impractical, since fuel economy is a primary customer concern. Moreover, a fuel-specific approach lends itself very conveniently to on-board vehicle testing, since it does not require determination of engine work.

Though devices are currently available for the direct measurement of torque, they are generally complex and prohibitively expensive. These devices are placed in the driveline and measure the torque transmitted through the drive shaft. The intrusive nature of such devices often makes their use infeasible – either due to design constraints or the refusal of the equipment owner. Drive shafts used in off-road equipment are generally enclosed and very difficult to access, which compounds the problem. More importantly, on a large number of off-road vehicles there is no exposed driveshaft that can be replaced or outfitted.

Since there are inherent problems associated with the direct measurement of engine torque, indirect torque inferences must often be implemented. Common approaches to quantification of engine torque have generally relied on the measurement of the engine-fueling rate. To accomplish this, the rack displacement in the injection pump has been measured with a linear position sensor in order to estimate engine fuel consumption and, hence, load. The problems with this approach are measurement inaccuracies, difficulties related to the instrumentation of the injection pump, and vibration-induced sensor problems. Using the linear position sensor to determine rack position often requires the disassembly and modification of the injection pump, which is labor intensive and often not permitted by the owner of the test vehicle.

An additional approach for the determination of fueling rate can only be used on modern engines with electronically controlled fuel injection pumps. An interface can be used to retrieve desired fueling rate commanded by the ECU (Engine Control Unit), which is calculated based upon fuel pressure and injector pulse-width. Component degradation as well as inherent algorithm inaccuracies are identified shortcomings of this

inference method. Moreover, electronically controlled diesel engines were introduced into the off-road industry during the last decade; therefore the vast majority of off-road equipment encountered is mechanically injected. Obviously for such vehicles, the aforementioned method is not viable. However, as the current inventory of equipment is replaced by more modern electronically injected machinery, this could become the most desirable method for power prediction inferred from engine fueling rates.

For this study, in-field engine torque output was inferred from raw exhaust CO_2 concentrations and engine speed measurements, which were collected using a portable on-board emissions measurement and engine speed logging system during normal vehicle operating conditions. Once the engine was removed and brake-specific CO_2 performance maps were developed under quasi-steady-state operation, the engine loads from the recorded in-field cycle were inferred. The engine was then operated according to these dynamometer set points while raw exhaust CO_2 emissions were recorded using the same methodology that was used during in-field testing. The raw CO_2 trace recorded from the engine operating according to the dynamometer test cycle was compared to the CO_2 trace recorded during in-field testing. The dynamometer set points were then optimized as necessary until convergence criteria were achieved.

1.2   Objectives

The global objective for this study was to determine vehicle activity information and measure exhaust mass emissions rates from four diesel-powered off-road vehicles operated in-field, in their real-world environment. In the absence of any valid transient cycles for off-road equipment, the key focus of the study was the investigation of the feasibility of formulating a test cycle by recreating raw exhaust CO_2 concentration and engine speed traces that were logged during in-field vehicle operations. Upon the successful development of these dynamometer test cycles, the mass emissions rates of exhaust gas pollutants could be measured while the engines were operated in the laboratory according to speed-load schedules that mimicked in-field operations. The mass emissions of PM particulate matter), HC (hydrocarbons), CO (carbon monoxide), NO_x (oxides of nitrogen), and CO_2 were measured and recorded for the street sweeper, front-end loader, and excavator engines during both transient cycle, which WVU derived from data logged during in-field operation, and steady-state testing with the engines being operated according to the ISO-8178 Cycle C1 8-mode steady-state test cycle. The collected data could then be compared to quantify the effect of particular engine use on these rates. The gaseous exhaust mass emissions produced by the track-type tractor were measured using WVU's Mobile Emissions Measurement System (MEMS), which is a portable, on-board unit capable of providing measurements of mass emissions of NO_x and CO_2. The MEMS unit is capable of producing laboratory grade emissions measurements, but it requires more time and effort to operate than the data logging system used for the other vehicles. The engines from the other vehicles tested under this study were able to be removed from the machine and placed on a dynamometer test bed in the laboratory to collect the necessary high quality emissions data. Thus it was determined that use of the MEMS would only be required for the track-type tractor testing since this engine could not be removed from the vehicle and be tested in-laboratory. Gravimetric exhaust PM

measurements were made using MARI's portable Real-time Particulate Mass Monitor (RPM100) that is capable of providing real-time particulate mass information.

The objectives of this study were:

- To derive a transient cycle that accurately represents the "real world" operations for each vehicle.

- To use the derived transient cycle trace during the full-flow testing in the laboratory to determine full-flow mass emissions rates for the test vehicles (street sweeper, rubber-tired loader, and excavator).

- To determine if the in-field CO_2 measurement can be used to accurately predict engine power output for future in-field testing.

- To perform exhaust emissions tests with the engine operating according to the ISO-8178 Type C 8-Mode test cycle to determine the mass emission rates (g/bhp-hr) of exhaust gas pollutants. These measurements were to be made with laboratory-grade equipment (dilute sampling) that complies with the requirements stated in the CFR 40, Part 86, Subpart N.

- To develop off-road vehicle test cycles to facilitate future emissions testing.

- To determine the effects of cycle recreation accuracy and cycle nature on emissions results.

- To measure the on-board, in-field mass emissions produced by a Caterpillar D11R CD Track-Type Tractor while it operated in the field.

1.3   Relevant Literature

The following section has been included in order to summarize relevant activities involving exhaust emissions research for off-road diesel engines. The review will be subdivided into off-road emissions research and on-board emissions measurement studies.

1.3.1   Previous Off-road Emissions Testing

A few noteworthy projects that involved the measurement of in-use emissions levels from off-road vehicles have been conducted in the past. While countless tests have been performed on off-road engines in a laboratory setting, far fewer have been performed in-field on the vehicle as it operates in its true environment. Stationary equipment, such as that used by the mining industry, has often been tested with cumbersome testing apparatus similar to what would be found in a fully equipped emissions testing facility. While this approach cannot be faulted for stationary emissions sources, it is expensive, labor intensive, and usually impossible to utilize for any mobile sources.

1.3.1.1 Northeast States for Coordinated Air Use Management ¾ 1997

The Northeast States for Coordinated Air Use Management (NESCAUM) conducted a study to evaluate the impact of exhaust aftertreatment devices on emission levels [33]. Four different technologies were tested on five vehicles: oxidation catalysts, fuel borne catalysts, and active as well as passive particulate filters.

Representative in-field test routes (cycles) were derived by collecting in-field exhaust gas temperature data, and exhaust temperatures were monitored during the tests to indicated adherence to the original test cycles. A mini-dilution tunnel was used for sample dilution, integrated bag samples were collected as well as gravimetric PM. During the testing raw exhaust constituent concentrations were continuously monitored with a compact multigas analyzer, but the researchers concluded that response times made all measurements, except CO_2, unreliable. The CO_2 results were used to determine vehicle fuel consumption during the test procedure. The project illustrated the need to develop representative testing cycles for off-road vehicles, and exhibited that methods were available to determine correlation of the actual test cycle with a predetermined cycle.

1.3.1.2 United States Coast Guard ¾ 1997

A system was developed by the United States Coast Guard to measure the emissions of three 82-ft. U.S. Coast Guard Cutters (powered by Caterpillar D3412 engines of 750-800hp ratings), as Part of the Clean Air Act instituted in 1990 for non-road air pollution [4,1]. The test protocol used was one based on the ISO 8178 procedure, and a number of variables were investigated including water depth, effect of towing another boat, water current, sea state, and wind direction. Pollution emitted was determined quantitatively as a function of power and fuel consumption, but researchers concluded that propeller shaft speed had the greatest effect on emissions levels.

An Enerac 2000E emissions measurement system was used to measure nitric oxide (NO), CO, NO_2, sulfur dioxide (SO_2), oxygen (O_2), and HC in the raw exhaust stream, and CO_2 concentrations were inferred from the other gaseous component levels. Intake air flow rates were monitored digitally with the Electronic Flowhood manufactured by Shortridge instruments, and fuel consumption was measured with Hedland in-line flow meters. Engine torque was measured with driveshaft-mounted strain gauges that broadcast strain quantity through radio frequency.

The study was initiated, in part, out of the need for an emissions analysis system for on-board ship testing. The test system was adapted from commercially available stack gas monitoring components, and proved to be quite cumbersome. However, the study illustrated that on-board emissions testing with portable instruments was feasible, and that the use of strain gauges for in-field torque measurement was a viable, though complex and tedious, option.

1.3.1.3 VERT Study ¾ 1998

A European study was conducted to quantify the effects of exhaust aftertreatment devices on emissions levels at tunnel construction sites [34 At such sites, ventilation is often poor and workers can be exposed to high levels of pollutants originating from construction vehicles and equipment. Therefore, methods of reducing harmful pollutants

must be tested for effectiveness to improve the future air quality for worker safety. The study investigated thirty-two particulate traps of various types from different manufacturers, and focused on PM emissions, although CO, CO_2, and VOC levels were also recorded. The Switzerland VRV 59A smoke opacity test for free acceleration and a full-load exhaust blackening test were used to estimate PM emission levels.

For the smoke puff test, the engine is operated at steady load conditions and a sharp transient speed condition is administered. The change in opacity of the engine exhaust is used to identify the amount of diesel soot being emitted. While the test results for vehicles outfitted with particulate traps were near the detectable limits of the opacity meters, the results could be used to indicate trap failure during testing. The blackening measurements at full load were taken on construction vehicles equipped with torque converters that could be stalled for two to three minutes to allow sufficient time for an exhaust opacity test. Gaseous emissions were monitored only during steady-state loading conditions with computer-controlled instruments operating on the principles of electrochemical reaction and IR absorption (NDIR).

1.3.2   Previous On-Board Emissions Testing Devices

In-field data acquisition has required the development of a number of compact emissions measurements systems. For cycle development work, a system is needed that can be entirely contained on the vehicle being tested. This section describes a number of systems previously used for on-board exhaust emissions measurements.

1.3.2.1   Caterpillar ¾ 1982

A portable bag collection system was developed by Caterpillar for the determination of in-use NO_x emissions from diesel engines as part of the Point-of-Use Control program that required verification of in-field compliance to emissions regulations [14]. The measurement system was quite compact, and consisted of an exhaust probe, prefilter, sample line, pump, air-cooled condensing coil (for sample humidity control), and two gas collection bags. The system was operated remotely by the driver and was powered by its own on-board power supply. Researchers concluded that the valid data could only be obtained when the vehicle was operated at fully-loaded conditions, where the on-board system could report NO_x concentrations to within 10% of laboratory analyzers.

1.3.2.2   Southwest Research Institute ¾ 1992

A mobile system that measured diesel exhaust emissions was developed by Southwest Research Institute as part of a study initiated to develop testing methods that did not require the use of a chassis dynamometer [19]. The system was used for inspection and maintenance of buses and comparison with transient cycle chassis emissions data taken on buses by the EPA. The tests were limited to vehicles equipped with automatic transmissions, as the loading sequence required 30-second load operations on the vehicle at various throttle positions with the vehicle held stationary through locked brakes.

Gaseous emissions and PM were collected by the system. Raw gaseous measurements of CO, CO_2, NO_x, and O_2 were made using an Energy Efficiency Systems, Inc. Enerac 2000E from integrated bag samples collected during engine operation. PM

was collected with a mini-dilution tunnel system. Testing showed that measurement of CO, O_2, and NO_x were within 5% of measurements obtainable with laboratory grade analyzers

1.3.2.3 General Motors ¾ 1993

A 3.8-liter Pontiac Bonneville SSE gasoline-fueled passenger car was outfitted with emissions instrumentation by the General Motors Corporation and tested over numerous driving routes to obtain desired representative emissions data [21]. The system was capable of measuring HC, CO_2, CO, and NO using a variety of NDIR analyzers. A Horiba MEXA-311GE analyzer was used to measure CO_2 and CO, while measurements of HC and CO were performed with a MEXA-324GE. A Siemens Ultramat-22P analyzer was also used to make HC and CO measurements, and a Siemens NO analyzer was also used. In addition, a Draeger electrochemical gas sensor (EGS) cell was used to measure CO buildup levels within the vehicle driver compartment. Sample humidity conditioning was accomplished via an ice-cooled trap. A Kurz flow meter was used for exhaust gas flow rate measurements, while the intake air flow rates were monitored using the stock air meter, and a relationship between intake and exhaust flows was derived, which illustrated effects of intake flow on exhaust flow.

Data was collected along driving routes during high-traffic rush-hour conditions as well as during lighter traffic conditions to obtain a broad array of operating conditions. For comparative purposes, emissions rates of HC and CO were also recorded while the vehicle was loaded according to the Urban Dynamometer Driving Schedule (UDDS) on a chassis dynamometer. The system was unable to record transient events due to slow analyzer response times, and testing was limited to a single vehicle. However, the research did demonstrate that useful on-board emissions information could be obtained from a spark-ignited gasoline-fueled vehicle.

1.3.2.4 Ford Motor Company ¾ 1994

The Ford Motor Company developed a sampling system that was used to quantify emissions from three spark-ignited vehicles [7,15,24,25]. The vehicles tested in the study were a 1992 Aerostar van, a 1991 Taurus station wagon, and a 1991 flex-fueled Taurus sedan. The objective of the study was the comparison of real-time emissions measurements made with the on-board Ford system with those obtained with remote equipment.

The Aerostar van was equipped with an On-Board Emissions (OBE) system, comprised of a dilution tunnel and a Fourier Transform Infrared (FTIR) analyzer. CO_2, NO_x, CO, and HC emissions measurements were made, and results obtained with the OBE system were compared with those obtained from a chassis dynamometer laboratory. The researchers reported differences of 2% for CO_2, 10% for NO_x, 3% for CO, and 7% for HC, and indicated that the FTIR analyzer's response time was much too slow for transient emissions testing.

The Taurus wagon was outfitted with an infrared analysis system that was capable of measuring CO_2, NO_x, CO, and O_2 emissions. A non-dispersive ultraviolet (NDUV) analyzer was used for NO measurement. The results from the NDUV analyzer and a

laboratory grade chemiluminescent analyzer were compared and found to relate closely (slope of 0.8 and an R^2 value of 0.97).

1.3.2.5 University of Pittsburgh ¾ 1997

The University of Pittsburgh developed a system to measure emissions from a fleet of 20 natural gas passenger vans using an RG240 multigas analyzer produced by OTC SPX for the detection of CO, NO_x, CO_2, HC, and O_2 [36]. The system operated on 12v DC vehicle power and used stand-alone engine diagnostic equipment to monitor engine parameters. The sample was drawn from the exhaust stream with a 12 in. probe and conditioned with coalescing filters. Total exhaust flow rate was inferred from intake and fuel mass flow data collected by the diagnostic equipment. Data collection was performed with a laptop computer using software developed by the University of Pittsburgh.

The researchers reported problems associated with data time alignment, slow analyzer response times, mass emission rates measurement, and random analyzer auto zeroing. Also, since the analyzer unit was originally developed for testing gasoline-fueled vehicles and not NGVs, HC measurement bias was encountered. However, the system did provide on-board emissions data from natural-gas fueled vehicles operating in real-world applications.

1.3.2.6 Flemish Institute for Technological Research ¾ 1997

The Flemish Institute for Technological Research (VITO) conducted on-board emissions tests on gasoline-fueled passenger cars and diesel-fueled buses using a system developed in-house. The VITO On-the Road Emission and Energy Measurement (VEOM) utilized NDIR technology for CO and CO_2 measurement, an HFID for HC measurement, and a chemiluminescent analyzer for the detection of NO_x. The exhaust sample was diluted by means of a nitrogen-driven ejector located in the vehicle tailpipe, and heated sample lines were implemented to prevent the loss of heavy hydrocarbons from the sample stream. Emissions were reported in either g/s or g/km format by combining dilute sample amounts collected with data on fuel consumption, lambda values, and engine speed. Results showed that the VEOM data differed from chassis laboratory data by 25% for HC, 20% for CO, and less than 10% for CO_2 and NO_x. The weight of the VEOM system, which tipped the scales at approximately 500 lbs, made it unwieldy and difficult to use for acquiring in-use data.

1.3.2.7 United States Environmental Protection Agency ¾ 1999

A mobile testing system was developed by the Office of Mobile Sources of the United States Environmental Protection Agency (USEPA) to measure emissions from gasoline vehicles. The system, dubbed the Real-time On-Road Vehicle Emissions Recorder (ROVER), was later retrofitted to accommodate emissions analysis of diesel-fueled vehicles. A differential pressure device was used to determine exhaust flow rate, while a Snap-On Model MT3505 emissions analyzer was used for the determination of CO, CO_2, HC, and NO (no converter for NO_x determination). Vehicle speed can be determined with a global positioning system (GPS) and interface with the vehicle's ECU. Results were reported on a distance-specific basis - grams of pollutant emitted per mile the test vehicle travels (g/mile). .

1.3.2.8   Ford Motor Company/WPI Microprocessor Systems, Inc. ¾ 1999

Ford Motor Company and WPI-Microprocessor Systems, Inc. have recently developed a system known as the Portable Real-Time Emission Vehicular Integrated Engineering Workstation (PREVIEW) [8]. PREVIEW is a capable of measuring wet exhaust and was designed to be compact enough to allow it to fit into the passenger compartment of a sport-utility vehicle. PREVIEW is able to provide NDIR-based measurements of CO_2, CO, and HC, and ultra-violet detection of NO_x. A number of sensors can be used by the system for recording up to forty additional engine parameters, such as various engine temperatures or air/fuel ratio sensing devices. Control of the PREVIEW system is accomplished with a laptop computer and software that can record and display data simultaneously at a 1 Hz frequency.

Testing performed with the system included transient FTP cycle tests as well as Highway Fuel Economy tests in a laboratory setting. Comparative results with a chassis dynamometer laboratory showed that the PREVIEW system obtained results within 1.5% for CO_2, 12.3% for HC, 0.4% for NO_x, and 3.4% for CO of the laboratory-grade analyzers. It should be noted that the instantaneous mass measurements for NO_x with the system actually exhibited faster response times than the laboratory analyzer.

1.3.2.9   West Virginia University ¾ 2000

A system was recently developed at West Virginia University for the On-Board measurement of in-use emissions from heavy-duty on-road vehicles [32]. This work stemmed from the 1998 court settlement, wherein six heavy-duty diesel engine (HDDE) manufacturing companies (Caterpillar, Inc.; Cummins Engine Company, Inc.; Detroit Diesel Corporation; Mack Trucks, Inc.; International Truck and Engine Corporation[*]; and Volvo Trucks, Inc.) entered into individual agreements (referred to as Consent Decrees) with the US government as a result of the use of advanced injection timing strategies that could be responsible for increased engine emissions. The Mobile Emissions Measurement System (MEMS) provided real-time, on-board brake-specific measurement of NO_x and CO_2, and was comprised of the three primary components: an exhaust flow measurement apparatus, an emissions measurement component, and the data acquisition equipment. The MEMS was recently approved by the US-EPA for use in Phase III of the In-Use Testing program governed by the Consent Decrees that is currently being conducted by the authors of this report.

Engine exhaust flow was measured with an Annubar™, multi-port Pitot-tube differential pressure device. This flow rate measurement technique provided a low-restriction of the exhaust and proved to be very robust. The emissions sampling component consisted of a heated, filtered, and humidity-controlled sample conditioning system, a Horiba COM-11 NO_2 converter, Horiba BE-140 NDIR analyzer, a Horiba MEXA-120 NO_x sensor, and an electrochemical NO cell.

The data acquisition components of the MEMS were comprised of a National Instruments PXI-1025 computer, signal conditioning hardware, data acquisition, ECU-interface, and control software. The system provided records of a variety of signals from

---

[*] Formerly Navistar International Transportation Corporation

thermocouples, pressure transducers, emissions analyzers, and numerous ECU outputs. Engine torque output and speed was recorded with the aid of manufacturer-supplied ECU interfaces, and vehicle speed was measured with a Global Positioning System (GPS).

Reported results indicated that when compared to laboratory-grade analyzers during chassis-dynamometer testing, the MEMS was capable of providing brake-specific CO_2 data which differed from the laboratory data by 2.54%, and brake-specific NO_x data that differed by 11.54% (MEXA-120) and 5.68% (Electrochemical cell).

2 Materials and Methods

The following section is included in order to outline the equipment and procedures used for the in-field data logging and the engine emissions measurement activities.

2.1   Vehicles Tested

It should be noted that, unlike on-highway vehicles, recruitment of off-road equipment for emissions testing is a considerably greater challenge. The test vehicles procured for this project are typically used for production, maintenance, and construction and are therefore employed on, virtually, a daily basis. As a result, measures had to be taken to limit downtime and its negative impact on maintenance and construction. For instance, in the case of the rubber-tired loader, in-laboratory testing was performed on the engine while the vehicle was down for drive train repairs. This allowed the testing with no additional downtime being required for the vehicle, while construction and maintenance progress could still be made using the remaining operational loader. The street sweeper, on the other hand, is used daily and is the only one owned by WVU. This required the hiring of a contractor to perform the duty of sweeping the campus streets while in-laboratory testing was being performed. The excavator and track-type tractor involved both entailed equipment rentals and operator costs, as well as advanced scheduling to accommodate testing during non-production hours. All in-field testing was conducted in a manner that did not hinder the operation of the vehicle during its everyday routine. In-field testing routes and task descriptions will be described later in this chapter.

Prior to testing the vehicles, a diesel equipment questionnaire was provided to the owners in order to document maintenance history and vehicle condition. The completed questionnaires have been included in Appendix D. The questionnaires show that the vehicles were regularly maintained. However, contrary to what the questionnaire indicates, WVU found that the excavator was not well maintained. The usage of the vehicles varied from a steady rate for the sweeper and the track-type tractor, to a more variable rate for the loader and excavator. Table 1 summarizes the results of these questionnaires.

Table 1 Diesel Equipment Questionnaire Summary

Vehicle	Average Usage	Total Engine Hours	Fuel Used	Average Maintenance Window
Loader	15-20 hr/week	6841	D2	Weekly
Sweeper	15-20 hr/week	2756	D2	Daily
Excavator	0-20 hr/week	3263	D2	3 month or 100 hours
Track-type Tractor	100 hr/week	2750	D2	Daily

2.1.1 John Deere 444 Rubber-Tired Front End Loader

A John Deere 444 rubber-tired front-end loader was tested in field at a landfill site on WVU property. A picture of the rubber-tired loader can be seen in Figure 1. Data was collected with a portable multigas analyzer. The loader is powered by a pre-1995 John Deere 6059 diesel engine. This engine is a direct-injected, naturally aspirated, in-line six cylinder configuration. Detailed specifications for the 6059 engine are listed in Table 2. The engine, as tested in the laboratory, can be seen in Figure 2.

Figure 1 John Deere 444 Rubber-Tired Front End Loader

Figure 2 John Deere 6059D Engine on Eddy-Current Dynamometer Test Bed

2.1.2 Elgin Pelican Series P Street Sweeper

An Elgin Pelican street sweeper was tested in-field on WVU campus streets following its normal sweeping routes. A picture of the street sweeper can be seen in Figure 3. A multigas analyzer was used for the acquisition of all in-field data. The street

sweeper is powered by a post-1995 John Deere 4039T diesel engine. The engine is a direct-injected, turbocharged (non-aftercooled), in-line four-cylinder configuration. Specifications for the 4039T engine are given in Table 2. The in-laboratory testing setup for this engine can be viewed in Figure 4.

Figure 3 Elgin Pelican Series P Street Sweeper

Figure 4 John Deere 4039T Engine on Eddy-Current Dynamometer Test Bed

2.1.3   Komatsu PC400LC3 Excavator

A 1987 Komatsu PC400 LC3 Excavator with a turbo-charged in-line six-cylinder model S6D 125-1 engine was tested for the 250-500 hp engine class. The vehicle was leased to WVU by Richard Construction, Incorporated (RCI), for the duration of field and laboratory testing. RCI also provided operators for the field portion of testing (see Figure 5). The lease commenced on the seventh day of May, 2001.

In order to collect engine speed data, the vehicle alternator was modified in order to produce a TTL signal that could be recorded by the emissions measurement system. With the known quantities of CO_2 and engine speed, engine torque could be estimated and a test cycle produced, using an iterative approach that will be discussed in the methods section of this report. Detailed specifications for the S6D 125-1 engine are listed in Table 2. The engine, as tested in the laboratory, can be seen in Figure 6.

Figure 5 Komatsu PC400LC3 Excavator

Figure 6 Komatsu S6D 125-1 Engine installed onto GE dc dynamometer test bed

2.1.4   Caterpillar D-11 R CD Track-type Tractor

WVU procured the use of a 2001 model Caterpillar D-11R CD track-type tractor outfitted with a CAT 3508B TA, Vee-8, four-stroke diesel engine with electronically controlled direct injection. The machine is the property of Buffalo Coal Corp., and testing was performed on the company's #857 strip mine site near Mt. Storm, WV.

Figure 7 Caterpillar D-11R CD Track-Type Tractor Operating at Buffalo Coal Test Site

WVU was unable to remove the engine from the track-type tractor in order to perform emissions tests in the dynamometer laboratory. Not only did the engine output power exceed the dynamometer handling capabilities, but Buffalo Coal would not permit the extended downtime or potential damage that could have been caused by engine removal and dynamometer testing. As a result, WVU proposed to CARB, and received approval, to collect emissions and vehicle activity data for the dozer in the field. To do so, WVU's Mobile Emissions Measurement System (MEMS) was employed to record mass emissions rates of CO_2 and NO_x, while the Mid-Atlantic Research Institute's RPM-100 was used to provide real-time, on-board, gravimetric particulate mass emissions measurements. The MEMS utilizes an NDIR detector for the determination of CO_2, a zirconium-oxide sensor for measurement of NO_x, a quartz-crystal microbalance for determination of gravimetric PM, and an Annubar™ averaging pitot-static device for the measurement of engine exhaust flow rates. The system is capable of logging engine control unit data streams for the inference of engine torque, but the necessary engine load data stream was not publicly broadcast by the Caterpillar D11RCD engine control unit. Therefore, a representative from Caterpillar logged engine speed and estimated load, using a proprietary Caterpillar ECU-interface. The correlation of the MEMS with a full-flow CFV-CVS system operating according to CFR 40, Part 86, Subpart N was established before the unit was installed and tested on the Caterpillar D11RCD track-type tractor. Further details regarding the design, use, and correlation with a full-flow laboratory of the MEMS will be discussed in the methods section of this report.

Figure 8 Caterpillar D-11R CD Track-Type Tractor Outfitted with WVU's Mobile Emissions Measurement System

Table 2 Test Engine Specifications

Vehicle	Elgin Pelican Series P Street sweeper	John Deere 444 Rubber-Tire Loader
Engine Manufacturer	John Deere	John Deere
Engine Model	4039T	6059D
Displacement	239 in^3 (3.92 L)	359 in^3 (5.9 L)
Power Rating (Hp)	110 hp @ 2400 rpm	107 hp @ 2500 rpm
Torque Rating (ft-lb)	339 ft-lbs @ 1500 rpm	260 ft-lbs @ 1400 rpm
Configuration	In-line 4 cylinder, 4-stroke	In-line 6 cylinder, 4-stroke
Bore x Stroke	4.19 in. x 4.33 in.	4.19 in. x 4.33 in.
Compression Ratio	17.2:1	17.8:1
Induction	Turbocharged	Naturally Aspirated
Injection	Direct-Mechanical Control	Direct-Mechanical Control

Vehicle	Komatsu PC400LC3 Excavator	Caterpillar D11R CD Track-Type Tractor
Engine Manufacturer	Komatsu	Caterpillar
Engine Model	S6D 125-1	CAT 3508B TA
Displacement	674 in^3 (11.05 L)	2105 in^3 (35 L)
Power Rating (Hp)	250 hp @ 1800 rpm	850 hp @ 1800 rpm
Torque Rating (ft-lb)	745 ft-lbs @ 1350 rpm	N/A
Configuration	In-line 6 cylinder, 4-stroke	Vee-8 cylinder, 4-stroke
Bore x Stroke	125 mm x 150 mm	6.7 in. x 7.5 in.
Compression Ratio	N/A	N/A
Induction	Turbocharged	Turbocharged
Injection	Direct-Mechanical Control	Direct- Electronic Control

2.2   Test Fuels

The test fuel used for the engine emissions tests performed in the laboratory was a specified market basket blend California spec fuel per contract agreements. The fuel analysis results of this blend are included in Figure 9 and Figure 10. It is seen that sulfur content of the three different fuels in the market basket blend ranges from 173 ppm to 197 ppm, compared to a specification of 500 ppm (max.) for Federal Diesel No. 2, and California specification (for both on-highway, and off-highway applications). The aromatic content of the three fuels in the test blend was 15.2%, 15.4%, and 15.5% compared to a California specification of 20% for "small" refiners, and 10% for "large" refiners. The Federal Diesel No. 2 specification for aromatic content is 35% (max). The cetane numbers for the three fuels in the test blend were 48.4, 50.9, and 51.1, compared to a California specification of 52, and a Federal specification of 45. For the in-field on-board emissions tests that were performed on the Caterpillar D-11R CD track-type tractor, the vehicle was operated on Federal Diesel no. 2. Previous studies have shown that a 0.1% in fuel sulfur content increased total PM by 0.125 g/bhp-hr on an FTP cycle.

LABORATORY ANALYSIS REPORT
FUEL ANALYSIS AND METHODS EVALUATION SECTION
CALIFORNIA AIR RESOURCES BOARD

Project ID: WVU/CARB 98-317
Submitted by: Haviside Heastings Inc.　　Submitted: 5/19/00　　Contact: Mridul Gautam　　Affiliation: West Virginia Univ.

Fuel Analysis & Methods Evaluation Section (FAME)
Monitoring and Laboratory Division, CARB

ANALYTICAL LABORATORY METHOD		ASTM D5186 SFC/FID			ASTM D86 Automatic			ASTM D5453 Antek	ASTM D4052 Density Mtr
Analysis Date		5/26/00			5/24/00			5/24/00	5/24/00
Analyst		JC			MM			JS	JS
Sample I.D.	Sample Date	Total Aromatics (vol %)	Total Aromatics (mass%)	Polycyclic Aromatics (mass%)	T10 (deg C)	T50 (deg C)	T90 (deg C)	Sulfur (ppm)	Density @ 60 F (g/mL)
98-317-1		15.2	15.2	2.91	198	235	307	173	0.8268
98-317-2		15.5	15.4	2.93	198	234	304	197	0.8262
98-317-3		15.4	15.4	2.97	197	235	305	187	0.8266

Approved by: _____　　NR: Not Requested　　Date: 5/26/00

Figure 9　Test Fuel Analysis Results Provided by CARB Southern Laboratory Branch.

CORELAB

CORE LABORATORIES

LABORATORY   TESTS   RESULTS
05/25/000

JOB NUMBER: 100704   CUSTOMER: University Of West Virginia   ATTN: Byron L. Rapp

SAMPLE NUMBER: 1   DATE RECEIVED: / /   TIME RECEIVED: :   SAMPLE DATE: / /   SAMPLE TIME: :
PROJECT: IA, Diesel   SAMPLE: IA, Diesel   REM: 1-1gal can

SAMPLE NUMBER: 2   DATE RECEIVED: / /   TIME RECEIVED: :   SAMPLE DATE: / /   SAMPLE TIME: :
PROJECT: IIA, Diesel   SAMPLE: IIA, Diesel   REM: 1-1gal can

SAMPLE NUMBER: 3   DATE RECEIVED: / /   TIME RECEIVED: :   SAMPLE DATE: / /   SAMPLE TIME: :
PROJECT: IIIA, Diesel   SAMPLE: IIIA, Diesel   REM: 1-1gal can

TEST DESCRIPTION	SAMPLE 1	SAMPLE 2	SAMPLE 3				UNITS OF MEASURE
Nitrogen, Total	106	114	110				ppm wt.
Cetane Number, Neat	51.1	50.9	48.4				Cetane Number

21730 S. Wilmington Suite 201
Carson, CA   90810
(310) 513-2031

PAGE:1

Figure 10 Test Fuel Analysis Results Provided by CORE Laboratories.

2.3   Vehicle In-field Testing Routes

Emissions data was collected on four vehicles (street sweeper, rubber-tired front-end loader, track excavator, and track-type tractor) while they followed operational cycles that were typical of those encountered during day-to-day usage. Detailed graphs of CO_2/RPM vs. time can be viewed in the results section of this document. The representative cycle developed during in-field testing was later recreated in the laboratory using laboratory-grade analyzers and a dynamometer test bed. During laboratory testing, raw emissions were measured with the solid-state NDIR device that was employed in the field, and the speed and load settings applied to the dynamometer were adjusted until the in-laboratory emissions data closely correlated with emissions data taken in field. Brief descriptions of the testing routes and vehicle activity are included in Section 3.3.

2.3.1   Street sweeper Test Cycle

Data was collected on the street sweeper while it performed normal sweeping duties on the campus streets of WVU. In the case of the street sweeper, it was possible for the test engineer to ride aboard the vehicle to monitor data acquisition functions during testing. A typical sweeping route was followed on the hilly terrain that is characteristic of the Morgantown, WV area. Street sweeper functions performed while data was taken included: normal sweeping, normal transport mode with brushes off, dumping of collected debris, and extended idle periods. A short test was also performed to assess the effects of brush rotation and drag on CO_2 emission rates. These effects and in-field emissions data are illustrated in the in-field results section 3.6.2.

2.3.2   Rubber-Tired Loader Test Cycle

Data was collected on the rubber-tired front-end loader while it performed earth-moving activities at a landfill site on the WVU campus. Though space restraints prevented the test engineer from riding aboard the machine during the end loader testing, the vehicle was stopped several times during the test session to ensure that data acquisition system was functioning properly. No data logging was conducted during these stops. Activities encountered while following the operational route include: transport from the place of origin to the landfill site on hilly terrain, loading/lifting dirt with the bucket, transporting the dirt in the bucket, and dumping the dirt. These processes were repeated numerous times during the test. In-field emissions data can be found in the in-field results section 3.6.1.

2.3.3   Excavator Test Cycle

Data for the operation of the excavator was collected while it performed specified earthmoving activities that simulated the most common uses of this vehicle. The in-field test site is located in Star City, WV. Three primary operations were performed during the in-field tests: stationary digging/backfilling, tracking/hauling, and trench digging. Stationary digging involves digging from the dirt removal area, swinging the boom to another location, and dumping the dirt into a pile. Backfilling is the opposite procedure, and the bucket may be used to compress the dirt as it is placed back into the area it was removed from. A tramming/hauling operation is performed when the excavator is moved

in order to transport dirt from one location to another that is not within the reach of the boom. Trenching/digging is an operation by which a line of dirt is removed, with the removed dirt placed near the trench for ease of backfilling. In this operation, the bucket digs out the desired amount of material, dumps near the edge of the trench, the machine tracks to the next position and the process repeats. Several repeats of each test were exercised to determine repeating trends in each operation. Due to the inability for any person but the operator to safely ride the vehicle while in operation, test equipment had to be checked and calibrated between tests. Once the trends of each operation were determined, the testing cycle was modified to include three ten-minute sections of each operation. This test design was repeated for QC/QA measures, and designated as the cycle that would be recreated once the engine was in-laboratory. In-field emissions data can be found in the in-field results Section 3.6.3.

2.3.4   Track-Type Tractor Test Cycle

The track-type tractor tested in this study is used to remove overburden from coal seams after it has been blasted from the high-wall, and then to recover the area after coal has been extracted. The average duty cycle involves starting from one side of a pit, pushing down into the center and then up the other side of the pit removing earth at a rate of nearly 900 yards per hour. The machine then reverses and repeats the removal process. Occasionally when sandstone has not been sufficiently demolished by blasting, a ripper is used to move large rocks that cause the tractor blade to skip over an area and not remove the desired amount of material. In recovery operations, the machine pushes the pile of material removed to expose coal back into the pit. As the job is completed, the track-type tractor sculpts the landscape to designed parameters. For the in-field testing data recorded during this study, the machine was only used to remove overburden, and was not employed for landscape recovery. The in-field emissions results can be found in the in-field results section 3.6.4.

2.4   In-field Data Acquisition Equipment/Procedures

In-field emissions were measured using four main components. The Sensors AMB-II multigas analyzer with laptop, a power inverter to provide 120V AC power, an exhaust sampling probe that transferred the sample, and a signal-conditioning device for engine speed measurement. A schematic of the in-field testing setup can be viewed in Figure 11. The four components will be described in detail in the following three sections.
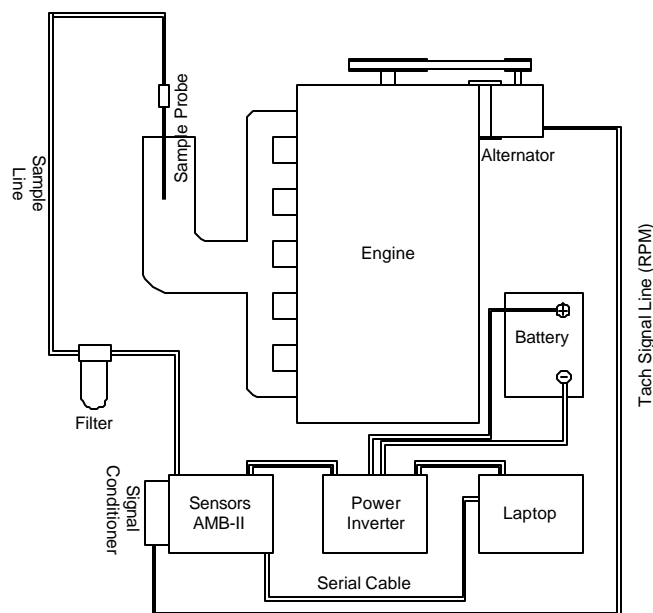
Figure 11 In-field Data Acquisition Setup

2.4.1   Sensors AMB-II Multigas Analyzer

As previously stated, a raw exhaust concentration measurement was collected with a five gas repair-grade analyzer on a continuous basis. The analyzer is an AMB-II manufactured by Sensors, Inc. It is a solid-state detector using Non-Dispersive Infrared (NDIR) technology that is capable of measuring CO_2, CO, and HC. The analyzer can be seen in Figure 12.

Theoretically, each gas has the ability to absorb a specific waveband of light in the infrared (IR) spectrum. This light is directed toward thermal detectors through a tube containing the sample gas. However, before the light can reach these thermal sensors it must first pass through optical band-pass filters. These filters transmit electromagnetic energies only within the critical IR waveband absorbed by the sample gas. Band-pass filters are utilized to increase resolution and account for the effects of absorption spectrum overlap. When the sample tube is filled with sample gases, the thermal detector measures the reduction in IR energy transmitted within the waveband of each gas being measured. Pressure and temperature variations in the sample tube are accounted for with a bench-mounted microprocessor. The AMB-II has measurement ranges of 2000 parts per million (ppm) for HC, 0-20% for CO2, and 0-15% for CO. The analyzer communicates with an onboard laptop computer via serial cable. Software supplied by Sensors, Inc. is used to control the calibration and data acquisition functions of the unit.
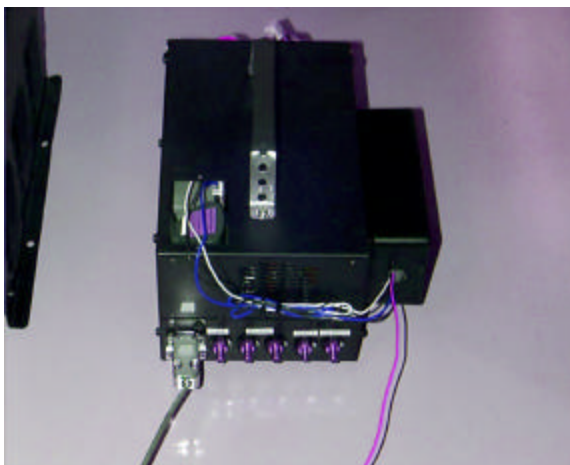
Figure 12 Sensors Inc. AMB-II Multigas Analyzer

2.4.2   Power Inverter

In order to supply power to the analyzer and the laptop, the use of a DC to AC power inverter was required. Tripplite, Inc manufactures the inverter, a model PV1200, used for the in-field testing. The inverter converts the 12V DC power supplied by the vehicle's alternator into 110V AC power that can be utilized for data acquisition. The power inverter can be seen in Figure 13.

Figure 13 Tripplite Inc. Model PV1200 Power Inverter.

2.4.3   Exhaust Sampling Probe

A stainless steel exhaust probe was used to sample from the vehicles' raw exhaust streams. The sample was passed through a non-heated sampling line and coalescing, high-temperature glass microfiber filter before it was introduced into the gas analyzer.

2.4.4 Engine Speed and Torque Measurement

A signal conditioning apparatus was constructed to aid in the measurement of the vehicles' engine speed. The engine speed was measured by tapping into the vehicle alternator. The signal coming from the alternator is a transistor-transistor logic (TTL) stepped-pulse signal. The voltage of the signal alternates between a value near zero volts and an upper limit near one volt. The Sensors AMB-II has the capability of measuring a TTL signal, but a problem was encountered due to the noise contained in the alternator signal. The signal was observed with an oscilloscope and it was found that it contained many very short duration spikes that were close enough to one volt that they were counted as a pulse. The signal-conditioning device constructed basically chopped the top of the signal off (voltages near one volt) and nullified the noise spikes that were significantly less than one volt, thus producing a substantially cleaner signal. The signal conditioner was mounted to the side of the AMB-II analyzer and can be viewed in Figure 14.

The torque produced by the engine is an exceedingly difficult parameter to quantify during in-field testing. Conventional methods of torque measurement, such as a dynamometer, are impractical for real world testing of off-road vehicles. In-line torque transducers are currently available for torque measurement, but transmission efficiencies must be known and taken into account. An additional shortcoming of in-line transducers is that parasitic engine losses such as water and hydraulic pump drag, alternator drag, air compressor drag, and fan windage losses are not accounted for. These parasitic loadings could be significantly different from those encountered during engine tests that are performed on an engine dynamometer, which would inevitably affect even brake-specific emissions results. It is also often very difficult to use in-line transducers for off-road vehicle testing because of short drive shafts that are usually not exposed for easy access.

In its simplest form, engine torque production can be inferred from the brake-specific fuel consumption of the engine. Many modern diesel engines use electronically controlled injection strategies that maximize power output and fuel efficiency. The injection is computer (ECU) controlled and optimized with various sensors providing feedback. These modern systems provide the ability to interface with them to allow the determination of the amount of fuel injected during each engine cycle. With the aid of sensors determining parameters such as intake pressure and temperature, exhaust backpressure, coolant and fuel temperatures, and intake air humidity, an accurate estimate of torque can be acquired from associated engine maps. Since the engines that were removed for dynamometer testing were mechanically fuel injected, this method was not an option for this research. However, this would be the method of choice for future torque determination on modern ECU-controlled vehicles.

In this study, engine torque was estimated with the BSFC determined by the mass of CO_2 amount present in the exhaust stream. This method allows the approximation of torque based on fuel properties, such as the hydrogen-to-carbon ratio and energy density. Many errors associated with the aforementioned parasitic loss parameters from engine accessories are eliminated with this approach. The vehicles in this study were tested in the laboratory with a dynamometer also, so the torque output approximation could be accurately checked.
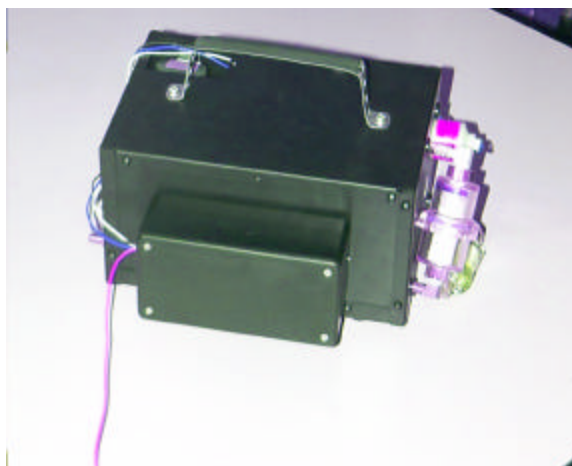
Figure 14 Engine Speed Signal Conditioning Unit and Sensors AMB-II Gaseous Microbench Analyzer.

2.5   West Virginia University's Mobile Emissions Measurement System

WVU has been involved in a study designed to evaluate the currently available on-board emissions measurement systems that are capable of measuring heavy-duty diesel exhaust emissions. This work stemmed from the 1998 court settlement, wherein six heavy-duty diesel engine (HDDE) manufacturing companies (Caterpillar, Inc.; Cummins Engine Company, Inc.; Detroit Diesel Corporation; Mack Trucks, Inc.; International Truck and Engine Corporation[*]; and Volvo Trucks, Inc.) entered into individual agreements (referred to as Consent Decrees) with the US government as a result of the use of advanced injection timing strategies that could be responsible for increased engine emissions. The agreements stated that, in addition to the standard FTP, engines had to be tested according to the Euro III test procedure, which incorporates the steady state test and emission weighting protocols identified as the "European Stationary Cycle" (ESC) Test in Annex III to the Proposal adopted by the Commission of the European Union on December 3, 1997. Further, engines were to demonstrate that they would not exceed prescribed emissions limits in a "Not-to-Exceed" (NTE) zone, Smoke or Alternative Opacity limits, and Transient Load Response limits. Engines are required to meet these limits when new and during in-use operations throughout their useful life. The six settling heavy-duty diesel engine (S-HDDE) manufacturers charged WVU to assess and propose a mobile measurement system that would be capable of testing emissions of heavy-duty diesel vehicles in order to comply with the conditions of the Consent Decrees.

In order to achieve accurate in-use brake-specific mass emissions, as required by the Consent Decrees, it is imperative that a viable on-board emissions measurement

---

[*] Formerly Navistar International Transportation Corporation

system not only be portable, but also be capable of accurately measuring several parameters in a repeatable manner with the highest level of precision. These include engine speed, engine torque, exhaust mass flow rates, and exhaust constituent concentrations. Based upon an extensive evaluation of the available technologies, WVU integrated and tested a Mobile Emissions Measurement System (MEMS). The MEMS has recently been approved by the US EPA for use in Phase III work of the "In-Use Testing Program" under the Consent Decrees. The MEMS is capable of measuring in-use brake-specific emissions of NO_x and CO_2 from diesel-powered vehicles operated under real-world conditions. The major sub-systems of MEMS include:

    i.   Exhaust mass flow measurement system
    ii.   Engine torque and speed measurement system
    iii.   Exhaust emissions analyzers
    iv.   Exhaust gas sampling, and sample conditioning systems
    v.   Vehicle speed and distance measurement system
    vi.   Data acquisition, reduction, and archival system
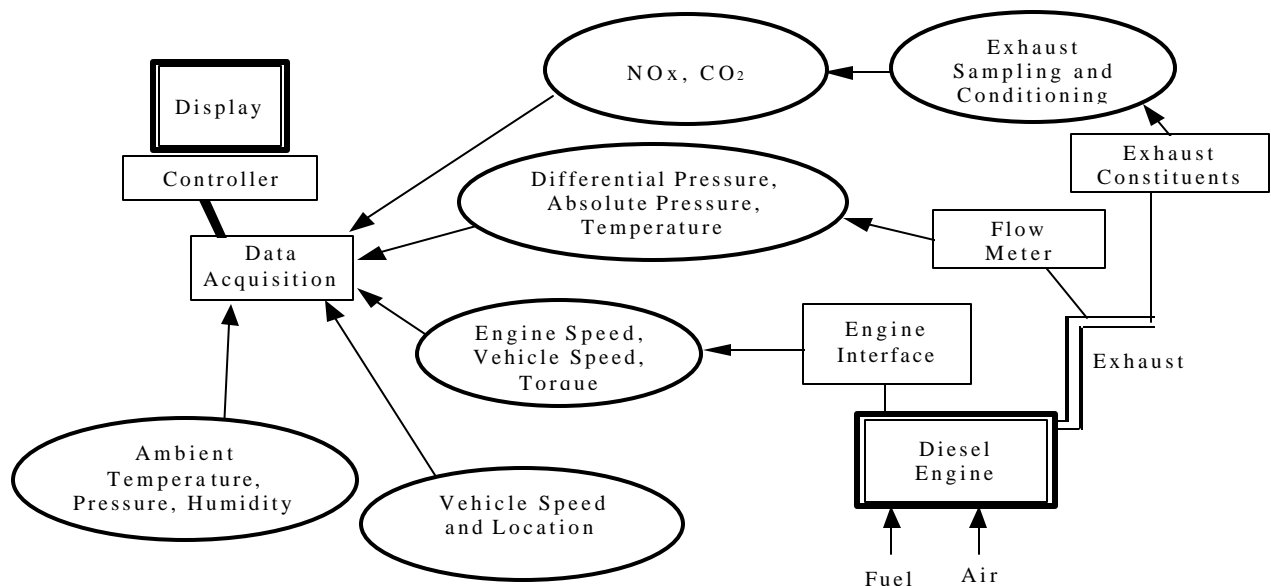
Figure 15 System integration of MEMS.

These subsystems are comprised of the components described in the following subsections and represented above in Figure 15.

The MEMS employs a filtered, heated sample handling and conditioning system, a solid-state non-dispersive infrared detector for CO_2 measurement, and a zirconium oxide sensor for NO_x measurement. It relies upon engine ECU broadcasts for torque, and engine/vehicle speed data. Exhaust flow rate is measured with a differential pressure device. All data is collected with a rugged data acquisition system, and a customized software package that allows sampling at a minimum sampling rate of 5 Hz. Currently, the WVU MEMS employs a portable generator set to power all components with a battery back-up for the data acquisition system and emissions analyzers.

A correlation study was performed between mass emissions results obtained from the MEMS and the full flow dilution tunnel system. The results of this are included in Section 3.3.4. It should also be noted that the US-EPA has recently approved the MEMS for use during the Phase III component of the "Consent Decrees" work for which WVU has been contracted.

2.5.1 MEMS Exhaust Mass Flow

An Annubar™ cross-sectional averaging flow meter is used to measure the exhaust flow rate, since it can account for the effects of pulsation in the exhaust stream that are produced by an internal combustion engine. When used in the same nominal pipe size as the vehicle's exhaust system, a minimal additional backpressure is placed on the engine. A Validyne P55D differential pressure transducer, Omega PXI213 absolute pressure transducer and J-type thermocouples were used to interpret the Annubar™ signal for calculation of mass flow rate.

2.5.2 MEMS Engine Torque and Speed

Engine torque and speed are available via an ECU protocol adaptor through an RS232 interface with the data acquisition system. Engine torque is inferred from the ECU's broadcast signal of the percent load, the measured curb no-load percent load, and the manufacturer's supplied lug curve. Engine speed is available directly from the ECU broadcast. Engine load and speed data are available at least on a 10 Hz rate.

The Caterpillar D11RCD bulldozer used for this study did not broadcast ECU data that could be interpreted with a standardized (public) protocol adaptor as used with the MEMS. Therefore Caterpillar provided a representative and interface to collect the ECU data. The engine speed signal was divided at the magnetic pickup and monitored by the WVU acquisition system as well as the Caterpillar system in order to provide a common means of data alignment. Caterpillar provided engine speed and load information (estimated from fueling information) so that engine work could be integrated to provide brake-specific emissions results.

2.5.3 MEMS Emissions Analyzers Component

The WVU MEMS employs an NDIR solid-state detection device for the inference of CO_2, (as well as CO and HC), whereas a ZrO_2 sensor is used for NO_x determination. An electrochemical cell is employed as a quality control/quality assurance (QC/QA) measure, due to the limited in-field performance data associated with the ZrO_2 sensor that serves as the primary NO_x measurement device. It should be noted that although the NDIR system is capable of measuring HC and CO, its resolution is substandard for diesel applications. Particulate matter emissions were measured with a quartz crystal microbalance sampling dilute exhaust provided by a sampling conditioning system.

2.5.4 MEMS Emissions Sample Conditioning System

The MEMS sampling system addresses three key design parameters: removal of particulate matter, sample temperature control, and minimization of water interference. Water interference may be minimized by preventing condensation or by removing the water vapor present in the sample stream. In order to prevent sample stream condensation, heated sampling lines were incorporated into the MEMS. In addition, a

thermoelectric chiller was placed immediately before the emissions measurement devices in order to remove water from the sample stream and lower the sample temperature to analyzer manufacturer's specifications.

A schematic of the sampling system for MEMS is shown in Figure 16. The generalized system consists of a sampling probe, a heated line, a heated filter, a heated-head pump, an external NO_2 converter, and a thermoelectric chiller. The MEMS sampling probe is designed in accordance with the Code of Federal Regulations (CFR) 40 Part 89.412.96. Specifically, a 0.25-inch diameter stainless steel tube with nine sampling holes was used, as shown in Figure 17. The multiple sampling ports on the probe provide a means of averaging the exhaust flow composition, which helps to reduce the dependency of the sampling accuracy on the specific flow rate regime. A differential pressure regulator, used in conjunction with a flow meter, provide for stable flow rate control. System components were sized according to the specific requirements of the emissions analyzers that are employed.

MEMS Sample Flow Schematic
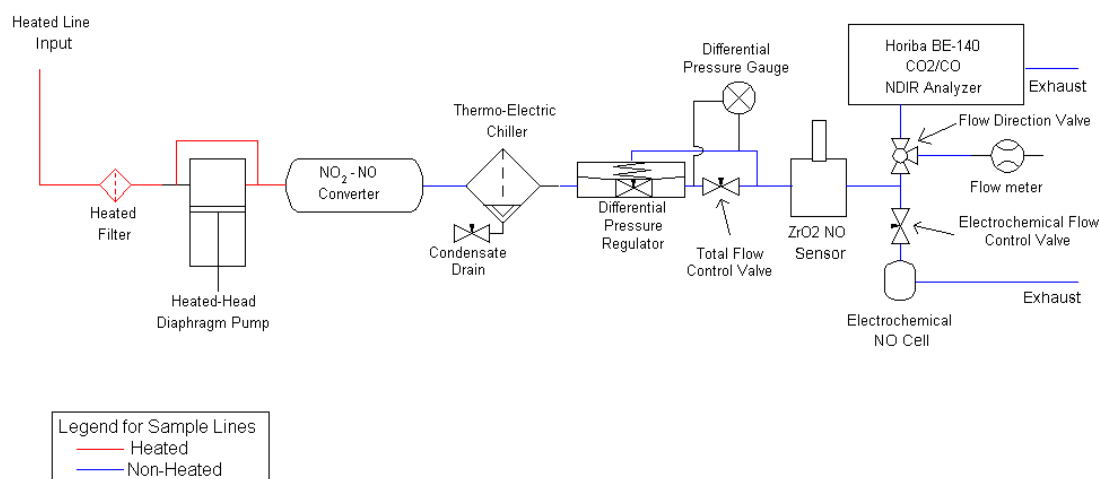
Figure 16 MEMS exhaust sampling system.
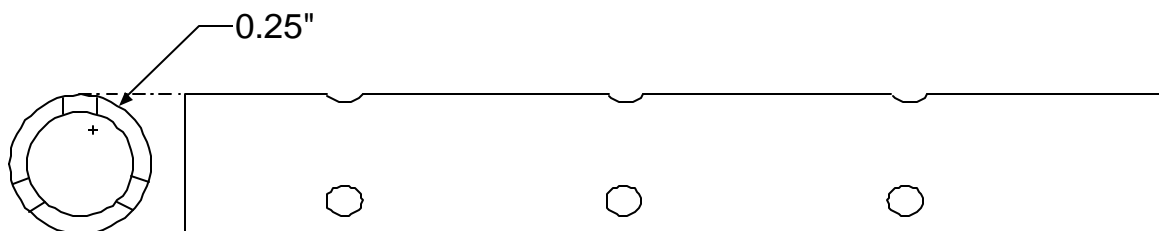
Figure 17 MEMS sample probe.

2.5.5 MEMS Data Acquisition, Reduction, and Archival System

WVU selected a National Instruments PXI-1025 as the computer platform for MEMS, due to its inherent ruggedness and expandability. The configuration consists of a National Instruments multifunction 6071E data acquisition card that interfaced to a signal conditioning box, a National Instruments Temperature/Voltage 4351 card, and a RS-232 serial card. The platform also employs a National Instruments PXI-8156B embedded computer, which allows access to two serial ports, a USB port, a GPIB interface, as well as hard, floppy, and CD drives. The portable platform utilizes a built-in monitor and keyboard, which is attached to the chassis, and required minimal setup effort.

2.5.6 MARI Real-Time Particulate Mass Monitor (RPM 100)

Total particulate matter emissions measurements that were recorded during the testing of the Caterpillar D-11R CD track-type tractor were made using the Mid-Atlantic Research Institute LLC. (MARI) Real-time Particulate Mass Monitor RPM100 (see Figure 18 and Figure 19). This prototype is essentially a quartz crystal microbalance (QCM) that has been integrated with a sample conditioning system. RPM100 has undergone evaluations under the US EPA Heavy-duty Engine FTP schedules. In addition, the units have been used extensively for on-road, on-board vehicle applications, chase studies, and cabin air quality studies. In order to provide a more thorough presentation of this system, the following descriptions regarding the theory of operation of the unit has been included.

Figure 18 MARI Real-Time Particulate Mass Monitor (RPM 100) – Adapted for On-board, Off-road Testing

2.5.6.1 Quartz-Crystal Microbalance

Quartz crystal microbalances were popular in the 1970's and 1980's, but, since these sensors were easily overloaded, the TEOM® and beta gauges became dominant for continuous ambient PM_{10} dust monitoring. More recently, the TEOM® for automotive

near-real-time particulate measurement has been introduced to provide particulate mass measurements. However, the current emphasis on vehicle emission particles in the environment (emitted from gasoline and diesel vehicles) has created a niche for a system, such as the QCM that can measure these often ultra-low mass concentrations. The greater sensitivity (100-1000 times more sensitive to mass than other harmonic oscillator-based microbalances), simplicity, and inherent design attributes (no vibration or temperature problems) of the QCM makes it better suited than other harmonic oscillators for measuring low particle concentration levels. Quartz crystal microbalances of the past suffered from diffusion losses, long residence times, and inability to hold particles to the collection surface. Since the 1980's, major technological advancements have been made in area of collection and measurement of very low masses of PM.

Preliminary data from heavy-duty engine dynamometer studies clearly show the benefits of the technique with respect to robustness, sensitivity for real-time measurements, and equivalency to regulatory filter mass measurements, when compared to other commercially available microbalances. Tests conducted with the MARI RPM 100 on a heavy-duty engine dynamometer have shown the PM mass emissions data to be within 10% of the CVS-based gravimetric method [5].

Figure 19 View of Internal Components of the MARI Real-Time Particulate Mass Monitor (RPM 100)

The MARI RPM 100 employs a piezoelectric crystal that is used as a sensitive microbalance. A point-to-plane electrostatic precipitator provides a very efficient collection of aerosol particles on the surface of the piezoelectric crystal. The electrostatic force has been demonstrated as an effective means for collecting aerosol samples, especially in the sub micrometer particle size range. The crystal is excited to its natural frequency, which decreases with increasing mass load on its surface. Thus, the particulate mass collected on the crystal can be determined by measuring the change in the crystal's natural frequency. A piezoelectric quartz crystal is externally driven by an electronic

oscillator attached to two metal plates (usually deposited by vacuum evaporation) placed on both sides of the quartz blank.

The RPM 100 is insensitive to pressure fluctuations in the pulsating flow of an internal combustion engine. The resonant frequency of the QCM used is normally 5MHz but can be varied depending on the application. Also, the MARI RPM 100 is insensitive to workplace vibrations typically encountered in on-board vehicle applications. While some microbalances may have to rely either on mass to dampen the oscillations, or software fixes based on signals from accelerometers mounted on the unit, both these solutions to vibrations problems are considered unacceptable for continuous PM mass measurement applications.

2.5.6.2   Sampling Conditioning System

Sampling from vehicle emissions (both raw exhaust and from dilution tunnels) requires the careful consideration of both the influences of sampling on the characteristics of the sampled exhaust (i.e. changes to the particulate size and composition) and to the needs of the particulate measurement instrumentation.

Sampling uncertainties arise from many artifacts, including:

- Source to receptor changes to the physical and chemical nature of the aerosol

- Sampling effects

- Temporal behavior

- Volatility, humidity and temperature effects

- Changes to the aerosol components

- Field-use robustness

For example, it has been well documented that changes in dilution ratio, in the presence of volatile material in the exhaust, can affect the size distribution and concentration of the sampled aerosol. To overcome this potential sampling artifact, various research projects have employed thermal denuders to remove volatiles. Similarly, current particulate matter emissions measurement instrumentation has uncertainties arising from poor presentation of the sample to the analyzer, which include:

- Pressure fluctuations at the inlet (caused by pressure changes in the raw exhaust or dilution tunnel)

- Sample concentration outside "best" performance range of the analyzer

- Temperature and humidity effects

With reference to Figure 20, the overall system is controlled by the Sampling Conditioning System (4) and includes 12V DC pump(s) (7, 12), an optional thermal denuder (13), a filter (6), automated minor and major flow controllers (8, 9) and control options/valves (3, 14, 15, 16, 17) for the selection of the "most-appropriate" sampling configuration. The configuration of the system has been designed to minimize particle losses, provide great flexibility for measurement, avoid pressure fluctuations at the

instrument inlets and improve measurement repeatability and reproducibility by having a "fixed" and "well-defined" sampling geometry.

Key features of the system include:

- A computer controlled SCS (diluter) that can dilute the aerosol to a pre-programmed levels or proportionally (range 3:1 – 3000:1 - comprising selectable ranges using laminar flow capillaries).

- Sample dilution accuracy of better than 5%

- Atmospheric pressure sampling conditions for the particulate instrumentation

- Adaptive provisions for accommodating filters for mass-based regulatory measurements

- Minimized particle losses and bias to the size distribution.

- A HEPA filter and Carbon Capsule Filter connected to the inlet (via a control value) to enable base-line measurements.

Figure 20 Schematic of the Sampling System

To manage the lifetime of the crystal (maximum loading typically less than 30 μg after which it needs to be cleaned), the RPM 100 uses a high-performance dilution system.   The integration of the unique diluter with the QCM (currently by utilizing a CAN network) offers a fully flexible automated system that can both manage the crystal lifetime and moreover potentially offer an automatic and traceable route for determining the volatility component of the exhaust particulates– a prerequisite for good equivalency performance.

The Sampling Conditioning System is based on the Brockmann et al. paper [6]. This paper describes a diluter that was designed for sampling high concentrations ($\sim 10^{10}$ cm^{-3}) of ultrafine aerosols. In its design particular care was taken to minimize the effects of coagulation and diffusional deposition within the diluter. Moreover, the diluter was also designed so that the effects of these processes on the size distribution of the sampled aerosol could be calculated and minimized.

A schematic diagram of the diluter within the Sampling Conditioning System is shown Figure 21. The gas sample is extracted through a needle and immediately mixed with the primary dilution flow. This diluted gas / aerosol then flows through a second transport tube to the throat of the Venturi where it mixes with the secondary dilution air. The Venturi is used to create the suction needed to draw the sample. This allows a sample to be extracted and the diluted sample to be delivered at atmospheric pressure.
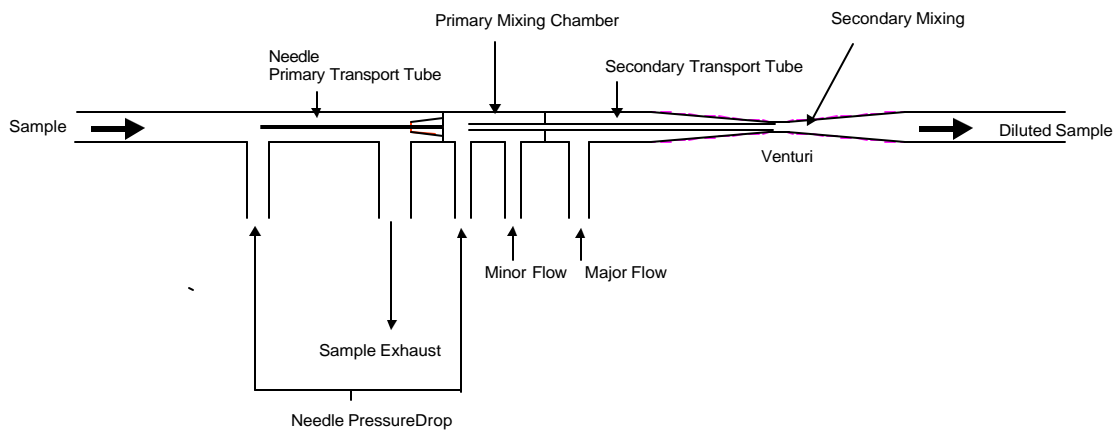
Figure 21 Schematic of the sample conditioning system

Using Bernoulli's equation, the pressure balance for the diluter can be expressed as:

$$P_s - (P_E - \tfrac{1}{2}pV_t^2) = \Delta P_1 + \Delta P_2$$

Equation 1.

Where,

P_s = static pressure at the sample point

P_E = static pressure at the exhaust point

ΔP_1 = pressure drop across the sample capillary (primary transport tube)

ΔP_2 = pressure drop across the transport capillary (secondary transport tube)

V_t = gas velocity (average) at Venturi throat

p = gas density (g/cm^3)

If the pressure at the sample and exhaust points are equal (assumptions that are often valid in practical situations), Equation (1) reduces to

$$\Delta P_1 + \Delta P_2 = 1/2pV_t^2$$

Equation 2.

The pressure drops in the sample (ΔP_1) and the transport (ΔP_2) capillaries are functions of volumetric flow rates, Q, through the capillaries. In fully developed laminar tube flow, pressure drop is linearly related to volumetric flow rate. However, if the flow develops from a flat velocity profile, as is the case in the sample and transport capillaries, the pressure drop has an additional contribution equal to $0.58pu^2$ [31]. Therefore, for flow through the capillary tubes, pressure drop ΔP and volumetric flow rate Q are related by

$$\Delta P = aQ^2 + bQ$$

Equation 3.

Where,

$$a = 8(1.16)p/(\pi^2 d^4)$$

Equation 4.

$$b = 128\mu l/(\pi d^4)$$

Equation 5.

$$p = \text{gas density}$$

$$d = \text{capillary diameter}$$

$$\mu = \text{gas absolute viscosity}$$

$$l = \text{capillary length}$$

The overall dilution ratio R is given by:

$$R = (Q_2/Q_1)(Q_3/Q_2)$$

Equation 6.

where the subscripts 1, 2, and 3 refer to the flow rates through the sample capillary tube, the transport capillary tube, and the Venturi, respectively.

The sample flow rate Q1 depends on P, which in turn depends on Q2, Q3, and the dimensions of the capillary tubes and Venturi. The relationship between Q1 and these parameters is determined by substituting Equation (3), for both capillary tubes, into Equation (2).

Brockmann et al. [6] found that the agreement between experiment and Schlichting's equation was excellent, and the experimentally determined diameter values fell within the manufacturing tolerance limits.

The experimental results were subsequently used to determine flow rates. Because the expression for pressure drop is applicable only so long as the capillary length exceeds the entrance. This is supplied by Schlichting [31]:

$$l_{10\%} = 0.29 \, Re_d$$

Equation 7.

where $l_{10\%}$ is the length required for the flow centerline velocity to approach to within 10% of fully developed centerline velocity, and Re is the Reynolds number.

The equations presented above provide the basis for the design of this diluter, and indeed the design of any sample extraction device using Venturi suction and capillary flow metering.

2.6   In-Laboratory Data Acquisition Setup – EERL Components

All in-laboratory testing for this research was performed at the West Virginia University Engine and Emissions Research Laboratory located on the WVU campus in Morgantown, WV. The laboratory utilizes a full-scale CFV-CVS (critical flow venturi-constant volume sampler) system with all laboratory components and equipment constructed according to the specifications outlined in the CFR 40, Part 86, Subpart N. These components will be briefly discussed in this section. A schematic of the laboratory testing setup is shown in Figure 12.

2.6.1   Full-Flow Exhaust Dilution Tunnel

The primary goal of engine emissions testing is to determine the effects that exhaust constituents have on the environment. In order to simulate "real world" conditions and produce accurate data, it is necessary to simulate the dilution process that occurs when hot exhaust gases mix with ambient air. The effects of this exhaust gas dilution are threefold. The primary reason for dilution is to allow any in-use exhaust-air interactions to take place, but it also quenches post-cylinder combustion reactions and lowers the exhaust gas dew point, thus inhibiting condensation. Exhaust line quenching is necessary to prevent measurement inconsistencies. The elimination of water in the sampling stream is of utmost importance as certain gaseous components are soluble in water (such as nitrogen dioxide (NO_2)), which could adversely affect measurement accuracy. Water presence in sample lines can also affect certain instruments as well, such as NDIR analyzers, and particulate matter measurement accuracy could be reduced.

The dilution tunnel used for this research was a full-flow tunnel. In a full-flow tunnel, all of the exhaust gases emitted by the test engine are routed into the tunnel where they are mixed with the required amount of air to achieve the desired dilution ratio. Mini-dilution tunnels have also been developed that dilute only a small portion of the total exhaust stream for sampling. While these systems are decidedly more compact and portable, the CFR only recognizes full-flow dilution tunnels as certifiable means of exhaust sampling.

The full-flow system housed at the EERL is based upon the CFV-CVS principle where a large centrifugal blower draws the diluted exhaust gas mixture from the tunnel through critical flow venturis. The dilution tunnel is constructed of stainless steel to prevent oxidation contamination and degradation from occurring and is approximately 0.4572 m (18 in.) in diameter and 12.2 m (40 ft.) in length. The blower is driven by a 56.2 kW (75 Hp) electric motor. There are four venturis that can be selected singly or in any combination necessary to achieve the required dilution ratio. There are three 28.32 m^3/min (standard) (1000 scfm) well as an 11.32 m^3/min (400 scfm) venturi that allow

total tunnel flow rates ranging from 11.32-68 m³/min (400-2400 scfm). The exhaust gases enter the tunnel at its centerline and pass through a mixing orifice plate located three feet downstream. The orifice plate is 8 inches in diameter and creates turbulence in the flow path that promotes thorough mixing. Dilute gaseous samples are collected at a distance of 4.6 m (15 ft.) downstream of the plate with heated sampling probes. These probes transfer the sample to the analyzers via electrically heated Teflon lines. The particulate sampling system utilizes a 0.10 m (4 in.) stainless steel secondary dilution tunnel located at the end of the sampling region to provide additional dilution air. Air can be injected into the secondary tunnel to increase the dilution ratio, which lowers the sample temperature to less than 51.7° C (125° F). The purpose of this is to keep the face of the particulate sampling filter at a sufficiently low temperature as to prevent any damage to it. After exiting the analyzers and particulate sampling system, the exhaust gases are collected and vented away.

2.6.2   Critical Flow Venturi

A CVS system is used to regulate the flow of diluted exhaust gases passing through the dilution tunnel for compliance with the CFR 40. When the critical flow venturi reaches sonic conditions (choked flow), a constant mass flow rate is maintained in the dilution tunnel. When the choked condition is attained, the flow rate of the gas through the venturi is a function of the diameter of the throat and the pressure and temperature of the gas upstream. Pressure data was collected with a Viatran model 1042 AC3AAA20 pressure transducer while the temperature was recorded with a resistive temperature device, or RTD. With these two parameters quantified, the mass flow rate can be determined with the following equation:

$$Q = (K_nP)/\sqrt{T}$$

Equation 8.

Where,

Q   =   the flow rate in scfm at standard conditions (20° C and 101.3 Kpa)

K$_n$ =   the calibration coefficient of the venturi

P   =   the absolute pressure at the inlet of the venturi in Kpa

T   =   the absolute temperature at the inlet of the venturi in °K

The venturis were calibrated with a subsonic venturi traceable to the standards set forth by the National Institute of Standards and Technology (NIST).

2.6.3   Particulate Sampling System

Total particulate matter sampling and the subsequent gravimetric analysis was conducted to determine the mass emission rates of particulate matter. Total particulate matter is defined as the material collected on a specified filter medium after diluting

exhaust gases at a temperature of less than or equal to 51.7ºC (125ºF). Diesel PM is primarily carbon, condensed hydrocarbons, sulfates, wear metal and associated water.

The particulate sampling system housed at the EERL incorporates a secondary dilution tunnel to provide a double dilution, proportional-sampling method for particulate matter collection and analysis. This system draws a diluted exhaust sample from the sampling region of the primary full-flow dilution tunnel into a secondary dilution tunnel. The flow rate through the secondary dilution tunnel is varied, via mass flow controllers, throughout the emissions test in order to draw a proportional sample from both dilution tunnels. Further dilution in the second tunnel can be varied with the amount of air necessary to reduce the face temperature of the sample filter to less than 51.7ºC (125ºF). The sample filter collects the PM matter from the diluted exhaust to enable the determination of the amount of PM emitted by the engine during a test cycle with a gravimetric analysis. The PM sampling system was designed to reduce thermophoretic losses of particulate matter. The PM collected consists primarily of elemental carbon as well as sulfates, the soluble organic fractions (SOF), and bound water.

In detail, the PM sampling system draws the diluted sample through a 1.3 cm in. (0.5) diameter transfer tube, 17.8 cm (7 in.) in length that links the secondary dilution tunnel to the sampling region of the primary dilution tunnel. The secondary dilution tunnel is constructed exclusively of stainless steel and is 7.62 cm (3 in.) in diameter and approximately 76.2 cm (30 in.) long. The secondary tunnel was designed in order to provide a sufficient residence time to allow the exhaust to thoroughly mix with dilution air to cool it to less than the desired 51.7ºC (125ºF). The sample flow exits the secondary tunnel and passes through a stainless steel filter holder that contains two Pallflex 70mm Model T60A20 flourocarbon-coated glass microfiber filters used for PM collection. Two filters, a primary and a secondary, are used in the filter holder to extract the maximum amount of PM from the sample stream for analysis. The total secondary dilution flow is maintained by two Gast Model 1023-101Q-583X rotary vane pumps each governed by a single Sierra 740-L-1 mass flow controller. A secondary check of PM sample flow is provided by corrected data from a roots-style positive displacement flow meter. The total diluted flow possible is 0-0.17 m^3/min (0-6 scfm) with the maximum amount of air injected variable between 0 and 0.08 m^3/min (0 and 3 scfm). The Sierra mass flow controllers are routinely recalibrated by the manufacturer and additionally checked with a Merriam Instruments Model No. 50MW20 laminar flow element (LFE) rated at 0-0.65 m^3/min (0-23 scfm).

The filters are conditioned before and after sampling in a controlled environmental chamber maintained at 50% RH and 70°F. The blank and loaded filters are weighed in a calibrated Cahn C-32 microbalance that has an accuracy of 1μg. The balance is recalibrated periodically during filter weighing to ensure measurement consistency.

2.6.4   Particulate Sizing Equipment

Promulgation of fine-particle standards warrants a re-evaluation of the currently established protocols for measurement of particulate matter from combustion sources in general, and diesel engines in particular. In light of such activity, the particle size distributions and concentrations of the exhaust emitted from the test engines were

measured using a TSI Scanning Mobility Particle Sizer (SMPS) unit in conjunction with a TSI 3025 condensation particle counter (CPC), and gravimetric size information was provided using PM_{10} and $PM_{2.5}$ cyclones. A limited number of cyclone samples were drawn directly from the laboratory's full-flow dilution tunnel, whereas the SMPS-CPC samples were conditioned in a mini-dilution tunnel in order to avoid the effects of low dilution ratio on particle size distributions and concentrations.

The mini-dilution tunnel that was utilized for this testing was specifically designed to provide enhanced control of dilution ratio in order to provide realistic profiles of particle size distributions.   WVU's past research supports that of other researchers who have indicated that particle size distributions and concentrations are greatly impacted by the dilution ratio used in the sampling stream.   At primary dilution ratios above 1:20 (approximately) the dilution ratio effects are not as significant, but it is well known that depending upon the engine size, the dilution ratios encountered in full-flow dilution tunnels can be very low. For this reason, a nominal dilution ratio set-point of 1:30 was used for this study.   The system employed for this study conditioned only a slip-stream of raw exhaust, and provided precise measurement and control of the air flow rate and subsequent dilution ratios. Two Sierra Model 760 mass flow controllers were employed to maintain the desired diluted sample and dilution air flow rates, but the determination of dilution ratio was accomplished by measuring both the raw and dilute exhaust CO_2 concentration. This approach reduces the inherent inaccuracies that plague mass flow controller-based systems in that the raw quantity contribution is directly measured rather than inferred as a difference of two large numbers. The raw exhaust sample was drawn within two meters of the engine exhaust manifold and diluted with HEPA-filtered air, but as a precautionary measure, background samples were also collected to account for system history contributions to measured particulate matter. The sampling trains were leak checked and particulate matter stratification and deposition in the sampling lines was minimized by proper design and choice of sample line material.

In order to provide a more thorough presentation of the experimental set-up used for the determination of particle size distributions and concentrations, the following description regarding the theory of operation of the test equipment employed for this study has been included.

2.6.4.1   Scanning Mobility Particle Sizer (SMPS)

The SMPS uses the electrical mobility technique that is based on the electrical mobility of aerosol to achieve the size distribution data. During operation the sample aerosol first passes through a single stage inertial impactor, which removes any large particles above 1.0 μm aerodynamic diameter, since they may carry more electrostatic charge than the data reduction procedure will permit, resulting in the propagation of large errors throughout the measured size distribution. The aerosol is then charged in a Kr-85 bipolar charge equilibrator. The aerosol is charged according to the Boltzmann distribution with most of the charged particles being charged with either one positive or one negative electronic charge. It should be noted that, although most of the particles remain uncharged, the adherence to the Boltzmann equilibrium allows the software to calculate the total particulate flux in each size range. As the overall aerosol remains uncharged, the charged particles are formed as "correlated pairs", one positive and one negative. The particles then pass through an electrostatic classifier where they are

separated according to their electrical mobility. An electrical field inside the classifier, generated by a cylindrical rod at potentials of 0 to 11,000 volts, influences the trajectory of the charged particles. Negatively charged particles are repelled into the chamber wall while the positively charged particles are attracted to the central electrode. A narrow electrical mobility range of the positive ions passes through an open slit and exits the classifier as a monodisperse aerosol. Therefore, the size of the monodisperse aerosol exiting the classifier is selected by adjusting the mobility analyzer voltage and air flow rates. The aerosol then enters a condensation particle counter (CPC) where each individual particle is counted. The SMPS enables a full scan of the size distribution in less than 30 seconds. The SMPS collects the size data in 147 channels with 64 channels per width. The particle size range is 0.005 μm to 1.0 μm.

The size-selective measurements with the SMPS were conducted on both steady state and transient conditions. This provides size distribution and concentration data during targeted engine operating set-points. For steady-state tests, a complete scan of the size distributions was performed, whereas a single particle size was monitored for transient test cycles. By setting the SMPS for a single particle size range and running several transient cycles, the emissions profile of that particle size could be obtained for the entire cycle. Transient data could be collected for several sizes during the test cycle and a size distribution could be established for the transient cycle operation.

2.6.4.2   PM$_{2.5}$ and PM$_{10}$ Cyclones

Cyclones operate by using particle inertia to segregate a sample according to a pre-determined cut-size that is governed by cyclone geometry and sample flow rate. The tangential entry of an aerosol near the top of a typical reverse flow cyclone sampler creates a double vortex pattern within the cyclone body. The gas-solid flow swirls down the outer free vortex and then reverses and spirals up through the inner forced vortex to the exit. Particles with sufficient inertia are unable to follow the air streamlines and impact onto the cyclone walls. The particles are either retained on the cyclone walls or migrate to the bottom of the cyclone cone. Cyclones have several advantages in air sampling, including their relatively low cost of construction and ease of operation. They have no moving parts and are easily maintained. Unlike impactors, they are not subject to errors due to particle bounce or re-entrainment and do not require special collection surface coatings. The 2.5 μm cut-point cyclones have been widely used for size-fractionated sampling. It should be noted that isokinetic sampling is not an issue for diesel particulate matter, due to its very small relative size. The sampling nozzles will be designed to minimize turbulence effects at the nozzle entry. Past experience has shown that aerosol sampling with cyclones could lead to a non-uniform deposition of particles on the filters. However, the problem can be rectified by installing straight length of pipe between the cyclone outlet and the filter holder. This provides sufficient distance for flow development of both the gas- and solid-phases. Background samples were collected in addition to dilute exhaust samples from dilution tunnel in order to account for system history contributions to measured particulate matter.

For this study diluted diesel exhaust PM$_{2.5}$ and PM$_{10}$ samples were drawn from the total exhaust dilution tunnels in the engine test cells using a University Research Glassware (URG) Model 2000-30-EH cyclone with a 50 % cutpoint (d$_{50}$) of 2.5 μm at a

nominal flow rate of 16.7 lpm ($PM_{2.5}$) and a URG Model 2000-20EAM cyclone with a cutpoint of 10 μm at 15 lpm. The mass fractions were determined by drawing the samples through the appropriate cyclone and collecting them on 47-mm Teflon filters and then measuring the net mass addition of particulate matter.

2.6.5 Gaseous Emission Sampling System

The EERL's gaseous sampling system consists of heated probes located in the dilution tunnel and heated sampling lines connecting the probes with the gas analyzer bench. A picture of the gas analyzer bench can be seen in Figure 22. There are three heated sampling probes located ten tunnel diameters (approximately 4.57 m, or 180 in.) downstream of the origin of the mixing zone to ensure complete turbulent mixing of the exhaust gases with the dilution air. The tips of the probes project six inches into the tunnel and are oriented so the opening is directed upstream toward the entrance of the tunnel. The connection between the sampling probes and the analyzer bench is made with electrically heated sampling lines. The HC sampling line was maintained at a temperature of 190.5ºC ± 5ºC (375ºF ± 10ºF) using Fuji model No. 223-1806 temperature controller. This prevented the high molecular weight hydrocarbons from condensing in the sample line. The sample lines and probes for the NO_x and CO/CO_2 sampling systems were maintained at 112.8ºC ± 5ºC (235ºF ± 10ºF) to prevent the condensation of water in the line which could induce measurement error as well as cause damage to the analyzers.

The gas analysis bench houses four major analyzer components: HC analyzer, CO analyzer, CO_2 analyzer, and NO_x analyzer. The analyzers are all produced by the Rosemount Company and will be described in greater detail in the following sections. The bench also houses the sample flow meters, the temperature controllers for the heated sampling components mentioned previously, and a NO_x efficiency tester. The efficiency tester is made by the Beckman Co. and ensures that the NO_x analyzer is operating above 90% converter efficiencies, as is mandated by the CFR 40, Part 86, Subpart N.

Figure 22 The EERL's Gaseous Emissions Analyzer Bench.

2.6.6 Exhaust Gas Analyzers

A brief description of each analyzer and its components as well as theory of operation will be given in this section. A more in depth look into operational theory can be found in the Rosemount analyzer operation manuals.

2.6.6.1 Oxides of Nitrogen Analyzer

The NO/NO_x analyzer used for testing was a Rosemount Model 955 Chemiluminescent analyzer. The analyzer is capable of detecting the concentration of NO or NO and NO_2 together, which is commonly referred to as NO_x. When measurement of NO is desired, the sample NO is converted into NO_2 by gas-phase oxidation with molecular ozone (O_3). During this reaction, about 10% of the NO_2 becomes electrically excited, followed by an immediate return to the non-excited state. This phenomenon is known as photon emission. A photomultiplier tube is used to detect the photon emission quantity, which is proportional to the amount of NO present in the sample. For the detection of NO_x, the sample is first passed through a NO_x converter that converts the NO_2 into NO, which is then measured with the principle described previously. If the determination of NO concentration only is desired, the sample can bypass the converter and be measured directly by selecting the NO mode of the analyzer. In the case of NO_x detection, the total analyzer response would determine the amount of NO present in the original sample, as well as the NO created through the dissociation of NO_2 in the converter. A NO_x efficiency tester is used to ensure that the converter in the Model 955 analyzer is operating optimally.

2.6.6.2 Hydrocarbon Analyzer

The hydrocarbon analyzer used was a Rosemount Model 402 Heated Flame Ionization Detector (HFID) analyzer. The counting of the elemental carbon atoms in the sample is used to determine the amount of hydrocarbon levels in the exhaust stream. The sample gas flow is regulated and flows through a hydrogen/helium-fueled flame that causes the production of ions. These ions are collected with polarized electrodes in the analyzer. This absorption of ions by the electrodes produces a current flow in the analyzer's measurement circuitry, which is quantified and related to the number of carbon atoms contained in the sample [29]. The measurement range of the HC analyzer is up to 250,000 ppm with a linear full-scale output. A multiplier switch located on the front of the Model 402 allows selection of measurement ranges with the best resolution for the particular gas concentration being sampled.

2.6.6.3 Carbon Monoxide/Carbon Dioxide Analyzers

The gaseous constituents of CO and CO_2 were determined with Rosemount Model 880 and Model 868 analyzers. Both of the analyzers utilize NDIR technology for gas measurement. An NDIR analyzer operates using the principle of infrared light absorption. In its simplest form, the NDIR analyzer uses the fact that a particular gas will absorb a certain wavelength of light somewhere within the infrared spectrum, with the other spectral wavelengths still being able to transmit through the gas. The analyzer detects the amount of infrared energy able to pass through the sample gas and uses it in the determination of the amount of the measured absorbent gas in the sample stream. An NDIR analyzer does not produce a linear output, so calibration curves were generated for

the analyzers before each testing session began. The range of the CO_2 analyzer is from 0-5% and from 0-20%. Two analyzers are available for the sampling of CO; a high range and a low range. The low range CO analyzer has a range of 0-1000 ppm and 0-5000 ppm while the high range analyzer has a range of 0-2% and 0-10%. For testing performed in this study, it was only necessary to use the low range CO analyzer.

2.6.7 Bag Sampling

In addition to being sampled by the analyzers during the test, a portion of the diluted exhaust is also collected in 80-liter Tedlar bags. The reason for doing this is to allow an additional gas analysis for each test before the bag is evacuated and a new test is initiated. There are two Tedlar bags used in the EERL's sampling system. One bag is used to collect a diluted exhaust gas sample and the other bag is used to collect a sample of the dilution air to account for any trace gas concentrations that might be contained in it. This allows for the background concentrations contained in the dilution air to be subtracted from the analyzer measurements to quantify actual exhaust stream concentrations. The primary reason for using the dilute sample bag is to allow comparison between it and the integrated sample for a quality control/quality assurance check for the testing performed.

2.6.8 Fuel Metering System

In order to create accurate exhaust dilution ratios, it is necessary to determine total tunnel flow rates and engine exhaust mass flow rates. The total tunnel flow rate, as described previously, is determined with the CFV-CVS system. The problem lies in the determination of raw exhaust mass flow rates. A number of factors inhibit a direct measurement of the exhaust flow rate, such as engine backpressure limits, high temperatures, and high particulate matter concentrations. An alternative approach to estimating exhaust mass flow rate is to use the intake airflow rate along with engine fuel consumption rate to calculate the exhaust flow.

The fuel flow rate is accurately metered and monitored with a Max Flow Media 710 Series Fuel Measurement System. The fuel supplied to the engine is first drawn from the storage tank through a filter and into a vapor elimination device that maintains a constant pressure of 206.8 kPa (30 psi) with the system's transfer pump. The fuel then encounters a bypass system where excess fuel is routed via a pressure regulator through a heat exchanger and back to the storage tank. The heat exchanger uses the bypass supply fuel to cool the engine return fuel. Fuel that is not returned to the tank enters a Model 214 piston-displacement flowmeter. From there the metered fuel supply enters a level-controlled tank. In this tank the metered fuel is mixed with the unused engine return fuel that has already passed through and been cooled by the internal heat exchanger. The volume of the tank is kept constant, so the fuel used by the engine is the amount of metered fuel recorded during a given test period. The fuel is drawn from the tank with a secondary fuel pump. The purpose of the second pump is to further increase the pressure of the fuel to levels needed by high-pressure diesel injection systems. A bubble detector eliminates any vapors in the system by controlling a solenoid valve that connects to-engine and from-engine fuel lines. The removal of any vapor bubbles in the system is necessary to prevent any engine performance problems or metering inaccuracies. After

exiting the solenoid valve, the fuel enters an external heat exchanger that maintains a constant fuel temperature with a Fuji Model 223-1806 temperature controller.

2.6.9   Intake Air flow Measurement

A Laminar Flow Element (LFE) manufactured by Meriam Instruments is used for quantification of intake airflow rates. The LFE is made up of a series of small capillary tubes oriented parallel to the direction of airflow. The purpose of the capillary matrix is to produce a laminar flow of air from the turbulent flow entering it. A pressure drop is created in the LFE from the friction of the air passing through the tiny capillaries. Meriam Instruments supplies a calibration equation and coefficients that are unique to each LFE unit. Meriam determines these coefficients with a flow meter that is traceable to NIST standards. The absolute temperature and pressure upstream of the capillary matrix and the pressure downstream of the matrix are the only parameters needed for intake volume flow determination. The equation used for this calculation is:

$$\overset{\bullet}{V}_{Actual} = \left[B \times (\Delta P) + C \times (\Delta P)^2 \right] \times \left(\frac{m_{std}}{m_{flow}} \right)$$

Equation 9.

Where,

$\overset{\bullet}{V}_{Actual}$ = volume flow rate of air through LFE

B = coefficient supplied by Meriam Instruments

C = coefficient supplied by Meriam Instruments

μ_{std} = standard kinematic viscosity

μ_{flow} = actual flow kinematic viscosity

ΔP = differential pressure across LFE

A correction factor is used to account for viscosity variations and is as follows:

$$CorrectionFactor = \left(\frac{529.67}{459.67 + T(^{o}F)} \right) \times \left(\frac{181.87}{m_g} \right)$$

Equation 10.

$$m\!e = \dfrac{14.58 + \left(\dfrac{459.67 + T(^{o}F)}{1.8}\right)^{1.5}}{110.4 + \left(\dfrac{459.67 + T(^{o}F)}{1.8}\right)}$$

Equation 11.

The LFE used for all in-laboratory testing was a Meriam Model 50MC2-4 LFE that had a 10.2 cm (4 in.) I. D. and was capable of flowing a maximum of 11.32 m^3/min (400 cfm). Differential pressure across the element was measured with a MKS 223 B differential pressure transducer, while absolute upstream pressure was determined with a Setra Model C280E pressure transducer. The temperature of the inlet air upstream of the LFE was recorded with a Resistive Temperature Device (RTD). The pressure transducers and the RTD were calibrated before the start of each test.

2.6.10 Instrumentation Control/Data Acquisition

All in-laboratory data obtained during the testing undertaken in this study was collected with software and hardware previously developed and installed in the EERL [27]. The software uses an RTI-815F data acquisition board for data collection as well as rack-mounted signal conditioning units (Analog Devices Model 3B). All data was recorded in ADC codes and later converted to the proper engineering units with a reduction program developed in-house at WVU.

2.7 Steady-State Operating Conditions

The three engines that were removed and tested in the laboratory on the dynamometer test-beds were operated at eight different modes for the steady-state portion of the laboratory testing. The engine speed and load factors of the 8-Mode test are shown in Table 4. The operating speeds and loads are obtained from the ISO/DIS 8178-4 Section 6.3.1.1 standards entitled "Test Cycles Type C – Off-Road Vehicles and Industrial Equipment," and resemble the set points outlined by CFR 30, Part 7. The weighted 8-mode data given in Chapter 4 of this document was reduced based on the associated weighting factors outlined in Table 3.

Table 3 ISO 8-Mode Cycle.

Mode Number	Engine Speed	Load Factor (Percent Load)	Weighting Factor
1	Rated	100	0.15
2	Rated	75	0.15
3	Rated	50	0.15
4	Rated	10	0.10
5	Intermediate	100	0.10
6	Intermediate	75	0.10
7	Intermediate	50	0.10
8	Idle	0	0.15

Figure 23 Schematic of West Virginia University's Engine and Emissions Research Laboratory Emissions Measurement System.

3 Experimental Results

3.1 Introduction

The objectives of this study were threefold: first, to log activity data for off-road diesel-powered equipment while they were operating in-field; second, to develop representative test cycles with in-field vehicle activity data; and, third, to use these cycles to exercise the engine in a dynamometer laboratory in order provide real-world emissions data from these vehicles. It should be noted that even though cycle development was not a stated objective of this study, this team of investigators had to develop dynamometer test cycles because none were available for laboratory emissions testing of off-road engines. The task first involved some preliminary evaluative testing with the portable Sensors multigas analyzer. The analyzer was then used onboard to collect desired in-field raw emissions data on a John Deere T444 rubber-tired front-end loader, an Elgin Pelican street sweeper, and a Komatsu PC400 LC3 Excavator as they carried out their operational duties. The collected data were used to develop representative transient testing cycles that could then be used in a laboratory setting to accurately recreate the real-world vehicle emissions scenario. Fully diluted emissions were measured while each vehicle's engine operated on the developed transient cycle on a dynamometer test bed at the EERL. Steady-state emissions data was also collected as each engine was operated according to the ISO 8178 steady-state cycle – the current certification test cycle.

In order to compare emissions data obtained with the Sensors multigas analyzer with laboratory emissions data, a plot of CO_2 data was created during each test. The time averaged emissions result was obtained with the following formula:

$$I = \frac{\sum_{i=1}^{N} x_i (t_i - t_{i-1})}{TotalTime}$$

Equation 12.

Where,

I	=	Integrated Result
N	=	Number of data points
x	=	Data point
t	=	Time

Any and all errors calculated and mentioned in this document were obtained with the formula for relative percent error given below:

$$\% \, \text{error} = \frac{\text{testvalue} - \text{refvalue}}{\text{refvalue}} \times 100$$

Equation 13.

The refvalue in the above equation is considered to be the "known" value, such as the laboratory data obtained during testing. The testvalue is the value that is being compared to the "known" value, such as the data taken with the Sensors portable analyzer.

The data presented herein will be instrumental in developing protocols pertaining to the testing of off-road equipment as well as providing a more accurate description of contributors to air inventories. It also illustrates the ability to estimate engine power for a particular engine family based on the amount of CO_2 emitted by the vehicle, which could be very useful for future cycle development work. The in-field testing data presented in this document also adds to the recent research activities focused on on-board vehicle emissions measurement.

3.2   Preliminary Analyzer Testing

In order to accurately measure in-field vehicle emissions, a thorough evaluation of the Sensors multigas analyzer was necessary. Three areas were investigated in the testing of the analyzer. The first testing performed consisted of steady-state testing of the measurement accuracy of the analyzer using various known gas concentrations. The steady-state testing was followed by transient testing of the analyzer performed with a step input of a known gas to evaluate the response time, as well as the settling time of the instrument. This data was later implemented, along with line length lag time to determine total system lag time, as an aid in the recreation of the transient testing cycle in the laboratory. The final analyzer testing performed consisted of comparative tests on the detection of raw exhaust concentrations between the Sensors AMB-II analyzer and the laboratory grade analyzers housed at the EERL.

One problem encountered while using the Sensors AMB-II analyzer was the fact that it did not record data at a constant time rate for successive runs. It recorded at a rate close to one data point every 0.6 seconds, or 1.667Hz. This rate would vary somewhat from test to test, however. The problem arose when comparisons of the 1Hz laboratory data and the slightly frequency-varying in-field data were made. In order to make point-to-point correlative comparisons for the cycle development portion of the research, the data had to be of the same frequency, so linear interpolation was used to convert the variable frequency Sensors AMB-II data to 1Hz.

To compound the sampling frequency problem, the Sensors AMB-II would often randomly change the sampling frequency during a test. This could be determined by performing a visual inspection of the time aligned engine speed data. This made it necessary during some tests to evaluate only the portion of the test run prior to the change in sampling frequency of the Sensors analyzer.

3.2.1   Steady-State Analyzer Testing

Preliminary testing of the measurement accuracy of the Sensors AMB-II analyzer was performed using gas bottles of known concentration. A broad measurement range was investigated by diluting the test gas with nitrogen using a Stec, Inc. Model SGD-710C capillary flow gas divider. This allowed the testing of the analyzer at different levels from 0% test gas concentration to 100% concentration in increments of 10%. The results of the steady-state testing can be seen in Table 4. The test gas used on the AMB-II was 19.9% CO_2. Gas divider viscosity effects were neglected. Results showed that the Sensors analyzer bench performed well with a range of error between 0% and 4.27%.

Table 4 Results of Steady-State Gas Bottle Tests on Sensors AMB-II (19.9% CO_2).

Gas Divider Position	Actual Gas Concentration (%)	Measured Gas Concentration (%)	Percent Error
100%	19.9	19.9	0.00
90%	17.91	18.1	1.06
80%	15.92	16.2	1.76
70%	13.93	14.2	1.94
60%	11.94	12.2	2.18
50%	9.95	10.3	3.52
40%	7.96	8.3	4.27
30%	5.97	6.2	3.85
20%	3.98	4.1	3.02
10%	1.99	2.0	0.50
0%	0.0	0.0	0.00

3.2.2   Transient Analyzer Testing

It was necessary to investigate the transient recording ability of the analyzer to determine if response times would be sufficient to capture the sharp transient events that would often be encountered during the in-field testing. A test apparatus was developed that allowed for computer-controlled switching of a solenoid valve that routed either the test gas or nitrogen to the analyzer. Over-pressurization of the unit was prevented by placing an atmospheric vent in the line upstream of the analyzer sample port. A series of timed pulses were used to switch between zero and span gas streams. The pulses were tested in groups of five with the first group being 10s in length, followed by a group of 8-second pulses, then 5-second, 4-second, 3-second, 2-second, and finally a group of 1-second pulses. It was found that the analyzer was able to respond fast enough to allow the attainment of 100% relative concentration readings on all but the 2-second and 1-second pulse groups. This was believed to be sufficiently fast to accurately record nearly all of the transient events that would be encountered during the in-field testing. A test was then performed to determine the T_{90} and T_{100} times (response times needed for the analyzer to reach 90% and 100% of span value) of the analyzer by routing 100% component gas to it and measuring the analyzer response as a function of time. It was

found that the analyzer had a T_{90} time of 0.75 seconds and a T_{100} time of 2 seconds. It should be noted that these times were estimated from the graphical data and are therefore approximations. In addition, the span gas used for the transient testing was 30% CO_2, which resulted in a dynamic range of nearly twice that which would be encountered during onboard, in-field testing of raw diesel exhaust CO_2 concentrations. The graphical data can be seen in Figure 24.
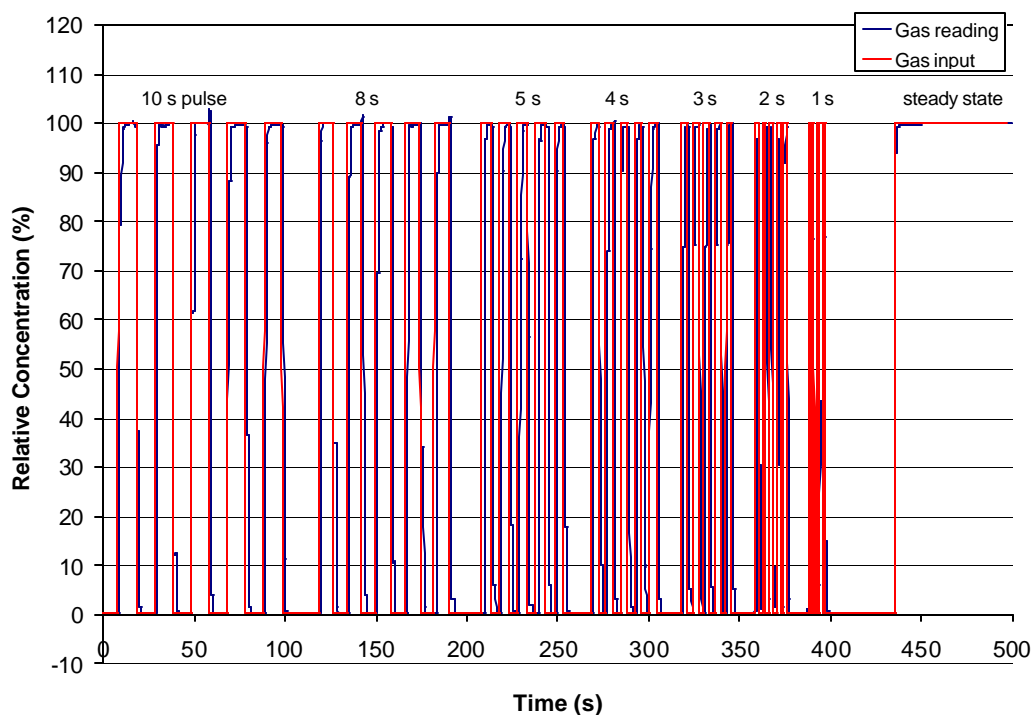
Figure 24 Sensors AMB-II Step Response on 30% CO₂

3.2.3 Analyzer Comparative Testing

In order to establish a performance benchmark, preliminary tests between the Sensors AMB-II analyzer and the EERL's laboratory-grade Rosemount 880 CO_2 analyzer were performed. A raw exhaust sample stream from a 10.8L Cummins ISM 370 ESP diesel engine, following the Federal Test Procedure (FTP) transient cycle, was conditioned and introduced to both the AMB-II and the Rosemount 880 in order to provide an equivalent comparison. Results indicated less than a 4% difference between the integrated measurements provided by the two analyzers throughout the cycle. The continuous concentration vs. time traces is included as Figure 25.
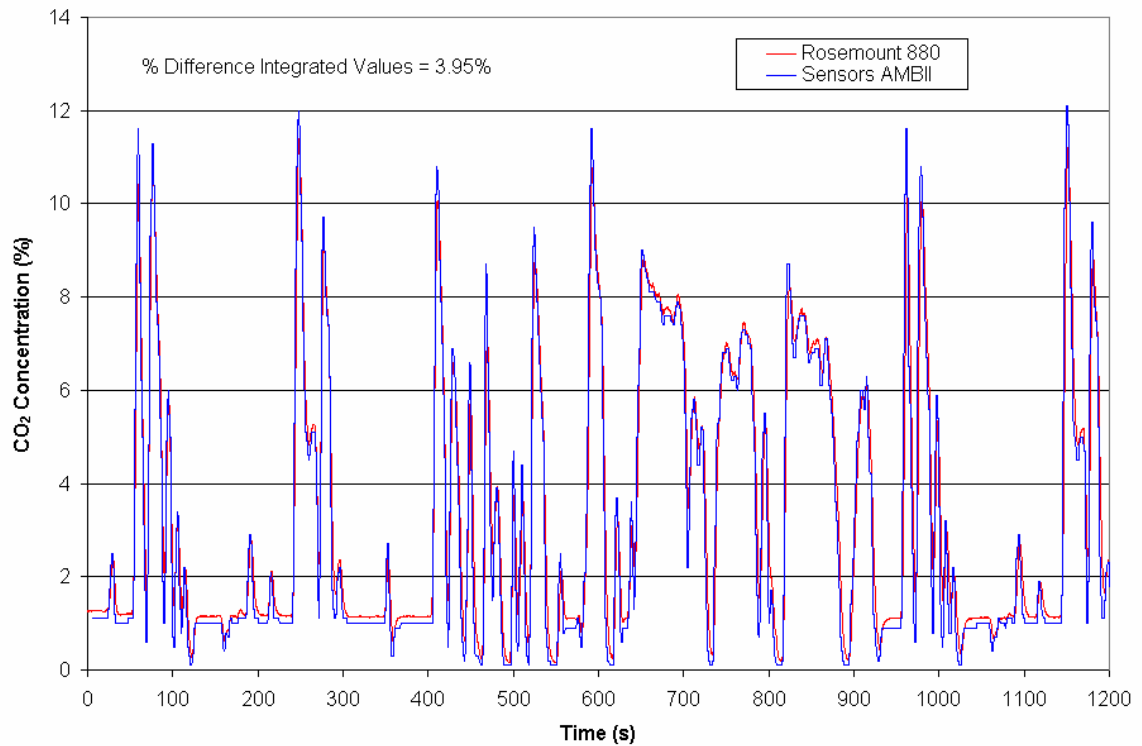
Figure 25 Rosemount 880 and Sensors AMB-II CO$_2$ Measurement Comparison (Cummins ISM 370; Torque Inference Prediction Testing).

3.2.4 Torque Inference Prediction Testing

In order to evaluate the feasibility of inferring torque based on CO$_2$ emissions, preliminary tests were performed to determine torque prediction accuracy. A Cummins ISM 370 was exercised over a series of steady-state operating conditions that spanned the engines operating range while continuous raw CO$_2$ emissions (in % volume) were recorded with the Sensors AMB-II analyzer. To eliminate effects of ambient CO$_2$ levels, the analyzer was zeroed on ambient air. A graphical representation of the steady-state testing cycle can be seen in Figure 26. The engine was then operated through a series of mapping exercises at motored, 0%, 25%, 50%, 75%, and 100% load conditions while raw exhaust CO$_2$ concentrations were again recorded using the Sensors analyzer. Graphical results of the mapping exercises can be seen in Figure 27 through Figure 32. This data was then used to develop correlation curves for the various engine speeds that were measured from the test cycle shown in Figure 26. Correlation curves for the five selected engine speeds can be seen in Figure 33 through Figure 37. These figures show that the relationship between CO$_2$ emissions and engine torque produced is very close to linear, as expected. Since the CO$_2$ mapping points were discretized at 100 rpm increments, and to further test the sensitivity to engine speed interpolation, the results for the 970 rpm and 1160 rpm were linearly interpolated from neighboring values. The resultant error between the inferred torques for the five randomly selected data points is shown in Figure 38
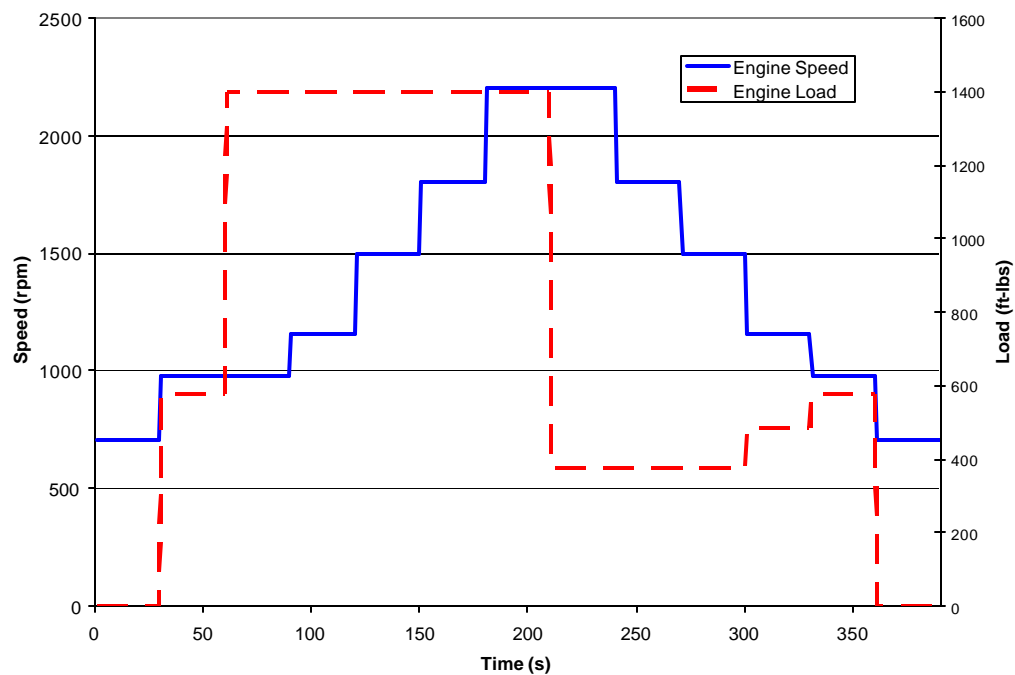
Figure 26 Cycle used for Cummins ISM 370 Torque Inference Prediction Testing.
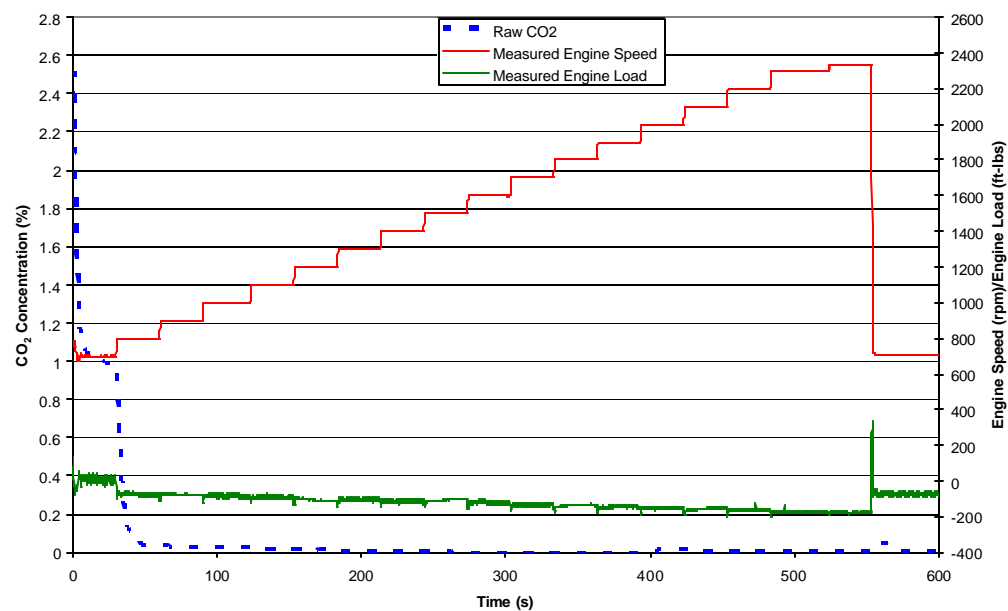
Figure 27 Engine Exhaust CO_2 Concentration Map for Motored Condition (Cummins ISM 370; Torque Inference Prediction Testing).
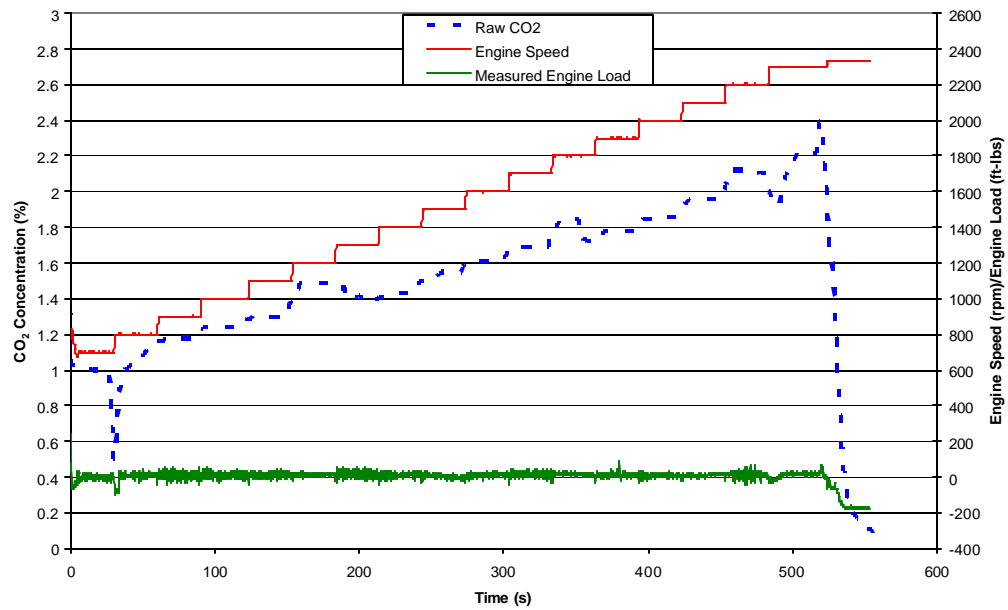
Figure 28 Engine Exhaust CO_2 Concentration Map for 0% Applied Load (Cummins ISM 370; Torque Inference Prediction Testing).
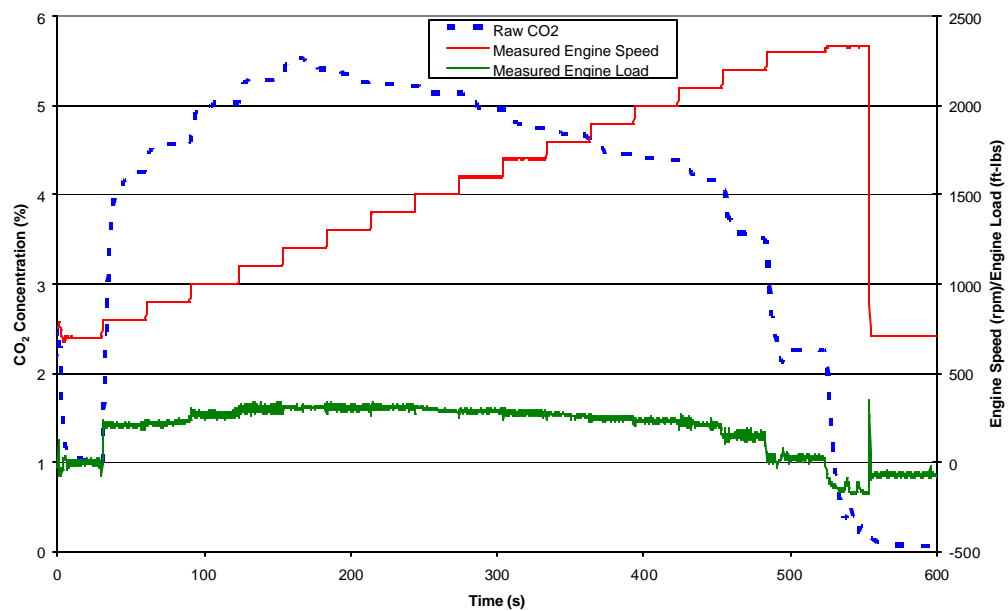
Figure 29 Engine Exhaust CO_2 Concentration Map for 25% Applied Load (Cummins ISM 370; Torque Inference Prediction Testing).
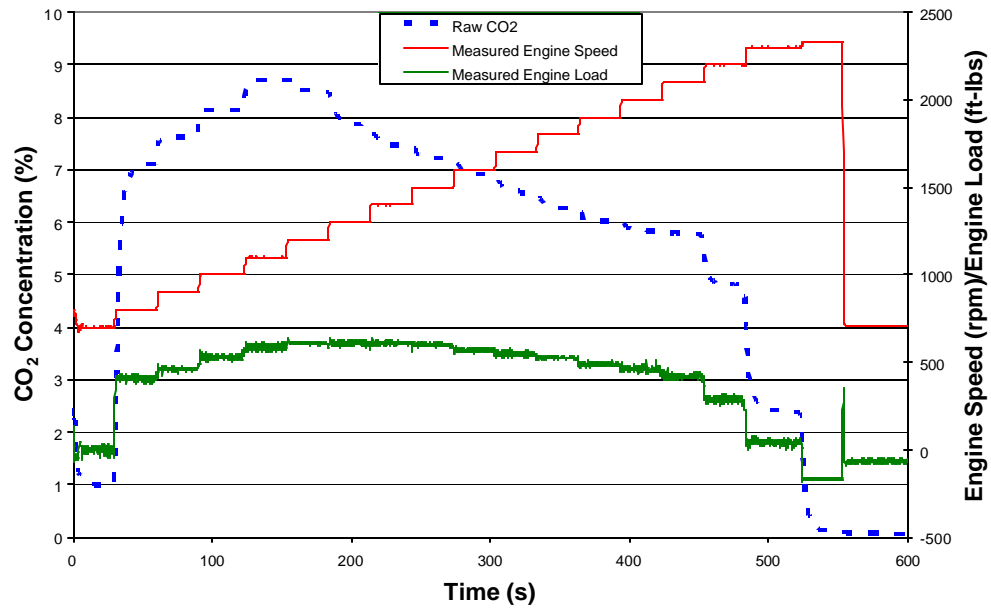
Figure 30 Engine Exhaust CO_2 Concentration Map for 50% Applied Load (Cummins ISM 370; Torque Inference Prediction Testing).
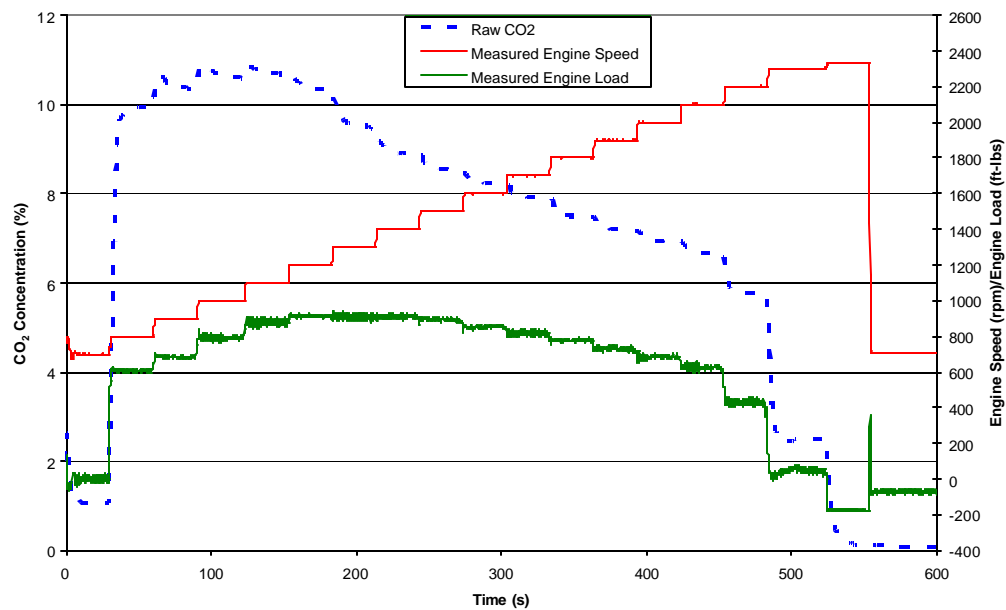
Figure 31 Engine Exhaust CO_2 Concentration Map for 75% Applied Load (Cummins ISM 370; Torque Inference Prediction Testing).
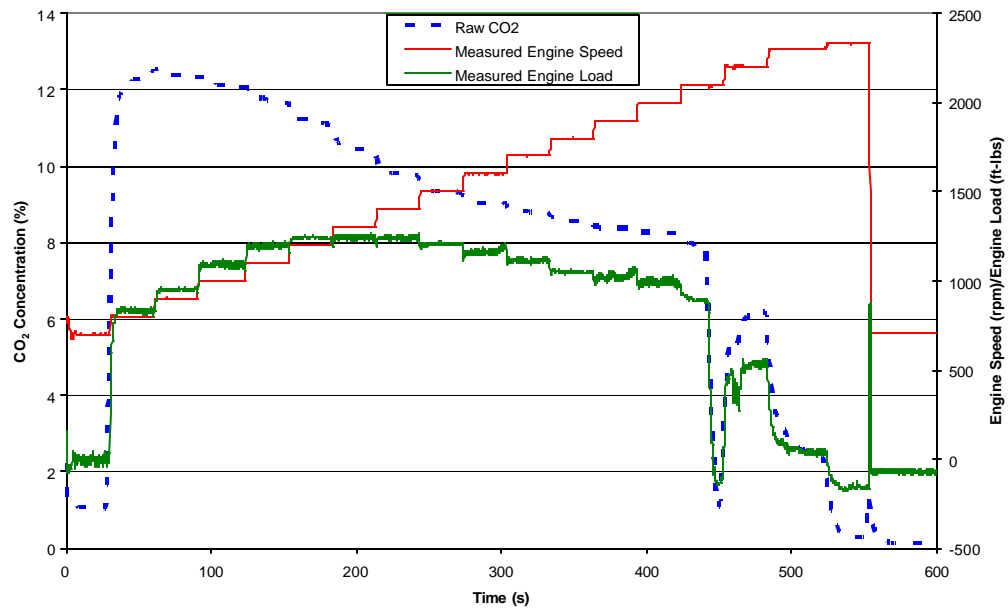
Figure 32 Engine Exhaust CO$_2$ Concentration Map for 100% Applied Load (Cummins ISM 370; Torque Inference Prediction Testing).
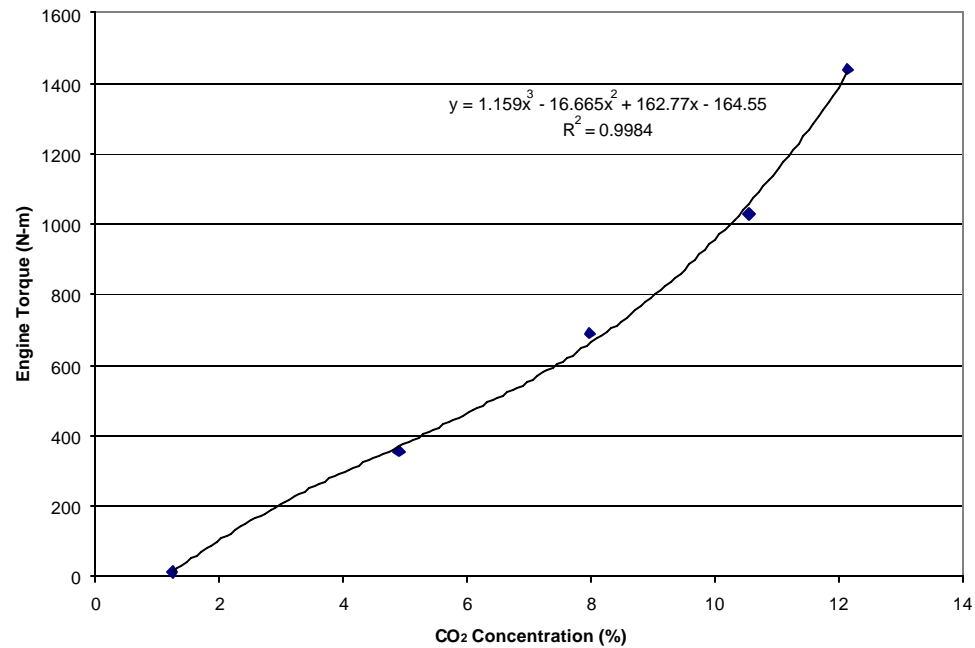
Figure 33 Interpolated CO$_2$ vs. Engine Load Correlation for 970 rpm (Cummins ISM 370; Torque Inference Prediction Testing).
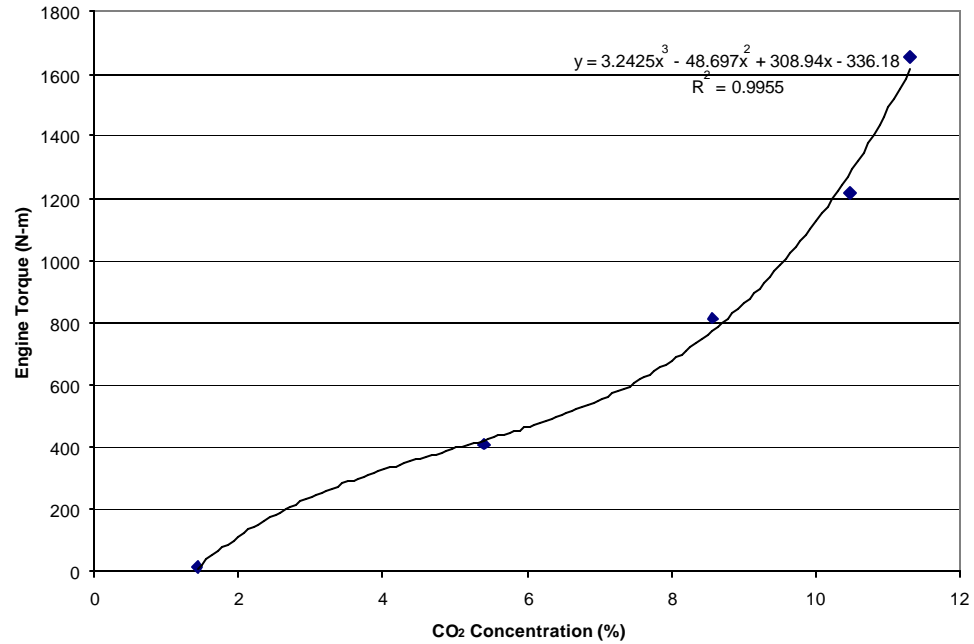
Figure 34 Interpolated CO_2 vs. Engine Load Correlation for 1160rpm (Cummins ISM 370; Torque Inference Prediction Testing).
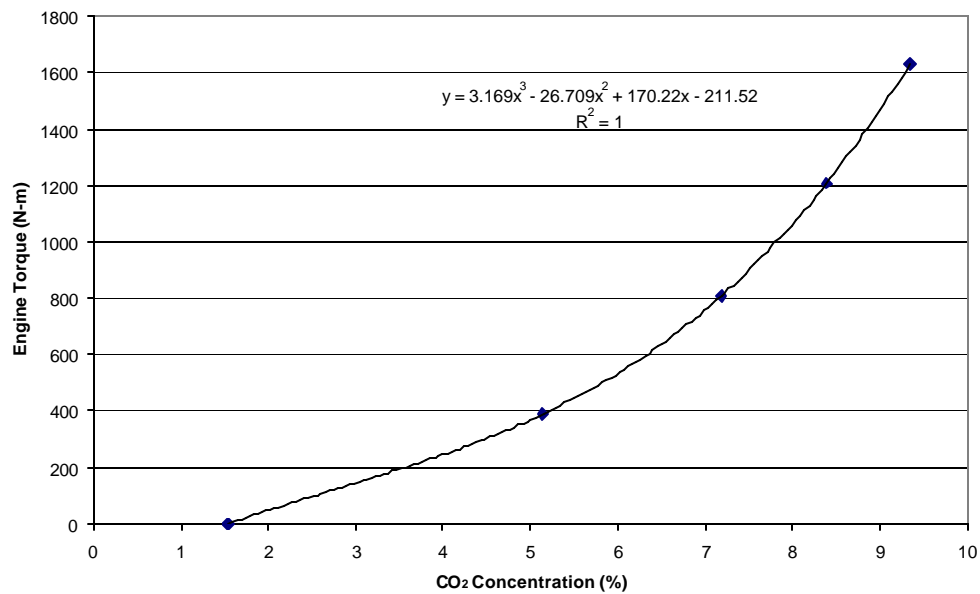
Figure 35 Interpolated CO_2 vs. Engine Load Correlation for 1500 rpm (Cummins ISM 370; Torque Inference Prediction Testing).

$$y = 0.0856x^3 + 22.056x^2 - 27.454x - 8.8133$$
$$R^2 = 1$$
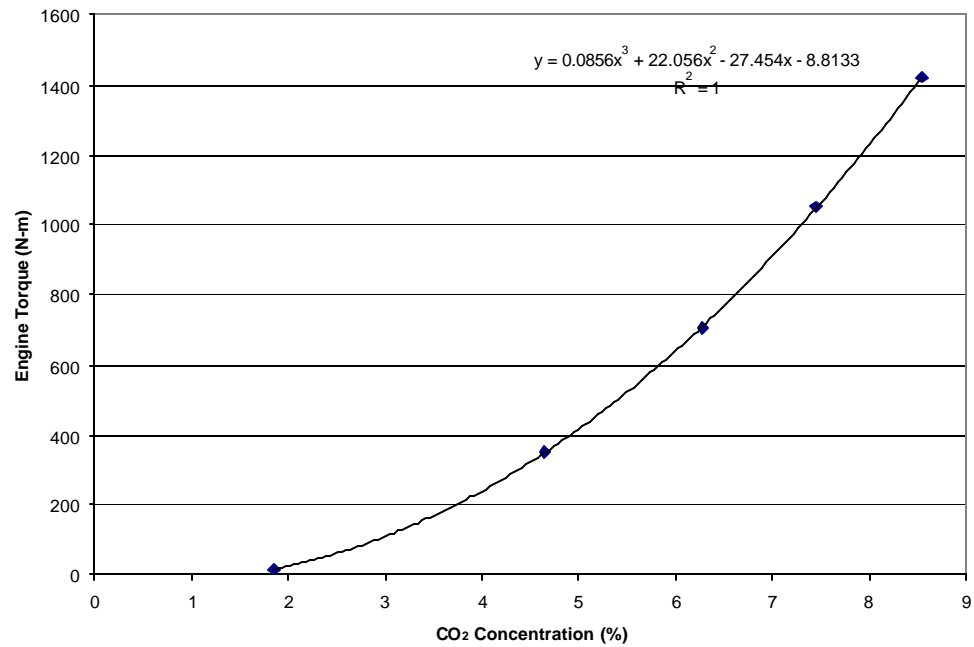
Figure 36 Interpolated CO_2 vs. Engine Load Correlation for 1800 rpm (Cummins ISM 370; Torque Inference Prediction Testing).

$$y = 18.503x^3 - 206.16x^2 + 848.1x - 1031.9$$
$$R^2 = 0.9969$$
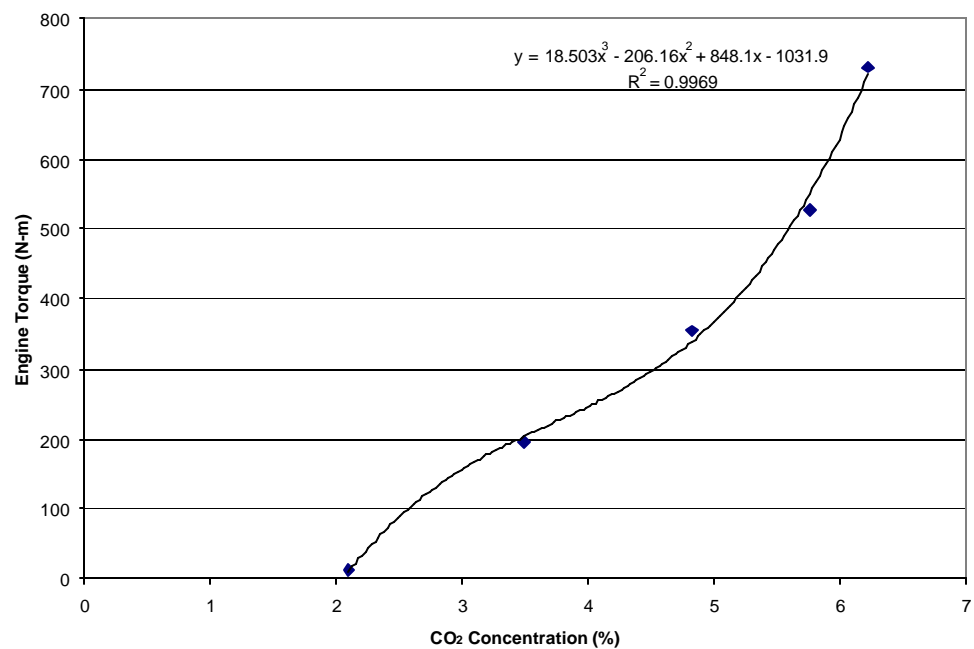
Figure 37 Interpolated CO_2 vs. Engine Load Correlation for 2200 rpm (Cummins ISM 370; Torque Inference Prediction Testing).
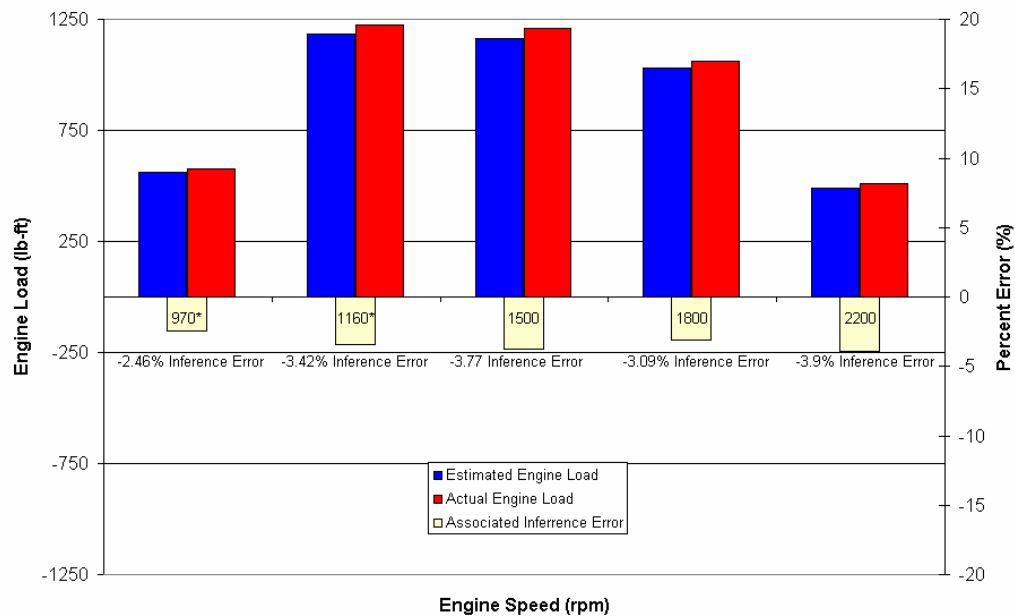
Figure 38 Torque Inference Error Estimates for Preliminary Engine Testing (Cummins ISM 370; Torque Inference Prediction Testing).

3.3 In-field Vehicle Testing Results

The results of the in-field data that were collected for the development of the representative transient testing cycles can be found in this section. All in-field data were collected with the Sensors AMB-II multigas analyzer bench and associated data acquisition components. Though a number of tests were performed in-field for a thorough evaluation of the "real-world" operating conditions of each vehicle, only one cycle was chosen as most representative and used in the recreation of the cycle for the in-laboratory testing. A brief description of each testing route is also given with approximate inclination angles provided for the various slopes encountered during in-field data collection in the following two sections. A graphical representation of raw CO_2 exhaust concentrations and engine speed for each cycle is also presented. In order to reduce the amount of dynamometer test time, as well as associated operating expenses, in-field cycles were shortened, but in such a manner that they still accurately represented all activities of the full in-field cycle. A detailed explanation of the cycle shortening process is described in Section 3.4.

3.3.1 Rubber-Tired Loader In-field Results

The testing route followed during the collection of in-field CO_2 emission data for the rubber-tired loader consisted of two primary operations. The two operations were a transport mode to the landfill site on hilly terrain and a scoop loading/unloading mode that was repeated numerous times during data collection. The graph of the in-field CO_2 emissions and engine speed versus time can be seen in Figure 39 below. The sharply

transient nature of the loader cycle was somewhat more difficult to recreate in the laboratory and required a number of iterations to be performed before a satisfactory correlation could be achieved. This iterative process is explained in the Cycle Development section of this chapter.
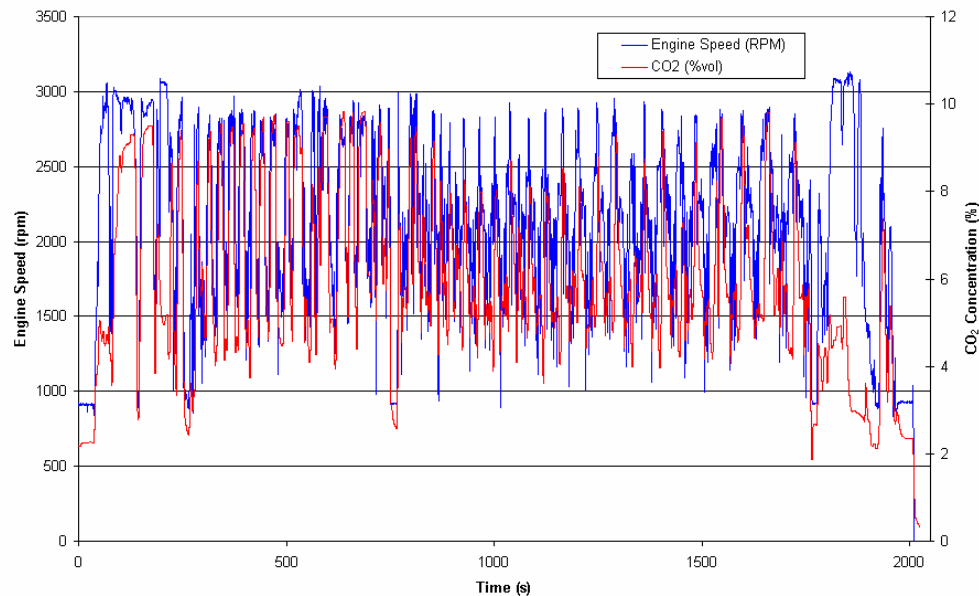
Figure 39 In-field CO$_2$ and Engine Speed vs. Time Results for the Rubber-Tired Loader

3.3.2   Street sweeper In-field Results

As stated previously, one of the goals of the in-field testing was to accurately measure CO$_2$ emissions during each vehicle's routine operation. Figure 41 shows a street map of the route followed by the street sweeper during its normal operation, while Table 5 describes the time spent in each operation mode during the in-field test. The CO$_2$ emissions were continuously collected to allow the estimation of the engine load throughout the in-field route. A description of the in-field testing route with approximate inclination angles for the slopes encountered can be seen in Table 5. The inclination angles were approximated with a pendulum apparatus. The graphical representation of the street sweeper CO$_2$ emissions and engine speed as a function of time can be seen in Figure 40. The amount of CO$_2$ emitted is useful because it can be directly related to the amount of fuel being combusted by the vehicle, which can then be used to estimate engine horsepower output. The engine speed was also continuously monitored during testing. With the estimated power derived from CO$_2$ emissions and known engine speed, an approximation of the produced engine torque can be determined.

This estimation of engine torque output can be used to account for drive train and accessory losses during the operation of the vehicle. In the case of the street sweeper, a test was performed to quantify the effect of brush rotation and drag on CO_2 emissions. The results can be seen in Figure 42. The estimated horsepower output of the engine based on in-field data was further refined during the in-laboratory portion of the testing by actually measuring engine horsepower with the dynamometer while raw CO_2 data was taken with the same experimental setup and procedures used during the in-field testing. The results were compared with brake-specific CO_2 maps to estimate in-field engine loads.
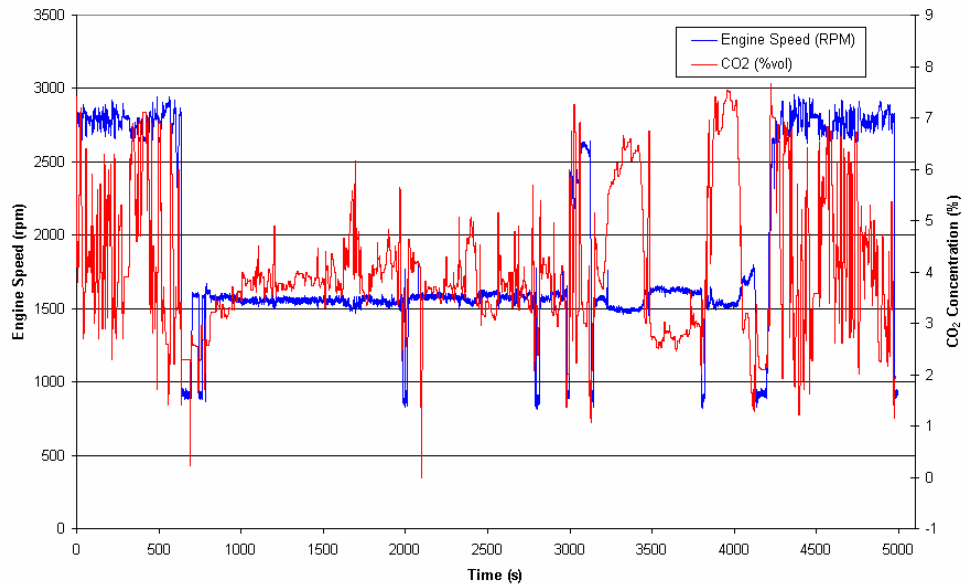
Figure 40 In-field CO_2 and Engine Speed vs. Time for Series P Street sweeper.
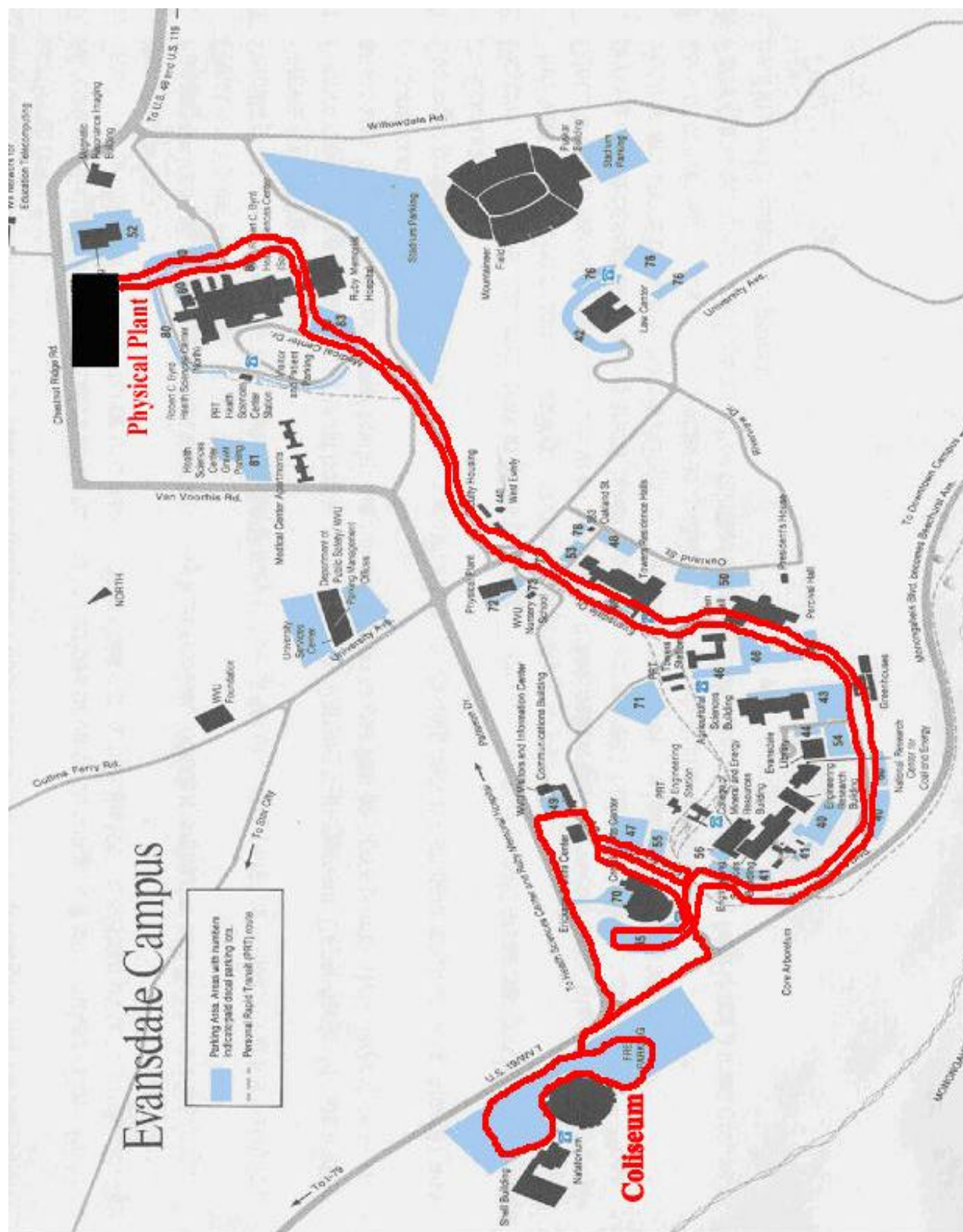
Figure 41 Map of Route taken for In-field Street sweeper Testing.

Table 5 Route Description for the Full In-field Street sweeper Testing Route.

Time (s)	Description
0.0	start test
228.0	end of Ruby Memorial hospital cruise (4-way)
349.5	in front of Brooke Tower
380.8	uphill in front of ERC (5.5% grade)
417.9	uphill Percival Hall Crosswalk (5.5% grade)
451.5	library 4-way
529.0	bus stop turn
570.1	downhill to CAC stoplight (4.5% grade)
641.3	idle
780.4	brushes on/speed up engine
809.5	brushes down to pavement
841.4	move
857.4	Engine speed=1500 rpm
991.9	around Coliseum
1192.0	turn around before Shell Building parking lot drop off
1525.5	turn around on other side of Coliseum
1621.3	turn out of Coliseum circle
1714.2	turn around (180) at Coliseum stoplight
1791.7	turn onto Coliseum circle c-clkwise
1949.6	shell Building turn -around
1982.7	stop/check hopper
2015.2	start again
2081.9	zero bench
2100.7	sample again
2280.3	turn around on other side of Coliseum
2428.5	turn around at light again
2778.0	stop/check hopper again
2808.7	start again
2975.8	transport mode
3061.3	down Patterson Dr. from Coliseum
3117.7	turn into Alumni Center road
3141.1	take off sweeping
3209.5	passing old Towers shortcut starting uphill (4.5 % grade)
3363.4	pass top parking lot by PRT track uphill (4.5% grade)
3448.9	stop at top of hill for pedestrians
3477.4	turn around and go back downhill (4.5% grade)
3791.0	stop and check hopper at hill bottom
3819.5	turn around at Patterson Dr.--head back uphill (4.5% grade)
4033.3	top hill turn downhill toward Beechurst Ave (4% grade)
4118.8	check hopper at CAC parking lot (bottom of hill….full)
4184.3	transport mode back uphill on Evansdale Dr. (4.5 % grade)
4280.1	behind shop
4365.0	downhill past Percival Hall crosswalk stop (5.5% grade)
4412.4	towers crosswalk in front of ERC
4475.1	stoplight (University Ave./Evansdale Dr.)
4564.6	hospital 4-way
4780.6	dump debris above Physical Plant on hill
4956.2	stop to refill water tank
4976.7	stop recording data
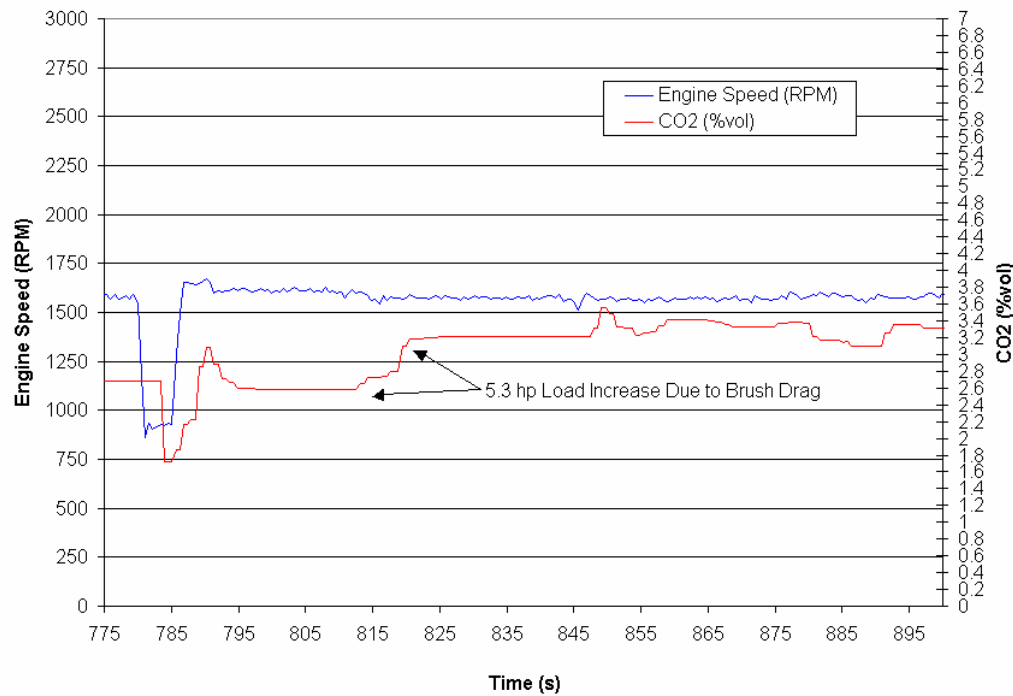
Figure 42 Effect of Sweeper Brush Drag/Inertia on CO_2 Emission Levels.

Table 6 Description of Sweeper Brush Drag Test.

Time (s)	Description
752.5	Idle
780.4	Brushes on/speed up engine
809.5	brushes down to pavement
841.4	move
857.4	RPM==1500
991.9	around Coliseum

It can be seen from the Engine Speed/CO_2 trace of Figure 42 and the test description (Table 6) above that sweeper brush drag and inertial forces did produce a measurable change in CO_2 emissions. The small peak in CO_2 emissions occurring at about 790 seconds is the result of the vehicle's engine having to overcome the rotational inertia of the sweeper brush as it came up to speed. It can be seen from the CO_2 trace that the extra load placed on the engine to overcome the rotational inertia resulted in an increase in CO_2 level of about 0.5%vol over the steady-state value of about 2.6%vol after the brushes were up to speed.

After the rotational inertia test was completed, a test was performed to check the effects of frictional brush drag on CO_2 levels when the sweeper brush was lowered to the pavement. The added load placed on the engine in overcoming this drag resulted in an increase in CO_2 emissions from about 2.6%vol to 3.2%vol. Examining the street sweeper CO_2 matrix data of Section 4.4.2.2 and noting that a 1%vol change in CO_2 emissions equates to a horsepower change of about 10.6hp, the brush drag can be quantified in terms of horsepower consumed. The increase in engine load from the frictional brush drag is approximately 5.3hp, calculated from the CO_2 level increase of 0.5%vol. While this is obviously a rough estimate, it illustrates the idea that vehicle drivetrain and accessory losses can be quantified through CO_2 emissions measurements.

The small CO_2 spike occurring at about 845 seconds (see Figure 46) is from the vehicle beginning to move to sweep the Coliseum parking area (see Table 5). The remainder of the CO_2 trace shows data collected while sweeping the nearly flat parking area.

3.3.3 Excavator In-field Results

The first test was a stationary digging operation in which the first half of the test was digging and the second half of the test was spent back-filling. This operation is common in construction situations like digging a basement; or burying a culvert or a storage tank. The continuous CO_2 map from this test was used for the development of the first transient test cycle.

Figure 43 Excavator Digging Operation

The second test simulated hauling or tramming. A tramming/hauling operation is performed when the excavator is moved in order to transport dirt from one

location to another that is not within the reach of the boom. The second test cycle was derived from this in-field activity.

Figure 44 Excavator Hauling Operation

For the third test a trench was dug and then filled. This is probably the most common industrial use of the excavator. Trenching is used when cables or pipelines are to be buried and in digging building footers. Cycle three was developed from this data.

Figure 45 Excavator Trenching Operation

Testing continued through early summer 2001. The three tests were combined into one operation for CO_2 measurement. The final test of the combined cycles was used as the ultimate source for the laboratory test cycles. The test started with digging for ten minutes followed by hauling for ten minutes and finished with trenching for the last ten minutes. The following graph shows the CO_2 levels recorded during this test.
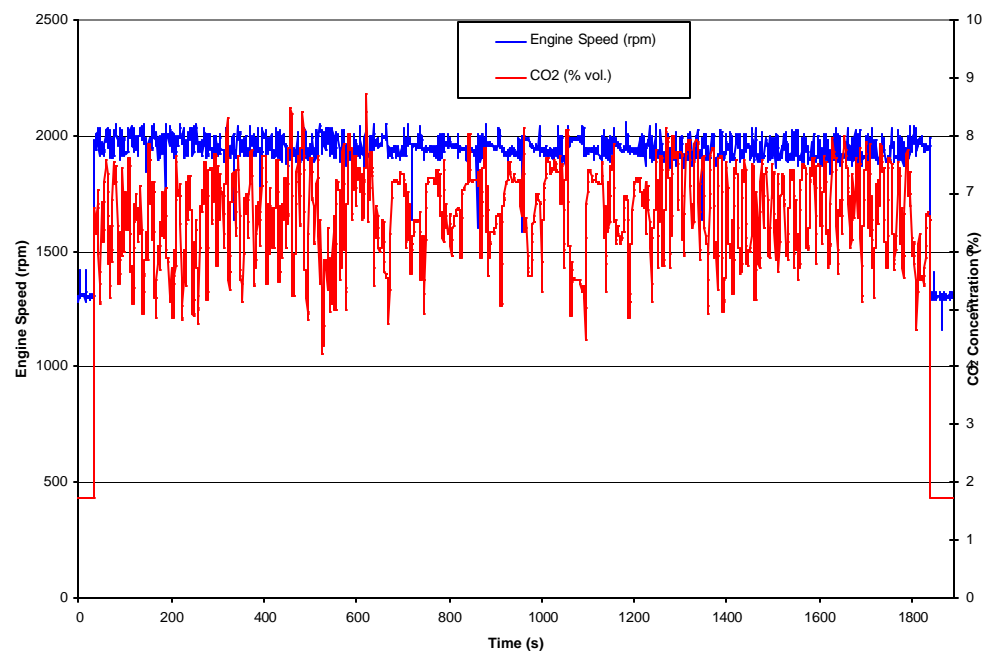
Figure 46 In-field test cycle

3.3.4   Track-Type Tractor In-field Results

Once the test vehicle was identified, the task of designing and qualifying emissions measuring equipment for the purpose of on-board in-field testing began. WVU proposed that Mobile Emissions Measurement System (MEMS), developed for on-board testing of diesel-powered over-the-road trucks, would be the best available device to use for the collection of gaseous emissions data. The MEMS has recently been approved by the US EPA for use for in-use emissions testing for "Consent Decrees" work that WVU is conducting. This system was employed to collect CO_2 and NO_x concentration levels as well as engine speed data, and information used to calculate exhaust flow rates. In order to collect particulate matter data, a Real Time Particulate Mass Monitor was used. This device uses a quartz crystal microbalance in order to measure total particulate concentrations. Modifications were made to the device to incorporate engine speed measurement such that PM data could be time aligned with MEMS data. The following describes the process by which testing equipment was verified and modified to accommodate the challenging task of measuring in-field emission rates for a large off-road diesel engine powered track-type tractor.

Exhaust flow rate was calculated from measurements acquired with an Annubar™ averaging pitot tube device coupled with absolute and differential pressure transducers. Emissions from the two exhaust stacks of the track-type tractor were tested individually due to the complexity and additional backpressure that would be associated with combining the two stacks into a single larger stack. As there is a crossover between the two flows, it was expected that emissions from each stack would be the same. The flow sections, rolled from 16 gauge mild steel, were 0.55 m (22 in.) long with an inside diameter of 0.175 m (6.875 in.). Four ports provided for the collection of temperature, absolute pressure, gaseous emissions, and particulate matter. These ports were 90° from the plane of the Annubar™, and were evenly spaced along the direction of flow. The flow section was designed to slide over the existing exhaust stack and be clamped to it, with approximately 0.05m (2 in.) of overlap onto the existing exhaust stack. Design goals of these flow sections included keeping the setup lightweight and compact while avoiding major flow restrictions.
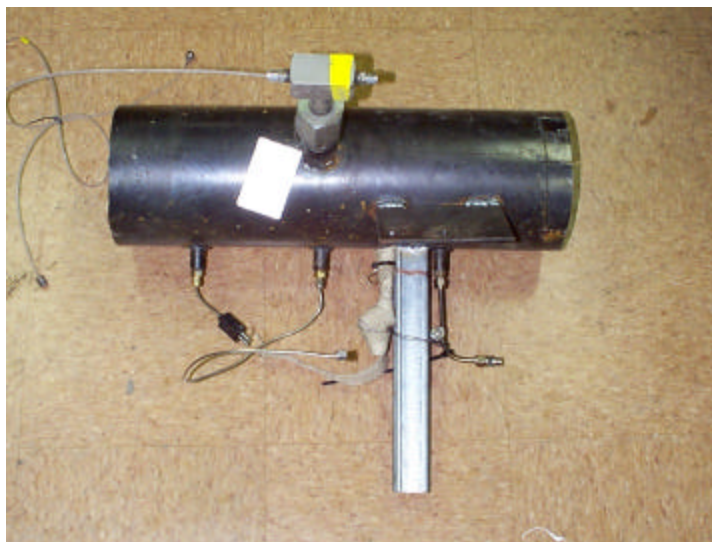
Figure 47 Exhaust Test Section with Annubar™ Flow Measurement Device and Gaseous and PM Sampling Probes

In order to verify the exhaust test section, a prototype was built and tested to compare flow rate measurements with measurements from a NIST-traceable sub-sonic venturi and a laminar flow element. During this bench testing it was discovered that a three-lobed venturi section exists in the engine's exhaust stack that is used to provide vacuum for an intake pre-filter system. In order to determine the effects of this obstruction, an exhaust section was purchased, and the flow section was tested with and without the exhaust section inline. Various configurations of exhaust stack sections and flow meters were investigated in order to quantify entrance and exit effects and their subsequent impact on flow rate measurements. Transition regions between devices (except for exhaust section and flow section) were sized in accordance with the needs of the flow measurement device.

After completion of the bench testing, the track-type tractor exhaust stack and exhaust test section, including the Annubar™ and sampling probes, were installed in the exhaust system of a DDC Detroit Series 60 12.7 liter engine for evaluation in an engine test cell. Several test cycles were run to compare the emissions data between MEMS and the laboratory instruments using the track-type tractor exhaust stack. The flow rates of the exhaust from the Series 60 engine are comparable to those through each exhaust stack on the track-type tractor. The previous flow rate testing results indicated that flow rate measurements were inaccurate at higher flow rates. These errors were attributed to the wake effects created by the exhaust venturi, which affected the Annubar™ pressure readings, and therefore induced a 20% error in the calculated flow rate and the mass emission rates of CO_2 and NO_x. In order to combat this problem, tests were performed to determine correction coefficients that could be applied to the Annubar™ flow rate calculations. The engine was operated at steady-state setpoints for sufficient time to stabilize the pressure readings, and the gaseous emissions concentrations measured with the MEMS. The calculated mass emissions rates were compared to those recorded by the full-flow dilution tunnel and laboratory emissions analyzers. The Annubar™ flow rate equation coefficients were adjusted accordingly in order to provide adequate correlation.

After these correction factors were applied, steady-state and transient engine test cycles were designed based on expected engine loading conditions of the track-type tractor. Emissions measurements were again performed using these transient cycles, and results of the MEMS were compared with those obtained with the laboratory's full-flow dilution tunnel.

Emissions data were collected using the MEMS System, the RPM 100, and the laboratory for the test cycle designed to mimic the operation of the track-type tractor. Figure 49 is included as a comparison of NO_x mass emissions rates and Figure 50 of CO_2 mass emissions rates.
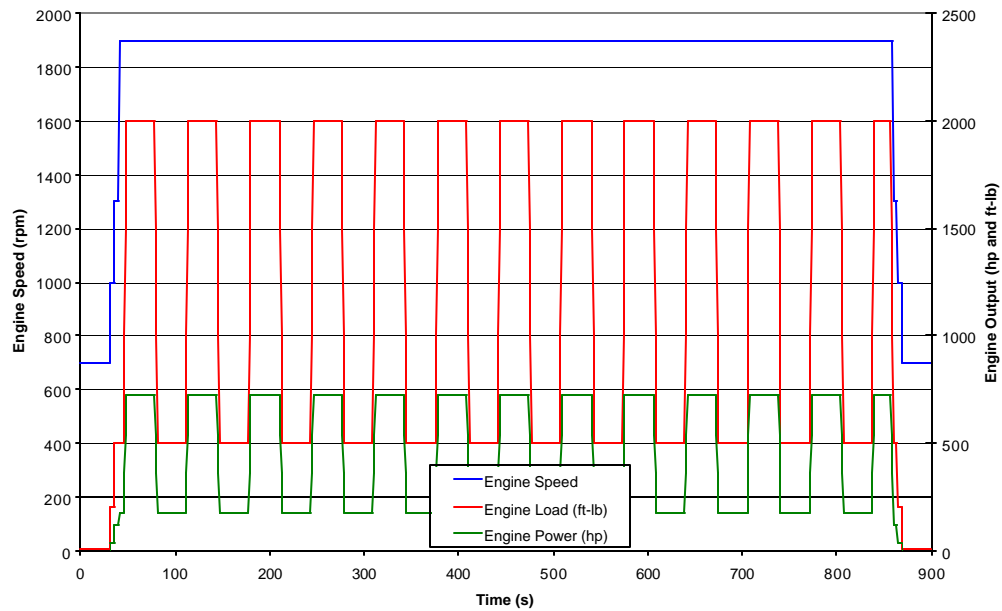
Figure 48 Dynamometer Test Cycle Designed to Evaluate the On-board Emissions Testing System (MEMS and RPM 100) in the Laboratory.
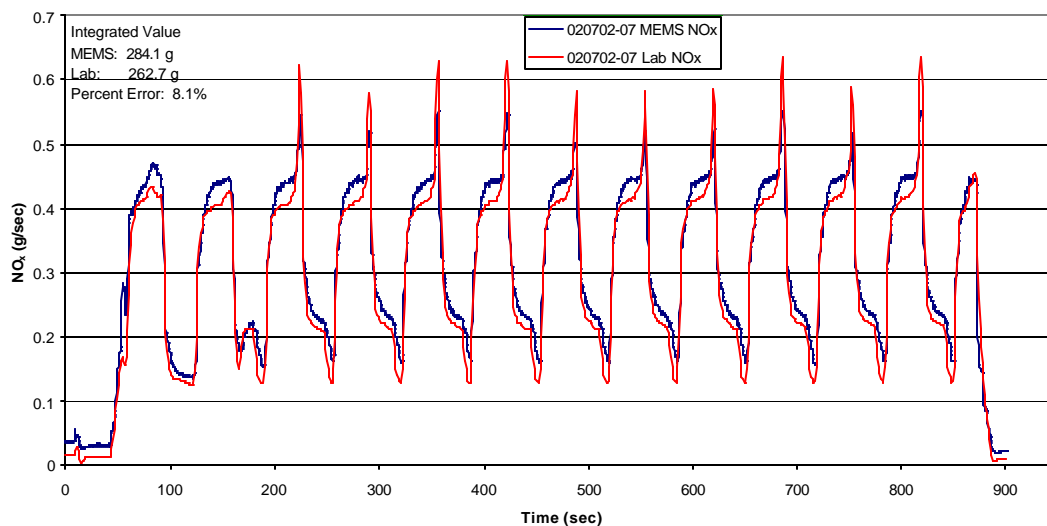
Figure 49 Comparison of Mass Emissions Rates of NO$_x$ over a Transient Cycle Designed to Mimic In-field Track-type Tractor Operation – MEMS Results and Laboratory Results
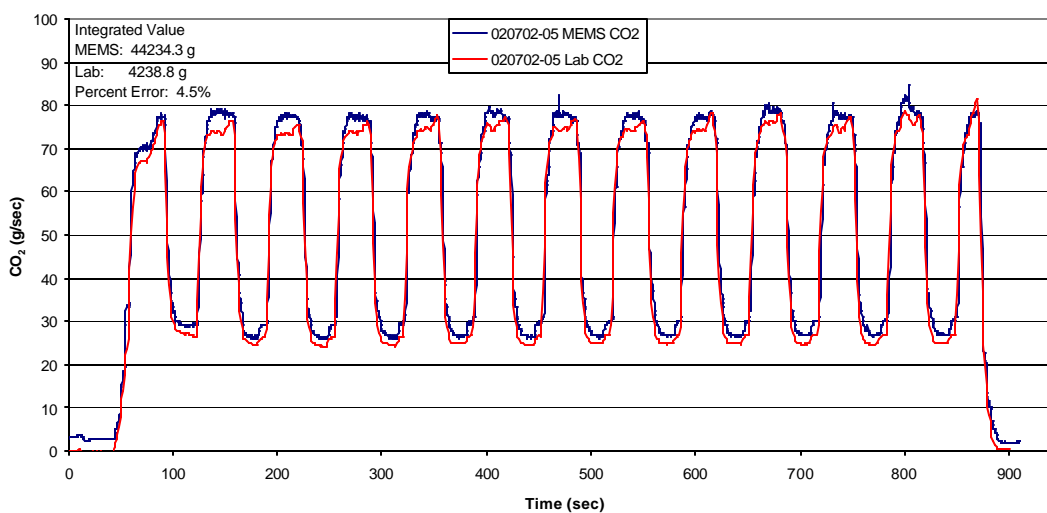
Figure 50 Comparison of Mass Emissions Rates of CO$_2$ over a Transient Cycle Designed to Mimic In-field Track-type Tractor Operation – MEMS Results and Laboratory Results

Coinciding with the validation of MEMS equipment was the adaptation of the MARI RPM 100 for use as an on-board measurement system for off-road vehicles. As explained earlier, the RPM 100 provides for fully arbitrary control of the dilution of a

slip-stream sample from the raw exhaust stream, and measures PM mass with a quartz crystal microbalance. The inherent system properties of compact size, robustness, and resistance to vibration made the RPM 100 well suited for on-board testing of the track-type tractor. However, provisions had to be made to enclose the system in order to protect it from possible inclimate weather and less-than-optimal mounting locations. As a result, the system was mounted in an independent enclosure. In addition, modifications to the sample probe design were implemented in order to accommodate the anticipated exhaust pressures and flow rates that are characteristic of engines that are comparable to that used in the D-11R CD Track-type Tractor. For a complete description of the system, see Sections 2.5.6 and 2.5.6.2. When the dilution ratio, particulate concentration, and total engine exhaust flow rate are combined, engine-out particulate mass emissions rates can be calculated. The MARI unit was compared against the full-flow dilution tunnel laboratory. For this comparison, particulate mass emissions were measured from a DDC Detroit Series 60 12.7 liter engine that was operated according to a designed transient test cycle (see Figure 48), which was developed by WVU to simulate engine operating points that would be encountered while testing the track-type tractor during in-field operations. The results from these comparison tests are summarized in Table 7. It should be noted that the resultant error is an integration of all error sources in the emissions measurement system (raw exhaust flow rate measurements, mass measurements, inherent data acquisition errors, and general errors related to test procedures).

Table 7 Gravimetric PM Comparisons between the MARI RPM 100 and the Full-flow Dilution Tunnel (g)

	Test 01	Test 02	Test 03
MARI RPM 100 Integrated PM Mass	0.74	1.97	1.73
Full-Flow Dilution Tunnel Gravimetric Integrated PM Mass	0.71	1.75	1.79
Percent Difference	4.2%	12.6%	-3.4%

Since the tractor engine could not be removed and tested in the emissions laboratory, all emissions results from the track-type tractor in-field testing that were generated using the on-board Mobile Emissions Measurement System will be presented in the in-field results section, Section 3.6.4.

3.4 In-field Cycle Shortening

Test cycle length is an important consideration when developing a cycle. In-laboratory test cycles need to be long enough to provide a sufficient amount of representative emissions data while not wasting resources by being too lengthy. Laboratory dynamometer testing is expensive, and excessively long test cycles would add significantly to total testing costs. Limiting wear on the engine and test equipment is also an important factor to consider when deciding on an appropriate test cycle length. These

considerations were the driving force for shortening the in-field cycles as the dynamometer test cycles were developed.

Likewise, it should be noted that in-field test cycles are arbitrary and the strict adherence to any transient test cycle does not necessarily provide data that is absolutely representative of all in-field operating conditions. Many parameters influenced all in-field data, and factors such as operator driving style, specific activity and load, ambient conditions, and the condition of the terrain encountered have significant impacts on any in-field results. The primary goal in the development of a cycle is to capture the basic nature of the modes most encountered during the test vehicle's operation. The shortened in-field cycle should include all the basic operational modes of the full in-field cycle with an adequate amount of time spent on each mode to allow a sufficient amount of data to be collected. For the test cycles developed, a proportional amount of time was dedicated to each of the identified modes, compared to the original in-field cycle.

For this study, presentation of the cycle shortening efforts was included as a separate section so as to provide a more detailed explanation of the methodology and reasoning that was applied. For the street sweeper and rubber-tired front-end loader, the in-field cycles were shortened, and then comparisons were made with the original cycle, based upon engine speed and inferred load factors. The subsequent shortened cycles were then used to create the dynamometer test cycles, using the iterative load inference techniques that are detailed in section 3.5.

3.4.1 In-field Loader Cycle Shortening

The in-field activities of the rubber-tired loader consisted of two modes of operation: a transport mode to the excavation site, and a loading/tramming/unloading mode. The in-field data was examined for areas of excessive repetitiveness of operation that could be shortened. Transport mode was identified as a time consuming, relatively steady, operation. However, the transport mode is not of a repetitive nature because the loader was descending hills on the way back to the test origin that it ascended on the way to the excavation site and vice-versa. For this reason, the transport modes, the first 240 seconds and the last 210 seconds of the in-field loader data were kept in their entirety for the shortened test cycle (Figure 52). Figure 51 shows the entire in-field loader cycle for comparative purposes. Sections of repetitive events in the loading/tramming/unloading mode of the in-field cycle were truncated. A total of 864 seconds were removed from the full in-field cycle to arrive at the shortened test length of 1144 seconds. Comparisons with respect to full in-field and shortened in-field cycle integrated values of continuous speed and CO_2 to make sure that the shortened speed/load ranges were representative of the actual full in-field ranges. Average engine speed for the full in-field loader cycle was 1806 rpm and the average CO_2 was 5.92%vol. The shortened cycle had average engine speed and CO_2 values of 1810 rpm and 5.80%vol, respectively. Considering the variability's encountered during testing, the differences in integrated values were negligible.
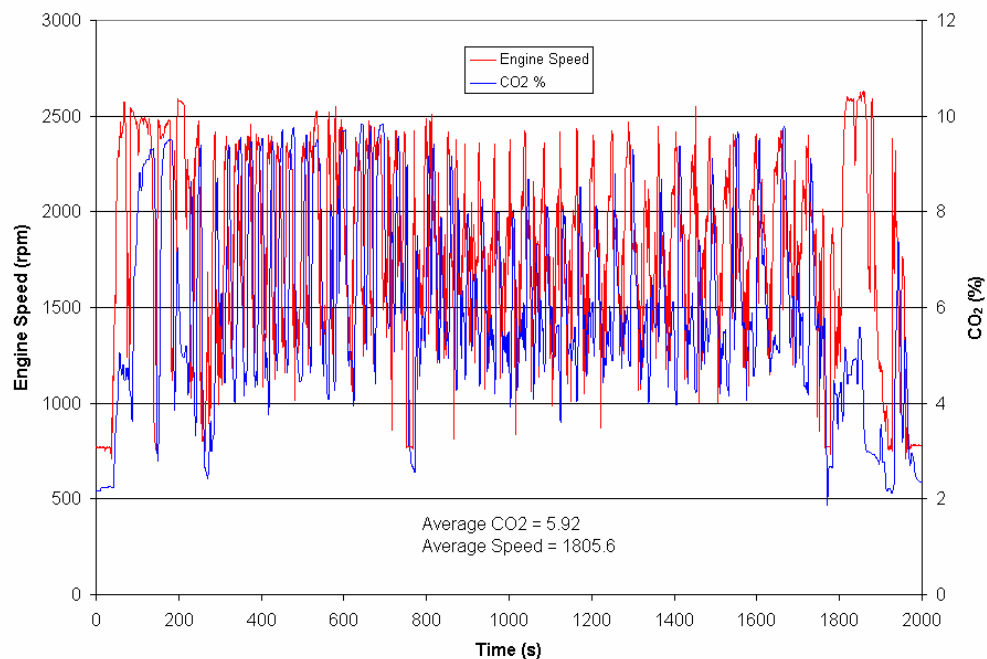
Figure 51 CO_2 and Engine Speed vs. Time for the Full In-field Loader Cycle.
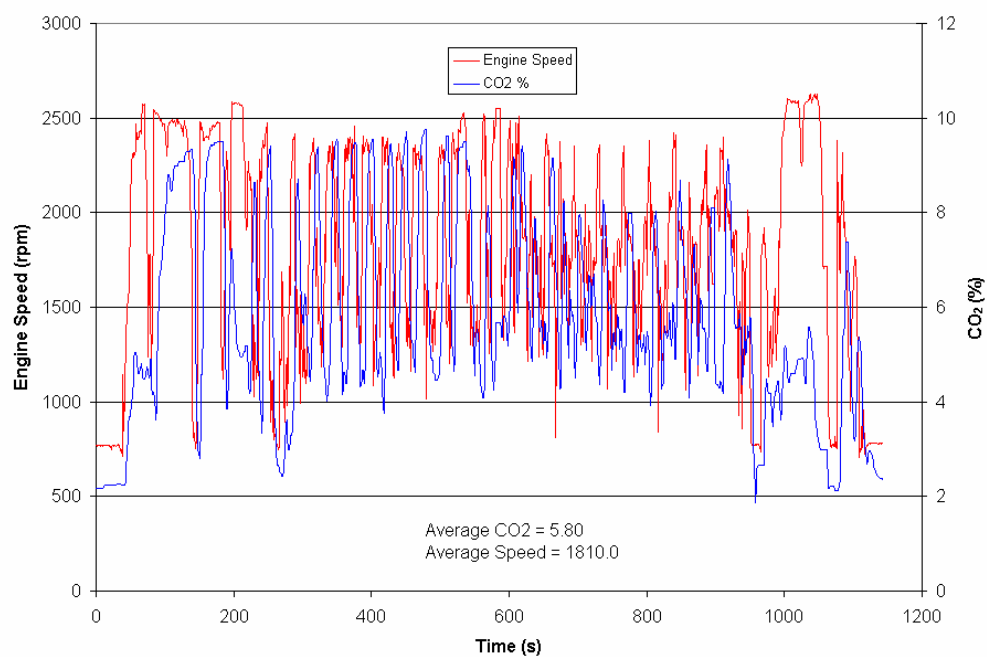
Figure 52 CO_2 and Engine Speed vs. Time for the Shortened In-field Loader Cycle.

A visual comparison was made between the normalized speed/load data of the shortened WVU loader test cycle (Figure 53) and the normalized speed/load data of a United States EPA wheel-loader transient testing cycle (Figure 54). The data was normalized in the following manner, engine speed was normalized against governed central speed and engine load was normalized against the maximum load per the engine speed exhibited at each data point. It can be seen from comparison of the two figures that they are consistent in their repetitive nature and total test length, with the major difference being that the EPA cycle does not have a transport mode at the beginning and end of the cycle. Rubber-tired loaders can spend a significant amount of time moving from site to site, therefore it was decided that the test cycle would be more representative of actual conditions encountered in the field if the transport mode data was included.
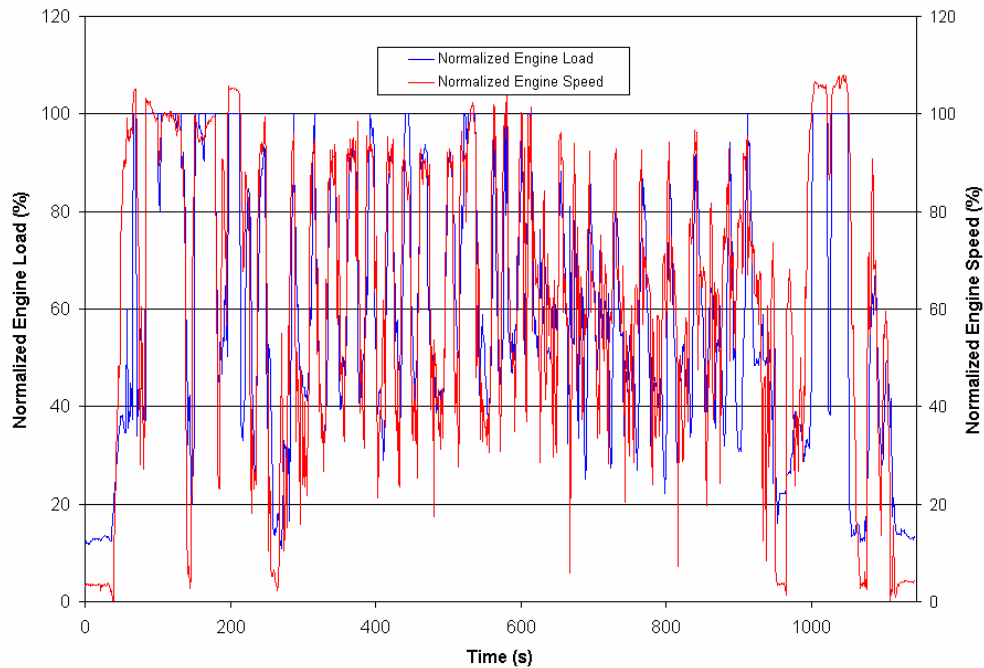
Figure 53 Normalized Engine Speed and Load for the Shortened WVU In-field Rubber-Tired Loader Cycle.
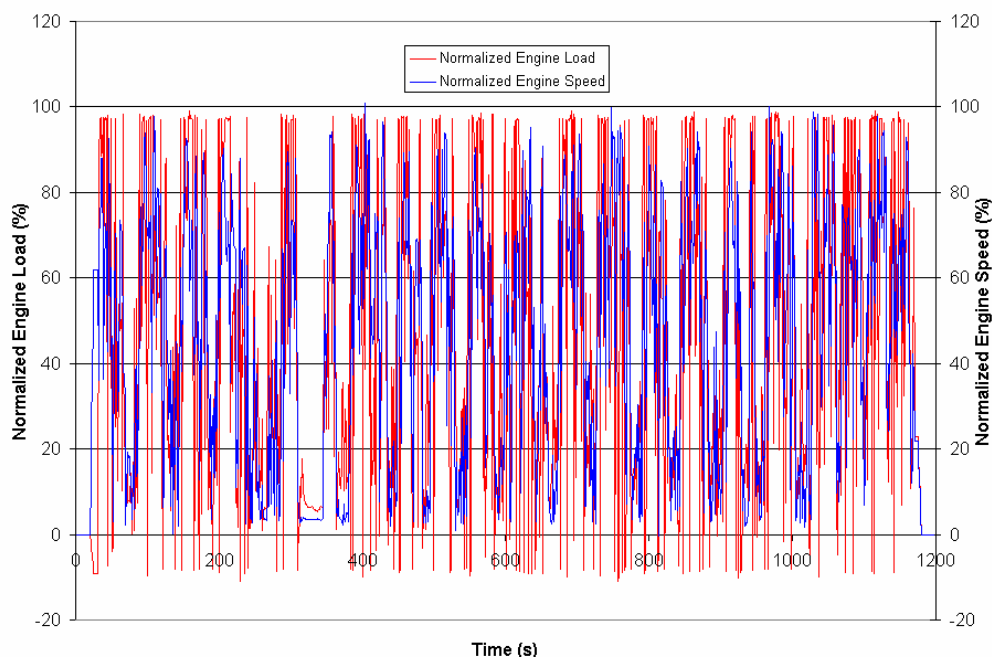
Figure 54 Normalized Engine Speed and Load for the EPA Rubber-Tired Loader Cycle.

The integrated values obtained for the two cycles discussed previously are an indication of total cycle work only, and do not reflect the accuracy of recreation of transient events in the shortened cycle. A much more in-depth assessment of the accuracy of the shortened cycle with respect to the full in-field cycle was made by discretizing the two cycles across small engine speed ranges and comparing normalized speed/load results.

The full and shortened in-field loader cycles were discretized into increments of 100 rpm each from 700 rpm to 2700 rpm, and average engine loads were estimated for each engine speed range using a normalized CO_2-load inference, which will be discussed thoroughly in the following sections. It was necessary to use small engine speed increments over the full range because the transient events of the loader cycle in the field indicated speed ranges from idle to full speed in rapid succession. The more steady-state operation of the street sweeper cycle permitted the use of only three broader speed ranges for discretization purposes, as will be seen in section 4.4.2. The average engine loads were found by multiplying the average normalized CO_2 values by the maximum torque, which was found for each speed range during the creation of the loader CO_2 map matrix discussed in section 4.5.1.2. This method yields the most accurate indication of the differences in engine load during transient events between the shortened and full cycles. Average load values for both the full and shortened in-field loader cycles, as well as percent difference in average load, can be seen in Table 8.

Table 8 Comparison of Engine Speed Discretized Average Load Values between the Full and Shortened In-field Loader Cycles.

Engine Speed (RPM)	Shortened Cycle Average Load (ft-lbs)	Full Cycle Average Load (ft-lbs)	% Difference
750	36.1	41.2	-12.47
850	100.4	95.6	4.99
950	73.8	59.5	24.10
1050	128.1	113.8	12.57
1150	109.4	98.8	10.71
1250	106.4	98.6	7.96
1350	115.8	114.3	1.26
1450	123.4	119.4	3.36
1550	116.4	119.5	-2.58
1650	124.0	119.8	3.49
1750	114.6	119.2	-3.85
1850	125.7	127.1	-1.03
1950	114.5	122.5	-6.50
2050	117.3	116.1	1.00
2150	95.3	100.3	-5.04
2250	100.3	104.7	-4.17
2350	103.1	106.0	-2.73
2450	140.5	134.6	4.37
2550	94.4	89.0	6.10
2650	1.4	1.4	0.00

3.4.2   In-field Street Sweeper Cycle Shortening

For the in-field street sweeper cycle, the activity was divided into three main categories: transport, sweeping, and idle. The sweeping and transport activities were then subdivided by the nature of the terrain encountered. These subdivisions were identified based on whether the sweeping/transport activity was performed on level ground, uphill, or downhill, with approximate percent grades assigned to the respective activity. The three basic operational modes of the full in-field sweeper cycle were examined for repetitiveness and excessive length and shortened accordingly. A total of 3760 seconds were removed from the lengthy in-field cycle to arrive at the shortened cycle length of 1221 seconds. The CO_2 and engine speed traces for the full in-field cycle can be seen in Figure 55 with an average CO_2 value of 4.06%vol and average engine speed of 1855.8 rpm. The CO_2 and engine speed traces for the shortened in-field sweeper cycle can be seen in Figure 56 with the average CO_2 values of 4.14%vol and 1716 rpm, respectively.
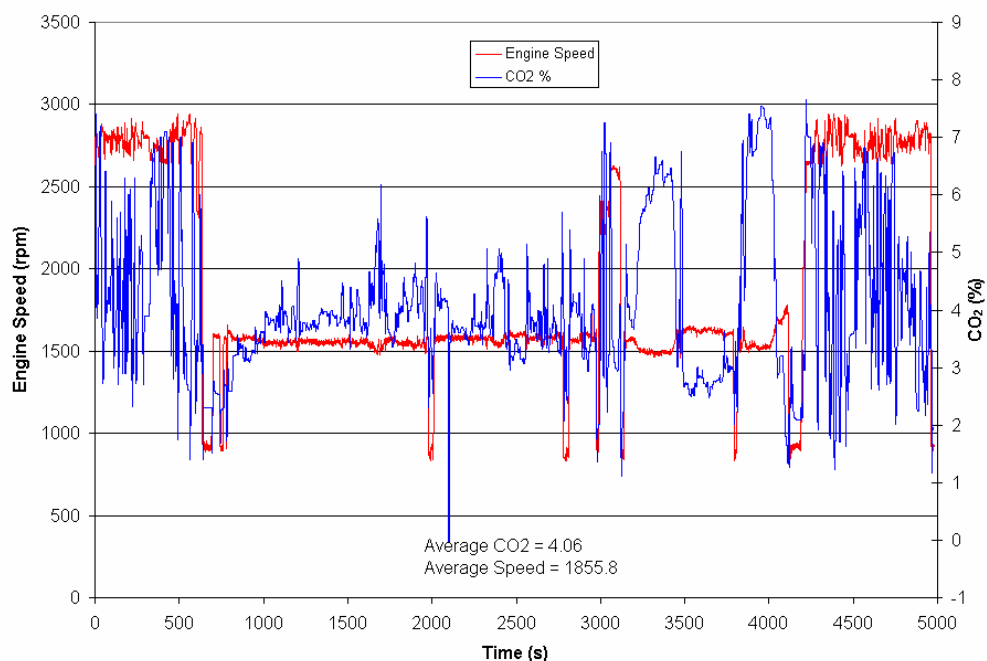
Figure 55 CO_2 and Engine Speed vs. Time for the Full In-field Street sweeper Cycle.
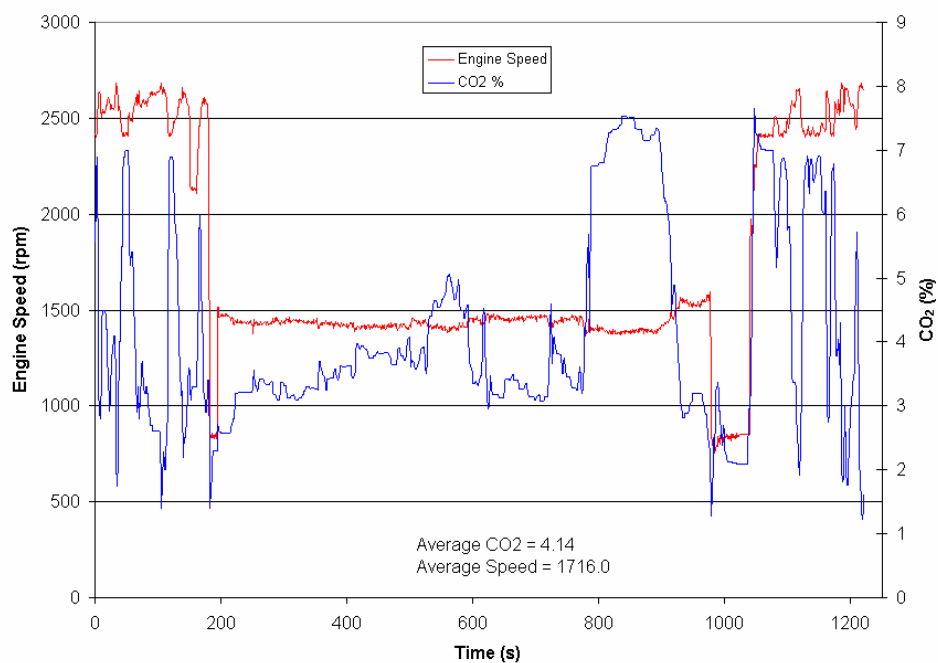
Figure 56 CO_2 and Engine Speed vs. Time for the Shortened In-field Street sweeper

Cycle.

The activities of the street sweeper were closely related to discrete ranges of engine speeds, therefore the in-field cycle was characterized according to the percent of total time allotted to each activity. The full and shortened in-field street sweeper cycles were divided into three engine speed ranges: 700 rpm-1000 rpm, 1200 rpm-1600 rpm, and 2300 rpm-2700 rpm. In contrast with the loader, the use of larger speed ranges for the sweeper was possible because it operated primarily within these three ranges in the field. The idle mode (700 rpm-1000 rpm), the sweeping mode (1200 rpm-1600 rpm), and the transport mode (2300 rpm-2700 rpm) were all covered by the selected ranges. The average engine loads were then found for each engine speed range. These average loads were found by multiplying the average normalized CO_2 values by the maximum torque that was measured for each speed range during the creation of the street sweeper CO_2 map matrix discussed in section 4.5.2.2. This method yields the most accurate indication of the differences in engine load during transient events between the shortened and full cycles. A graphical representation of the normalized engine speed and load can be seen in Figure 57. No comparison was made between the shortened WVU cycle and other transient sweeper testing cycles because no equivalent cycles for street sweepers were found in the literature searched. Average load values for both the full and shortened in-field loader cycles as well as percent difference in average load can be seen in Table 9.
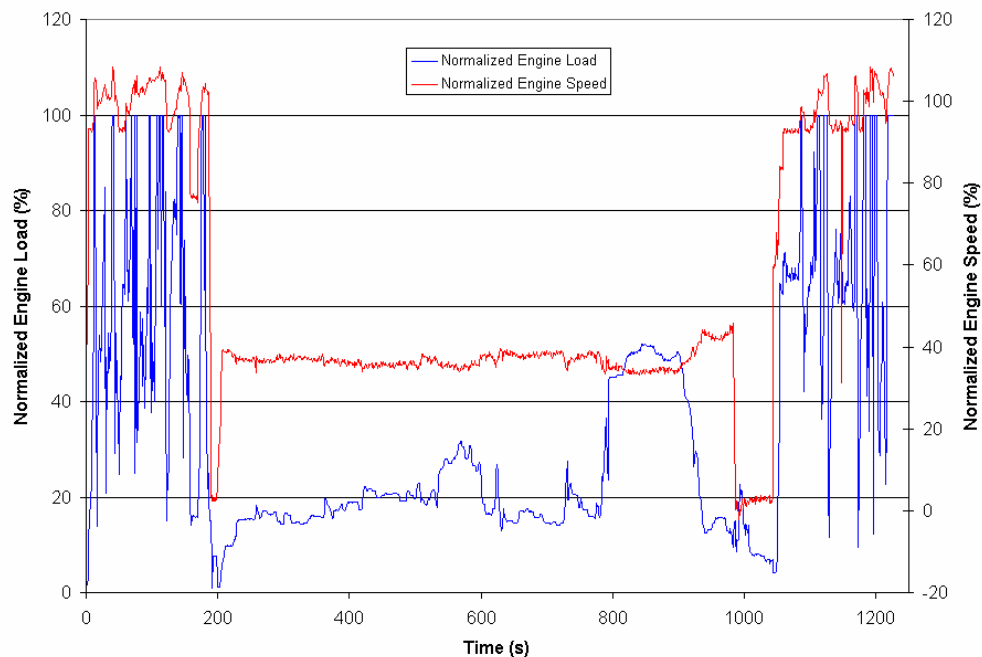
Figure 57 Normalized Engine Speed and Load for the Shortened In-field Street Sweeper Cycle.

Table 9 Comparison of Engine Speed Discretized Average Load Values between the Full and Shortened In-field Street sweeper Cycles.

Engine Speed (RPM)	Shortened Cycle Average Load (N-m)	Full Cycle Average Load (N-m)	% Difference
700-1000	195.1	120.9	61.34
1200-1600	197.8	181.7	8.88
2300-2700	102.1	110.2	-7.47

The large percent difference for the 700-1000 rpm range can most likely be attributed to the operation being performed by the street sweeper. The vehicle could have been idling in the field, had the brushes up and rotating, or it could have had the brushes rotating and contacting the road surface. It should also be noted that the amount of friction-related load the brushes place on the engine will change depending on the nature of the surface being swept.

3.4.3 In-Field Excavator Cycle Shortening

The excavator in-field test cycle data indicated that emissions were task specific and clear demarcations existed between operations. In order save time once the engine was placed in laboratory, the cycle was broken into ten-minute segments which could be iterated while another cycle was tested. These test segments were compared to the tests of each separate activity to satisfy that they were representative of the characteristic trends of each activity. Once acceptable convergence had been achieved between the CO_2 traces recorded in-field and in the laboratory for each section, they were combined once again to form the full dynamometer test cycle.

3.5 Cycle Development Work

The data taken in the field was used to develop a representative cycle for each vehicle, which would ultimately be used to load the engines during full-flow transient emissions tests at the EERL. The lengths of the in-field test cycles that were collected were too long to recreate in their entirety, so the in-field data was examined and representative micro-trips of each in-field cycle were compiled to produce a single shorter test cycle.

The task of creating a shorter dynamometer test cycle that truly represented the in-field cycle was a difficult and time-consuming one. The in-field operating cycles for each engine are very specific to the vehicle used and the operating site. Therefore, blind adherence to a cycle measured in the field provides only limited information regarding that vehicle's operation during the specific conditions that were present during data logging. To overcome this obstacle, the in-field cycle was characterized according to "micro trips" and specific activities. This process provides the researcher with the ability to apply such activity data to a broader range of engines/vehicles. The in-field raw CO_2 emissions data traces were used to infer the speed/load traces followed by the engine, while on the dynamometer. The full cycle for each vehicle, as measured in the field, was

characterized and specific "micro trips" were identified. Once the in-field cycle is characterized based on speed/load ranges, the micro-trips can be combined in order to produce alternative transient cycles that more accurately represent the actual duty cycle corresponding to a particular off-road vehicle. A detailed explanation of the in-field cycle shortening process can be found in the Section 3.4.1 for the rubber-tired loader, Section 3.4.2 for the street sweeper, and Section 3.4.3 for the excavator.

The method for deriving test cycle iterations consisted of exercising the engine in the laboratory on a dynamometer test bed according to the initial speed/load setpoints and then altering the cycle to produce the emissions and engine speeds recorded in-field. Speed and load setpoints that were used for the engine cycle were linearly interpolated between discretized speed and CO_2 setpoints. During the test, the in-field data measurement system was used to compare the continuous CO_2 laboratory data to the data collected in the field. The torque levels placed on the engine were then adjusted in an attempt to make the in-field and in-laboratory CO_2 data correlate more closely. The test was then repeated with the updated adjusted cycle and emissions data was again compared. This iterative process was continued until the laboratory cycle data and the in-field cycle data met correlation criteria described in this chapter. A flowchart of the steps involved for cycle iteration can be viewed in Figure 58.

In order to provide a starting point for the development of the cycle, a torque step map was performed on each engine while raw CO_2 emissions were collected with the AMB-II. During the mapping process, the engine was loaded in increments of 50% of maximum engine torque from 0% to 100% while CO_2 emissions data were collected. It should be noted that in the initial stages of the study the engine was loaded in increments of 10%, which required excessive time for iterations. However the results of the final cycle, which was converged upon via iteration and manual cycle adjustment, were not dramatically affected by the initial approximation. Hence, load increments of 50% were used in order to reduce test time. This map was then repeated at different engine speeds from idle to maximum speed in increments of 100 rpm. A table of the values for each engine in matrix form can be seen in the "CO_2 Map Matrix" portions of this chapter. The data was then examined to determine how engine torque levels and CO_2 levels compared at the various engine speeds. A Visual Basic program was developed that linearly interpolated engine load by comparing in-field engine speed and CO_2 versus time traces with the raw CO_2 versus engine speed matrix.

A significant amount of time was needed for the proper setup of the Dyn-Loc IV Dynamometer Controller and the DTC-1 Digital Throttle Controller. There are several hard-coded Proportional Integral Derivative (PID) parameter settings on both systems that govern the ability of the engine to accurately follow the desired cycle. The PID settings must be set up based on the nature of the transient events encountered in the cycle and on the rotational inertia of the system. Aspects such as signal overshoot and throttle opening speed must be optimized with the settings.

The Proportional (P) parameter instructs the Dyn-Loc how far the actual engine speed/torque values are from the desired values, the Integral (I) parameter allows the Dyn-Loc to close in on the desired values, and the Derivative (D) parameter dictates the speed at which the controller can close in on the desired value. Separate settings could be entered in for each of the three parameters of the PID, and it was found during the setup

process that the Derivative parameter was the most sensitive to set up. If the Derivative was set too high (quick closing on the desired value) signal overshoot was the result. If it were set too low, the engine would not be able to quickly follow any sharp transient events in the cycle. There are separate PID parameters for the dynamometer controller and the throttle controller, so care must be taken during the setup process to ensure harmonious operation. Several cycle iterations were run consecutively in the laboratory in order to optimize the PID settings of both controllers for each test cycle. The setup was further complicated due to the use of two PID controls. It is anticipated that one global PID controller would have greatly improve the transient control.

```
┌─────────────────────────────────────────┐
│  Collect In-field CO₂/Engine Speed Data  │
└─────────────────────────────────────────┘

┌─────────────────────────────────────────┐
│      Create Load/Engine Speed-CO₂        │
│                 Matrix                    │
└─────────────────────────────────────────┘

┌─────────────────────────────────────────┐
│      Use Matrix/Previous Cycle Results   │
│       to Create/Adjust Dynamometer       │
│            Speed/Load Setpoints          │
└─────────────────────────────────────────┘

┌─────────────────────────────────────────┐
│  Exercise Engine on the Test Bed According to │
│      the Created Setpoint File while Collecting │
│        Raw Emissions/Engine Speed Data   │
└─────────────────────────────────────────┘

┌─────────────────────────────────────────┐
│   Compare In-field and Laboratory Results │
│     through Correlation and Compare to   │
│     Predetermined Correlation Criteria   │
└─────────────────────────────────────────┘

┌────────────────────────┐   ┌──────────────────────────────┐
│ If Correlation Meets    │   │ If Correlation Does Not Meet │
│        Criteria         │   │           Criteria           │
└────────────────────────┘   └──────────────────────────────┘

┌────────────────────────┐
│  Run Final Transient Cycle and │
│  Collect Full-Flow Emissions Data │
└────────────────────────┘
```

Figure 58 Flow Chart of Steps Involved in the Cycle Iteration Process.

3.5.1 Rubber-Tired Loader Cycle Development

The fact that the John Deere 6059 loader engine was tested first made the recreation of its in-field cycle more time consuming. In addition to inexperience in the cycle recreation process, many details related to the dynamometer setup had to be addressed, such as the PID settings that were discussed previously. However, upon inspection of the in-field loader data, it is understandable that its cycle would be more

difficult to recreate in the laboratory than the street sweeper cycle, due to its sharply transient nature. This point is illustrated by the fact that correlation results between in-field and in-laboratory data for the street sweeper were much better than those for the rubber-tired loader.

3.5.1.1 Engine Map

An engine mapping procedure, outlined in the CFR 40 Part 86 Subpart N [1], was performed on the John Deere 6059 engine to determine peak horsepower (rated speed) and peak torque(intermediate speed) values and operating points. Quantifying these two points is necessary to determine the set points to be used for the steady-state 8-mode cycle and to allow the compilation of the CO_2 map matrix used for development of the transient cycle. The results were corrected with the eddy current dynamometer windage loss information supplied by Mustang Dynamometers, Inc. The resultant lug curve for the John Deere 6059 (Figure 59) indicated that peak horsepower was approximately 107 hp (80 kW) at 2375 rpm, while the torque peak occurred at 1010 rpm and was approximately 276 ft-lbs (375 N-m)
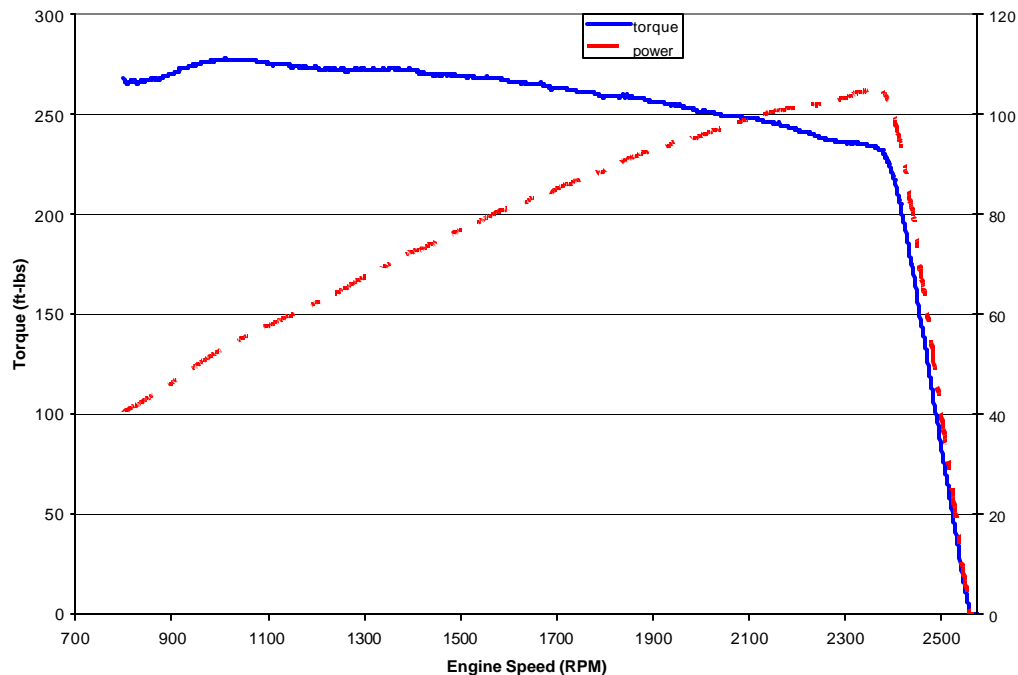
Figure 59 Engine Map for the John Deere 6059 Loader Engine.

3.5.1.2 CO_2 Map Matrix

The engine was operated according to a series of speed-load setpoints, while CO_2 levels were recorded with the in-field data collection system. The CO_2 levels were recorded in the laboratory for the loader engine at speeds from 700 rpm to 2700 rpm in increments of 100 rpm. Engine loadings used ranged from 0% to 100% load in increments of 10% load during the recording of CO_2 emissions. The system was allowed

to stabilize for 30-seconds at each speed/load point to ensure that the CO_2 data had time to reach a value of at least 90% of the fully stabilized steady-state value. The system was not allowed to stabilize for more than 30-seconds to prevent skewing of the often-quick transient events encountered during cycle testing. The full load value was determined from the engine map discussed in section 3.5.1.1 to be approximately 80 kW. The data collected was used to develop the first iteration of the loader transient cycle via the computer matrix interpolation program mentioned previously. Raw exhaust CO_2 data from the in-field testing was used to develop a torque estimate by interpolating the data collected in the laboratory, and is shown in Table 10 below.

The raw exhaust CO_2 data taken during the first iteration of the cycle was compared with the in-field data, and a correlation of the data was established. The speed and load set points of the previous transient cycle iteration were then manually adjusted in order to make the two traces converge. A graphical representation of continuous CO_2 and engine speed traces for the first and final iterations of the recreated in-laboratory cycle for the loader can be seen in Figure 60-Figure 63 along with graphical correlation data.

Table 10 Matrix for the John Deere 6059 Loader Engine.

Engine Speed	CO_2 (%vol) @ 0% Engine Load	CO_2 (%vol) @ 50% Engine Load	CO_2 (%vol) @ 100% Engine Load
700	1.29	6.06	11.77
800	1.31	5.82	12.24
900	1.34	5.85	12.29
1000	1.35	5.95	12.43
1100	1.39	5.94	12.21
1200	1.43	5.84	12.19
1300	1.46	5.83	12.08
1400	1.51	5.77	11.86
1500	1.55	5.77	11.99
1600	1.60	5.77	11.84
1700	1.66	5.80	11.75
1800	1.72	5.82	11.63
1900	1.81	5.84	11.61
2000	1.88	5.85	11.49
2100	1.97	5.94	11.28
2200	2.10	5.87	11.21
2300	2.23	5.86	11.02
2400	2.28	5.60	10.15
2500	2.35	3.36	4.65
2600	2.50	3.52	3.81
2700	2.50	3.52	3.81

3.5.1.3 Loader Cycle Iteration

As stated previously, a number of cycle iterations (9 iterations) were needed for the rubber-tired loader engine before the CO_2 and engine speed data sufficiently matched the in-field data. The repetitive nature of the loader cycle allowed a much shorter cycle to be run (about 600 seconds) for many of the iterations in order to save time and equipment wear. The first step performed after operating iterations of the test cycle was to time-align the laboratory data with the in-field data. This was done by examining a portion of the graphical continuous engine speed data from the laboratory, overlaying it on the in-field data, and adjusting the time of the laboratory data until the two engine speed traces aligned as closely as possible. The continuous CO_2 data was used for time alignment purposes. To minimize differences in analyzer disque times (time elapsed between sample collection and sample analysis) between laboratory and field tests, the same sampling system was used for all testing in an attempt to keep sample transfer time and overall system lag time nearly constant. Time alignment of engine speed and raw CO_2 traces were performed visually before comparison of in-field and laboratory results. An example of the time alignment difference for the initial portion of the first iteration of the loader cycle can be seen from the continuous engine speed data in Figure 60. The same data after time alignment can be seen in Figure 61. It should be noted that the time alignment difference for the data of the first loader iteration was approximately four seconds.
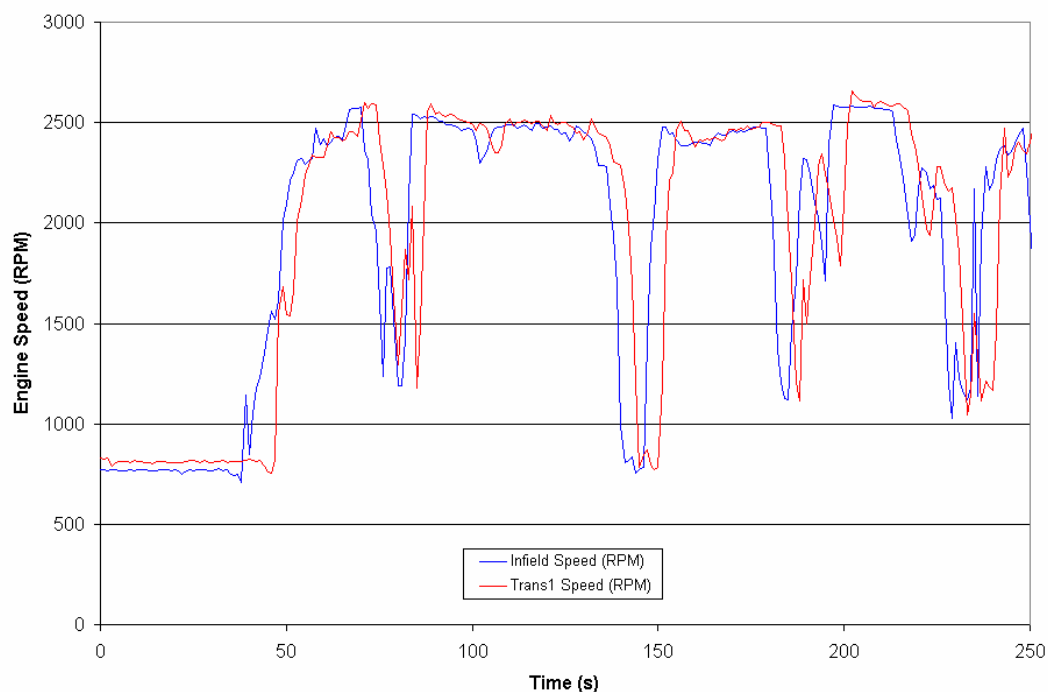
Figure 60 Comparison of In-field and First Laboratory Cycle Iteration (Trans1) Engine Speed Traces for the John Deere 6059 Loader Engine prior to Time Alignment.
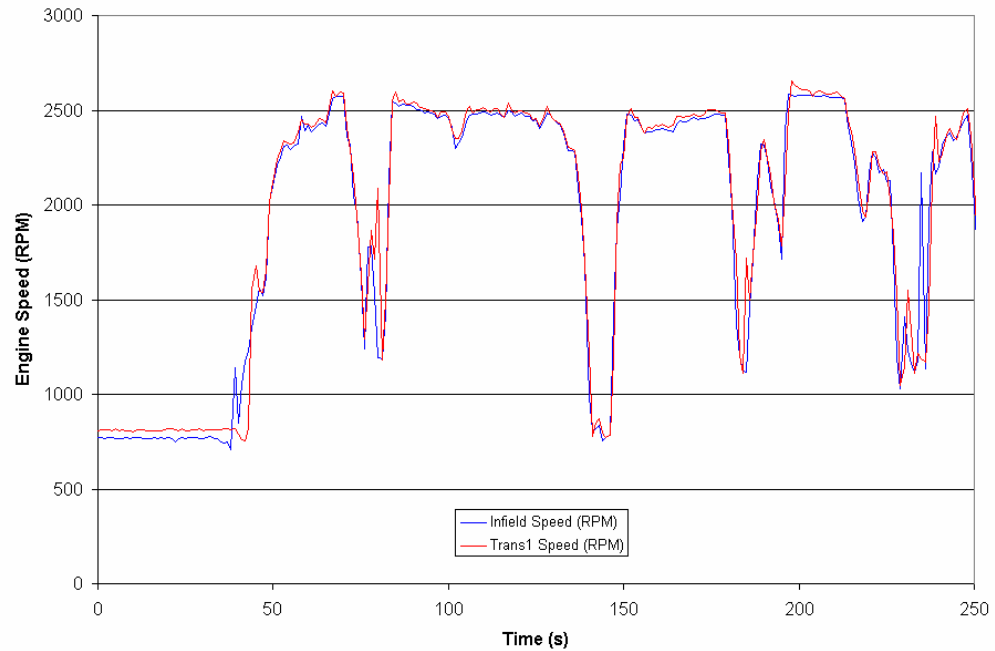
Figure 61 Comparison of In-field and First Laboratory Cycle Iteration (Trans1) Engine Speed Traces for the John Deere 6059 Loader Engine after Shifting Laboratory Data by 4-seconds for Time Alignment.
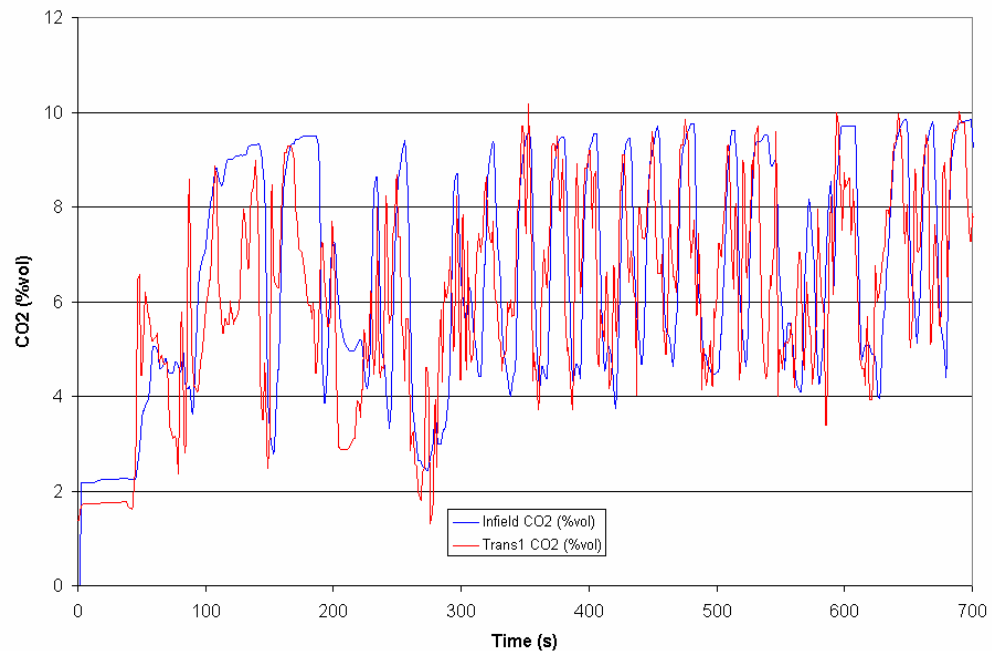
Figure 62 Comparison of In-field and First Laboratory Cycle Iteration (Trans1) CO₂ Traces for the first 700-seconds of the John Deere 6059 Loader Engine Cycle after Time Alignment.

The aligned in-field and in-laboratory CO_2 traces for the initial portion of the first iteration of the loader cycle can be seen in Figure 62. It can be seen from Figure 62 that a considerable amount of setpoint refinement was necessary to make the laboratory CO_2 data match the in-field data. Following the iterative technique and appropriate adjustments to the speed-load setpoints of the rubber-tired loader cycle, the laboratory results achieved satisfactory correlation. The final results are included in Figure 63.
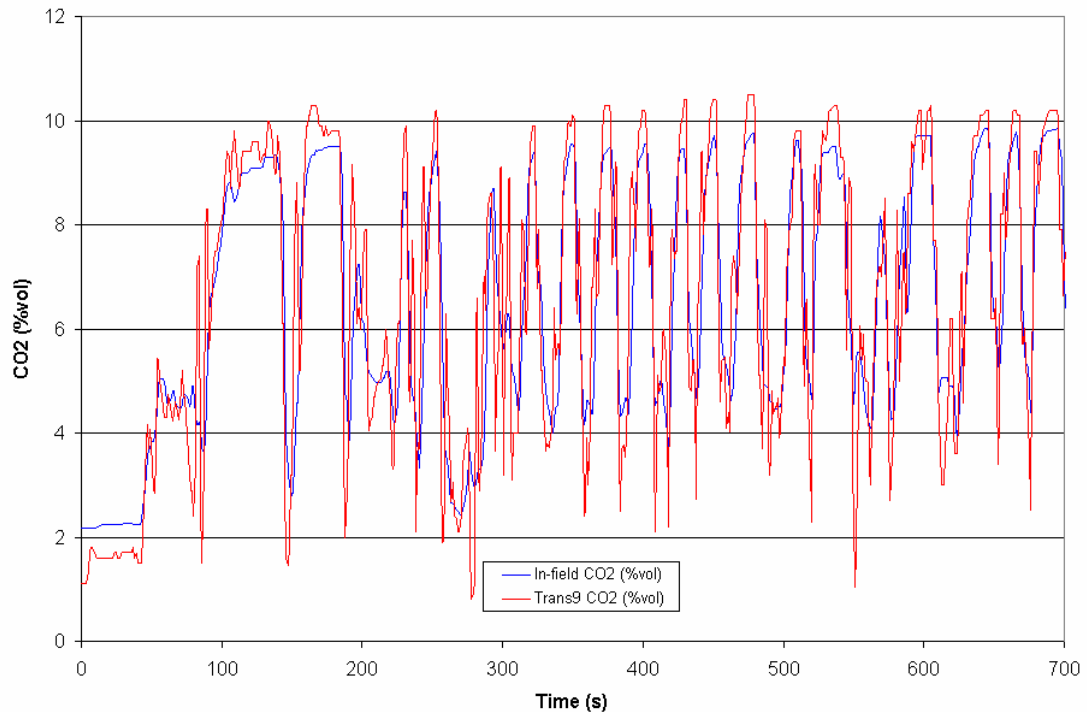
Figure 63 Comparison of In-field and Final (9th) Laboratory Cycle Iteration (Trans9) CO_2 Traces for the first 700-seconds of the John Deere 6059 Loader Engine Cycle after Time Alignment.

A number of repeat tests were run using the setpoints from the final iteration of the loader cycle for QC/QA purposes. A correlation was performed between two of the repeat tests to determine the best-expected correlation. While a perfect correlation would yield an R^2 value of 1 and a trendline equation with slope = 1 and a y-intercept of zero, many small factors present during testing prevent a perfect correlation from ever being obtained. The correlation results for repeat runs 1 and 2 using the setpoint file from the final iteration of the loader cycle can be seen in Figure 64 for the CO_2 data, while the engine speed data correlation can be seen in Figure 65.
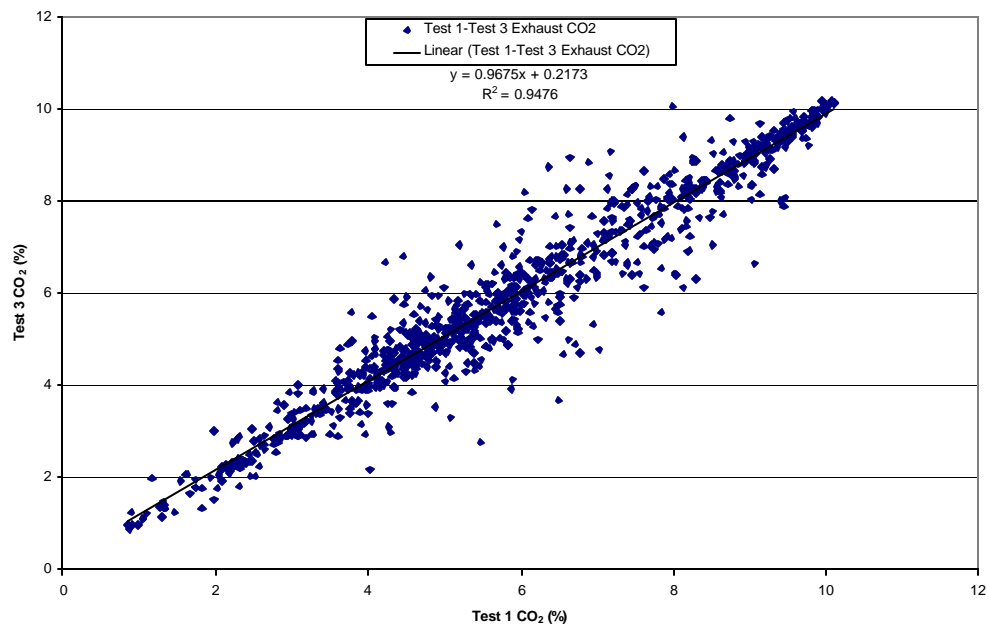
Figure 64 CO_2 Correlation Results for Two Repeat Runs of the Final Loader Cycle.
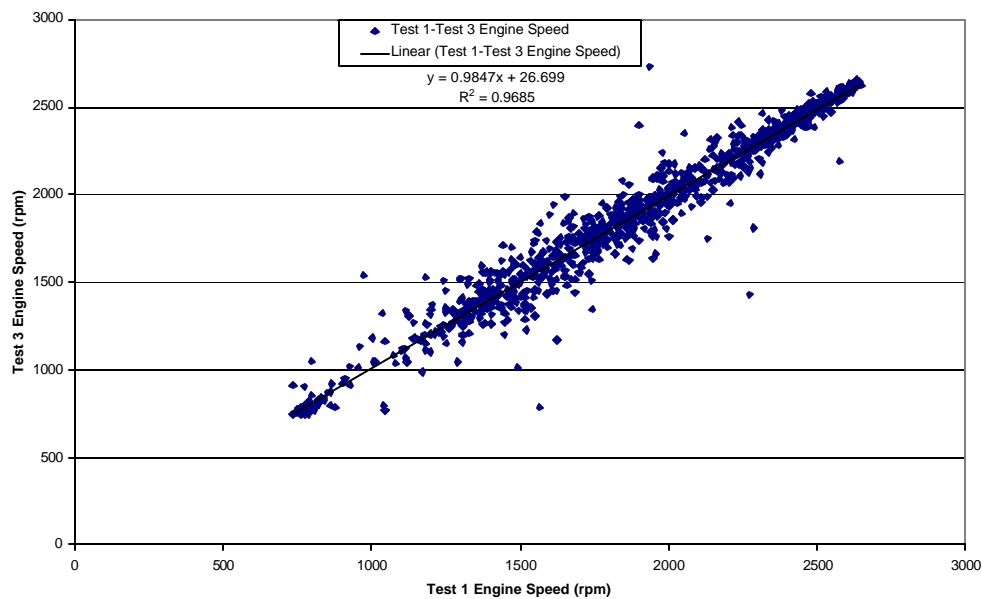
Figure 65 Engine Speed Correlation Results for Two Repeat Runs of the Final Loader Cycle.

The preceding two charts have been included to exemplify the repeatability limitations of the engine-dynamometer-raw gas measurement system. For the CO_2 data,

an R^2 value of about 0.9476 with a trendline slope of 0.9675 and y-intercept of 0.2173 was the test-to-test correlation established for the loader engine dynamometer system. The engine speed data correlated with an R^2 value of approximately 0.9685 with a trendline slope of 0.9847 and y-intercept of 26.7. While these numbers could slightly vary for any two runs of the same test, other test comparisons support the above correlation criteria. These criteria served as the target criteria for the in-field to derived cycle comparisons. Obviously with inherent differences between the characteristic response of the engine-in-vehicle and engine-dynamometer these criteria were likely not to be satisfied. However, iteration was conducted until asymptotic values were achieved. Moreover, exhaust emissions results between the first and final iterations are presented in Section 4.6 in order to illustrate the effect of cycle refinement on cycle-integrated emissions.

Figure 66 illustrates the large discrepancy between the in-field CO_2 trace and the laboratory trace collected during the running of the complete first cycle iteration. A perfect correlation, considering the test-to-test CO_2 variability discussed in the preceding paragraph, would yield an R^2 value of about 0.9476, a trendline with a slope of 0.9675, and a y-intercept of 0.2173. Considering that the first iteration regression values included an R^2 of 0.497, a slope of 0.697, and a y-intercept of 1.966, clearly considerable refinement was necessary.
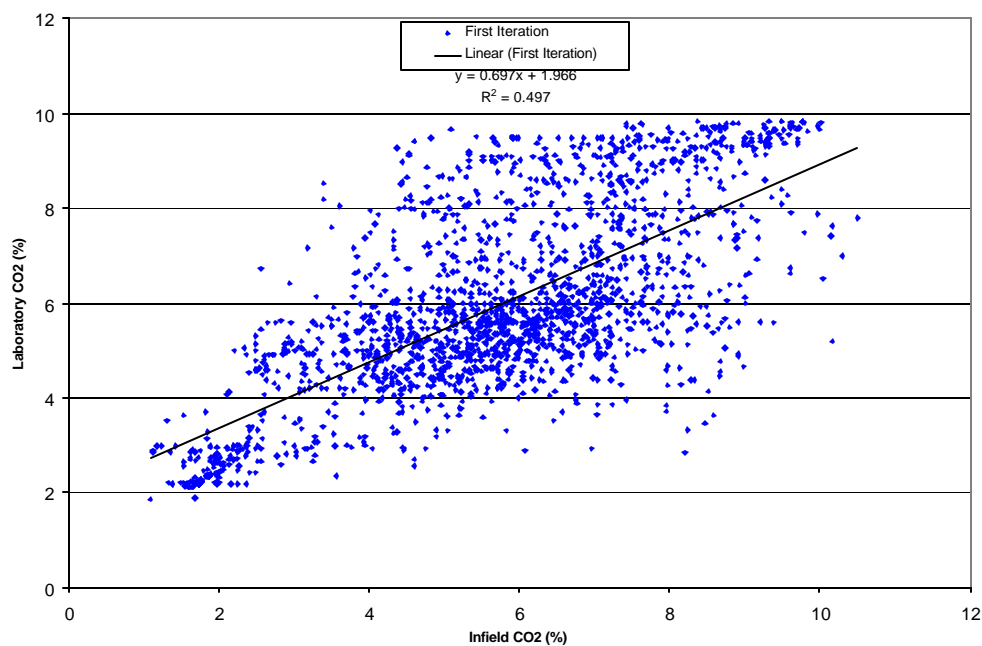
Figure 66 Correlation of the Loader CO_2 data Between the In-field and the Derived In-laboratory Cycles (First Iteration).

It was determined early in the testing that the most efficient approach for recreation of the shortened in-field cycle would be to divide it into smaller tests that could be repeated and modified (iterated) quickly. The rubber-tired loader shortened in-field cycle was divided up into three parts: 0-580-seconds, 580-900-seconds, and 900-1144-seconds. CO_2 correlation results for each portion of the final iteration of the loader cycle can be seen in Figure 67 through Figure 69.
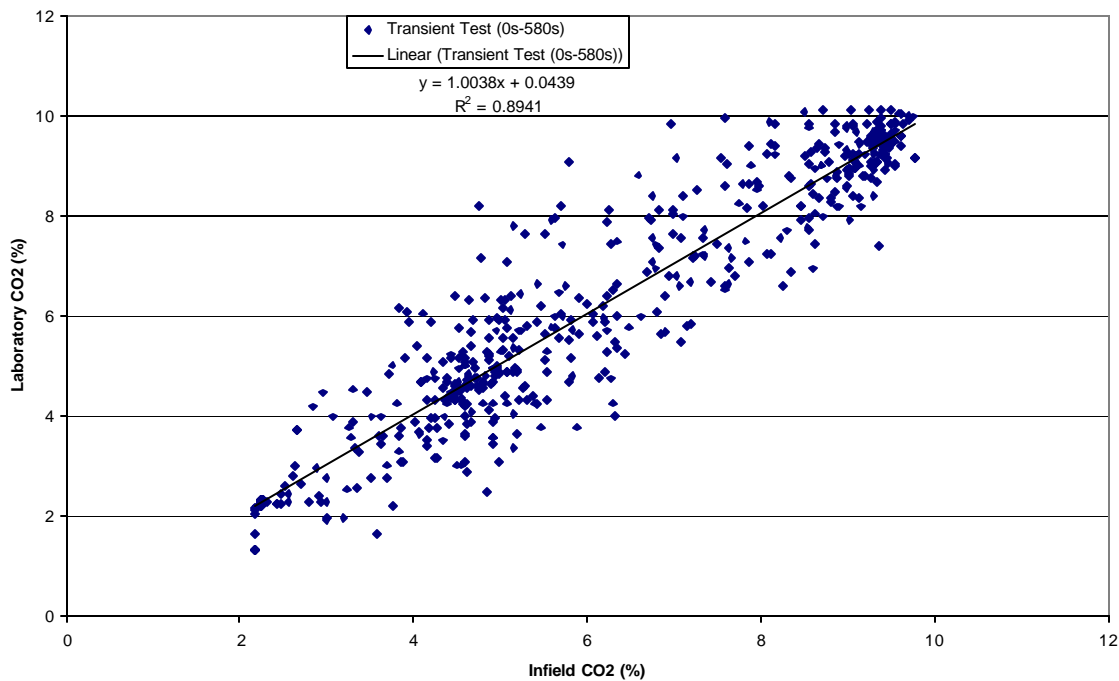
Figure 67 Correlation of the CO_2 Data between the In-field and the First Portion of the Final Iteration of the Derived In-Laboratory Loader Cycle (0s-580s).
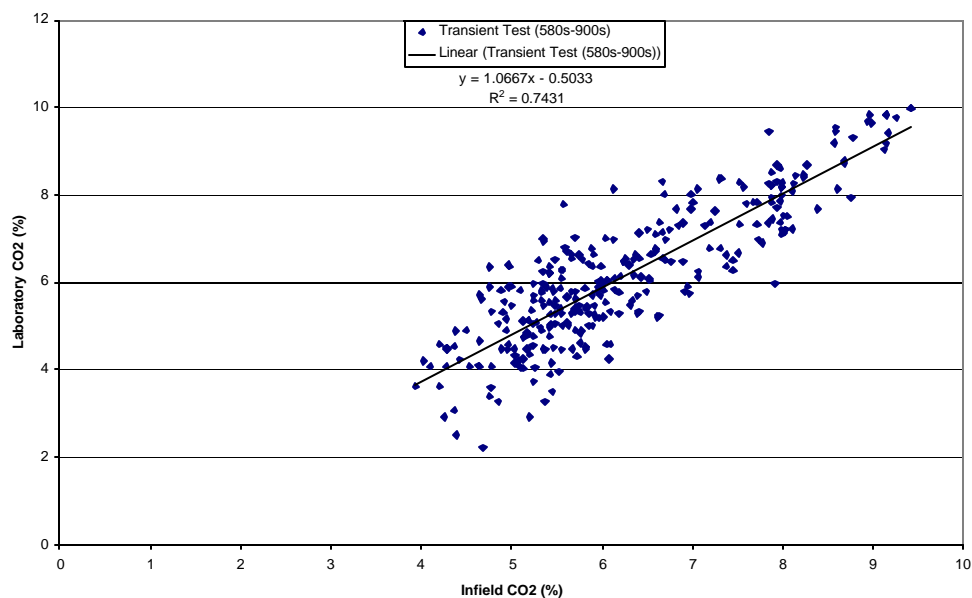
Figure 68 Correlation of the CO$_2$ Data between the In-field and the Second Portion of the Final Iteration of the Derived In-Laboratory Loader Cycle (580s-900s).
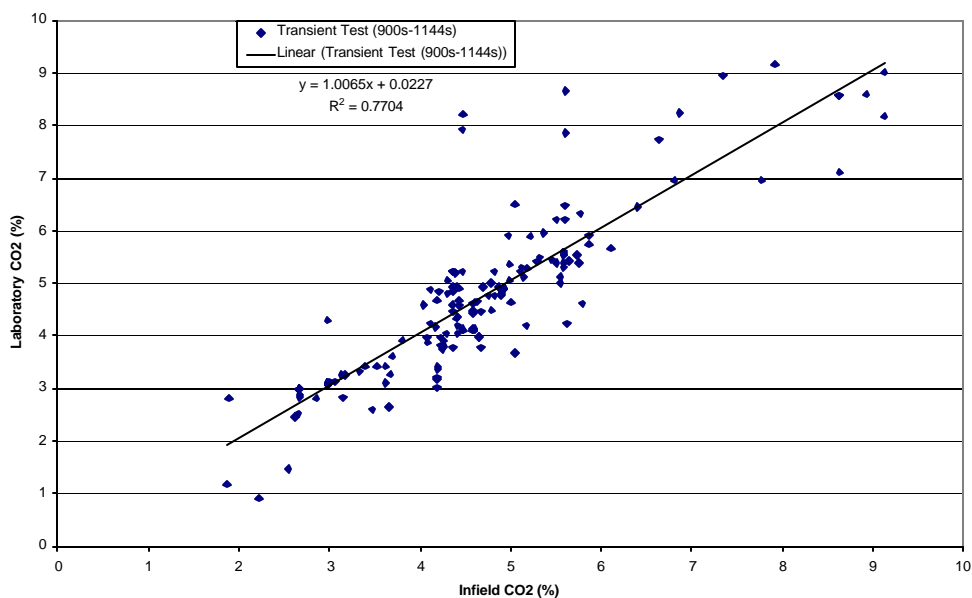
Figure 69 Correlation of the CO$_2$ Data between the In-field and the Final Portion of the Final Iteration of the Derived In-Laboratory Loader Cycle (900s-1144s).

It can be seen from the performed correlations that a significant improvement was achieved through the iterative cycle development process. The R^2 value improved from 0.497 for the first iteration to 0.8941, 0.7431, and 0.7704 for the first, second, and third portions of the final loader cycle iteration, respectively. The trendline slope improved from 0.697 to an acceptable value, and the y-intercept improved from 1.966 to a value of 0.0439, 0.5033, and 0.0227 for the first, second, and third portions of the final loader cycle iteration, respectively. While vast improvement was made through the iterative process as a whole, the changes made to the cycle for some test iterations actually reduced positive correlation. When this occurred, the speed/load setpoints from the previous iteration were restored and modified again. The new cycle was then used, and the results were checked for improvement over the previous iteration. The iterative process was continued until adjustment of the system produced no further enhancement of results.

Engine speed data was also compared during the cycle development process. It can be seen from the engine speed traces of Figure 70 and Figure 71 that the dynamometer control system was able to recreate the in-field engine speed trace much more accurately than the CO_2 trace. This is due to the fact that the engine speed signal is a direct electronic measurement with near zero lag time or calibration differences. The accuracy of engine speed recreation was improved slightly through the iteration process, mainly through adjustment of PID settings for the throttle controller. The CO_2 data, on the other hand, is affected by a number of parameters that can significantly alter results. The torque controlling aspect of the Dyn-Loc IV dynamometer controller relies on feedback from the dynamometer load cell to determine if more or less current needs to be supplied to the eddy-current dynamometer to achieve the desired torque demanded by the setpoint file. This feedback system produces the largest contribution to the difficulty in recreating the CO_2 trace that was measured in the field. Other variables such as sample line length, sample filter loading, barometric pressure, humidity, gas calibration accuracy, etc. are sources of possible deviations, but their impact was likely minimal when compared to the dynamometer torque control issues. While significant effort was put forth to minimize or eliminate the effects of these parameters, correlation results for the CO_2 traces were not realized that were equivalent to those obtained for the engine speed traces. Correlation data for the first and final cycle iterations can be seen in Figure 70 and Figure 71, respectively.
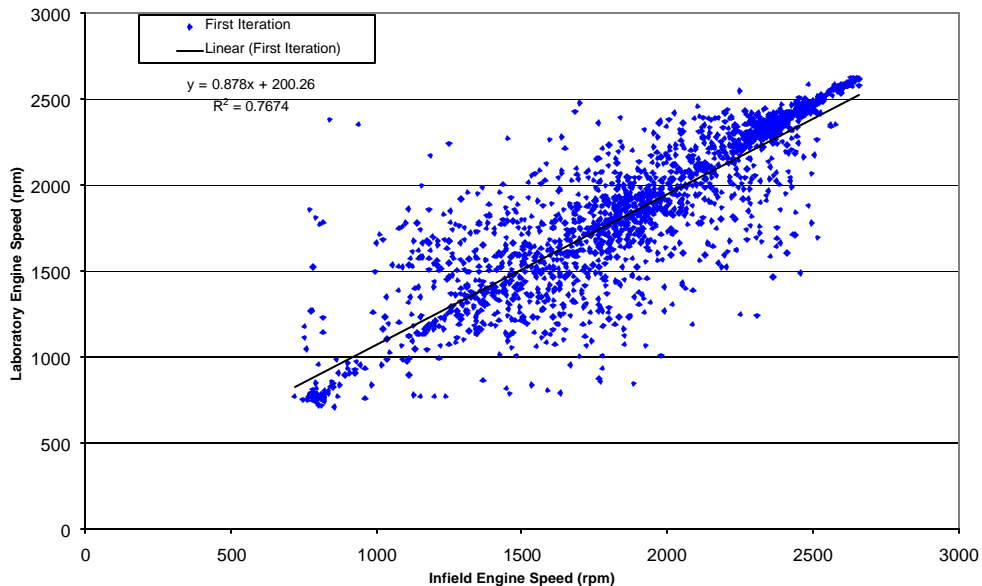
Figure 70 Correlation of the Loader Engine Speed Data between the In-field and the Derived In-Laboratory Cycles (First Iteration).
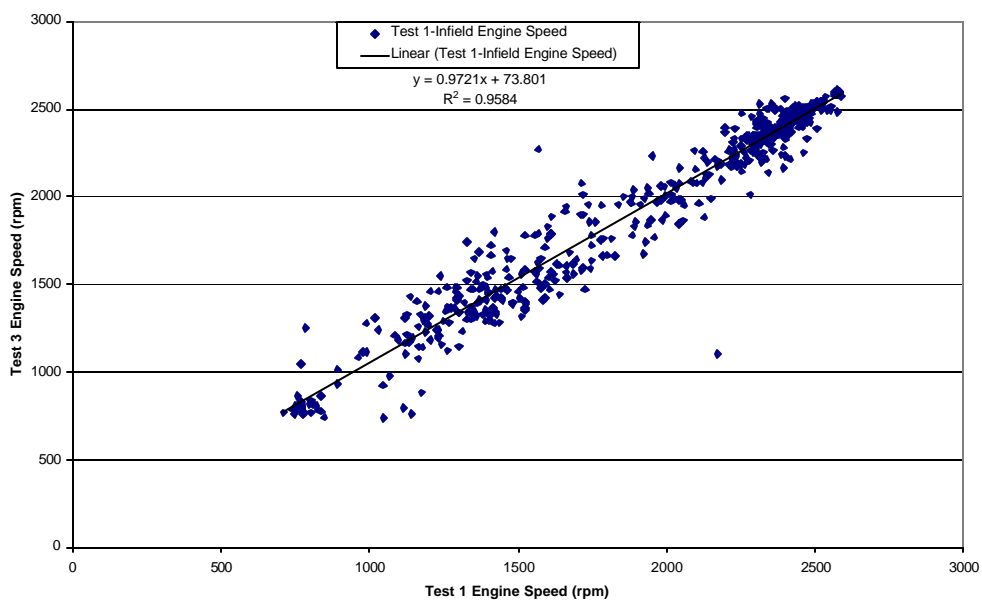
Figure 71 Correlation of the Loader Engine Speed Data between the In-field and the Derived In-laboratory Cycles (Final Iteration).

3.5.2   Street sweeper Cycle Development

The street sweeper cycle was easier to accurately recreate in the laboratory than the loader cycle due to inherent steady-state characteristics. The very nature of the sweeping process, which was less transient than the loader process, resulted in less drastic ramps of the CO_2 trace during operation. In contrast, the loader operation was relatively high-speed and very transient in nature because of the bucket loading/unloading process. Additionally, the engine speed for the street sweeper was set with a hand-twist knob during the sweeping process and an intermediate-speed governor kept engine speed relatively constant by adjusting fueling rate to compensate for differences in demanded engine load. The fueling rate of the loader, on the other hand, was controlled with a pedal operated directly by the operator's foot. For these reasons, the loader created much sharper transient events in both speed and load traces during its operation.

3.5.2.1   Engine Map

An engine mapping procedure, outlined in the CFR 40 Part 86 Subpart N [1], was performed on the John Deere 4039T street sweeper engine to determine at what engine speeds the horsepower peak (rated speed) and torque peak (intermediate speed) occur, and what values they had. The results were corrected with information supplied by Mustang Dynamometers, Inc. quantifying windage losses versus rotational speed of the eddy current dynamometer. It was found that the peak horsepower of the John Deere 4039T engine was approximately 110hp (82 kW) at 2100 rpm. The torque peak occurred at 1710 rpm and was about 295 ft-lbs (400 N-m). The engine lug curve for the John Deere 4039T can be seen in Figure 72.
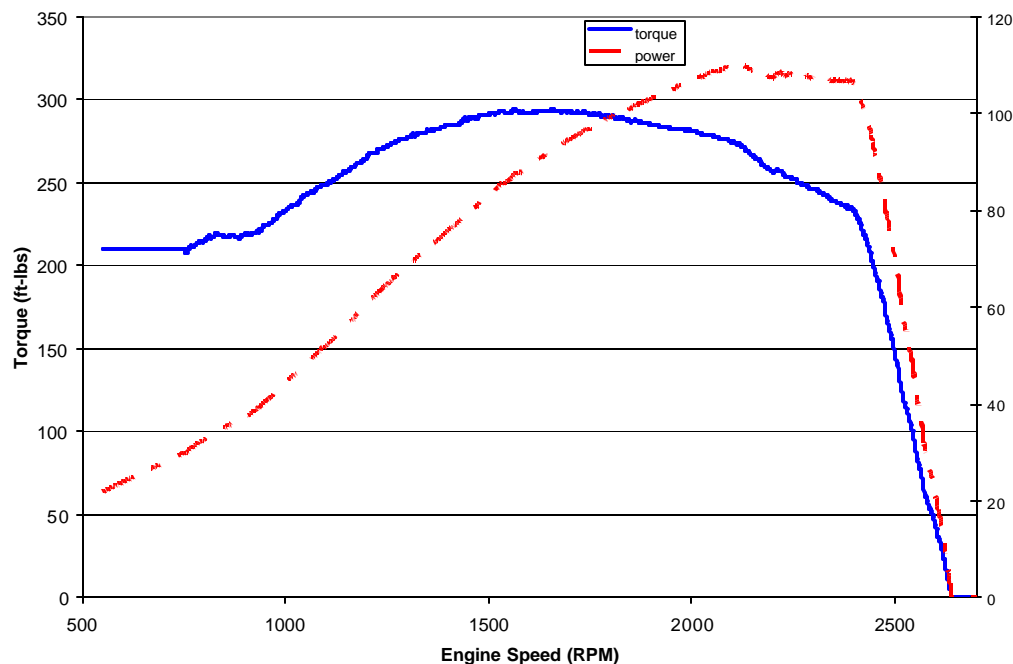
Figure 72 Engine Map for the John Deere 4039T Street sweeper Engine.

3.5.2.2   CO$_2$ Map Matrix

Just as was the case for the loader engine, the street sweeper engine was operated according to a series of speed-load setpoints and CO$_2$ levels were recorded with the in-field data collection system. For this testing, the same setup and procedures used for the in-field testing were followed. The CO$_2$ levels were recorded in the laboratory for the 4039T street sweeper engine at speeds from 700 rpm to 2700 rpm in increments of 100 rpm. Three different engine loadings were used during data collection. Load levels of 0%, 50%, and 100% of full load were used during the recording of CO$_2$ emissions. The system was allowed to stabilize for 30-seconds at each speed/load point to ensure that the CO$_2$ data had time to reach a value of at least 90% of the fully stabilized steady-state value. The system was not allowed to stabilize for more than 30-seconds to prevent skewing of the often-quick transient events encountered during cycle testing. The full load value was determined from the engine map discussed in Section 3.5.2.1 and was approximately 114hp. The data collected was used to develop the first iteration of the street sweeper transient cycle using the computer matrix interpolation program. Raw exhaust CO$_2$ data from the field was used by the program to develop a torque estimate by interpolating the data collected in the laboratory, shown in Table 11 below. The CO$_2$ data taken during the first iteration of the cycle was compared to the in-field data and a correlation of the results was performed. A manual process was then used to adjust the speed and load set points of the previous transient cycle iteration to make the CO$_2$ data match the in-field CO$_2$ data more accurately. A graphical representation of CO$_2$ data for the first and final (9th) iterations of the recreated in-laboratory cycle for the street sweeper can be seen in Figure 73 and Figure 74 along with correlations between the in-field and laboratory data.

Table 11 Matrix for the John Deere 4039T Street Sweeper Engine.

Engine Speed rpm	CO_2 (%vol) @ 0% Engine Load	CO_2 (%vol) @ 50% Engine Load	CO_2 (%vol) @ 100% Engine Load
700	1.50	6.22	10.67
800	1.55	6.42	10.67
900	1.59	6.63	10.67
1000	1.64	6.83	11.26
1100	1.69	7.04	11.91
1200	1.74	7.25	12.55
1300	1.80	7.45	12.89
1400	1.85	7.66	12.53
1500	1.91	7.76	12.17
1600	1.97	7.73	11.81
1700	2.03	7.71	11.44
1800	2.09	7.66	11.08
1900	2.15	7.55	10.72
2000	2.22	7.39	10.36
2100	2.28	7.21	9.99
2200	2.35	7.04	9.63
2300	2.43	6.84	9.27
2400	2.50	6.49	8.50
2500	2.58	5.71	5.95
2600	2.65	4.00	3.39
2700	2.73	2.73	2.73

3.5.2.3   Street Sweeper Cycle Iteration

The John Deere 4039T Street sweeper in-field cycle proved to be much easier to recreate, largely due to the experience gained through testing of the John Deere 6059 loader engine. The system setup was established during the loader engine testing, including the laborious process of optimizing the PID settings on the dynamometer controls. Another important reason for the relative ease of street sweeper cycle recreation was the cycle itself. The shortened in-field street sweeper cycle was much less transient in nature than the loader cycle due to a number of reasons discussed previously in this document. Just as was the case in the loader testing, the first step performed after running iterations of the cycle was to time-align the laboratory data with the in-field data. This was done by examining a portion of the graphical continuous engine speed data from the laboratory and overlaying it on the field data and adjusting the time of the laboratory data until the two engine speed traces aligned as closely as possible. To minimize differences in analyzer time lag between laboratory and field tests, the same sampling system and sampling line were used for all testing in an attempt to keep sample transfer time and overall system lag time nearly constant. The time difference, if any, determined by comparing the graphical engine speed data was applied to the CO_2 data as well. The aligned in-field and in-laboratory CO_2 traces for the full first iteration of the street sweeper cycle can be seen in Figure 73.
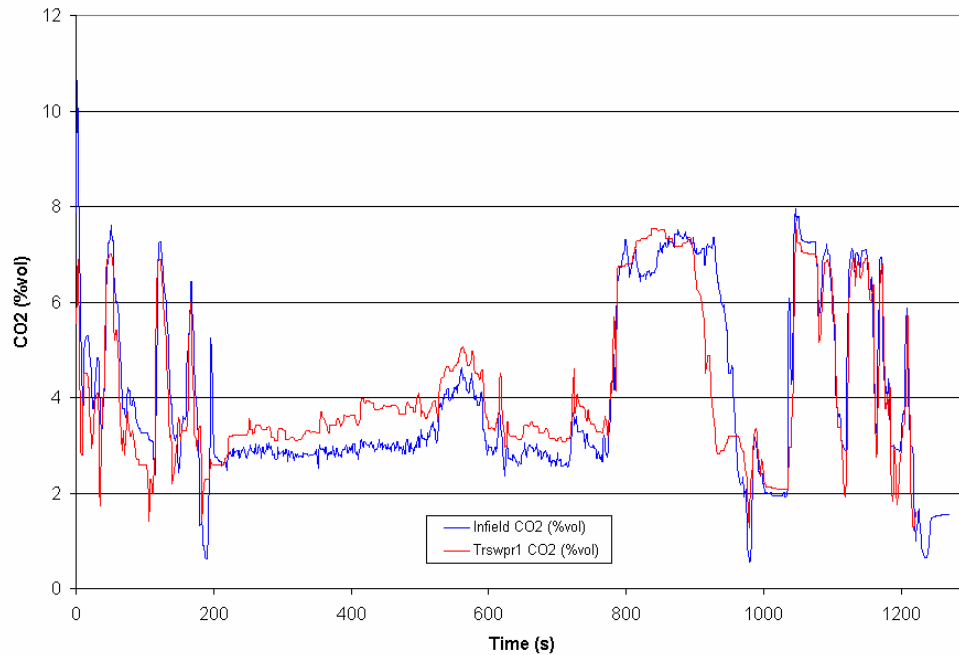
Figure 73 Comparison of In-field and First Laboratory Cycle Iteration (Trswpr1) CO_2 Traces for the John Deere 4039T Street Sweeper Engine after Time Alignment.

It can be seen from Figure 73 that a considerable amount of effort needed to be afforded in order to make the laboratory CO_2 data match the in-field data. Following the iterative technique and appropriate adjustments to the speed-load setpoints of the street sweeper cycle, the laboratory results achieved satisfactory correlation. The final results are included in Figure 74.
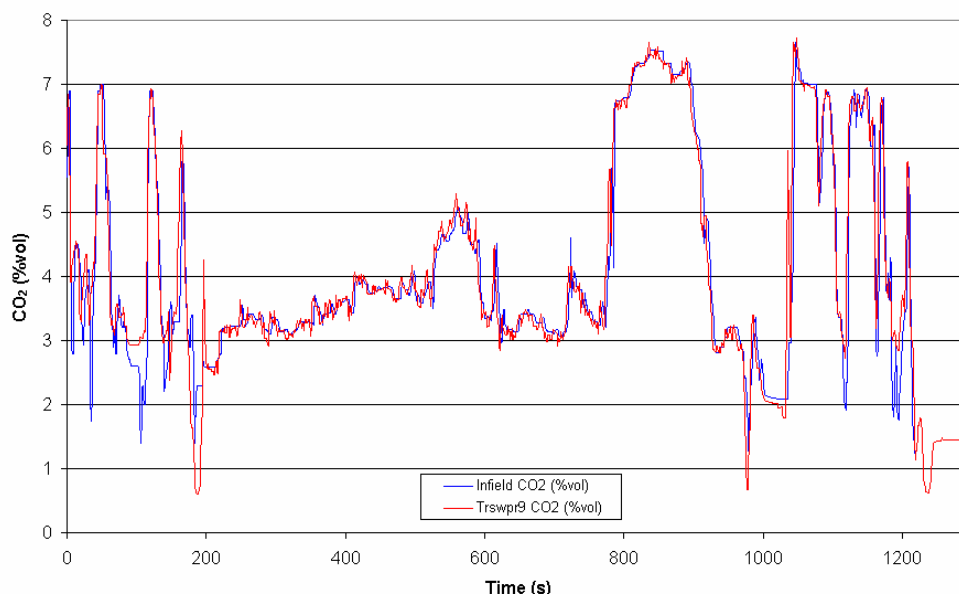
Figure 74 Comparison of In-field and Final Laboratory Cycle Iteration (Trswpr9) CO_2 Traces for the John Deere 4039T Street Sweeper Engine after Time Alignment.

A number of repeat tests were performed using the setpoints from the final iteration of the street sweeper cycle to check test-to-test variation of the CO_2 and engine speed data. A correlation was performed between two of the repeat tests to see what the best expected correlation could be. While a perfect correlation would yield an R^2 value of 1 and a trendline equation with slope = 1 and a y-intercept of zero, many small factors present during testing prevent a perfect correlation from ever being obtained. A repetitive test was performed using the setpoints from the final iteration of the street sweeper cycle to estimate what the expected "best fit" values for the linear regression could be. The correlation results for repeat runs 1 and 2 using the setpoint file from the final iteration of the street sweeper cycle can be seen in Figure 75 for the CO_2 data, while the engine speed data can be seen in Figure 76.
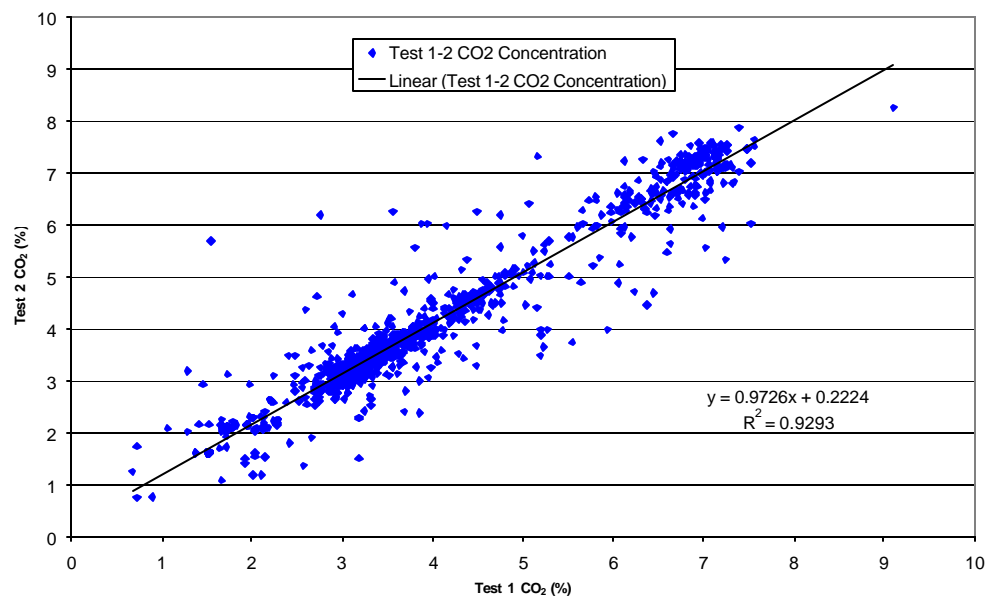
Figure 75 CO$_2$ Correlation Results for Two Repeat Runs of the Final Street Sweeper Cycle.
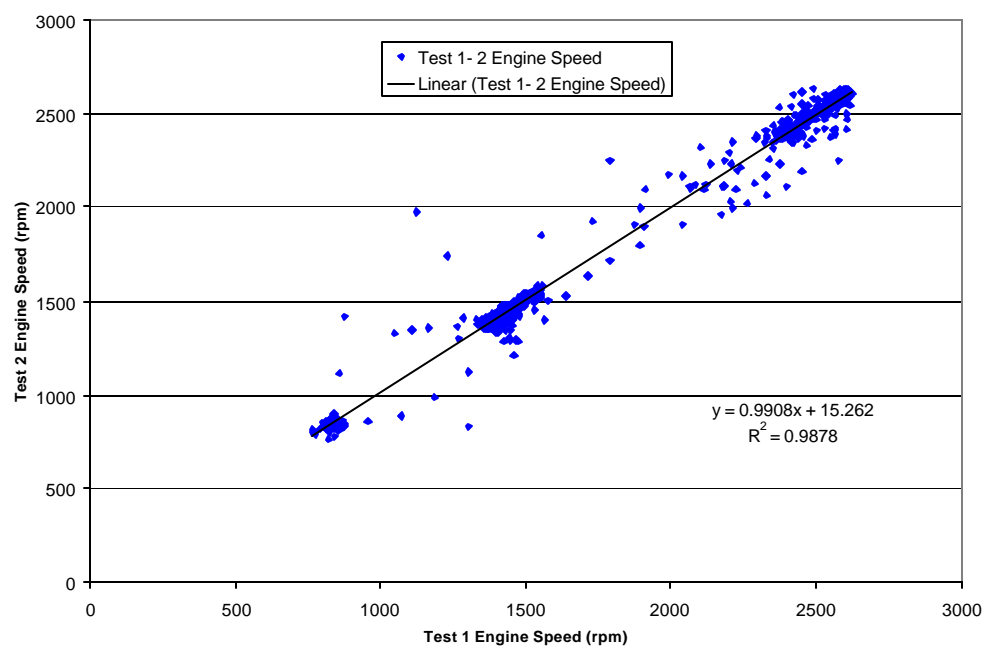
Figure 76 Engine Speed Correlation Results for Two Repeat Runs of the Final Street Sweeper Cycle.

A graphical correlation (Figure 77) illustrates the large discrepancy between the desired in-field CO_2 trace and the in-laboratory trace collected during the running of the complete first cycle iteration. The first iteration regression values of $R^2 = 0.7653$ with trendline slope of 0.7695 and y-intercept of 0.9849 were obtained. While these results are considerably better than the first iteration values for the loader cycle ($R^2 = 0.497$, slope = 0.697, y-intercept = 1.966), more work was needed on the first iteration street sweeper cycle load setpoints. The CO_2 correlation for the first iteration of the street sweeper cycle can be seen in Figure 77.
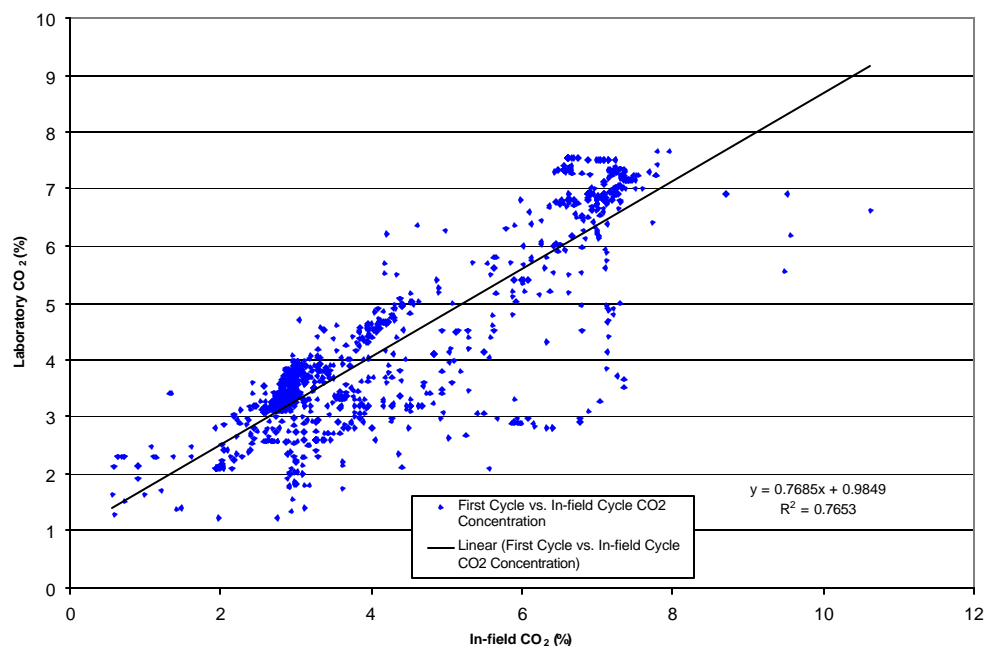
Figure 77 Correlation of the CO_2 Data between the In-field and Derived In-Laboratory Street Sweeper Cycles (First Iteration).

Significant improvement was made through cycle development with the street sweeper cycle. An R^2 value for the data of 0.8968 was obtained as well as a trendline slope of 0.9481 and a y-intercept of 0.2504. Graphical correlation results for the final iteration of the street sweeper cycle can be seen in Figure 78.
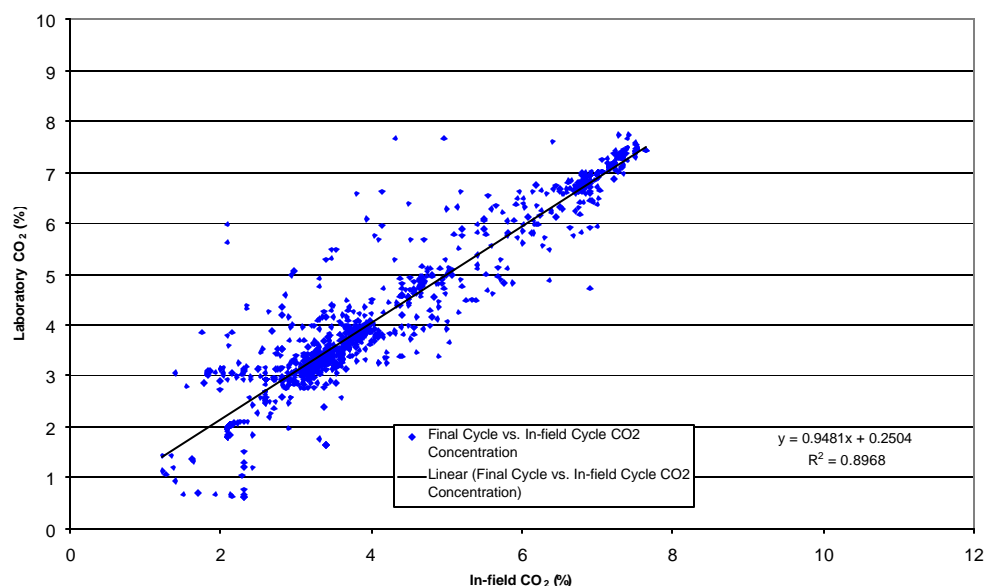
Figure 78 Correlation of the CO_2 Data between the In-field and Derived In-laboratory Street Sweeper Cycles (Final Iteration).

Engine speed data was also compared during the cycle development process. It can be seen from the engine speed traces of Figure 79 and Figure 80 that the dynamometer control system was able to recreate the in-field engine speed trace much more accurately than the CO_2 trace. This was due to the fact that the engine speed signal was a direct electronic measurement with no lag time or calibration differences. The accuracy of engine speed recreation was improved slightly through the iterative process, mainly through adjustment of PID settings for the throttle controller. The CO_2 data, on the other hand, was affected by a number of parameters that can significantly alter results. The torque controlling aspect of the Dyn-Loc IV dynamometer controller relied on feedback from the dynamometer load cell to determine if more or less current needed to be supplied to the eddy-current dynamometer to achieve the desired torque demanded by the setpoint file. This feedback system produced the largest contribution to the difficulty in recreating the CO_2-derived load cycle from the field. Other possible sources of errors that were identified: sample line length, sample filter loading, barometric pressure, humidity, and gas calibration accuracy. While significant effort was put forth to minimize or eliminate the effects of these parameters, correlation results for the CO_2 traces were not as good as they were for the engine speed traces. Linear regression results for the first iteration engine speed data were $R^2 = 0.9688$, trendline slope = 1.0097, and y-intercept = -4.9756 and were $R^2 = 0.9559$, trendline slope = 0.9624, and y-intercept = 45.484 for the final street sweeper cycle iteration. The apparently less desirable engine speed correlation results for the final iteration of the street sweeper cycle can best be explained by the backlash in the mechanical throttle linkage and the fuel

injection pump. Graphical engine speed correlation data for the first and final cycle iterations can be seen in Figure 79 and Figure 80, respectively.
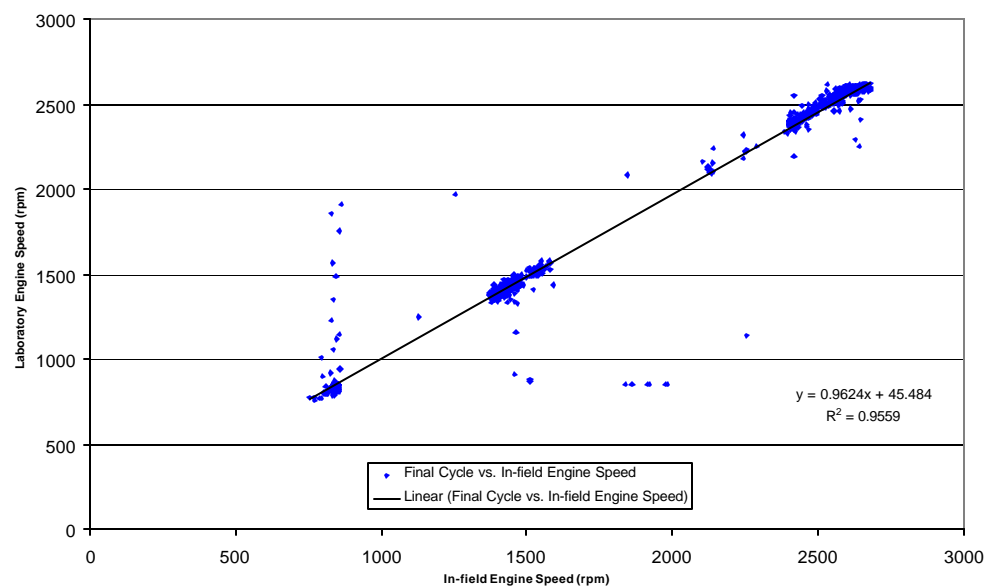

Figure 79 Correlation of the Engine Speed Data between the In-field and Derived In-laboratory Street Sweeper Cycles (First Iteration).

The chart shows a scatter plot with axis labels "Laboratory Engine Speed (rpm)" on the y-axis (0 to 3000) and "In-field Engine Speed (rpm)" on the x-axis (0 to 3000). The equation shown is:

$$y = 0.9624x + 45.484$$
$$R^2 = 0.9559$$

Legend:
- Final Cycle vs. In-field Engine Speed
- Linear (Final Cycle vs. In-field Engine Speed)
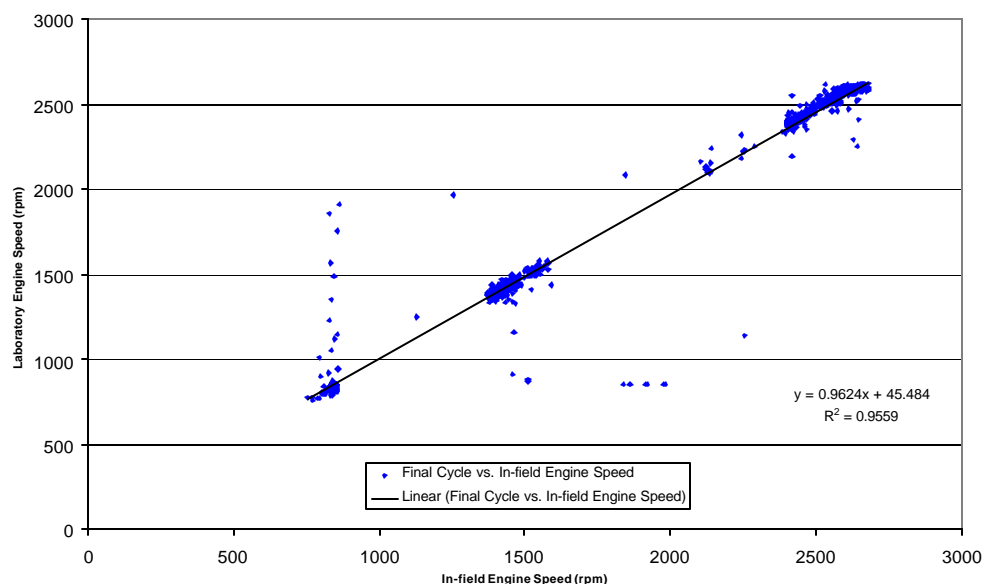
Figure 80 Correlation of the Engine Speed Data between the In-field and the Derived In-laboratory Street Sweeper Cycles (Final Iteration).

3.5.3 Excavator Cycle Development

Largely due to experience in torque inference from previous testing, the first laboratory approximations of the in-field cycle provided CO_2 traces that were relatively close to those collected in-field. First cycle results are shown in Figure 82, Figure 85, and Figure 88, for test cycles 1, 2, and 3, respectively. Visual inspection of the cycles revealed, during in-field testing, that the operation of the excavator varies from highly transient to nearly steady-state loading. As all drive and subsystems on the excavator operate via hydraulics, the engine speed will remain relatively constant and the engine load will change as more or less power demand is placed on the shaft mounted hydraulic pump. The fueling is controlled by a hand-operated lever, or by governing actuators that mount to the pump rack in order to bring engine speed up to meet loading demands to avoid stalls. During normal operation, this lever is in the full fueling position, thus simplifying cycle recreation, since varying throttle position was not present to induce error.

3.5.3.1 Engine Map

An engine mapping procedure, outlined in the CFR 40 Part 86 Subpart N [11], was performed on the Komatsu S6D125-1 engine to determine at what engine speeds the horsepower peak (rated speed) and torque peak (intermediate speed) occur, and what the respective values were. Quantifying these two points is necessary to determine the set points to be used for the steady-state 8-mode cycle and to allow the compilation of the CO_2 map matrix used for development of the transient cycle. The resultant lug curve for the Komatsu S6D125-1 (Figure 81) indicated that peak horsepower was approximately

250 hp (186 kW) and occurred at 1800 rpm, while the torque peak occurred at 1010 rpm and was approximately 745 ft-lbs (1010 N-m).
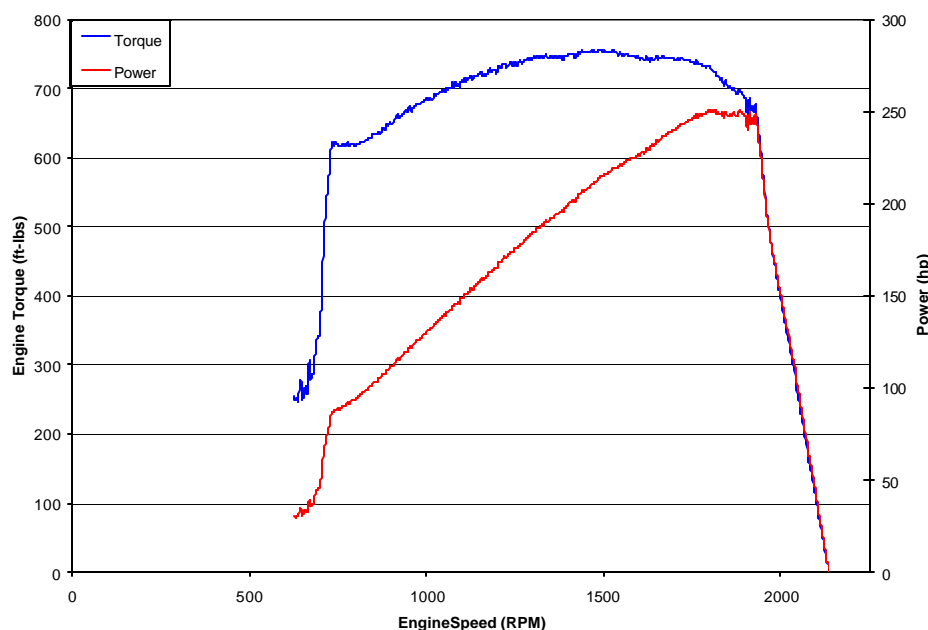
Figure 81 Komatsu Excavator S6D125-1 Engine Map

3.5.3.2 CO_2 Map Matrix

Similar to the other engines, the excavator engine was operated according to a series of speed-load setpoints and CO_2 levels were recorded with the in-field data collection system. For this testing, the same setup and procedures used for the in-field testing were followed. The CO_2 levels were recorded in the laboratory for the S6D125-1 excavator engine at speeds from 650 rpm to 2250 rpm in increments of 100 rpm. Three different engine loadings were used during data collection. Load levels of 10%, 50%, and 100% of full load were used during the recording of CO_2 emissions. The system was allowed to stabilize for 30-seconds at each speed/load point to ensure that the CO_2 data had time to reach a value of at least 90% of the fully stabilized steady-state value. The system was not allowed to stabilize for more than 30-seconds to prevent skewing of the often-quick transient events encountered during cycle testing. Results from this procedure are summarized in Table 12. The full load value for each speed was determined from the engine map discussed in Section 3.5.3.1. The data collected was used to develop the first iteration of the street sweeper transient cycle using the computer matrix interpolation program. Raw exhaust CO_2 data from the field was used by the program to develop a torque estimate by interpolating the CO_2 matrix data collected in the laboratory. The CO_2 data taken during the first iteration of the cycle was compared to the in-field data and a correlation of the results was performed. A manual process was then used to adjust the speed and load set points of the previous transient cycle iteration to make the CO_2 data match the in-field CO_2 data more accurately.

Table 12 Matrix for the Komatsu S6D125-1 Excavator Engine

Engine Speed (rpm)	CO_2 (%vol) @ 10% Engine Load	CO_2 (%vol) @ 50% Engine Load	CO_2 (%vol) @ 100% Engine Load
650	1.12	1.09	1.13
750	2	5.95	12.23
850	2.12	5.98	11.86
950	2.2	6.18	11.35
1050	2.33	6.34	11.04
1150	2.4	6.44	10.66
1250	2.55	6.57	10.33
1350	2.6	6.48	9.84
1450	2.65	6.29	9.63
1550	2.64	6.05	9.1
1650	2.7	5.93	8.66
1750	2.79	5.89	8.4
1850	2.72	5.82	8.14
1950	2.65	5.24	7.42
2050	2.43	3.44	4.95
2150	1.19	1.32	1.38
2250	1.19	1.32	1.38

A graphical representation of CO_2 data for the first and final iterations of the recreated in-laboratory cycle for the excavator can be seen in Figure 82 and Figure 83, along with correlations between the in-field and laboratory data.

Upon conference with CARB regarding vehicle activity, it was decided that three identified operations – digging/loading (cycle 1), shown in Figure 83, transport (cycle 2), shown in Figure 86, and trenching (cycle 3), shown in Figure 89, – would be investigated as separate test cycles. By doing so, the emissions results and vehicle activity could be combined so as to be most representative of actual vehicles in a given study area. The continuous CO_2 data from the first cycles was compared to the field data, and the iterative approach, similar to that discussed earlier in the report, was used to arrive at an acceptable correlation between laboratory and in-field data. The correlation graphs are shown in Figure 84, Figure 87, and Figure 90, for cycles 1, 2, and 3, respectively.
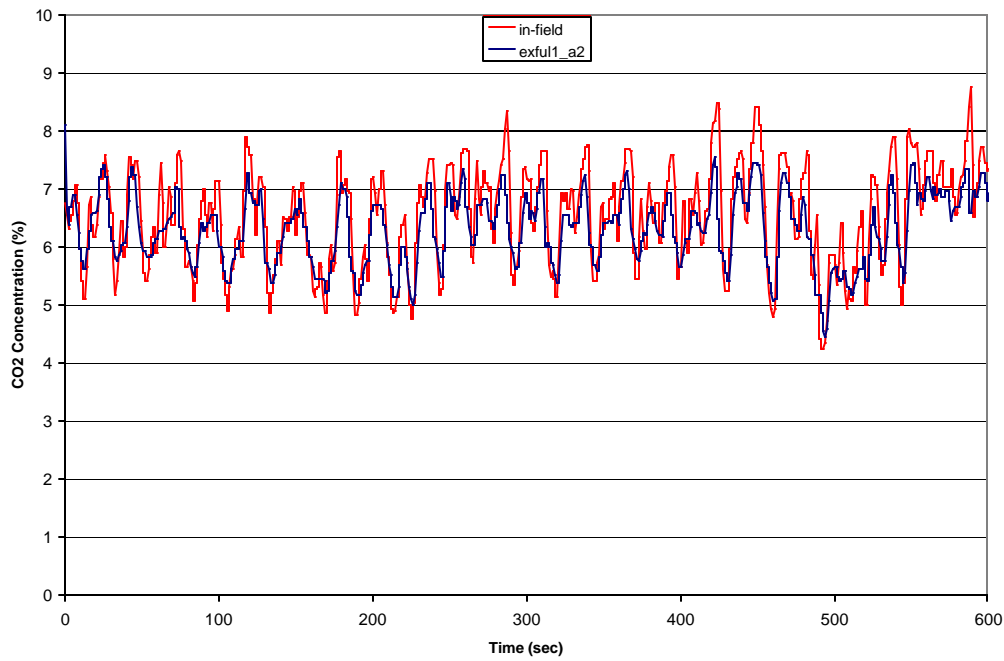
Figure 82 Excavator Test Cycle 1 First Approximation Results
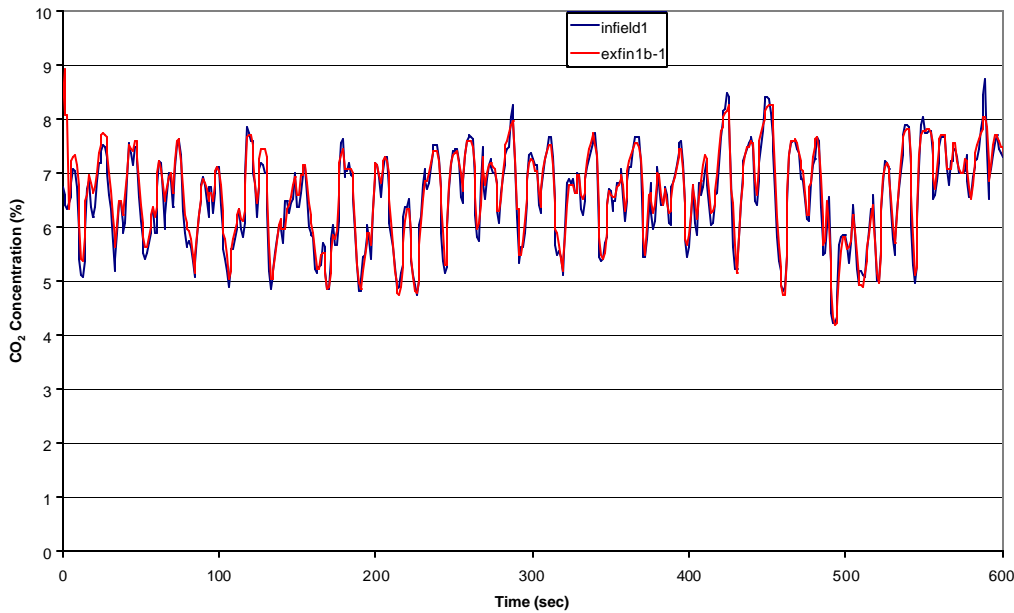
Figure 83 Excavator Test Cycle 1 Final Test Results
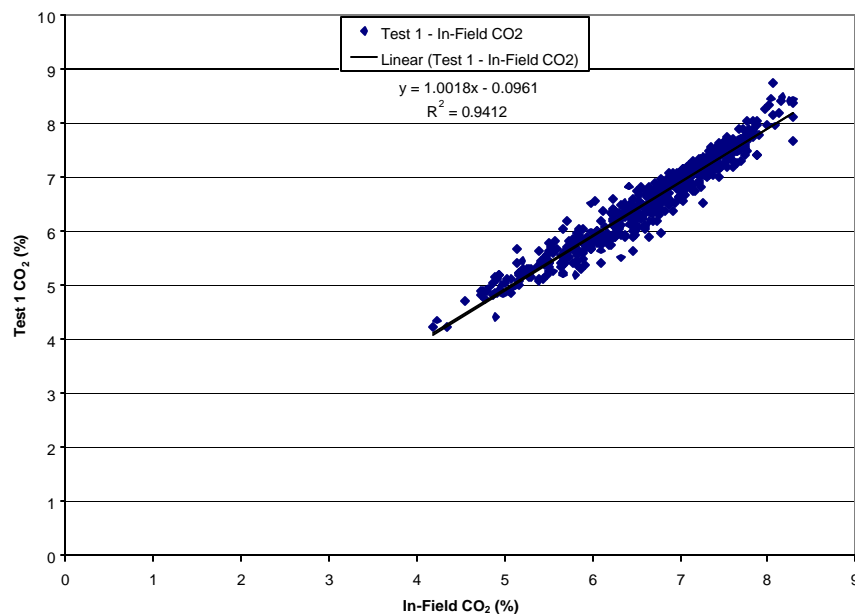
Figure 84   Excavator Test Cycle 1 Correlation

Review of this figure suggests excellent correlation between the test cycle and in-field raw CO_2 measurements. The correlation returned a slope very near to 1 and an intercept very near to zero. The R^2 value for this regression is 0.9412, indicating very close correlation.
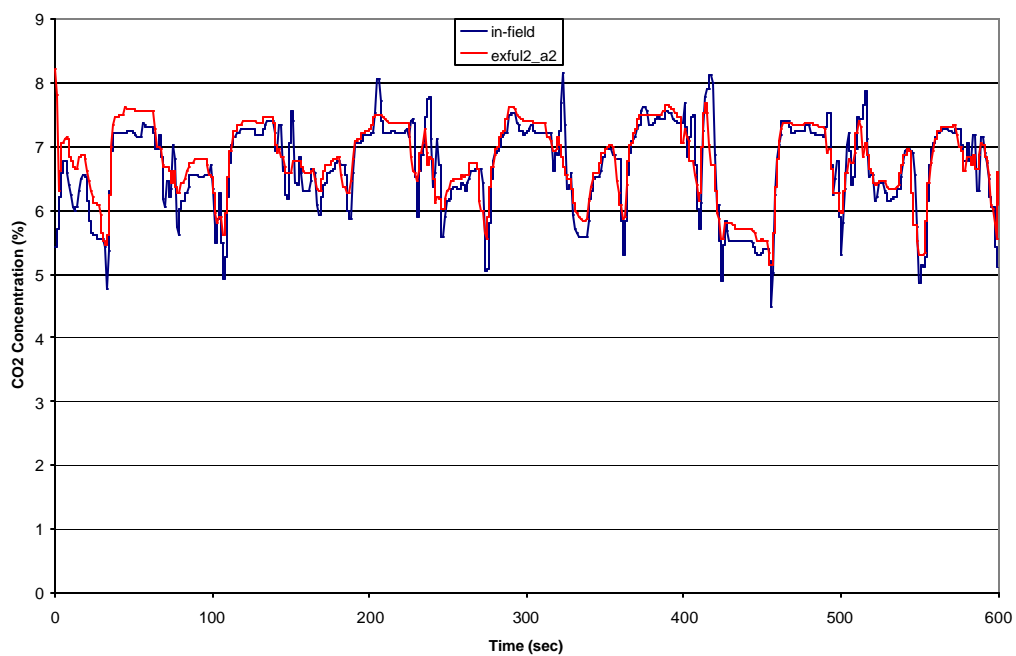
Figure 85 Excavator Test Cycle 2 First Approximation Results
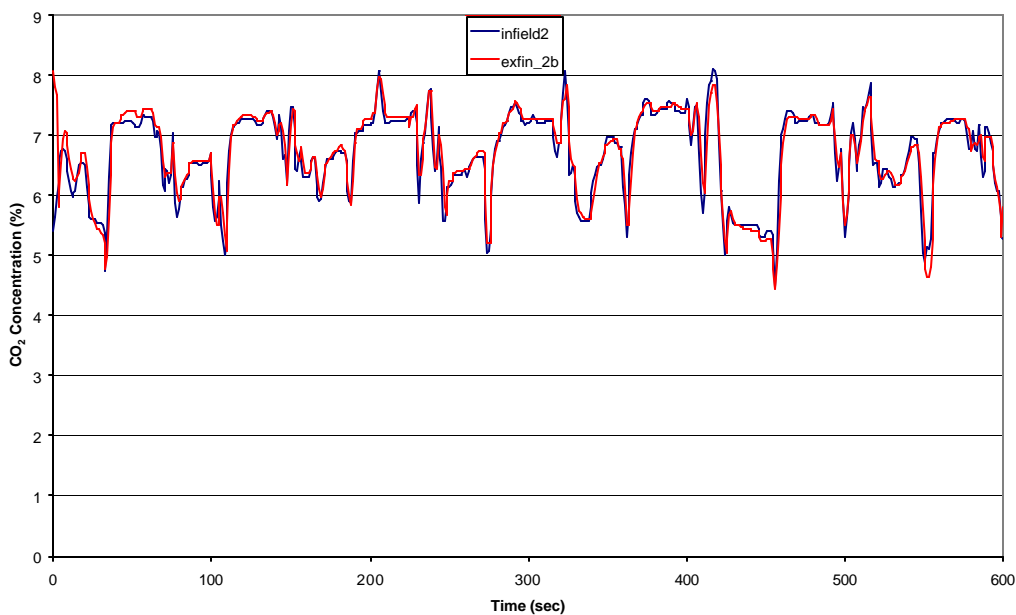
Figure 86 Excavator Test Cycle 2 Final Test Results
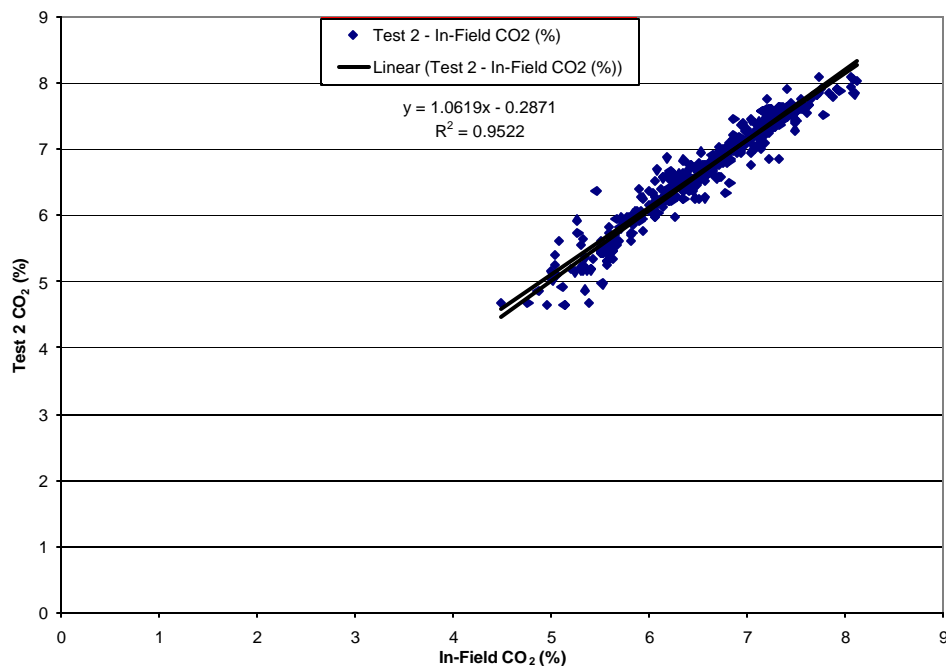
Figure 87 Excavator Test Cycle 2 vs. In-field CO$_2$ Correlation

Review of cycle 2 indicated a very close correlation between in-field and in-lab results, with a slope of 1.0619, an intercept of 0.2871, and a R^2 value of 0.9522.
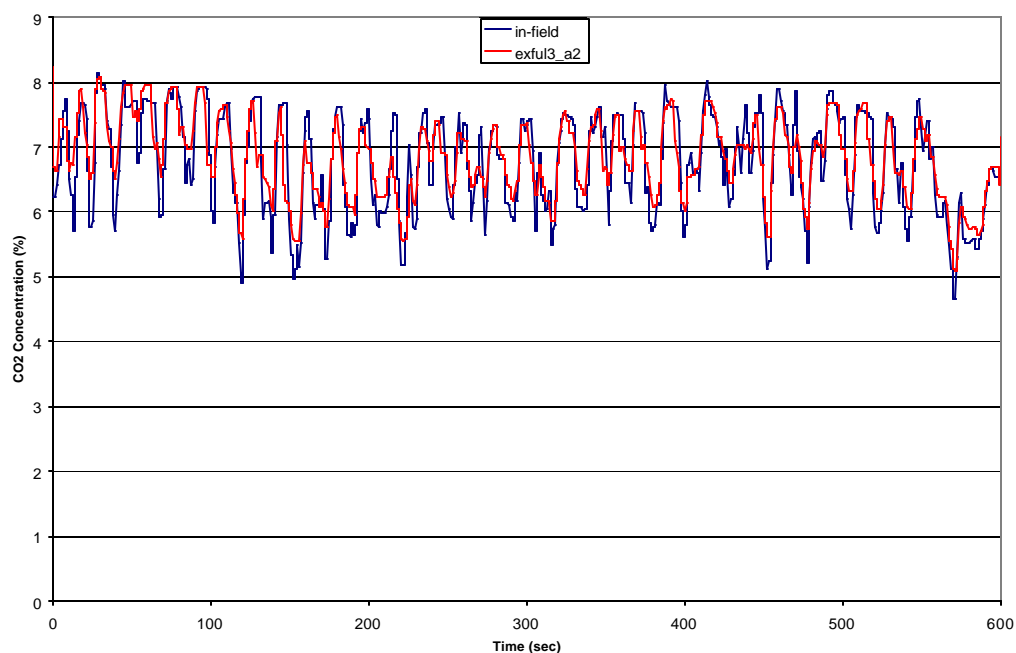
Figure 88 Excavator Test Cycle 3 First Approximation Results
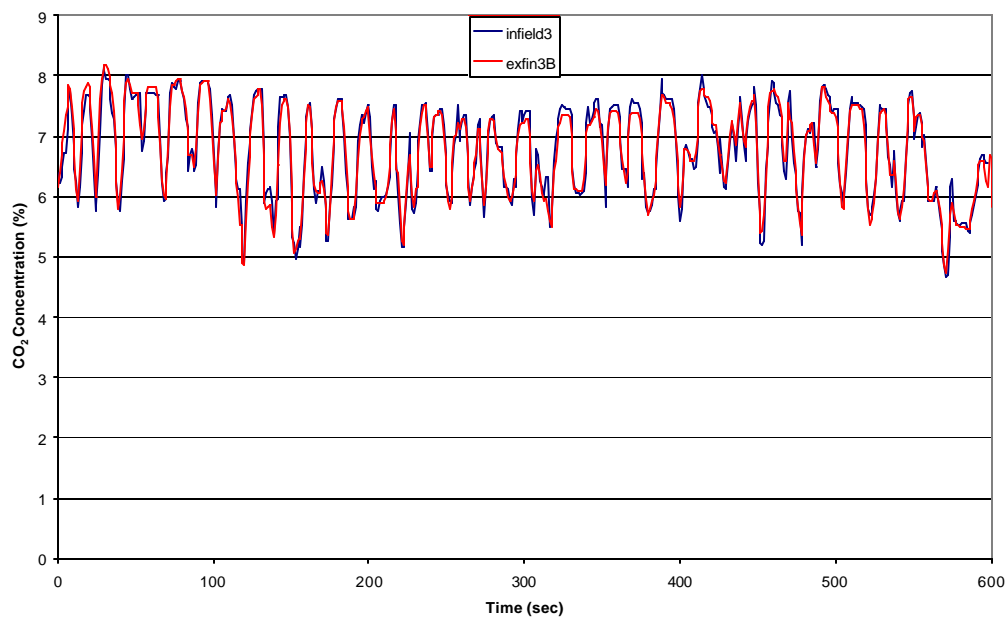
Figure 89 Excavator Test Cycle 3 Final Test Results
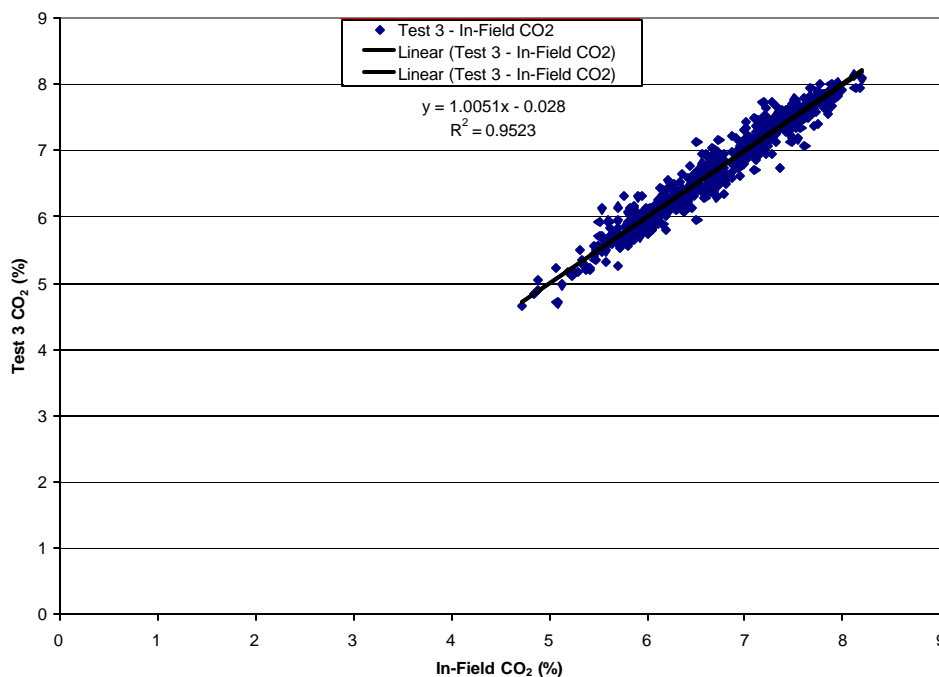
Figure 90 Correlation of CO$_2$ Data from Excavator Final Cycle 3 Test and In-field Results

Cycle 3 returned the best correlation results of all three cycles, with a slope of 1.005, an intercept of 0.028, and a R^2 value of 0.9523. The results indicate that all cycles returned CO$_2$ traces that were as close to the in-field data as could be expected.

3.6 In-Laboratory Emissions Testing Results

Full-flow dilution tunnel emissions tests were performed in the laboratory on the three engines that were removed from the vehicles (street sweeper, rubber-tired loader, and excavator). These engines were operated according to standardized steady-state 8-Mode, certification-type test cycles as well as transient tests that were developed from the in-field data. This transient test cycle development is discussed in detail in Section 4.4.

The steady-state engine dynamometer test cycles were adopted from the ISO/DIS 8178-4 Section 6.3.1.1 standards entitled "Test Cycles Type C – Off-Road Vehicles and Industrial Equipment," and resemble the set points outlined by CFR 30, Part 7 [1]. The engine speed and load factors of the 8-Mode test are shown in Table 13 and the weighted 8-mode data given in Chapter 4 of this document was reduced based on the associated weighting factors outlined in the Table 13.

Table 13 The ISO 8-Mode Cycle.

Mode Number	Engine Speed	Load Factor (Percent Load)	Weighting Factor
1	Rated	100	0.15
2	Rated	75	0.15
3	Rated	50	0.15
4	Rated	10	0.10
5	Intermediate	100	0.10
6	Intermediate	75	0.10
7	Intermediate	50	0.10
8	Idle	0	0.15

3.6.1   Rubber-Tired Loader In-Laboratory Results

Two types of in-laboratory testing were performed on the loader engine. The first tests performed were steady-state emissions tests that followed the ISO-8178 Test C 8-mode test cycle. The second series of testing consisted of final transient cycle emissions tests that followed the speed/load setpoints derived from the in-field data and discussed in detail in the Cycle Development section of this thesis.

3.6.1.1   Loader Steady-State 8-Mode Test Results

The ISO-8178 8-mode steady-state tests that were conducted consisted of four modes run at rated speed, three modes run at intermediate speed, and a "no-load" idle mode. Parasitic windage losses of the eddy current dynamometer were determined for all 8-mode testing speeds and the data was corrected for these losses when reduced. Mustang Dynamometers, the dynamometer manufacturer, provided estimates of the windage losses (in ft-lbs) of the dynamometer at any speed point. The rated and intermediate speeds were obtained from the engine maps run on the engines prior to testing. The setpoints were determined using the rated and intermediate speed from the engine map and the percentages of maximum torque described in Table 13 of Section 4.6 of this document. A graphical representation of the engine map for the loader engine can be seen in Figure 59. The 8-mode speed and load set points for the 6059 loader engine can be seen in Table 14.

The average emissions results for all gases and PM of the three 8-mode repeat tests performed can be seen in Table 15 with a graphical representation seen in Figure 91. The weighted results illustrated in Figure 92 were determined by multiplying the average results of Table 15 by the weighting factors outlined in Table 13 of Section 4.6. Results for all three runs of the 8-mode test are included in tabular form in the appendix of this report.

Table 14 Loader 8-Mode Engine Speed/Load Set Points.

Mode Number	Engine Speed (rpm)	Torque (ft-lbs)	Horsepower (hp)
1	2375	232.3	105.0
2	2375	174.2	78.8
3	2375	116.2	52.5
4	2375	23.2	10.5
5	1010	277.9	53.4
6	1010	208.4	40.1
7	1010	139.0	26.7
8	≈ 800	0.0	0.0

Table 15 Average of 8-Mode Results for the John Deere 6059 Loader Engine (g/bhp-hr).

	Mode 1	Mode 2	Mode 3	Mode 4	Mode 5	Mode 6	Mode 7	Mode 8	Weighted Results
HC	0.33	0.48	0.99	9.74	0.48	0.40	0.73	22.48	4.77
CO	2.02	2.86	3.18	18.48	4.17	0.30	1.09	35.32	8.91
CO_2	483.7	497.3	556.0	1236	471.3	334.6	483.0	4235	1118.0
NO_x	11.72	10.32	7.90	9.21	20.78	13.03	16.64	107.1	26.51
PM	0.188	0.367	0.347	0.849	0.172	0.083	0.094	1.641	0.502
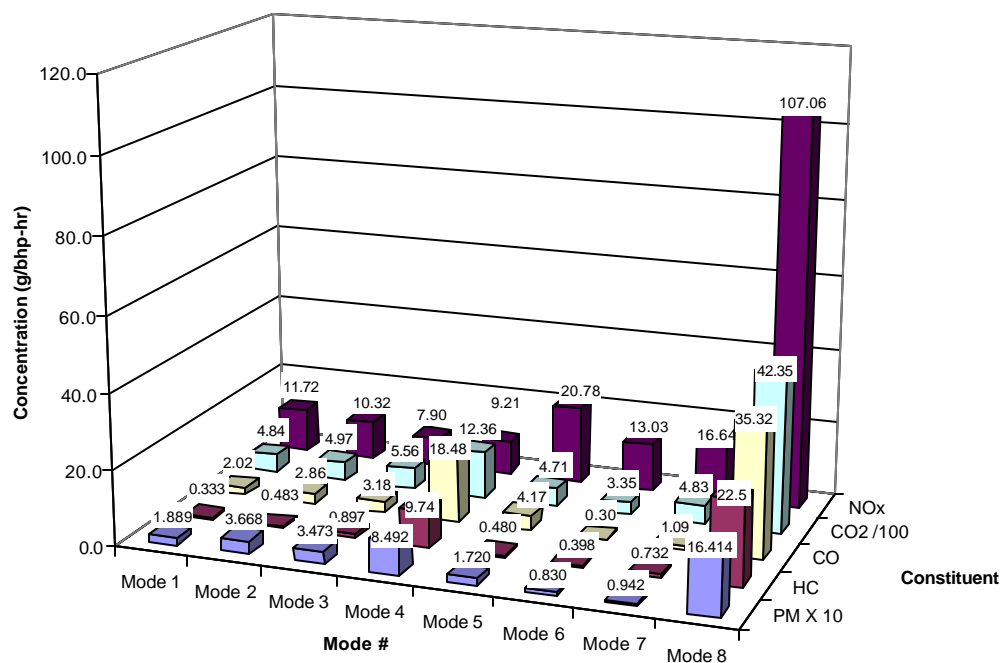
Figure 91 Average of 8-Mode Emissions Results for the John Deere 6059 Loader Engine (g/Bhp-hr).
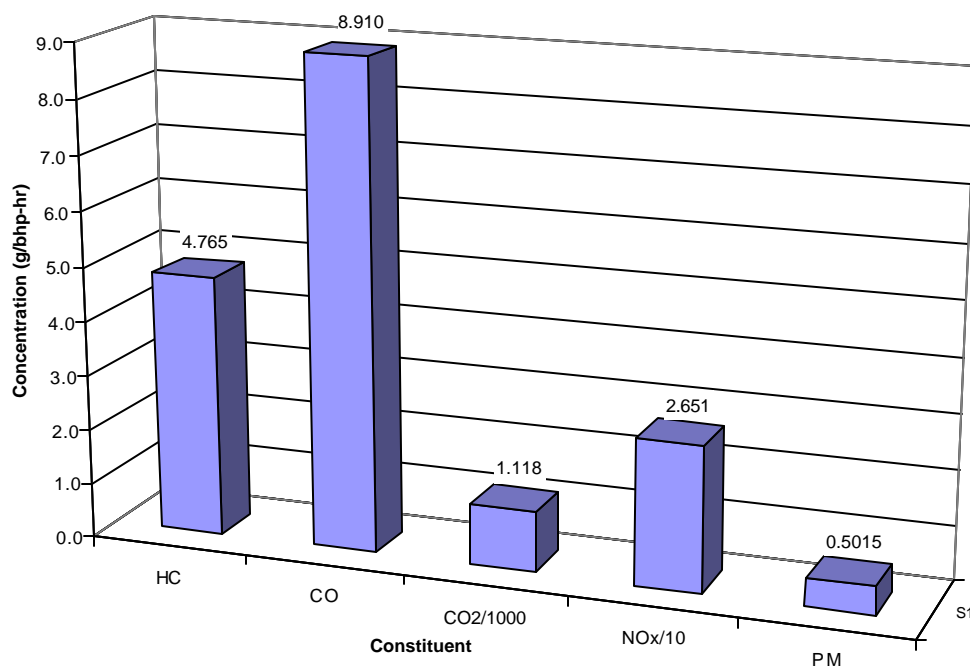
Figure 92 Average Weighted 8-Mode Results for the John Deere 6059 Loader Engine (g/Bhp-hr).

3.6.1.2   Loader Transient Cycle Test Results

In-laboratory transient cycle results for the John Deere 6059 loader engine can be seen in Table 16 with a graphical representation shown in Figure 93. All gaseous emissions data was found to be repeatable, with PM varying slightly from test to test. A total of five emissions tests were performed using the final iteration of the loader cycle for repeatability analysis. A graph of two repeated continuous CO_2 data traces can be seen in Figure 94 while the repeat engine speed traces are illustrated in Figure 95. A correlation of the CO_2 and engine speed data can be seen in Section 4.5.1.2 in Figure 64 and Figure 65, respectively. In the case of the loader, no full flow emissions data was collected in the laboratory during any of the previous cycle iterations with the laboratory-grade analyzers. Full-flow laboratory data was collected for the first and final iterations of the street sweeper cycle in order to investigate the effects of cycle refinement on emission levels, the results of which are included in Section 4.6.2.2.

Table 16 Transient Cycle Emissions Results for the John Deere 6059 Loader Engine (g/bhp-hr).

	Test 1	Test 2	Test 3	Test 4	Test 5	Average
HC	0.70	0.76	0.72	0.75	0.78	0.74
CO	2.05	2.17	2.19	2.17	2.27	2.17
CO$_2$	543.8	547.7	547.7	545.8	547.6	546.4
NO$_x$	8.15	8.12	8.05	8.03	8.13	8.10
PM	0.183	0.168	0.174	0.199	-	0.181
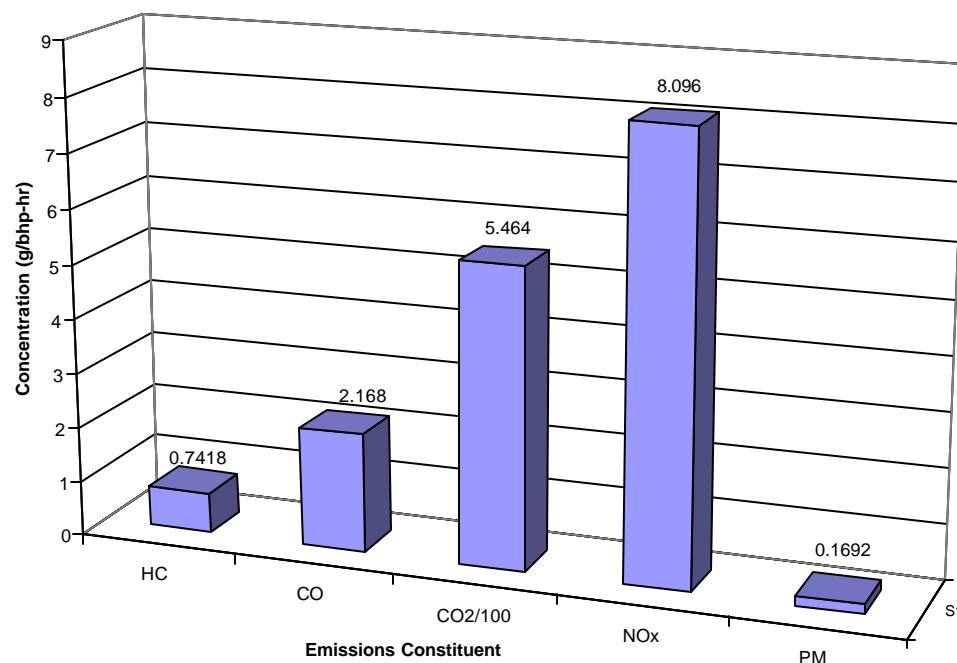
Figure 93 Transient Cycle Emissions Results for the John Deere 6059 Loader Engine (g/bhp-hr).
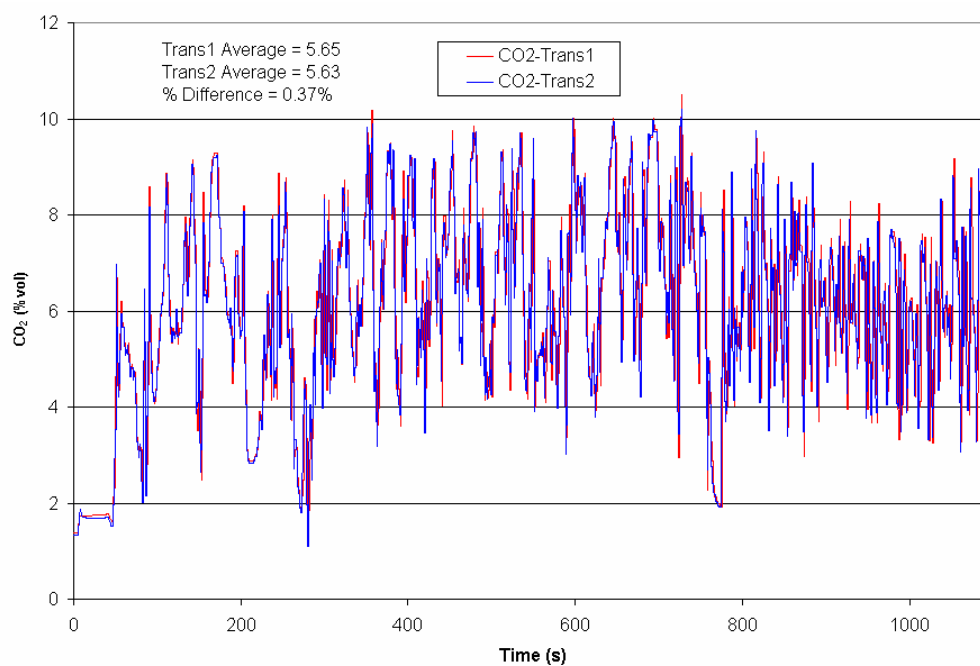
Figure 94 Comparison of Continuous CO_2 Traces for Two Repeat Tests of the Final Loader Transient Cycle.
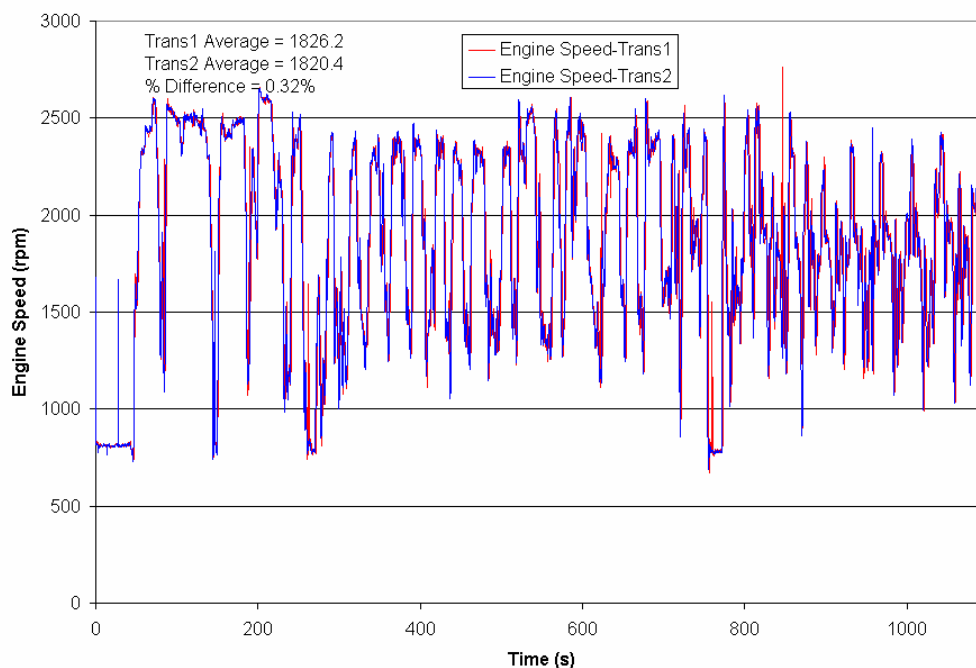
Figure 95 Comparison of Continuous Engine Speed Traces for Two Repeat Tests of the Final Loader Transient Cycle.

3.6.1.3 Comparison of Loader Steady-State and Transient Test Results

A comparison was made between 8-mode and transient results to determine how representative the 8-mode test cycle is of actual real world emissions. Brake-specific transient and weighted 8-mode results can be seen in Table 17.

Table 17 Comparison of Transient and Weighted 8-Mode Results for the John Deere 6059 Loader Engine (g/bhp-hr).

Mode Number	Weighted 8-Mode Results	Transient Results	% Difference
HC	4.77	0.74	544.6
CO	8.91	2.17	310.6
CO_2	1118.0	546.4	104.6
NO_x	26.51	8.10	227.3
PM	0.502	0.181	177.3

The feasibility of creating weighting factors that more accurately represent actual in-field emissions was investigated. The setpoint file for the finalized street sweeper

cycle was first discretized in 100 rpm increments from 700 rpm to 2800 rpm. The percentage of the total cycle time that the vehicle spent in each 100rpm speed range was determined and can be seen in Figure 96.
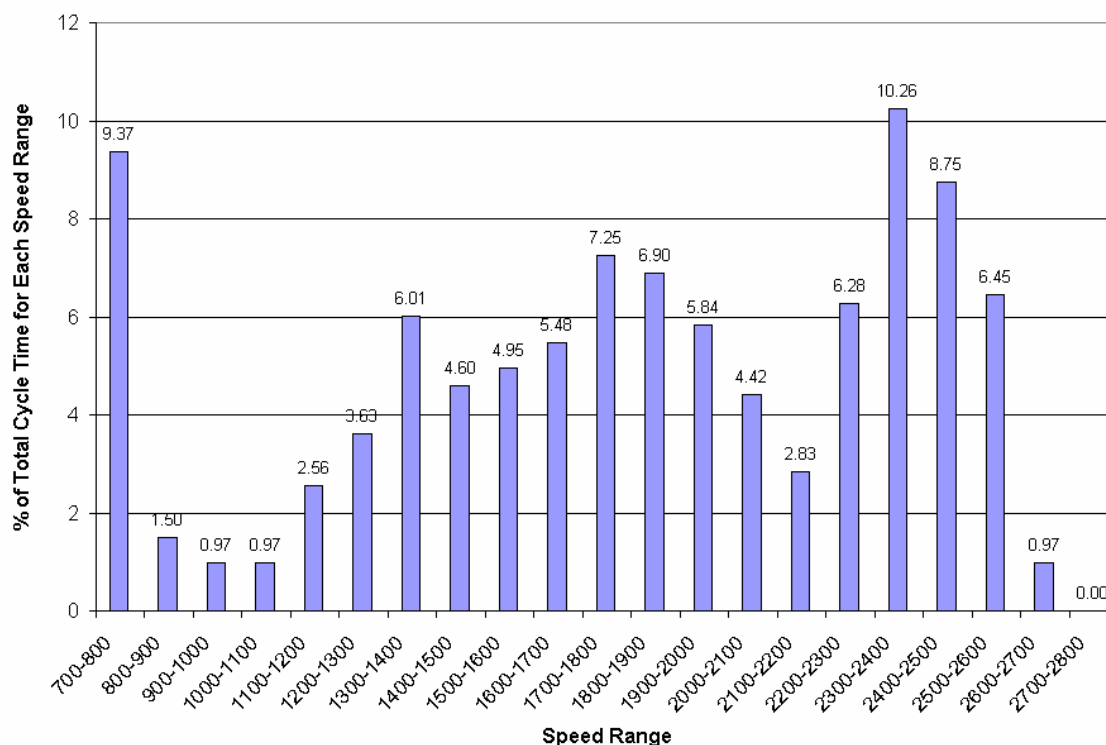
Figure 96 Percentage of Total Cycle Time Spent In Each Speed Range for the John Deere 6059 Loader Engine.

The speed discretization indicates a "tri-modal" distribution with idle, intermediate, and rated engine speed operating peaks. The data of Figure 96 was then examined for an approximate rated and intermediate speed range for the street sweeper. Due to the local maximas at 1700 rpm-1800 rpm and 2300 rpm-2400 rpm, these were chosen as representative of intermediate and rated speed conditions for comparative purposes. Both the intermediate and rated speed ranges were then discretized from 0 to 100% load in increments of 5% and the percentage of the selected speed range time the vehicle spent at each load range was plotted. Other speed bands before and after the selected intermediate and rated speed bands were also discretized for the percentage of time spent in each load range to see how they compared to the intermediate and rated load range time percentages. A graphical representation of the results for the speed ranges adjacent to the selected intermediate and rated speed ranges can be seen in Figure 97. The results of this operation for the intermediate speed range can be seen in Figure 98 while the rated speed range is illustrated in Figure 99.
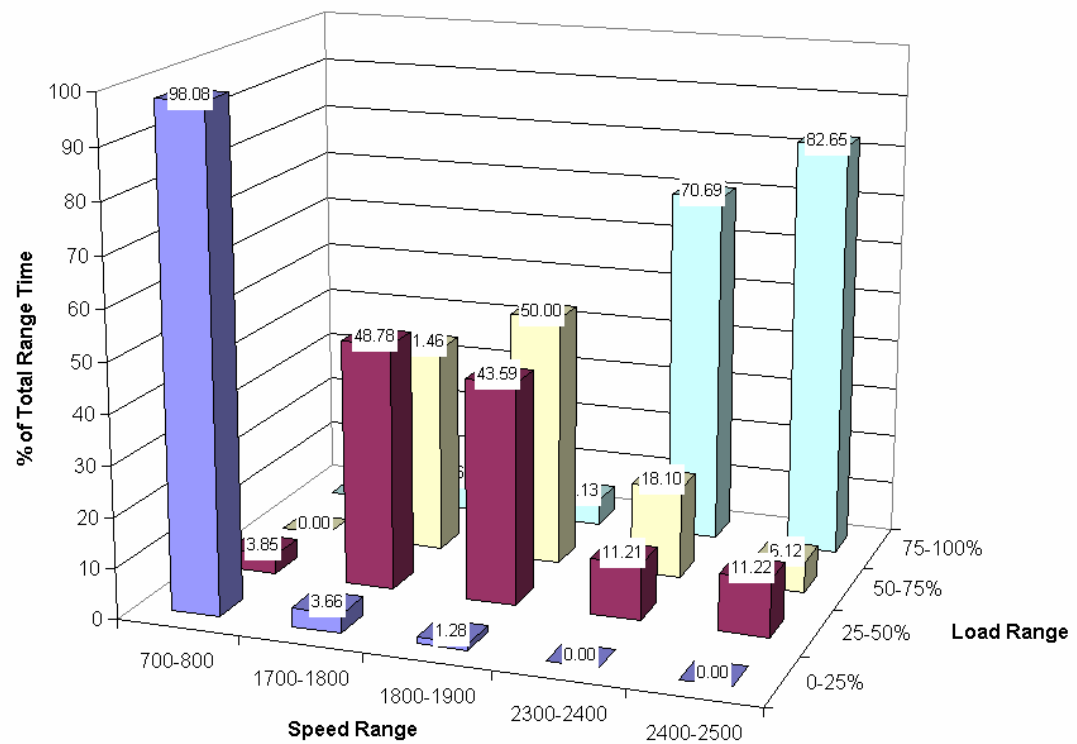
Figure 97 Comparison of the Time Spent at Different Load Ranges for Adjacent Speed Ranges.
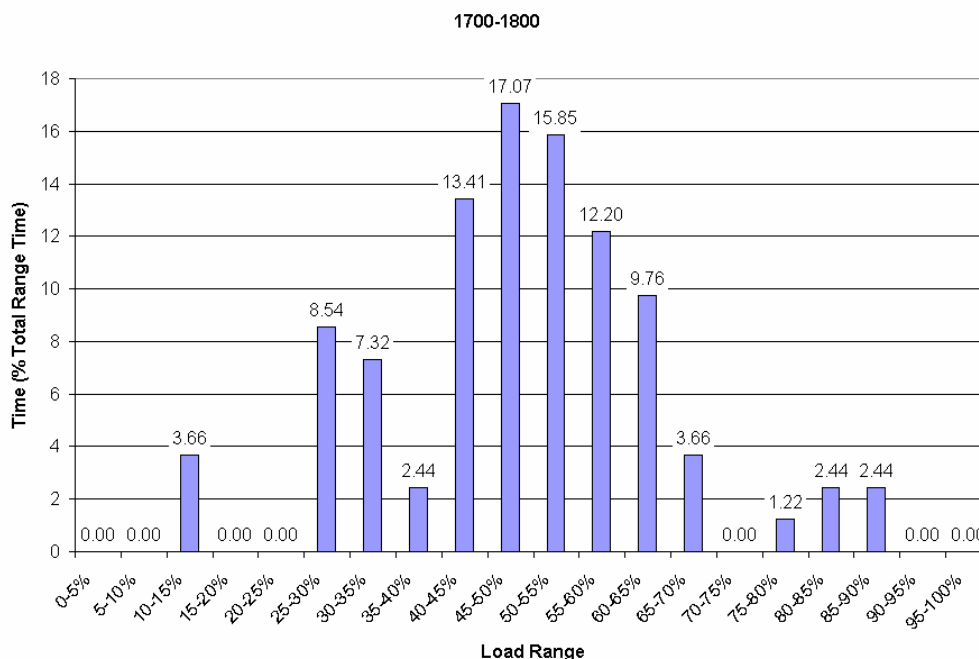
Figure 98 Percent Load vs. Percent Total Intermediate Speed Time for the John Deere 6059 Loader Engine.

It can be seen from Figure 98 that the load range that the engine operated at most in the field for an intermediate speed range (1700 rpm-1800 rpm) was 50-55%. This would be comparable to the Intermediate 50% load point in the 8-mode cycle, which has a weighting factor of only 0.1. It can also be deduced that the loader, as tested, did not spend an appreciable amount of time operating in the field at the other 8-mode intermediate points of 75% and 100% load – both of which have weighting factors of 0.10. This indicates that the intermediate speed percent load points in the 8-mode cycle may be unrepresentative of actual "real world" load levels and, therefore, emissions data would also be unrepresentative.
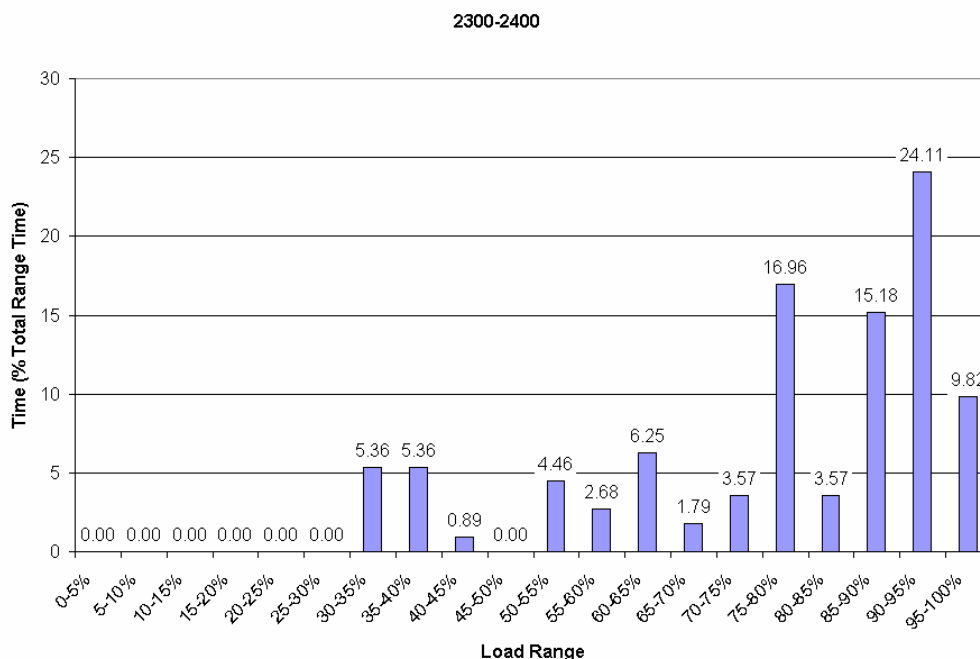
Figure 99 Percent Load vs. Percent Total Rated Speed Time for the John Deere 6059 Loader Engine.

It can be seen from Figure 99 that the load range that the engine most operated in during in-field testing was the rated speed range (2300 rpm-2400 rpm) and was primarily above 75% full load. This would be comparable to the rated 75% and 100% load points in the 8-mode cycle, which both have a weighting factor of 0.15. It can be deduced that the loader does not operate much in the field at the other rated 8-mode points of 10% and 50% load, which have 8-mode weighting factors of 0.10 and 0.15, respectively. This indicates that the rated speed percent load points in the 8-mode cycle may be unrepresentative of actual "real world" load levels and, therefore, emissions data would also be unrepresentative.

It should be noted that the transient cycle setpoint file was used for this analysis rather than the actual measured speed/load data. A regression was performed between the speed/load commanded by the setpoint file and the actual speed/load levels achieved. The CFR 40 Part 86 [1] provides regression analysis criteria to assess the validity of a transient cycle with respect to its setpoint file. These criteria can be seen in Table 18.

Table 18 Regression Criteria for Transient Certification Test Validity Analysis as Outlined in the Code of Federal Regulations.

Criteria	Speed	Torque
Slope of Regression Line, m	0.970-1.030	0.83-1.03
Coefficient of Determination, R^2	0.9700	0.8800
Regression line y intercept, b	+-50 rpm	+-15 ft-lb

It should be noted that the criteria listed in Table 18 are meant for engine certification purposes and were merely used as guidelines in this research as they did not have to be strictly adhered to. However, it can be concluded from viewing Figure 100 that the loader engine met the criteria for torque outlined in Table 18. The coefficient of determination for the torque was 0.8973, the slope of the regression line was 0.9417, and the y-intercept was 8.0222 ft-lb. For the speed regression analysis performed, the results did not meet the criteria. The coefficient of determination for the speed was 0.7252, the slope of the regression line was 0.8322, and the y-intercept was 307.24 rpm. The speed regression criteria could not be achieved with the eddy-current dynamometer and throttle controller setup used for the transient testing.
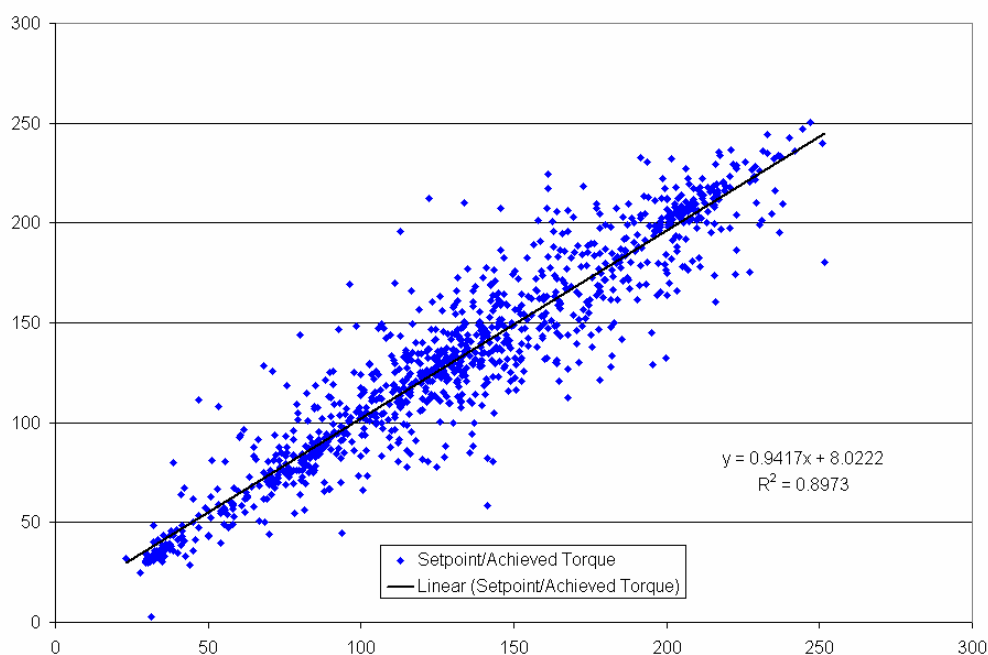
Figure 100 Regression Analysis for the Input vs. Achieved Torque for the John Deere 6059 Loader Engine.
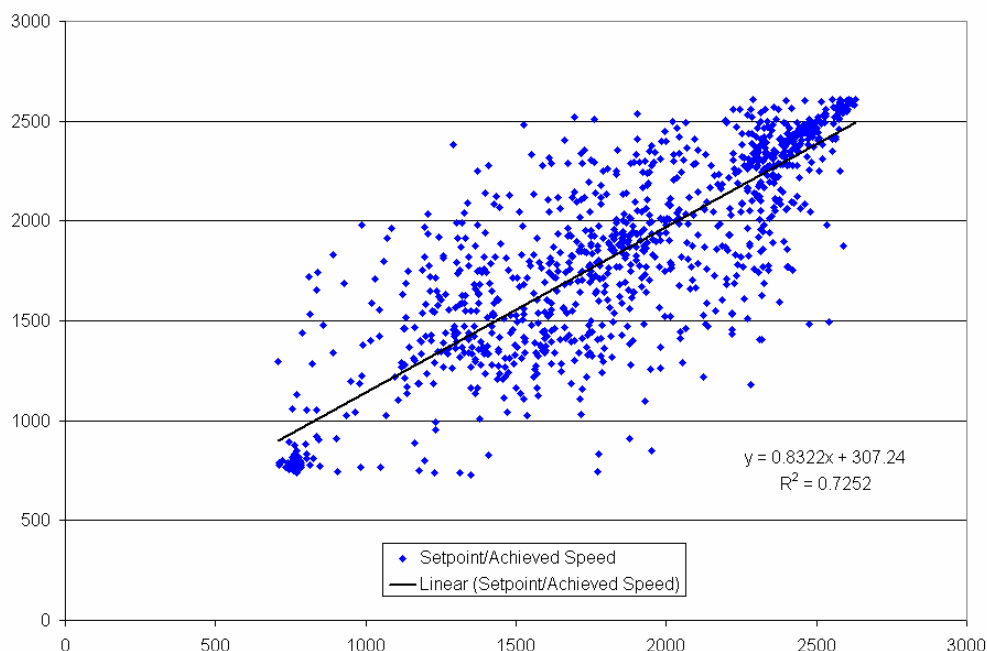
Figure 101 Regression Analysis for the Input vs. Achieved Engine Speed for the John Deere 6059 Loader Engine.

3.6.2   Street Sweeper In-Laboratory Results

Three types of in-laboratory testing were performed on the street sweeper engine. The first tests performed were steady-state emissions tests that followed the ISO-8178 8-mode testing protocols. The second series of testing consisted of final transient cycle emissions tests that followed the speed/load setpoints derived from the in-field data and discussed in detail in the Cycle Development section of this report. The third test performed was a transient test that consisted of the street sweeper engine being operated according to the normalized cycle that was developed for the loader engine.

3.6.2.1   Street Sweeper Steady-State 8-Mode Test Results

The ISO-8178 8-mode steady-state tests that were conducted consisted of four modes run at rated speed, three modes run at intermediate speed, and a "no-load" idle mode. Parasitic windage losses of the eddy current dynamometer were determined for all 8-mode testing speeds and the data was corrected for these losses when reduced. Mustang Dynamometers, the manufacturer of the eddy current dynamometer, provided estimates of the windage losses (in ft-lbs) of the dynamometer as a function of operating speed. The rated and intermediate speeds were obtained from the engine maps run on the engines prior to testing. The setpoints were determined using the rated and intermediate speed from the engine map and the percentages of maximum torque described in Table 13 of Section 4.6 of this document. A graphical representation of the engine map for the

street sweeper engine can be seen in Figure. The 8-mode speed and load set points for the 4039T street sweeper engine can be seen in Table 19.

The average emissions results for all gases and PM of the three 8-mode repeat tests performed can be seen in Table 20 with a graphical representation seen in Figure 91. The weighted results illustrated in Figure 92 were determined by multiplying the average results of Table 20 by the weighting factors outlined in Table 13 of Section 3.6. Results for all three runs of the 8-mode test are included in tabular form in the Appendix of this report.

Table 19 Street Sweeper 8-Mode Engine Speed/Load Set Points.

Mode Number	Engine Speed (rpm)	Torque (ft-lbs)	Horsepower (hp)
1	2100	274.7	109.8
2	2100	206.0	82.4
3	2100	137.4	54.9
4	2100	27.5	11.0
5	1712	295.4	96.2
6	1712	221.6	72.2
7	1712	147.7	48.1
8	≈760	0.0	0.0

Table 20 Average of 8-Mode Results for the John Deere 4039T Street Sweeper Engine (g/bhp-hr).

	Mode 1	Mode 2	Mode 3	Mode 4	Mode 5	Mode 6	Mode 7	Mode 8	Weighted Results
HC	0.13	0.16	0.27	2.17	0.04	0.20	0.23	9.82	1.95
CO	1.60	0.59	0.53	4.96	11.31	2.04	0.34	16.29	5.65
CO_2	508.4	514.3	545.2	974.7	527.4	516.4	521.6	3297.0	1111.0
NO_x	9.33	8.29	5.49	4.51	8.37	9.78	7.54	24.49	11.67
PM	0.181	0.134	0.143	0.228	0.882	0.269	0.117	1.207	0.474
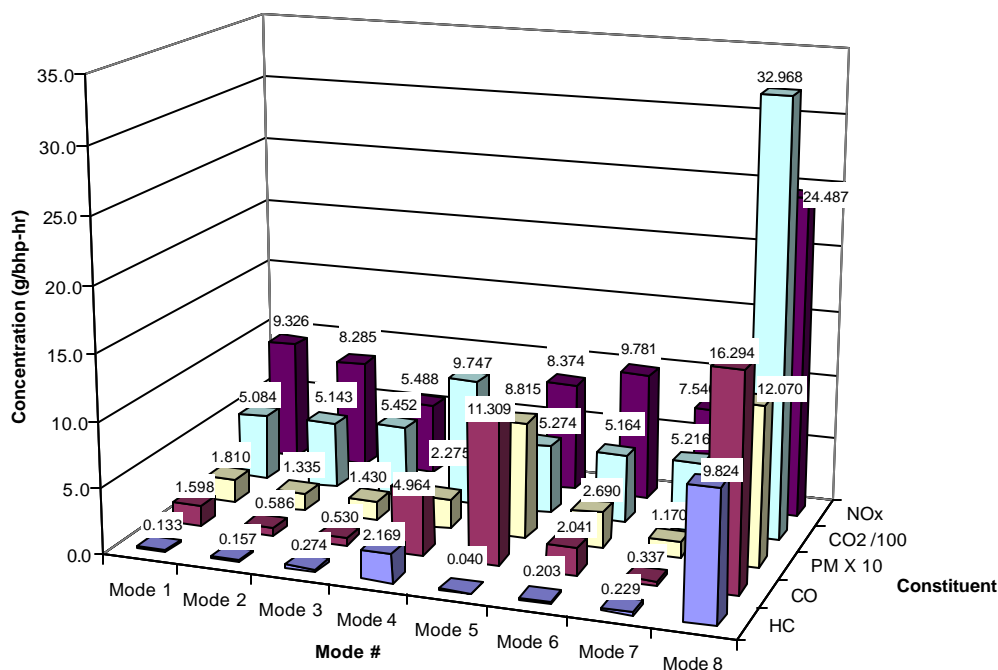
Figure 102 Average of 8-Mode Results for the John Deere 4039T Street sweeper Engine (g/bhp-hr).

It should be noted that the results for mode 8 are higher than all the other modes because of the brake-specific format. During mode 8, the "no load" idle mode, the power absorbed by the dynamometer is resultant of windage drag, and is therefore very low. This makes any data specified on a brake-specific basis have a disproportionately higher value. For brake-specific (g/bhp-hr) data, there is some load on the engine even at idle. If there were actually no load on the engine, the emissions for the "no load" idle mode (mode 8) would be infinite. For this reason, a time-based format, such as g/cycle, g/test, or g/mode, should complement brake specific emissions data in order to avoid misinterpretation of steady-state (such as the 8-Mode cycle) cycle data.
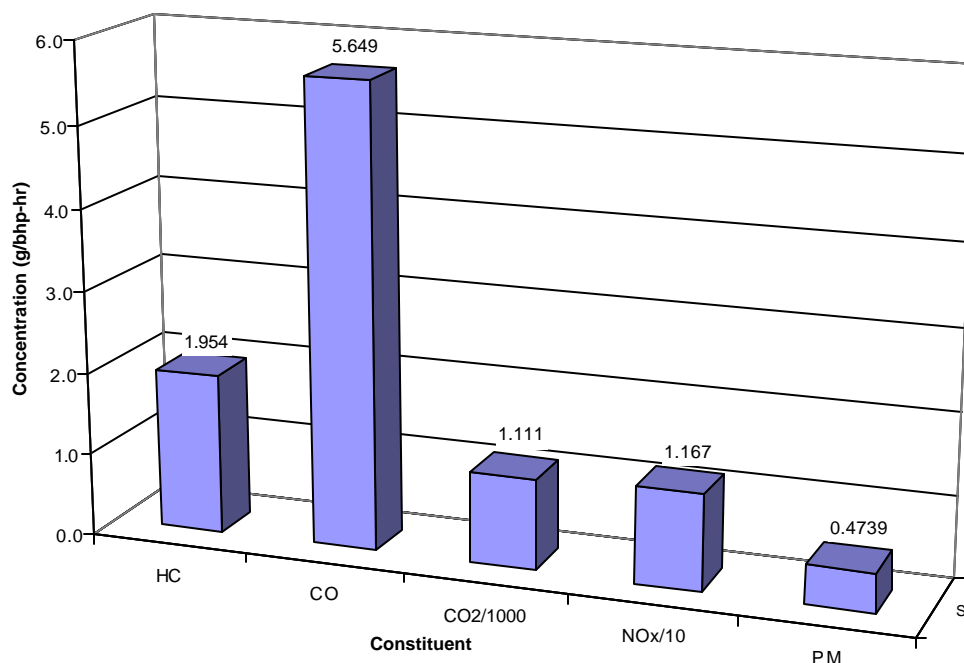
Figure 103 Average Weighted 8-Mode Emissions for the John Deere 4039T Street Sweeper Engine (g/bhp-hr).

3.6.2.1.1 Particle Sizing Results from the Steady-State Street Sweeper Engine Tests

Prior to the start of any testing in this study, the program manager at CARB suggested that PM sizing may be omitted from the study. The suggestion stemmed from the fact that there were no universally accepted procedures for PM sizing. Moreover, the E-43 study, funded by the Coordinating Research Council (CRC), was initiated nearly coincident with this program, and this study was expected to provide guidelines for PM sizing methodologies. However the authors did acquire limited PM sizing data for this study, and the results are presented herein.

Pure carbonaceous aerosol is hydrophobic (26) and it shows almost no water uptake in a humid atmosphere (37).   However, treatment of carbon particles with sulfuric acid improves their hydration properties so that sulfuric acid treated carbon particle become activated at very low super-saturations of less than 0.3% (23,28).   The oxidation of SO_2 to SO_3 occurs very early in the post-cylinder reactions, leads to formation of gaseous H_2SO_4 in the presence of H_2O. Karcher et al. (20) estimated that the formation of SO_3, in aircraft engines, is restricted to a very young plume with less than 10 ms in age. The subsequent binary nucleation of sulfuric acid-water systems has been discussed by Doyle (13), Heist and Reiss (16), Roedel (30), Baumgard (1), Baumgard and Johnson (2), and Kulmala et al. (22). Nucleation modes are brought about by the build-up of concentration of condensable vapor in the atmosphere. The initial formation of droplets from vapor is a complicated process. Droplets can be formed in the absence of condensation nuclei. The driving force for gas-to-particle conversion processes is the

saturation ratio. For nucleation to occur, saturation ratio should be greater than unity. Homogeneous nucleation or self-nucleation requires large saturation ratios (saturation ratio is a ratio of the partial pressure of an organic species to the saturation pressure of the same species) usually in the range of 2-10 to form nuclei particles. The more common modes of PM formation are nucleated condensation or heterogeneous nucleation. This process relies on existing sub-micrometer particles, called condensation nuclei, to serve as sites for condensation. The sub-micrometers particles are usually called ions, soluble or insoluble nuclei (17). There is a possibility that in diesel exhaust that there may be some ions and insoluble particles available to initiate heterogeneous nucleation, but homogeneous binary nucleation mode would be more likely to occur in the PM formation. When two or more vapor species are present, neither of which is supersaturated, nucleation can still take place as long as the participating vapor species are supersaturated with respect to a liquid solution droplet. In the classical binary nucleation theory the rate of nucleation, J, can be written in the form

$$J = C \exp (-\Delta G^*/kT)$$

Equation 14.

Where, ΔG^* is the free energy required to form a critical nucleus, C is the frequency factor, k is the Boltzmann's constant, and T is the temperature.

The binary clusters of H_2SO_4 and H_2O molecules undergo heterogeneous nucleation with the available carbon particles. These carbon particles may have their origin in the fuel, lubricating oil and/or both. Also, ash from the lubricating oil could contribute the particles that would participate in the heterogeneous nucleation process. The H_2SO_4-H_2O-carbon complex is susceptible to growth by condensation of heavier organic species, and a potential decrease in size by evaporation depending upon the partial pressures of the organic species in the exhaust. Nucleation has been shown to be a function of saturation ratio.

Most of the published literature on heavy-duty PM emissions has considered the binary nucleation (via the multi-component route) of water vapor and sulfuric acid, and the subsequent hetero-molecular nucleation and particle growth only in the exhaust dilution systems (laboratory or real-world). Exhaust samples extracted from a location close to the exhaust manifold provides a sample that is at an elevated temperature (approximately 900[O]F) compared to a temperature of 400[O]F at the exit of the tailpipe of a moving vehicle. It should be noted that sulfuric acid remains in a vapor state at temperatures above approximately 600[O]F. The sample extracted from the manifold is then diluted and cooled in a dilution tunnel system that employs filtered dilution air. Characteristics of particles formed in the dilution tunnel under these circumstances would be very different from those of particles formed in the dilution tunnel that uses a sample extracted from the end of a tailpipe on a vehicle operating in the field. The H_2SO_4-H_2O-carbon particles are now subject to growth by condensation, and coagulation. A sample extracted from the high temperature region of the exhaust system (close to the engine manifold) experiences the drop in temperature in a relatively cleaner environment of a dilution tunnel. The sample extracted from the end of the tailpipe has already experienced a history of cooling in an environment that is rich is carbonaceous particles, organic species and other particles.

Several research groups, including WVU, are currently studying diesel exhaust sampling techniques for particle sizing. There is no consensus amongst researchers on the most appropriate methodology for sampling and diluting exhaust samples for PM sizing and concentration measurements.

Figure 104 through Figure107 show the particle size distributions from the sweeper engine operated over ISO-8 mode steady state test. Particle concentrations are plotted against particle diameters. Particle concentrations are expressed in particles/cc (dN/dlogD). The figures show the particle size distributions, that is concentrations for each particle size in the exhaust sample stream. At least three replicate tests were conducted for each mode. The up scan time of 120 seconds and down scan time of 30 seconds was selected. It can be seen from these figures that the count median diameter of all the distributions were well over 100 nm with normalized number count in the order of 10^7, Mode 4 being the exception. During the mode 4 operation the engine was operated at rated speed with 10% torque at that speed. These conditions provided low fueling rates and relative cooler operation of the engine. It is possible that substantial amount of sulfates and/or low-volatility organics could have nucleated thus generating a particle size distribution with a smaller count median diameter. Mode 6 shows particle size distribution that has count median diameter of 150 nm. During this mode's operation, at intermediate speeds, the amount of excess air will be relatively low and due to the high load the fueling rate will be high. This condition promotes high degree of pyrolysis that is a precursor to formation of mainly elemental carbon. The elemental carbon will offer a nucleation site for the organics and sulfates to adsorb onto in the cooler exhaust stack so the particles will grow in size. It can be concluded from these two extreme cases that if the engine is operating at low A/F ratio the count median diameter will be the larger than in the case of high A/F ratio and cooler operation of the engine where the count median diameter may be smaller. However, given the high carbon content in the exhaust of the test engines, the saturation ratios were low. Hence, the nucleation mode was not distinct.
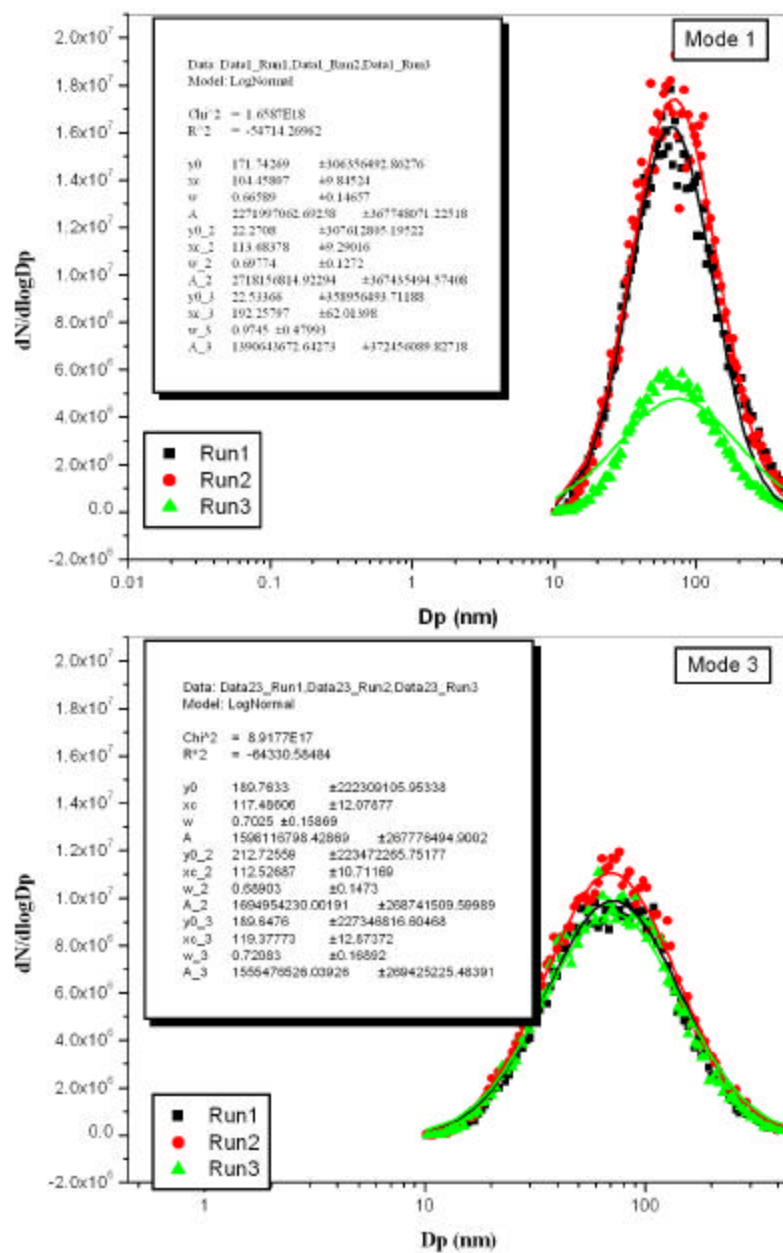
Figure 104 Particle Size Distribution from a Street Sweeper Engine Operated Over Steady-State Modes of ISO 8-Mode Test Cycle (Modes 1 and 3).
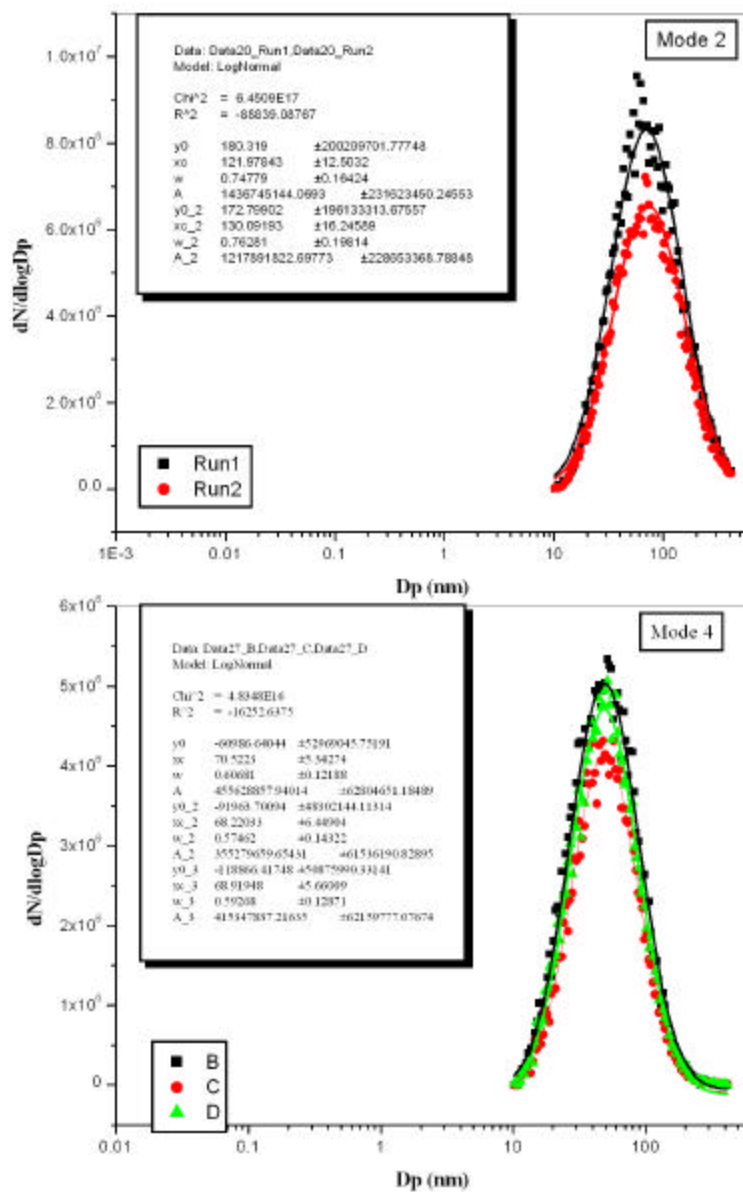
Figure 105 Particle Size Distribution from a Street Sweeper Engine Operated Over Steady-State Modes of ISO 8-Mode Test Cycle (Modes 2 and 4).
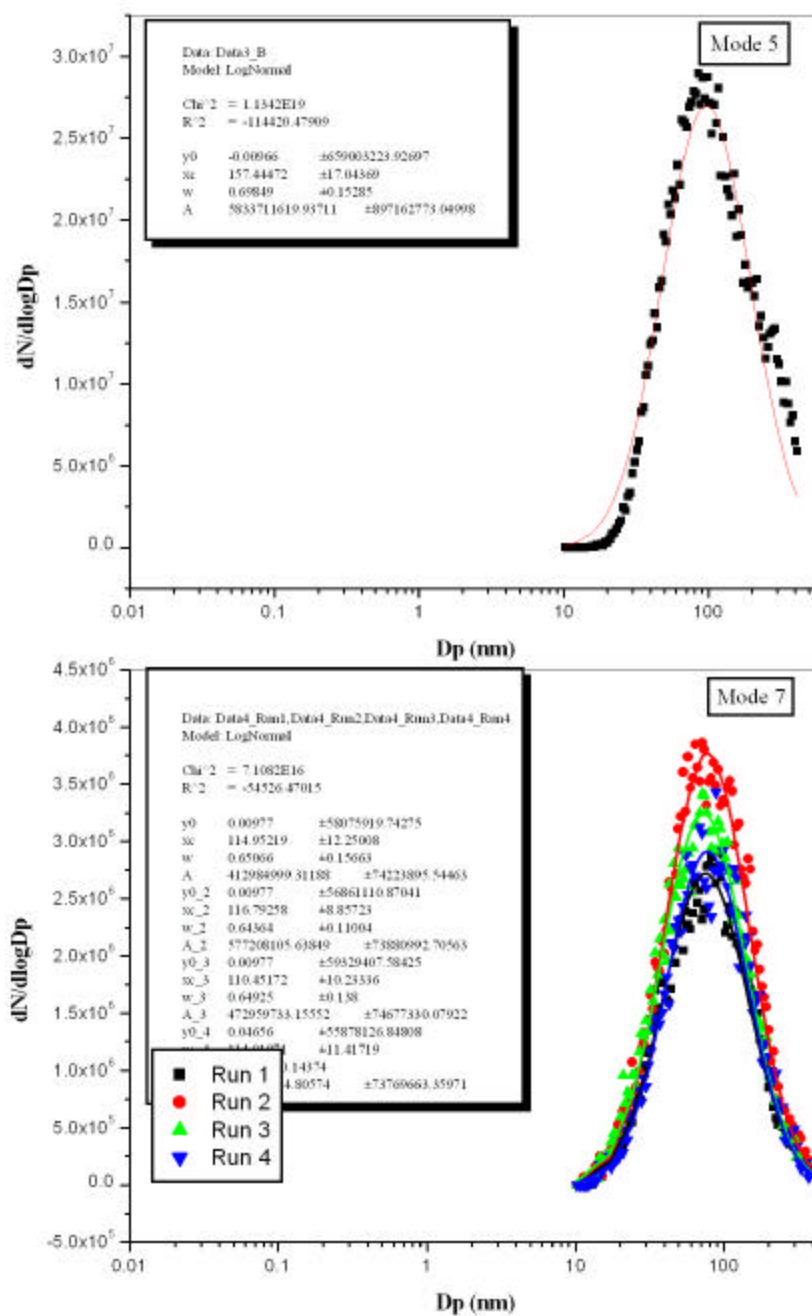
Figure 106 Particle Size Distribution From a Street Sweeper Engine Operated Over Steady-State Modes of ISO 8-Mode Test Cycle (Modes 5 and 7).
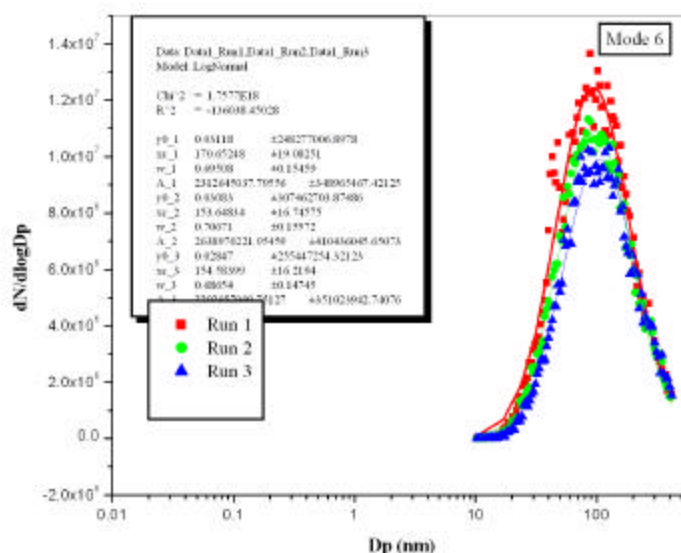
Figure 107 Particle Size Distribution From a Street Sweeper Engine Operated Over Steady-State Modes of ISO 8-Mode Test Cycle (Mode 6).

3.6.2.2 Street sweeper Transient Cycle Test Results

Several iterations were performed on the street sweeper cycle before the final transient cycle emissions data were collected. Two tests were conducted with the first cycle iteration and two were run with the final iteration for repeatability purposes. The data collected for the first cycle iteration can be seen in Table 21 while the data collected for the final iteration can be seen in Table 22. A graphical representation for the data of Table 21 and Table 22 can be seen in Figure 108. A comparison of average results between the emissions values from both test cases can be seen in Table 23. A graph of two final cycle repeated continuous CO_2 data traces can be seen in Figure 109 while the repeat engine speed traces are illustrated in Figure 110. A correlation of the CO_2 and engine speed data can be seen in Section 3.5.2.3, Figure 75 and Figure 76, respectively.

Table 21 Transient Cycle Emissions Results for the John Deere 4039T Street sweeper Engine Operating on the First Iteration (Trswpr1) of the In-field Data Derived Test Cycle (g/bhp-hr).

	Trswpr1-Run 1	Trswpr1-Run 2	Trswpr1-Run 3	Average
HC	0.55	0.573	0.351	0.491
CO	1.97	1.93	1.95	1.95
CO_2	623.8	631.4	635.7	630.3
NO_x	5.69	5.70	5.65	5.68
PM	0.261	0.264	0.267	0.264

Table 22 Emissions Results for the John Deere 4039T Street sweeper Engine Operating on the Final Iteration (Trswpr9) of the In-field Data Derived Transient Test Cycle (g/bhp-hr).

	Trswpr9-Run 1	Trswpr9-Run 2	Trswpr9-Run 3	Average
HC	0.44	0.58	0.47	0.50
CO	1.86	1.86	1.84	1.85
CO_2	624.7	623.9	629.4	626.0
NO_x	5.64	5.54	5.60	5.59
PM	0.243	0.242	0.248	0.245

Table 23 Comparison of Emissions Results for the John Deere 4039T Street sweeper Engine Operating on the First (Trswpr1) and Final (Trswpr9) Iteration of the In-field Data Derived Transient Test Cycle (g/bhp-hr).

	Trswpr1 Average	Trs wpr9 Average	% Difference
HC	0.49	0.50	1.83
CO	1.95	1.85	-4.83
CO_2	630.3	626.0	-0.68
NO_x	5.68	5.59	-1.51
PM	0.264	0.245	-7.350

It can be concluded from the data of Table 23 that the refinement of the cycle through the use of the manual speed/load adjusting process does have a fairly significant impact on emissions results. As can be seen, percent difference values between the averages of data collected for the two tests ranged from –7.53% to 1.83%. However, cycle appropriateness for the particular vehicle being tested plays a much more significant role in cycle-averaged results. It can be seen in the next section that when the street sweeper was run on the loader cycle, a large difference in cycle-averaged emissions results occurred.
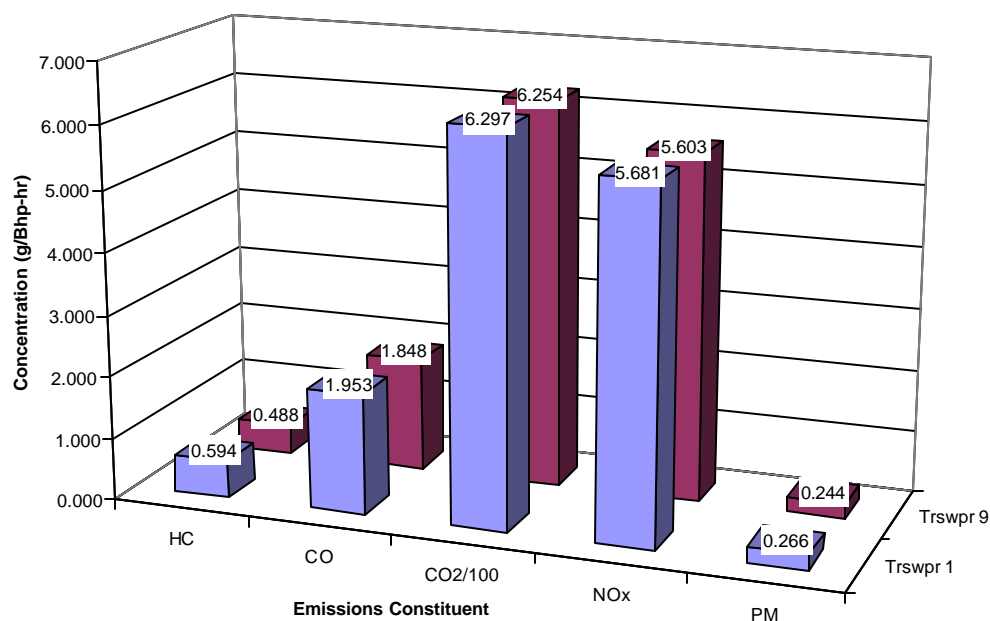
Figure 108 Average of Emissions Results for the John Deere 4039T Street sweeper Engine Operating on the First (Trswpr 1) and Final (Trswpr 9) Iterations of the Transient Cycle (g/bhp-hr).
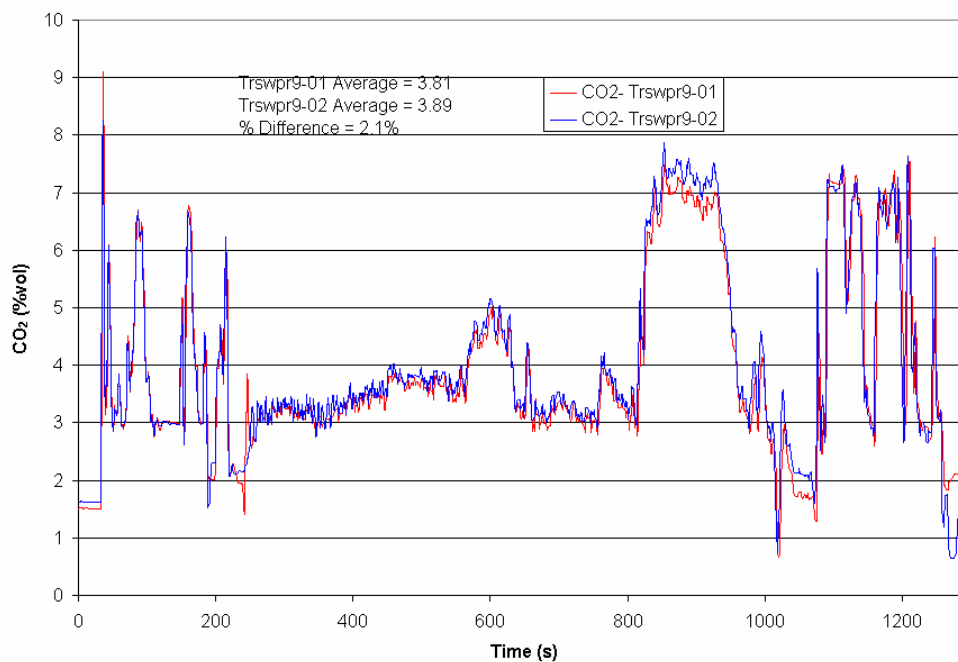
Figure 109 Comparison of Continuous CO$_2$ Traces for Two Repeat Tests of the Final (Trswpr9) Street sweeper Transient Cycle.
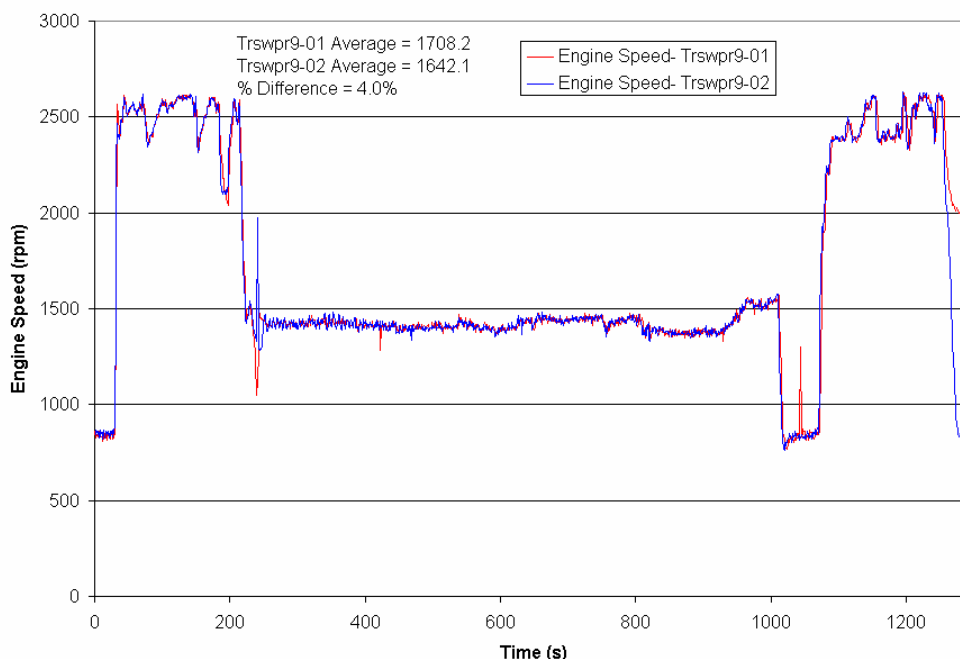
Figure 110 Comparison of Continuous Engine Speed Traces for Two Repeat Tests of the Final Street sweeper Transient Cycle.

3.6.2.3 Street sweeper-on-Loader Transient Cycle Test Results

The street sweeper was operated according to a normalized cycle developed previously for the rubber-tired loader. This test was performed to determine the feasibility of using the same cycle to test engines of different displacements but similar power levels and to determine the dependence of emissions levels on the cycles used. The turbocharged 4039T street sweeper engine, even though of smaller displacement, made slightly more horsepower than the 6059 loader engine. The test illustrates the need to create cycles that accurately represent the "real world" operating conditions of the vehicle in the field.

Table 24 Cycle Averaged Emissions Results for the John Deere 4039T Street sweeper Engine Operating on the Final Loader Transient Cycle (g/bhp-hr).

	Sweeper-on-Loader Run 1	Sweeper-on-Loader Run 2	Sweeper-on-Loader Run 3	Average
HC	0.39	0.35	0.36	0.37
CO	3.66	3.56	3.50	3.57
CO_2	561.9	561.1	562.4	561.8
NO_x	7.37	7.34	7.38	7.36
PM	0.389	0.376	0.343	0.370

Table 25 Average Results Comparison of Transient Tests Performed (g/bhp-hr).

	Sweeper-on-Sweeper Cycle	Sweeper-on-Loader Cycle	% Difference
HC	0.50	0.37	-26.54
CO	1.85	3.57	92.61
CO₂	626.0	561.8	-10.26
NOₓ	5.59	7.36	31.60
PM	0.245	0.370	51.19
Avg. Load %	33.7	57.8	41.7
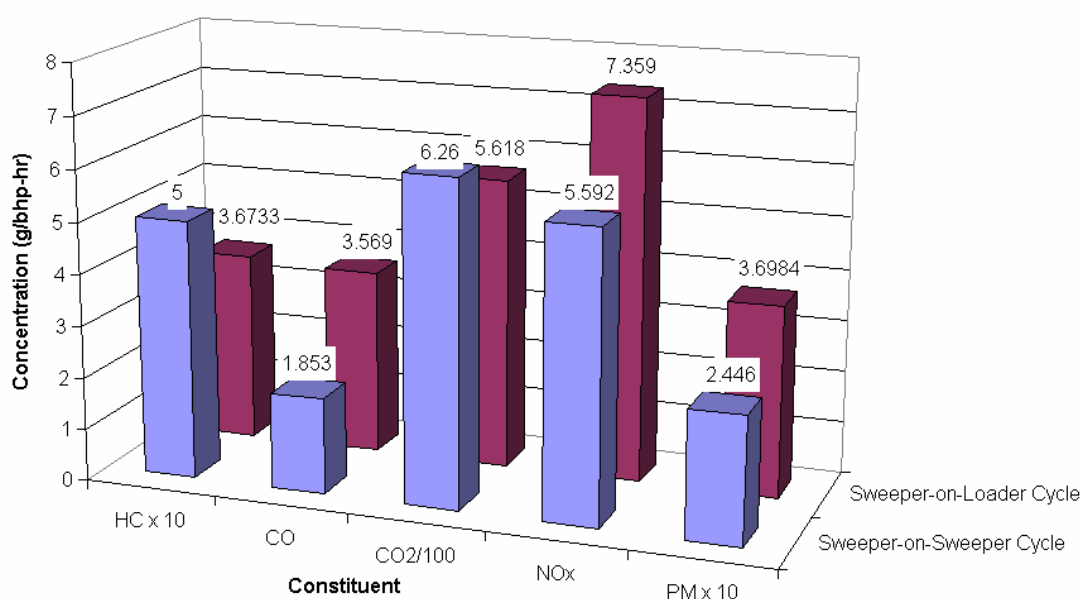
Figure 111 Graphical Comparison of the Effects of the Test Cycle on Engine Emissions (g/bhp-hr).

It can be seen from the data of Table 25 and Figure 111 that the nature of the cycle followed during testing had a dramatic effect on emission levels. In comparison with the Sweeper-on-Sweeper Cycle test, the Sweeper-on-Loader Cycle test yielded substantially higher CO (92.61%) and PM (51.19%) levels coupled with lower CO_2 (-10.26%) levels, which is an indication of less thorough combustion of the fuel consumed. This result can be explained in terms of the number of transient events encountered in the running of each cycle. The smoother, more steady-state sweeper cycle exhibited more complete combustion because of the steadier engine speed and much less transient torque

demands placed on the engine during the sweeping process. In contrast, the drastic engine speed changes and quick torque transients of the loader cycle combine to produce a less complete combustion of the fuel and the resultant increase of the CO and PM emissions.

It can be concluded from the data of this section that "real world" representation of test cycle activity plays a much larger role in emissions results than the accurate repeatability of the in-field cycle does. While the laborious and time-consuming process of cycle iteration changed the street sweeper cycle averaged CO_2 results by only 0.68%, running the street sweeper on the unrepresentative loader cycle changed cycle averaged CO_2 results by –10.26% on a brake-specific basis.

3.6.2.4   Comparison of Sweeper Steady-State and Transient Test Results

A comparison was made between 8-mode and transient results to determine how representative the 8-mode test cycle is of actual real world emissions. Differences between brake-specific transient and weighted 8-mode results can be seen in Table 26.

Table 26 Comparison of Transient and Weighted 8-Mode Results for the John Deere 4039T Street sweeper Engine (g/bhp-hr).

	Weighted 8-Mode Results	Transient Results	% Difference
HC	1.95	0.50	290.0
CO	5.65	1.85	205.4
CO$_2$	1111.0	626.0	77.5
NO$_x$	11.67	5.59	108.8
PM	0.474	0.245	93.5
Avg. Load (hp)	59.69	22.2	62.8

The feasibility of creating weighting factors that more accurately represent actual in-field emissions was investigated. To do so, the dynamometer cycle setpoint file for the finalized street sweeper cycle was first discretized in 100 rpm increments from 700 rpm to 2800 rpm. The results of this discretization indicating the percentage of total cycle time that the vehicle spent in each 100 rpm speed range can be seen in Figure 112.
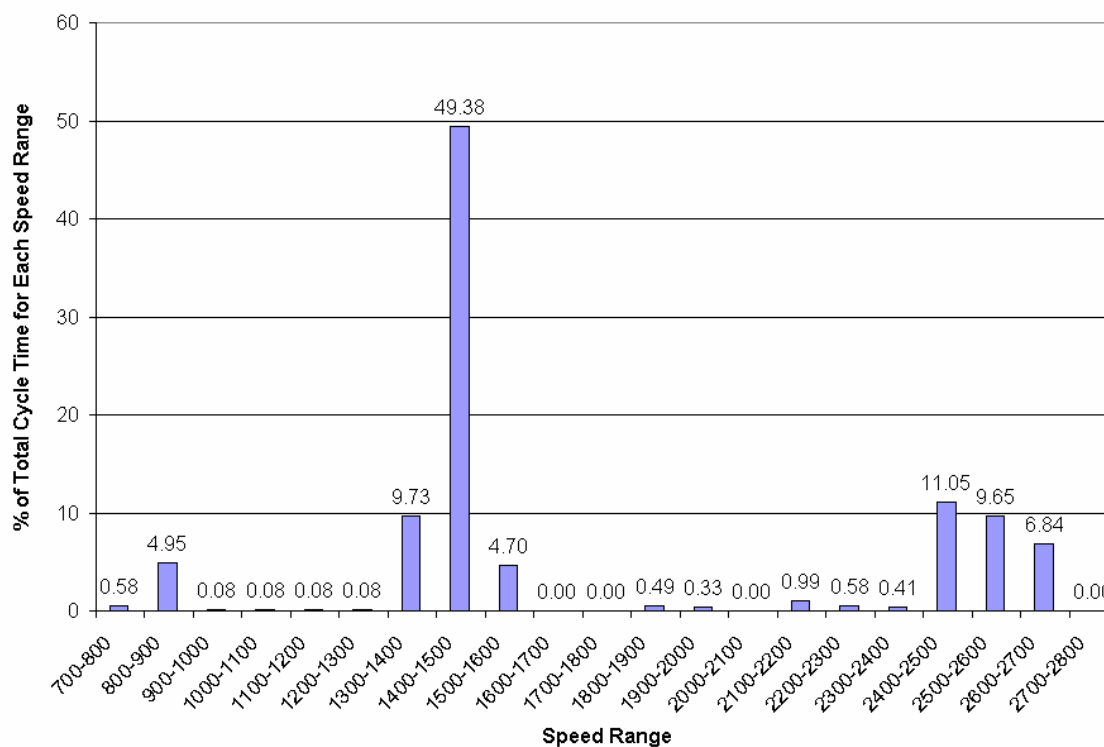
Figure 112 Percentage of Total Cycle Time Spent in each Speed Range.

The speed discretization results of Figure 112 indicate a "tri-modal" distribution with idle, intermediate, and rated engine speed operating peaks. The data of Figure 112 was then examined for an approximate rated and intermediate speed range for the street sweeper. Due to the local maximas at 1400 rpm-1500 rpm and 2400 rpm –2500 rpm, these were chosen to be representative of intermediate and rated speed conditions for comparative purposes. These identified speed ranges, loosely interpreted as intermediate and rated speeds, were then discretized according to load, from 0 to 100% load in increments of 5% for each of the two speed ranges. The results of this discretization indicating the percentage of the total time spent in the respective speed range that the vehicle operated within the discretized 5% load "bins" can be seen in Figure 113 for the intermediate speed range and Figure 114 for the rated speed range. Other speed ranges that were immediately before and after the selected intermediate and rated speed ranges were also discretized according to the percentage of time spent in each load range in order to compare with the intermediate and rated load ranges. The discretized results from the neighboring speed ranges were quite comparable to those obtained for the intermediate and rated speed ranges.
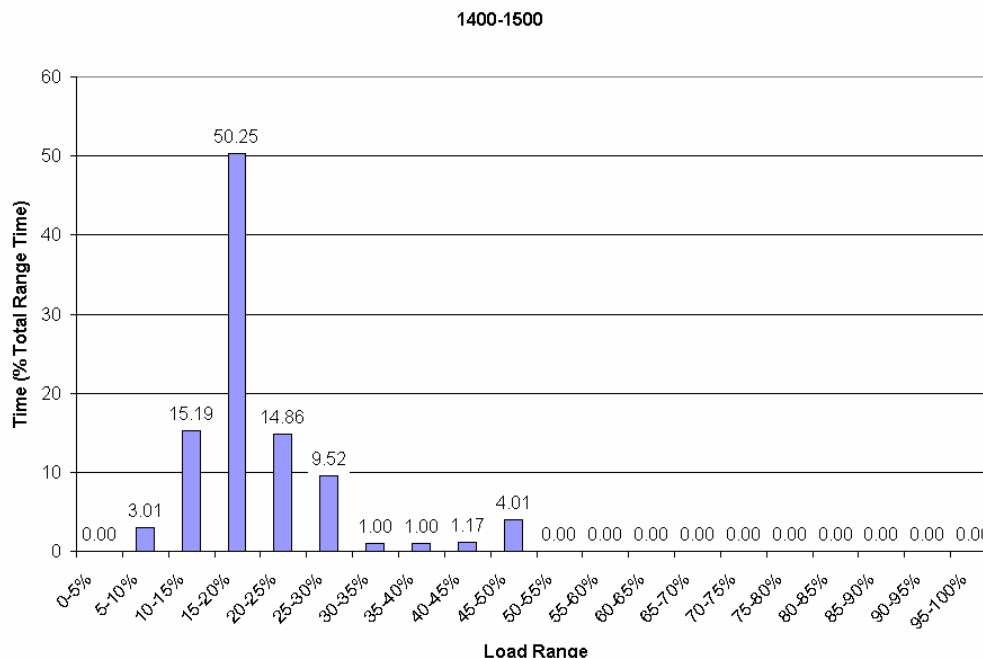
Figure 113 Percent Load vs. Percent Total Intermediate Speed Time for the John Deere 4039T Street Sweeper Engine.

It can be seen from Figure 113 that the load range the engine operated at the most in the field for the intermediate speed range (1400 rpm –1500 rpm) was 15-20%. By multiplying the time spent in the intermediate speed range by the time spent in the desired load ranges, one can arrive at an approximate weighting factor for the mode. For example, by multiplying the percentage of time the sweeper operated in the intermediate range (49.38%) by the percentage of time the street sweeper spent at a specific load, say 50% (which was 4%), one could arrive at a weighting factor of approximately 0.02 for this intermediate speed, 50% load condition. The weighting factor for intermediate 75 (intermediate speed, 75% load) and intermediate 100 (intermediate speed, 100% load) would be assigned values of zero for the cycle developed from the in-field street sweeper tests. In contrast, for the 8-mode certification test cycle, the weighting factor for intermediate 50, intermediate 75, and intermediate 100 are all 0.1. Thus the 8-mode data may not be representative of actual "real world" load levels and, therefore, emissions data may not provide a completely accurate picture of emissions contributions.

2400-2500
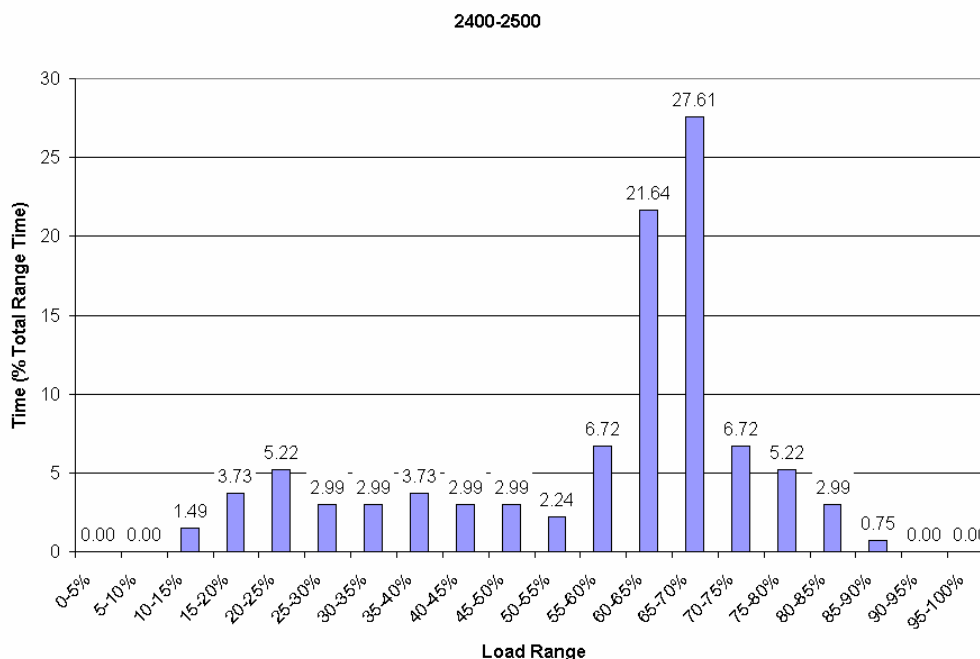
Figure 114 Percent Load vs. Percent Total Rated Speed Time for the John Deere 4039T Street Sweeper Engine.

It can be deduced from Figure 114 that the range the street sweeper most operated in during the in-field testing was the rated speed range (2400 rpm-2500 rpm) and was primarily around 75% load. The approximate calculated rated speed weighting factors for the street sweeper would be 0.12 for rated 10, 0.06 for rated 50, 0.56 for rated 75, and 0 for rated 100. In contrast, the actual weighting factors for the rated conditions of the 8-mode certification test cycle are 0.10 for rated 10, and 0.15 for rated 50, 75, and 100. This illustrates that the rated speed percent load points in the 8-mode cycle may be unrepresentative of actual "real world" load levels and, therefore, emissions data would also be unrepresentative. A comparison of 8-mode results with the integrated transient results, using the arrived-at "modified" weighting factors can be seen in Table 27 below. It can be deduced from a comparison of the percent difference data of Table 26 and Table 27 that the modified weighting factors produce a more accurate prediction of actual in-use emissions from the steady-state 8-mode data.

Table 27 Comparison of Transient and Newly Weighted 8-Mode Results for the John Deere 4039T Street Sweeper Engine (g/bhp-hr).

	New Weighted 8-Mode Results	Transient Results	% Difference
HC	0.42	0.50	-16.0
CO	1.03	1.85	-44.3
CO$_2$	552.4	626.0	-11.8
NO$_x$	7.17	5.59	28.3
PM	0.137	0.245	-44.1

It should be noted that the transient cycle setpoint file was used for this analysis rather than the actual measured speed/load data. A regression was performed between the speed/load commanded by the setpoint file and the actual speed/load levels achieved. The CFR 40 Part 86 [1] provides regression analysis criteria to assess the validity of a transient cycle with respect to its setpoint file. These criteria can be seen in Table 18.

It can be concluded from viewing Figure 115 that the street sweeper engine met the criteria for torque outlined in Table 18. The coefficient of determination for the torque was 0.954, the slope of the regression line was 0.97, and the y-intercept was 2.36 ft-lb. For the speed regression analysis performed, the results did not meet the criteria. The coefficient of determination for the speed was 0.9271, the slope of the regression line was 0.951, and the y-intercept was 80 rpm. The speed regression criteria could not be achieved with the eddy-current dynamometer and throttle controller setup used for the transient testing. Again, the criteria listed in Table 18 are meant for engine certification purposes and were merely used as references for comparative regression analysis of engine dynamometer test cycles.
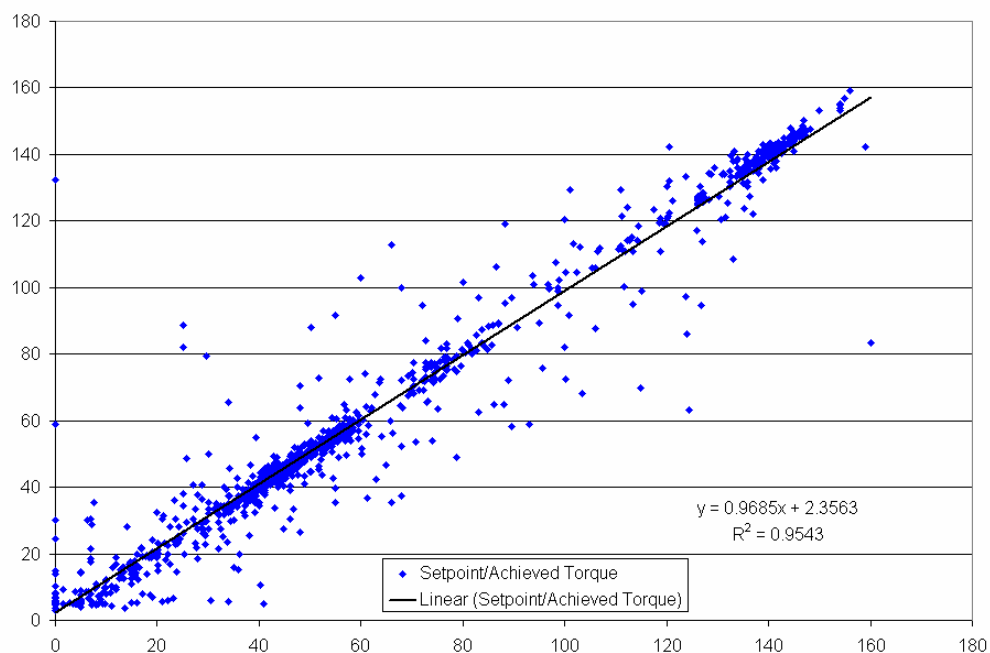
Figure 115 Regression Analysis for the Input vs. Achieved Torque for the John Deere 4039T Street Sweeper Engine.
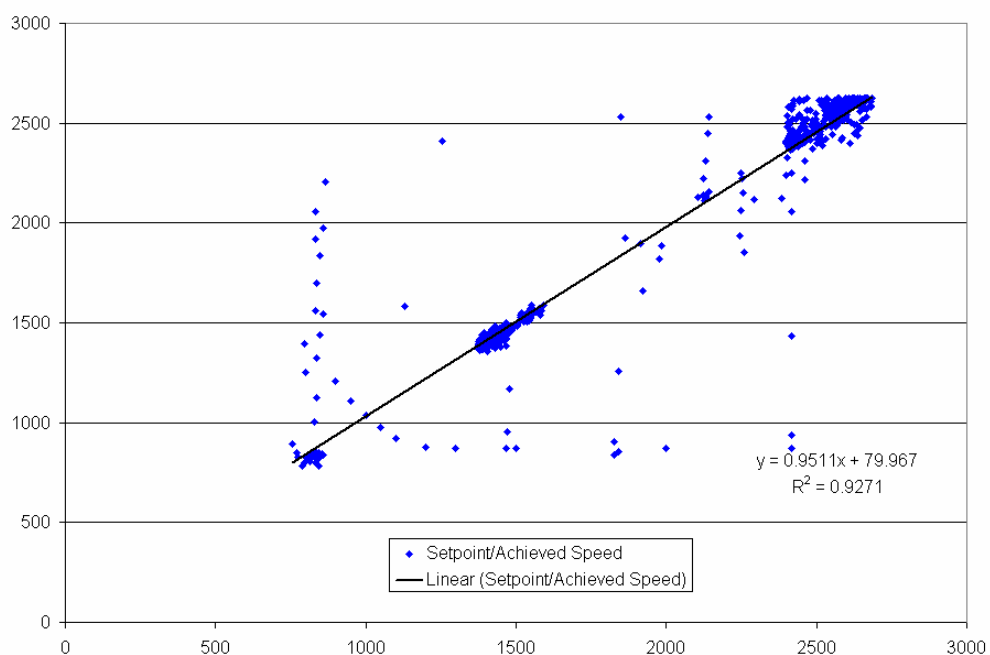
Figure 116 Regression Analysis for the Input vs. Achieved Engine Speed for the John Deere 4039T Street Sweeper Engine.

3.6.3   Excavator In-Laboratory Results

The engine was removed from the excavator in early summer 2001, and moved to the laboratory testing facility. The engine as tested on the dynamometer test bed is shown in Figure 117. Various small repairs and an extensive cleaning were performed before the engine was mounted onto the dynamometer test bed. The most significant of these repairs was to the turbo flange on the exhaust side as it had corroded away. The flange had to be repaired in order to affix exhaust lines to the engine, and could have been a source of an exhaust leak during field testing. While an exhaust leak in-field would be insignificant as only concentrations in the raw exhaust were measured, it would have a significant impact on the collection of mass emissions data in the laboratory CVS system. The condition of this engine may be representative of a large number of off-road equipment owned by smaller businesses. A sampling port for the Sensor's measurement device was placed in the exhaust line at approximately the same distance downstream as was used in-field.

Figure 117 Komatsu S6D125-1 Engine mounted on GE DC Dynamometer test bed

The engine was operated according to a series of discretized engine maps in order to provide information regarding the specific dependence of CO_2 emissions on engine load and speed. During these tests engine speed was increased in 100 rpm increments from curb idle to maximum governed speed while raw CO_2 emissions were recorded. Each of these operating points was held for 30 seconds in order to provide an asymptotic CO_2 measurement. Three separate series of tests were performed in which the engine was loaded at 0, 50, and 100 percent of maximum torque at the given engine speed according to the engine maps. The data recorded from these CO_2 maps were used to

develop the first transient cycles using a simple linear interpolation from the previously collected in-field data.

Upon conference with CARB regarding vehicle activity, it was decided that three identified operations – digging/loading (cycle 1), transport (cycle 2), and trenching (cycle 3) – would be investigated as separate test cycles. By doing so, the emissions results and vehicle activity could be combined so as to be most representative of actual vehicles in a given study area. The continuous CO_2 data from the first cycles was compared to the field data, and the iterative approach, similar to that discussed earlier in the report, was used to arrive at an acceptable correlation between laboratory and in-field data. The following figures are a comparison of each cycle with the corresponding field data, followed by a correlation between the normalized CO_2 curves for the in-field and final test cycle.
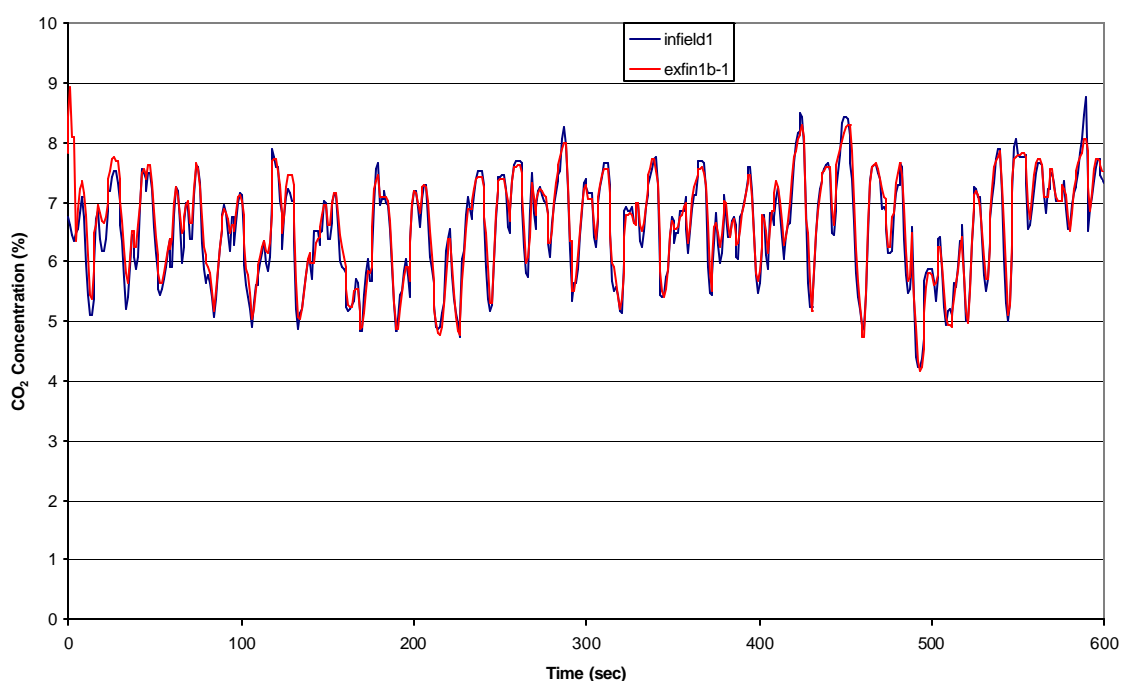
Figure 118 Test Cycle 1 Final Test Results

It is inherently evident that the final in-lab test cycle follows in-field continuous CO_2 data with more accuracy than the first test, thus it is more indicative of the sharp transient events that may have occurred during vehicle operation.   This process, however, is rather tedious and time consuming, and it's overall effect on brake specific emissions is relatively small, as is shown in Figure 120. The nature of this cycle shows peaks that coincide with engine loading as it digs a load of material. Heavy engine loads, which occur if the excavator encounters a large rock that is embedded in the material being moved, are demonstrated by the uncharacteristically high peaks. The swells in the cycle represent times when the excavator swings and unloads the material in another

location. This cycle shows that the nature of operation is very repeateable, depending largely on the nature of material, and operator tendencies.
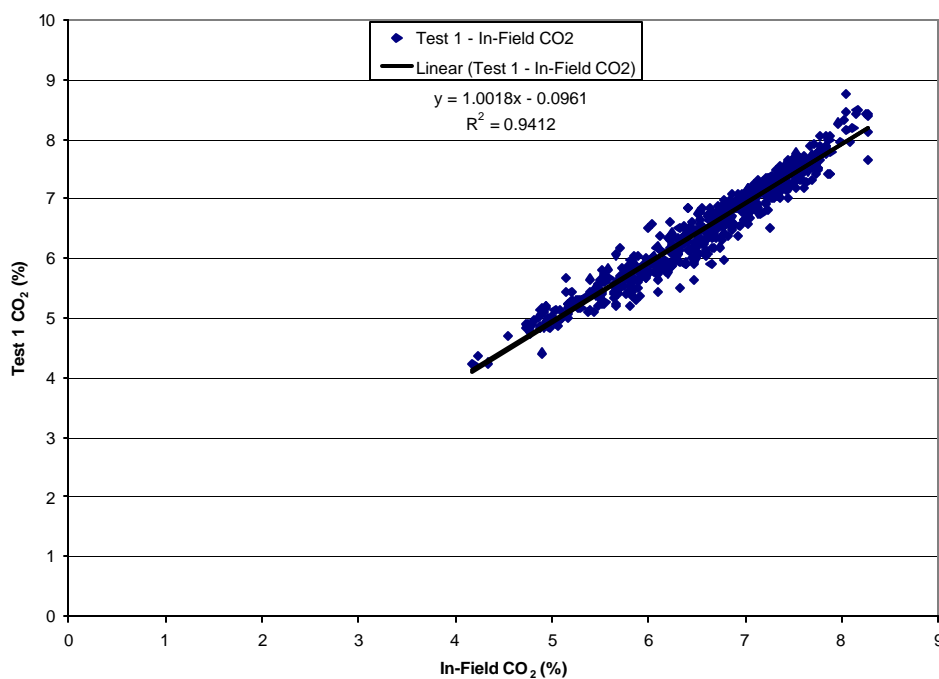
Figure 119   Test Cycle 1 Correlation

Review of this figure suggests excellent correlation between the test cycle and in-field raw CO_2 measurements. The correlation returned a slope very near to 1 and an intercept very near to zero. The R^2 value for this regression is 0.9412, indicating very close correlation. This correlation was simply performed by time aligning the CO_2 data from the in-field and the laboratory tests, and then plotting them against each other. In theory the data should be a straight line for perfect results.
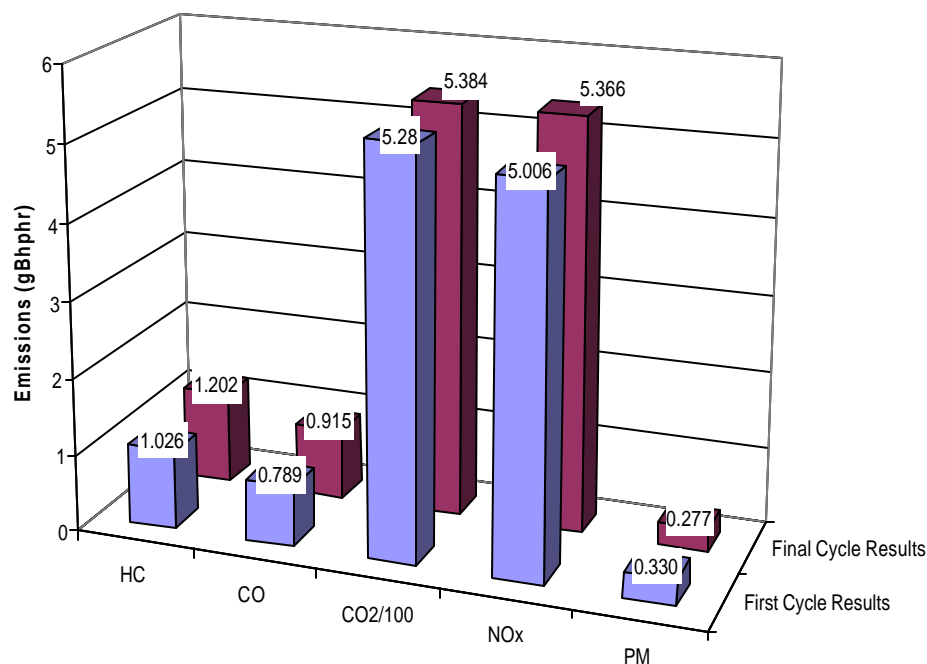
Figure 120 Comparison of Average Brake-specific Emissions Results from the First and Final Cycle 1 Tests

Review of this figure shows that the change in average emissions results did not rely heavily on cycle iteration and smoothing. The data persented herein indicates that the nature of the cycle will tend to affect the averaged emissions more than small changes in the same cycle for purposes of in-field cycle recreation. The first and last comparisons for cycles 2 and 3 demonstrate the same characteristic and are shown in Figure 123 and Figure 125. Therefore, should more work be performed in a manner consistent with this study, it is not reccomendable that much time be spent on transient cycle iteration as its cost would outweigh its worth to test results.
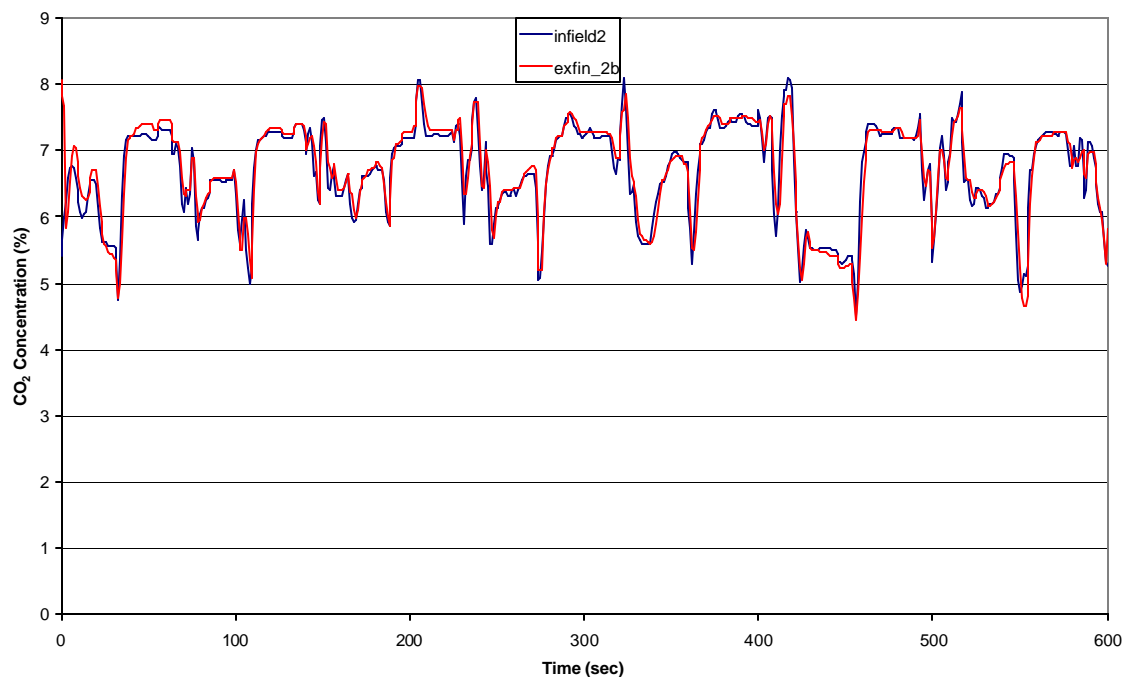
Figure 121 Test Cycle 2 Final Test Results

The results of cycle iteration again made the traces follow one another more closely in peaks and transient events. These cycles tend to show that the operating cycle of the excavator is very repetitive in nature, repeating many cycles of the same characteristic loading. This is largely due to operator tendencies and the nature of the work being performed by the machine. The longer peaks of high emissions rates represent the hauling operation as the excavator moves from one place to another and then returns to the material removal site. Smaller peaks indicate loading and unloading the bucket with material, and the high peaks indicate steering by locking one track and letting the other track turn the machine.
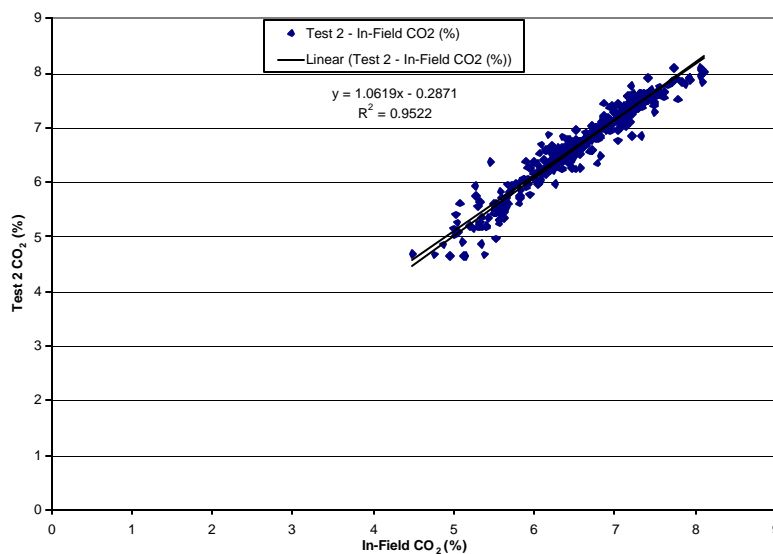
Figure 122 Test Cycle 2 vs. In-field CO$_2$ Correlation

Review of cycle 2 indicated a very close correlation between in-field and in-lab results, with a slope of 1.0619, an intercept of 0.2871, and R^2 value of 0.9522. The results of this test cycle showed closer correlation than the results of cycle 1, largely due to the fact that there are not as many transient events occurring through this cycle.
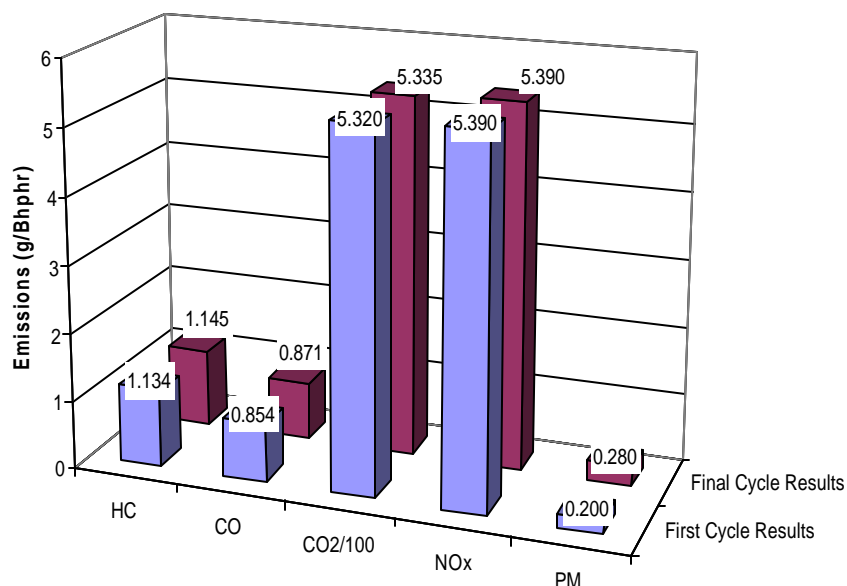
Figure 123 Comparison of Average First and Final Cycle 2 Iteration Brake-specific Emissions

Again it is shown that the iteration of cycles did not have nearly a significant enough impact on brake-specific emissions to warrant the effort involved in manually adjusting the test cycle to achieve the continuous in-field data trace.

Test 3 shows the same trends relative to cycle iteration as the first two cycles. The iterations provided a more accurate recreation of the in-field data, but averaged brake-specific cycle emissions were not changed significantly. Figure 124 shows the general trends of cycle 3 to be relatively close to those of cycle 1. This is largely due to similarity in the operations. Swells indicate periods of swinging and unloading material, or the period before loading, and peaks indicate periods of digging and/or maneuvering the vehicle.
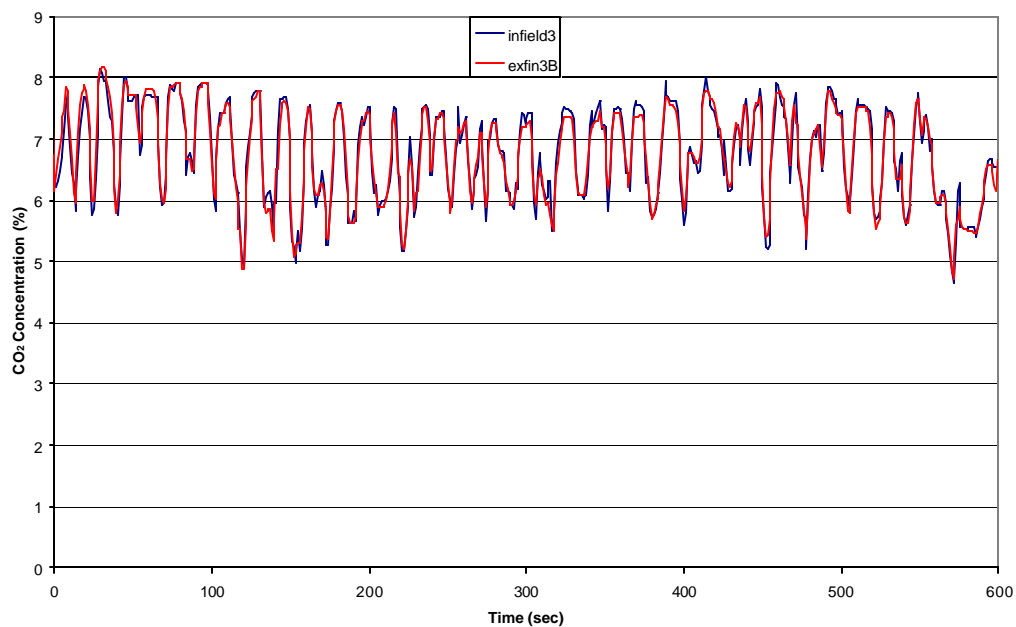
Figure 124 Test Cycle 3 Final Test Results
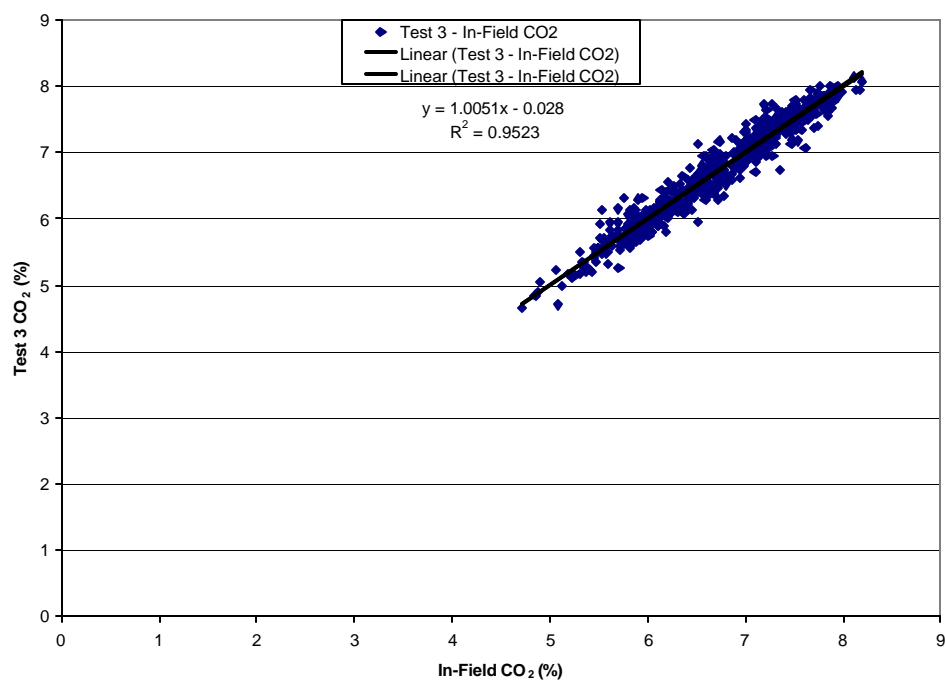
Figure 125 Correlation of CO_2 Data from final test and In-field Results

Cycle 3 returned the best correlation results of all three cycles, with a slope of 1.0051, an intercept of 0.028, and an R^2 value of 0.9523. The results indicate that all cycles returned CO_2 traces that were as close to the in-field data as could be expected, as they were within a determined value of test to test repeatability of the same cycle.

Figure 126 shows the averaged brake-specific emissions from the first and last cycle iterations. This again illustrates that the effort put into cycle adjustment produced little effect in brake-specific emissions.
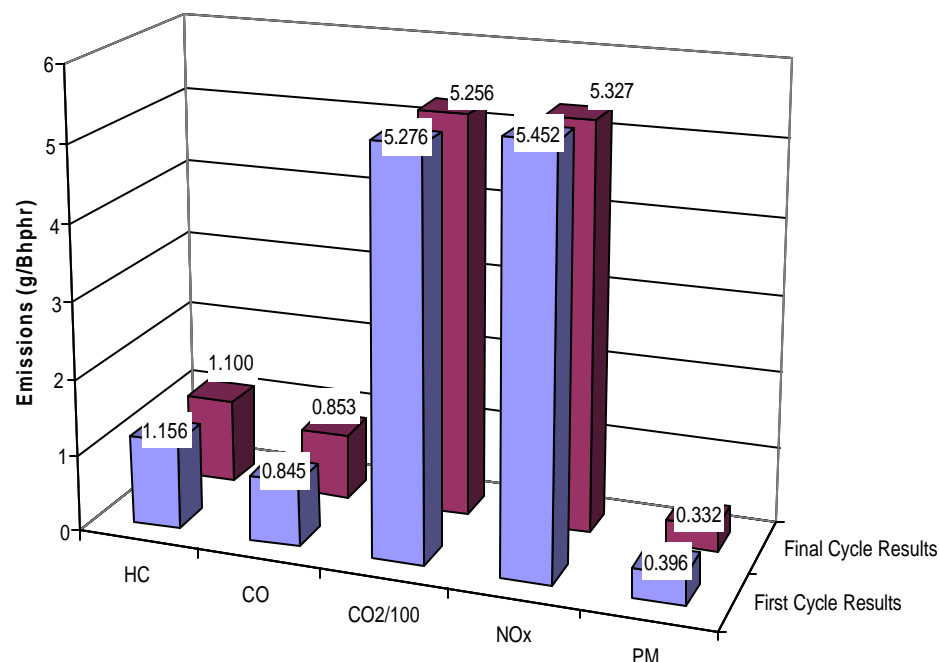
Figure 126 First and Final Cycle 3 Iteration Average Brake-specific Emissions Comparison

Upon achieving satisfactory correlation between in-field and laboratory-derived test cycles, the engine was operated according to the derived speed-load set points in order to investigate engine exhaust emissions production. Four tests of each cycle were performed to assure repeatability and QC/QA. The following is the cycle speed and load set points and the brake specific emissions results from these cycles. The reduced emissions from each cycle are presented with percentile differences shown between each test and the average value from all four tests. A comparison of average laboratory results from each of the three cycles is shown in Figure 133.
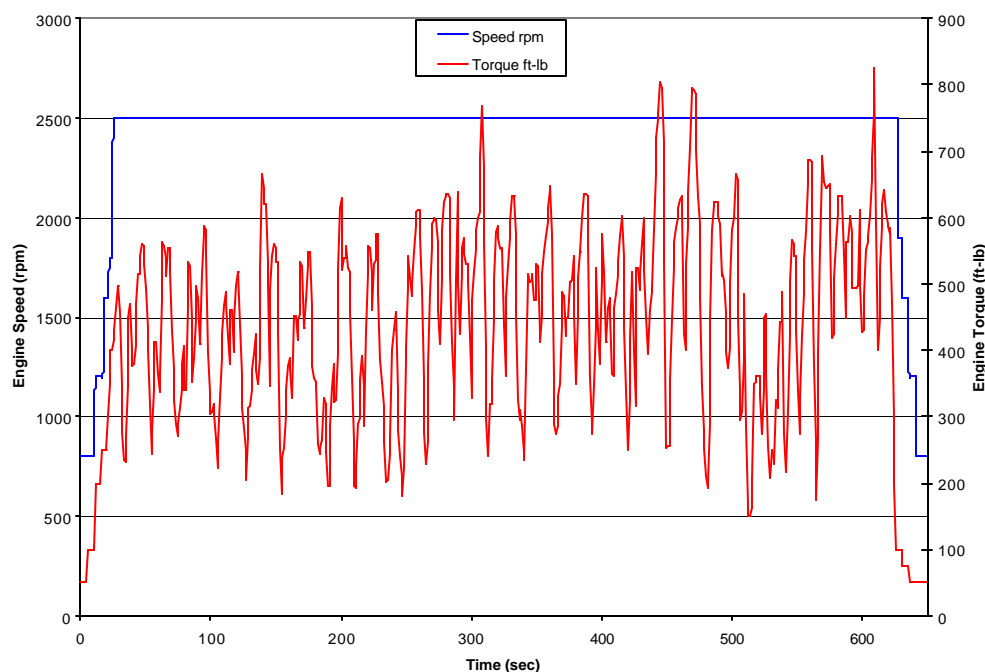
Figure 127 Cycle 1 Set-point curve

The speed was set at 2500 rpm in order to keep the laboratory fueling control at 100% by calling for an unattainable engine speed. This was the most reasonable solution to avoiding issues of fueling induced errors. The engine torque sometimes exceeded peak torque, which coincided with periods of the in-field data where the excavator encountered loadings due to embedded large rocks that would have stalled the engine if the operator had not repositioned the bucket and loaded material from another location. Most of the time, the loading tended to be between 50 and 75% of maximum load.
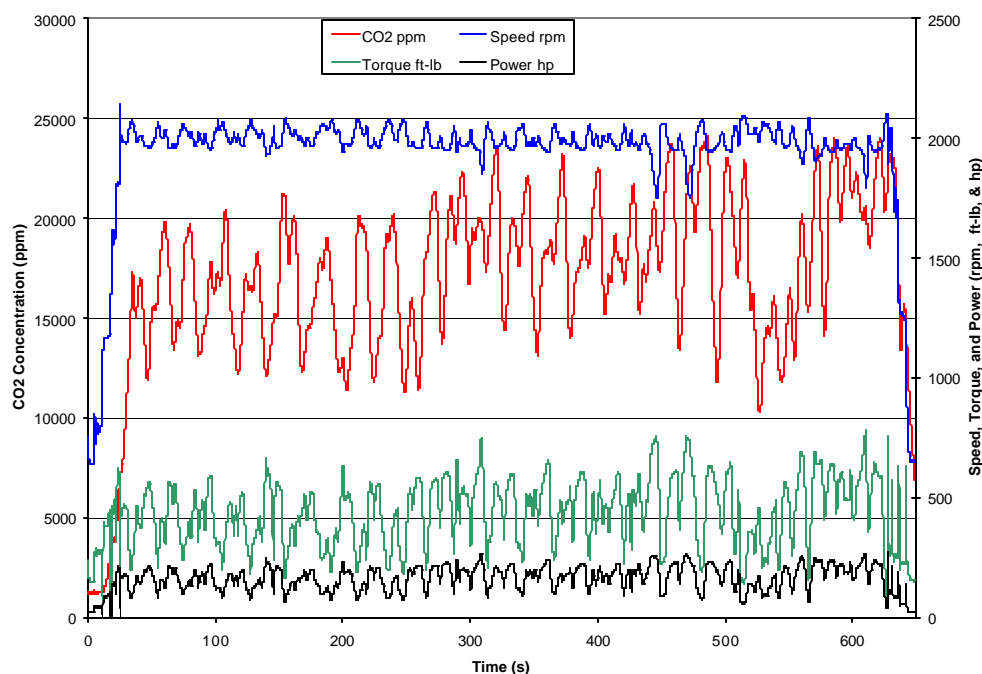
Figure 128 Continuous Cycle 1 Laboratory Results

This figure shows continuous laboratory data as recorded for speed, torque, and CO_2. Engine power was calculated from speed and torque data, and it is notable that the power curve shares notable similarities with the CO_2 curve.

Table 28 Transient Cycle Emissions Results for the Komatsu S6D125-1 Excavator Engine Operating According to the WVU Excavator #1 (Loading) Test Cycle (g/bhp-hr).

	Test 1	Test 2	Test 3	Test 4	Average
HC	1.212	1.252	1.159	1.183	1.202
CO	0.883	0.946	0.923	0.909	0.915
CO_2	536.79	538.97	539.04	538.94	538.43
NO_x	5.265	5.469	5.385	5.343	5.366
PM	0.267	0.297	0.260	0.283	0.277
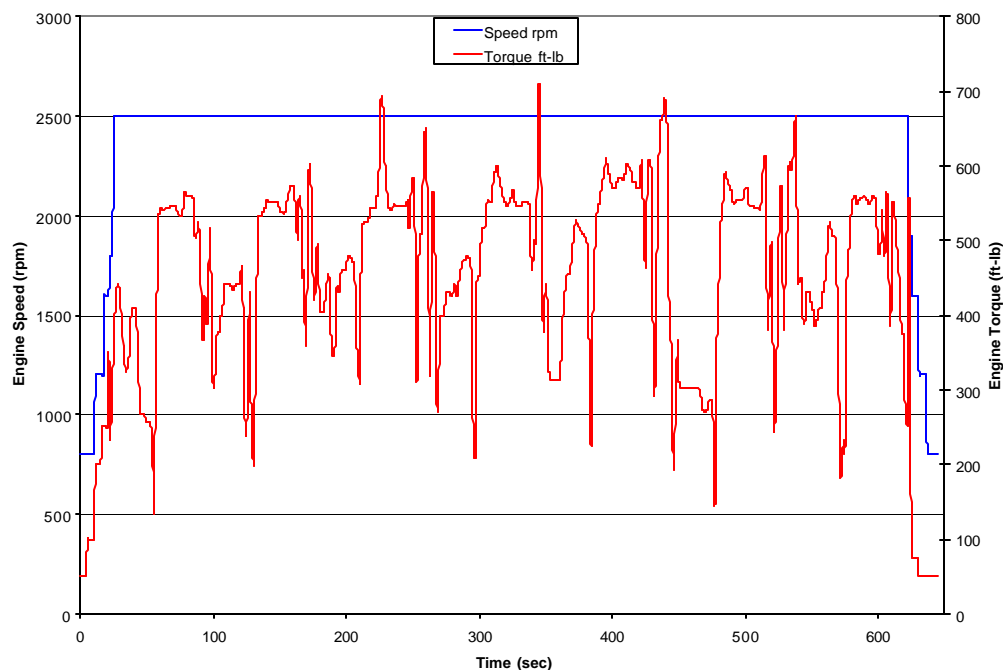
Figure 129 Final Cycle 2 Set-point File

Again, like cycle 1, the engine speed was set to an unattainable value to keep fueling at 100% and avoid fueling induced error. The long peaks indicate movement of the vehicle while spikes across these peaks indicate steering, the spikes in other areas represent periods of high loads due to filling the bucket with material. Swells indicate areas of unloading the material from the bucket, at times the swing on the excavator was operated during this time to simulate turning to load a truck with the material being hauled by the excavator.
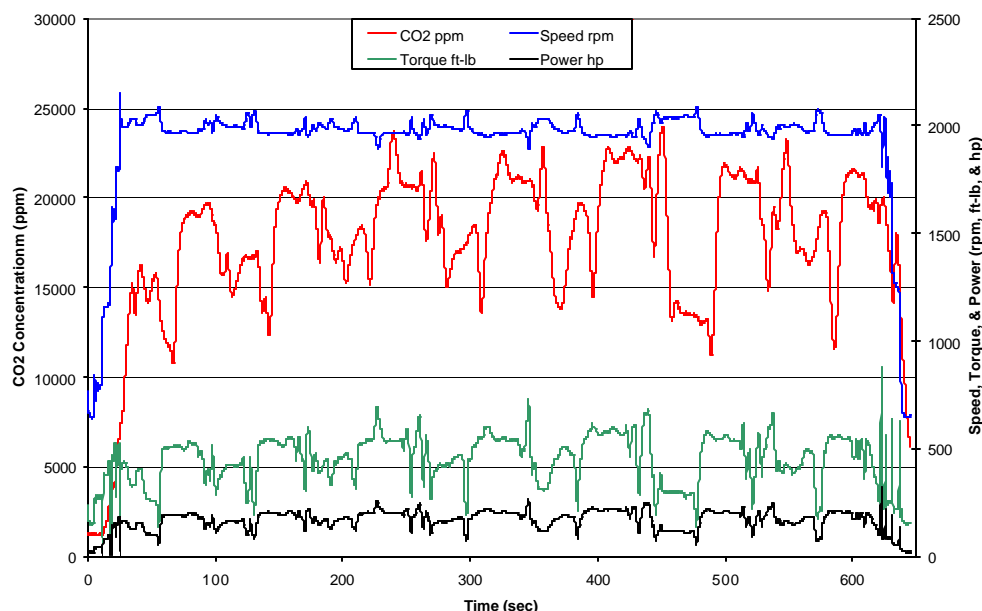
Figure 130 Continuous Cycle 2 Laboratory Results

The engine speed for this cycle did not vary as much as in cycle 1, largely due to the fact that the hauling operation did not usually cause a change in engine speed where as digging imposes variable loads on the engine that cause speed changes. Here, the CO_2, engine power, and torque traces are strikingly similar, which is a function of the relatively constant speed. Table 29 shows the averaged cycle brake-specific emissions results and the average value of the four repeat tests of this cycle that were performed.

Table 29 Transient Cycle Emissions Results for the Komatsu S6D125-1 Excavator Engine Operating According to the WVU Excavator #2 (Transport) Test Cycle (g/bhp-hr).

	Test 1	Test 2	Test 3	Test 4	Average
HC	1.156	1.158	1.169	1.095	1.145
CO	0.886	0.861	0.861	0.875	0.871
CO_2	534.00	533.67	533.91	532.381	533.49
NO_x	5.415	5.391	5.381	5.372	5.390
PM	0.305	0.274	0.290	0.251	0.280
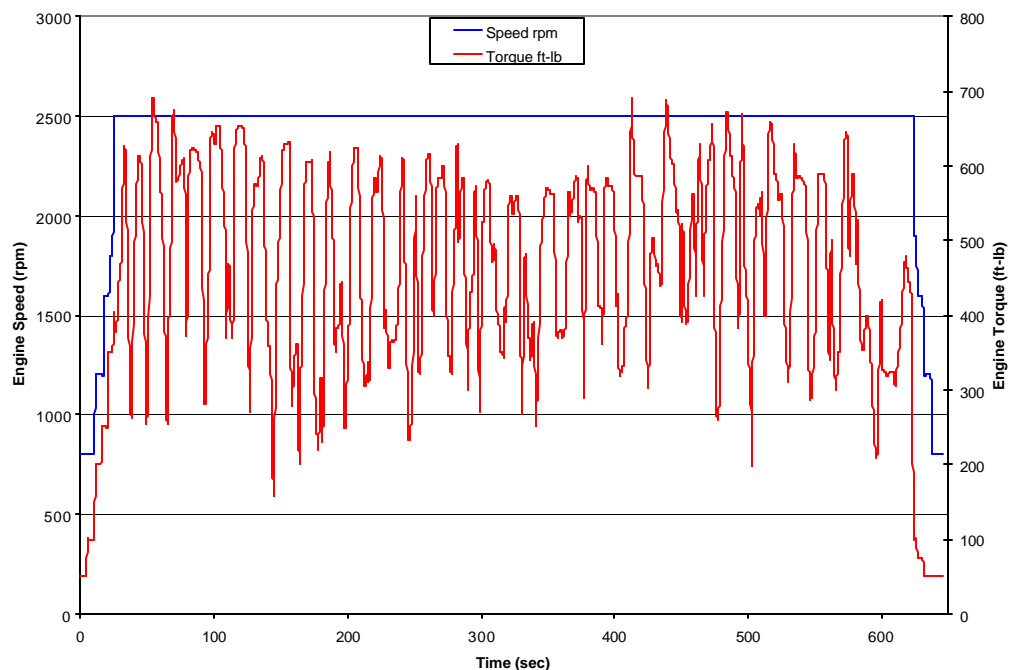
Figure 131 Final Set-point File for Cycle 3

Again the speed is set to an unattainable value, but here the loading takes characteristics from each of the two previous cycles. Short duration peaks indicate the digging of the trench while longer duration peaks indicate repositioning of the vehicle.
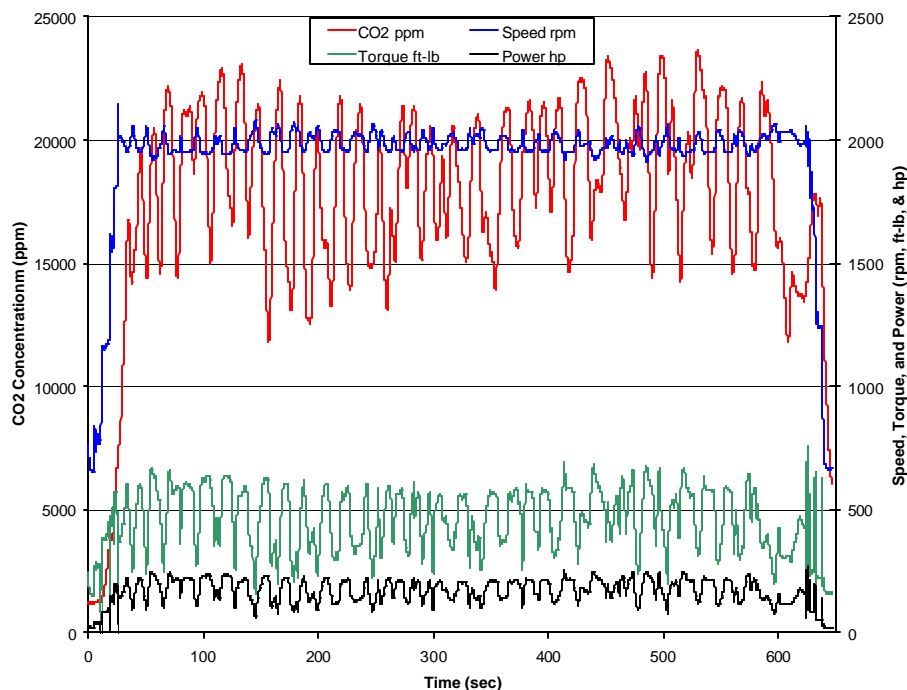
Figure 132 Cycle 3 Final Laboratory Results

Here the engine speed response tends to share more characteristically with cycle one as the trenching operation does not usually involve long periods of vehicle tramming. Thus the continuous power and CO_2 traces are characteristic of each other in this case, where torque is not as indicative of CO_2 emissions. Like the other cycles, four independent tests of this operation were performed in the laboratory, the average brake-specific results and the four test averages are shown in Table 30.

Table 30 Transient Cycle Emissions Results for the Komatsu S6D125-1 Excavator Engine Operating According to the WVU Excavator #3 (Trenching) Test Cycle (g/bhp-hr).

	Test 1	Test 2	Test 3	Test 4	Average
HC	**1.110**	**1.103**	**1.075**	**1.11**	**1.100**
CO	**0.859**	**0.856**	**0.861**	**0.837**	**0.853**
CO$_2$	**529.95**	**523.43**	**522.81**	**526.17**	**525.59**
NO$_x$	**5.338**	**5.358**	**5.324**	**5.287**	**5.327**
PM	**0.321**	**0.360**	**0.322**	**0.322**	**0.332**
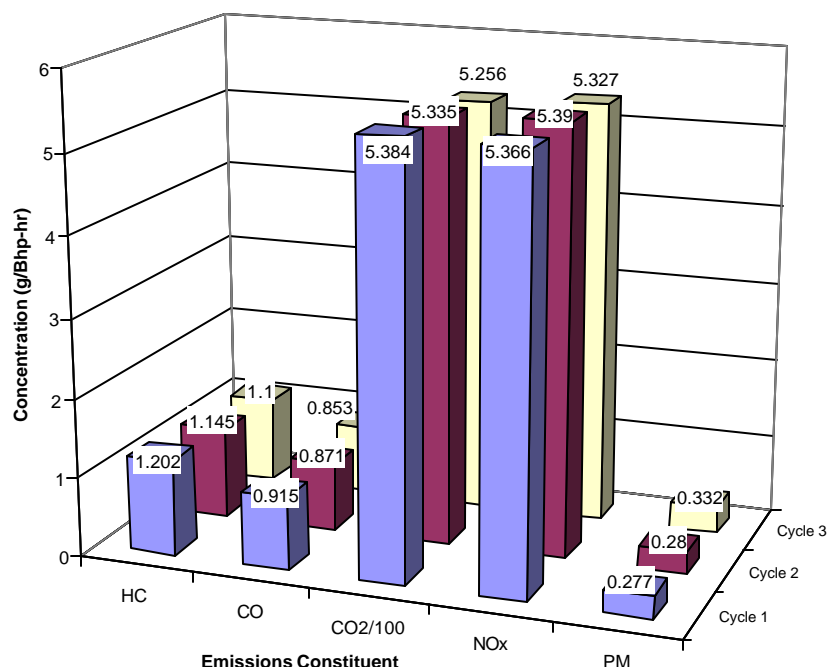
Figure 133 Average Laboratory Results Comparison for the Three Excavator Transient Cycles (g/bhp-hr).

This figure illustrates the average brake-specific emissions from the three transient test cycles. The cycles developed from the in-field data are all very similar in nature. They produce relatively similar brake specific emissions results. Although they may differ in instantaneous loading and response, the following figures demonstrate that the cycles are nearly the same when averaged. Figure 134 shows the speed range breakdown for transient cycle 1, the excavator digging operation. Values are a percentage of the total test cycle time spent in the associated speed range. Review of the figure shows that the significant operating ranges for this cycle are 1900 rpm-2000 rpm and 2000 rpm-2100 rpm. Using these speed ranges, the cycle was characterized as to the amount of time spent under different loading under the specific speed range. Figure 135 shows the amount of time that was spent at different loading ranges while the engine operated between 1900 rpm and 2000 rpm under test cycle 1. This figure shows that the engine encountered loads between 400 and 600 ft-lb for most of this time. This loading correlates with approximately 75% of max load for this engine speed.
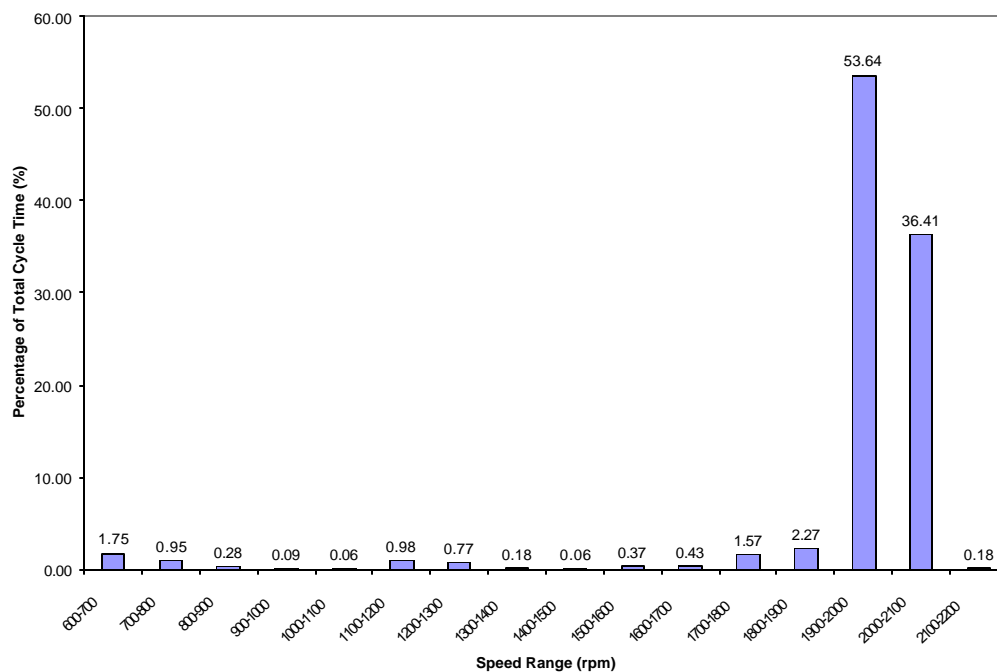
Figure 134 Speed Range Characterization for Excavator Cycle 1 (Digging)
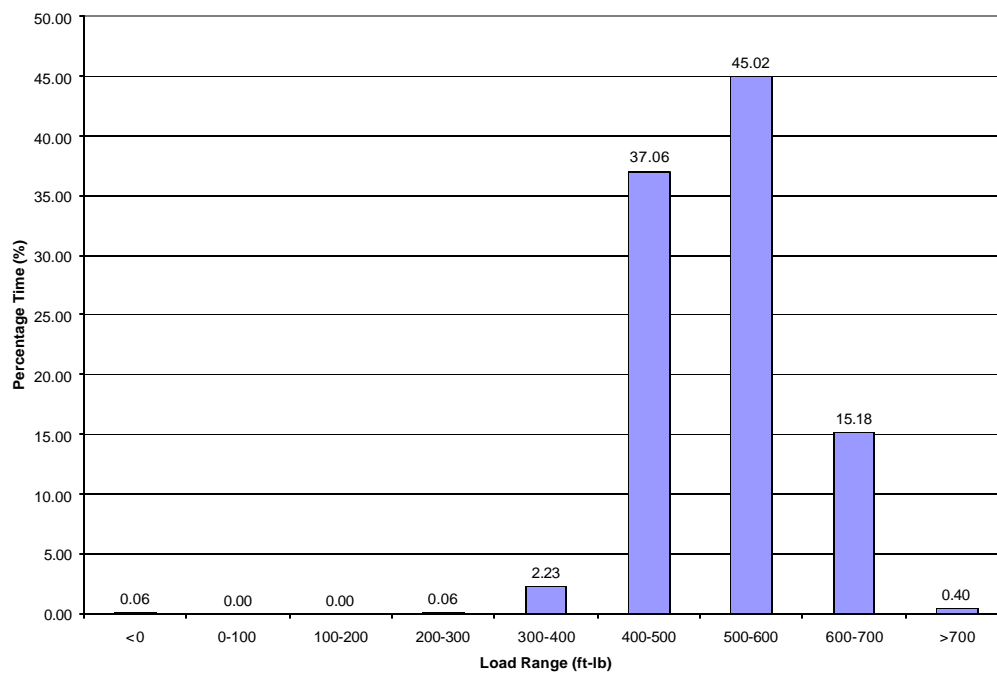
Figure 135 Load Range Characterization for 1900-2000 rpm Speed Range
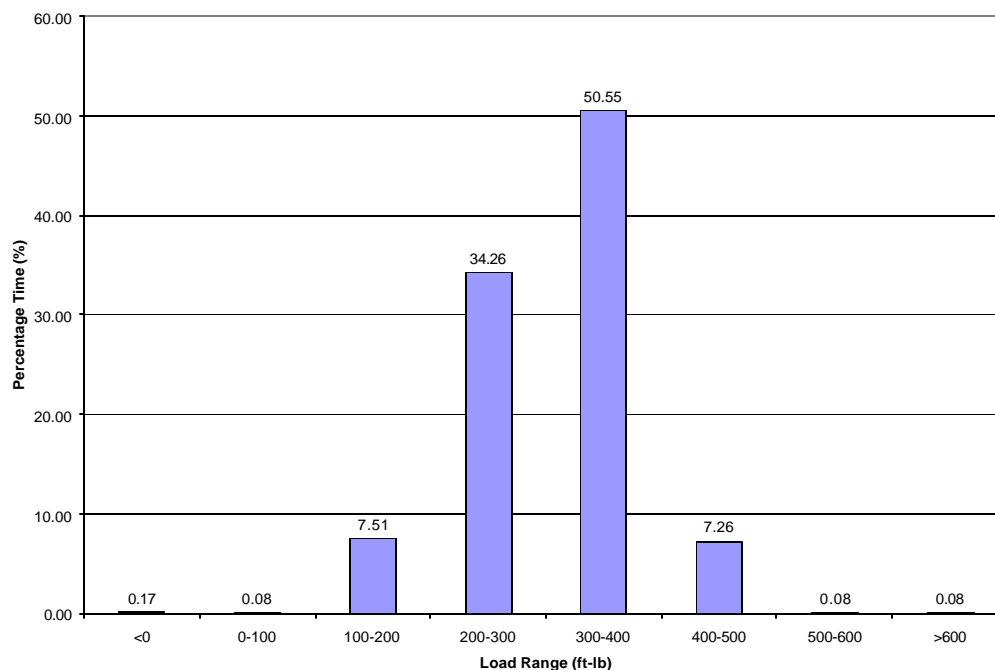
Figure 136 Load Range Characterization for 2000-2100 rpm Speed Range

Figure 136 shows the load range characterization for the 2000 rpm-2100 rpm speed range for excavator test cycle 1. As the max load significantly drops through this speed range, the 200-400 ft-lb loads that are most often encountered here represent nearly 100% loading. This is intuitively correct, as the nature of the operation would be that the engine would be operating at max speed, then speed would be reduced as the excavator digs a load of material to the point where the load introduced to the engine would be compensated by the ability of the engine to produce power.
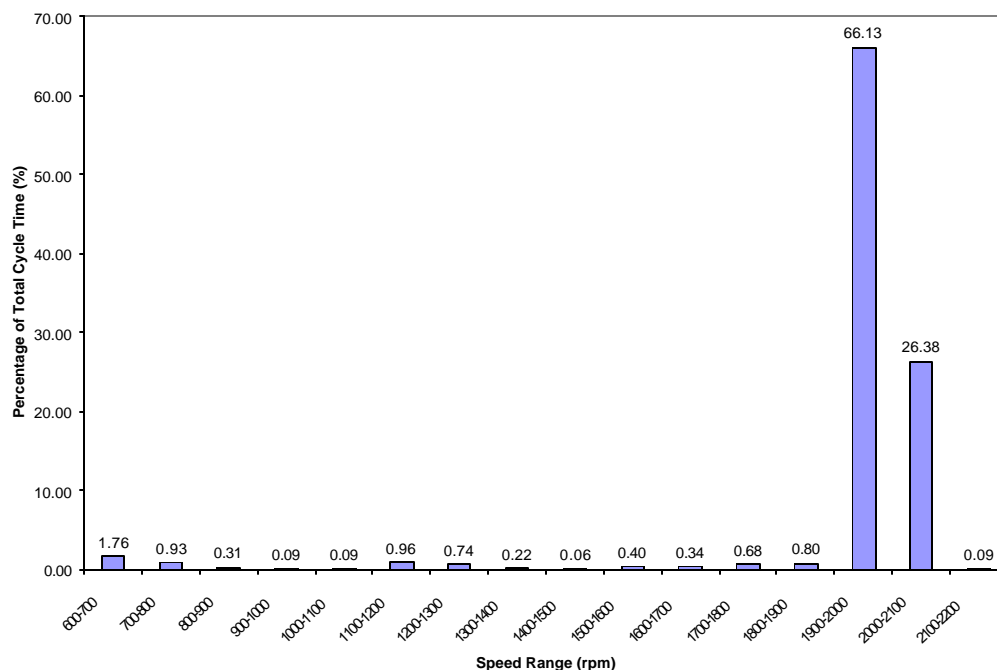
Figure 137 Speed Range Characterization for Excavator Cycle 2 (Hauling)

Figure 137 shows the speed range characterization for the excavator hauling cycle that was developed from in-field data. Again, like cycle 1, the significant speed ranges are 1900-2000 and 2000-2100. This is largely due to the same reason as the operation of the excavator tends to start from max speed and then loading causes changes in engine speed. Figure 138 shows the load incurred during the operation of the engine in the 1900 rpm-2000 rpm speed range under test cycle 2. This again indicates that the engine incurs nearly 75% of max load under this speed range for the majority of the time. Figure 139 shows the load ranges seen during operation of the engine in the 2000 rpm-2100 rpm speed range under this cycle. The 100-200 ft-lb range is the vast majority of this portion of the cycle, which is near 100% loading the higher speeds of this range. Review of the characterizations of cycles 1 and 2 reveals close similarities between the averaged cycles.
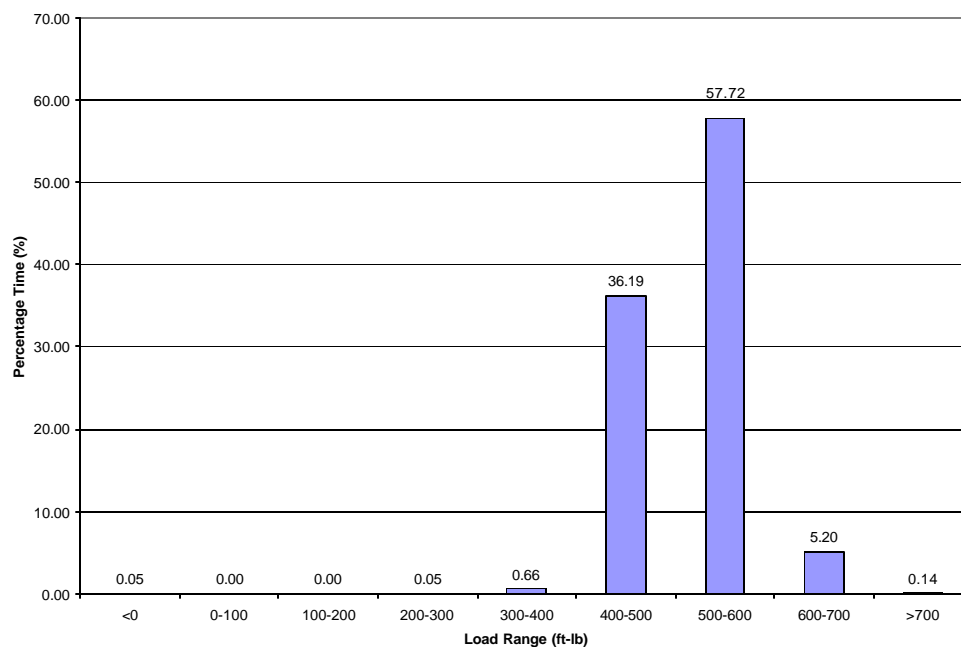
Figure 138 Load Range Characterization for 1900-2000 rpm Speed Range for Excavator Cycle 2
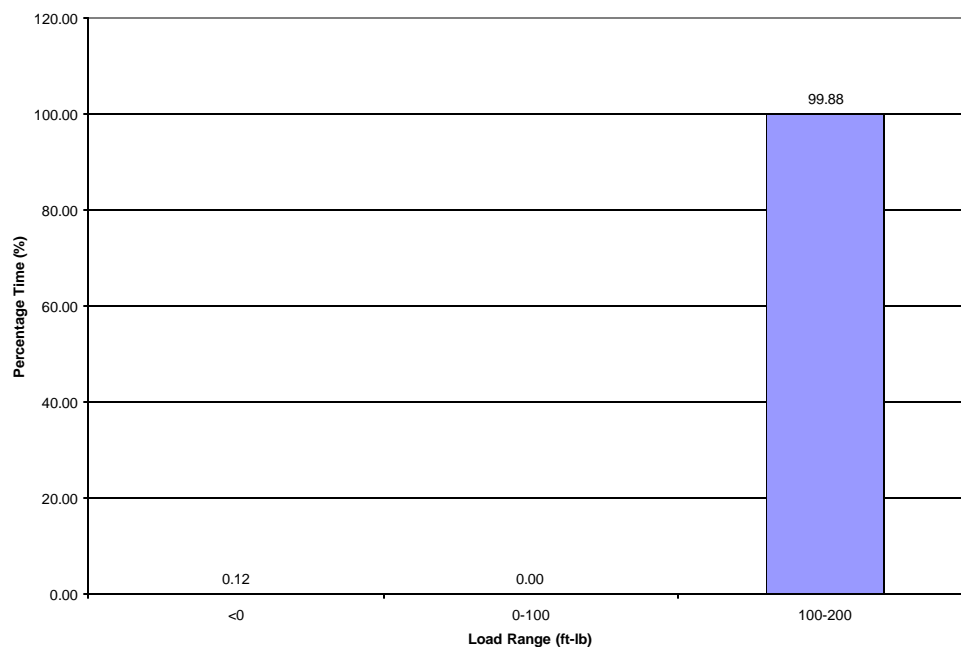
Figure 139 Load Range Characterization for 2000-2100 rpm Speed Range for Excavator Cycle 2

The final excavator cycle derived from in-field test data, the trenching cycle, again shows very similar characteristics to cycles 1 and 2. Again, as indicated in Figure 140, the significant speed ranges are 1900-2000 and 2000-2100 rpm.
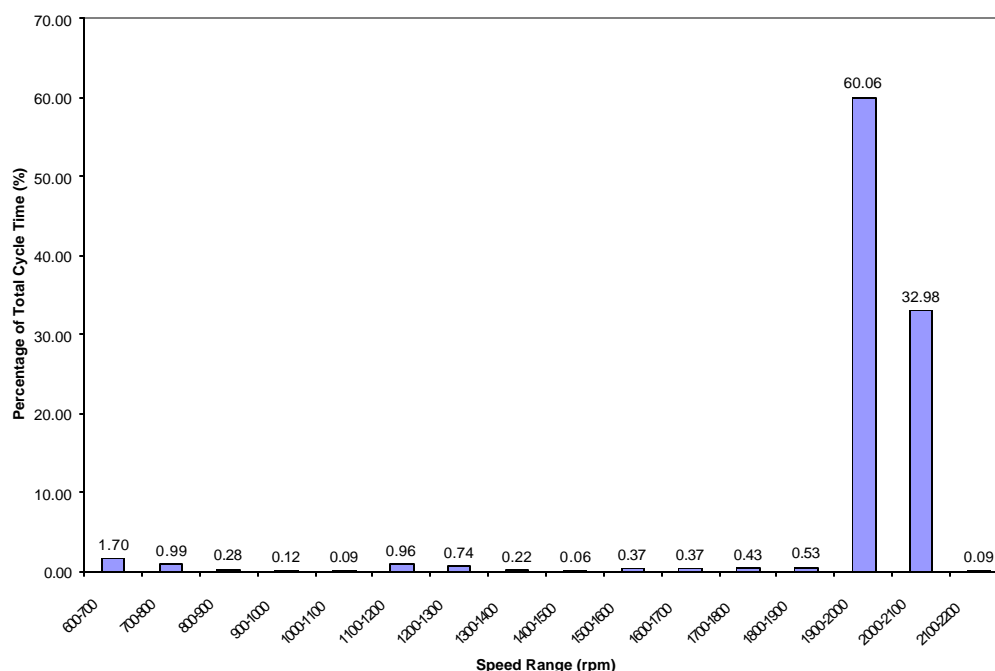
Figure 140 Speed Range Characterization for Excavator Cycle 3 (Trenching)

As the operations in cycle 3 combine those performed in cycles 1 and 2 (i.e. trench digging requires digging and tramming), the load characteristics should tend toward the average of both cycles 1 and 2. Figure 141 tends to agree with this as the percentage of time spent in the 500-600 ft-lb range is an approximate average of the time percentage values for cycles 1 and 2 in this speed and load range. The results shown in Figure 142 tend to favor the results of cycle 1 for this speed range. This is somewhat logical as the trenching cycle spends more time in digging than moving the machine, therefore, the characteristics of high speed operation will be more often influenced by introducing a digging load.
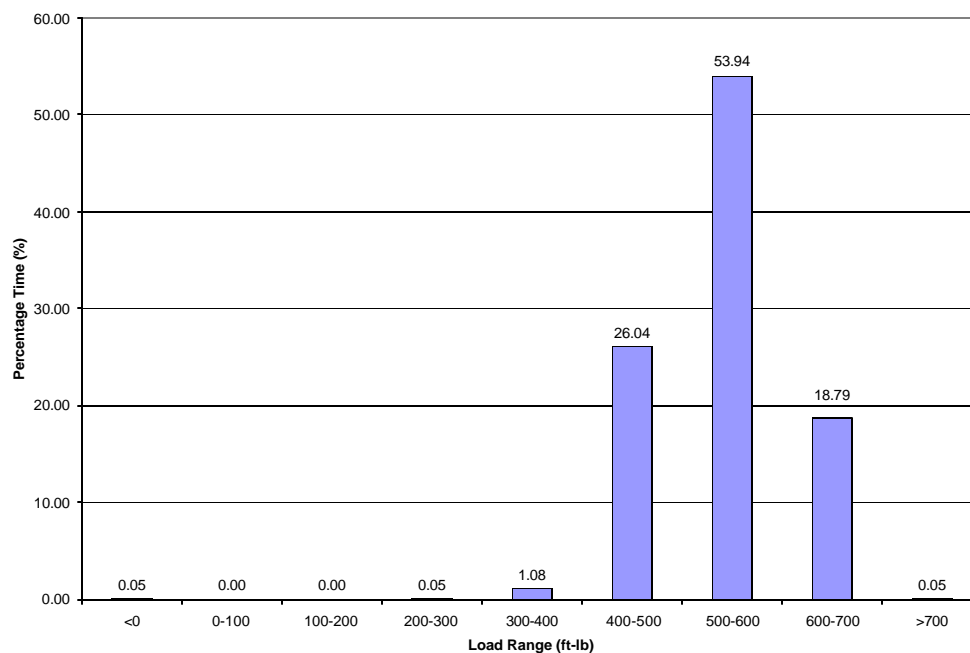
Figure 141 Load Range Characterization for 1900-2000 rpm Speed Range for Excavator Cycle 3
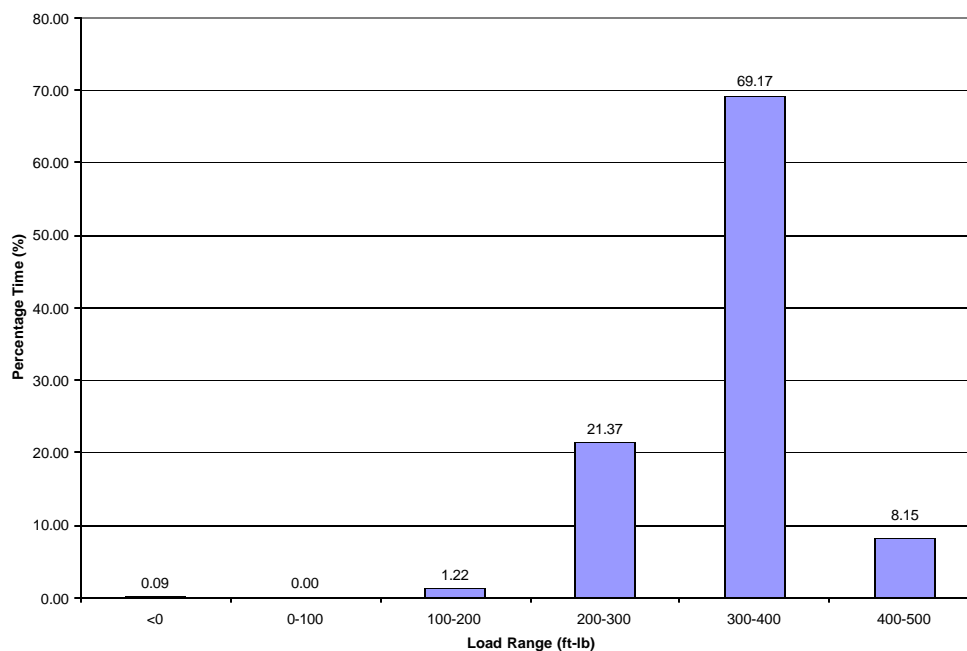
Figure 142 Load Range Characteriza tion for 2000-2100 rpm Speed Range from Excavator Cycle 3

In order that engine performance could be compared to manufacturer specifications such that the effects of age may be weighed, two ISO 8178-C steady state tests were performed. The test set points are listed and the results from these tests are tabulated below. At the request of CARB, the eighth or idle mode was performed separately as an extended idle mode at curb idle, the average results of the steady state test data is shown in Table 32, and Figure 143. Weighted 8-Mode results are shown in Figure 144.

Table 31 Excavator 8-Mode Engine Speed/Load Set Points.

Mode Number	Engine Speed (rpm)	Torque (ft-lbs)	Horsepower (hp)
1	1800	730.0	250
2	1800	547.5	188
3	1800	365.0	125
4	1800	73.0	25
5	1350	745.0	192
6	1350	558.8	144
7	1350	372.5	96
8	≈760	-	-

Table 32 Average 8-Mode Results (Test 1) for the Komatsu S6D125-1 Excavator Engine (g/bhp-hr).

	Mode 1	Mode 2	Mode 3	Mode 4	Mode 5	Mode 6	Mode 7	Mode 8	Weighted Results
HC	0.822	0.940	1.269	7.061	0.596	0.793	1.083	7.271	2.49
CO	0.842	0.563	0.788	6.449	1.829	1.036	0.799	8.061	2.55
CO_2	494.67	499.57	528.44	1036.54	488.86	489.415	507.15	862.10	610
NO_x	7.328	6.396	5.257	7.854	7.664	7.469	6.867	16.166	8.26
PM	0.362	0.295	0.328	1.449	0.582	0.432	0.360	1.354	0.633

These test results indicate that the engine usually operates at governed speed between 50% and 75% of maximum load. This confirms observations made during the collection of the in-field data. Particular attention was given to the idle mode as many machines spend a large amount of time at idle in any given day of operation while an operator may be awaiting instruction from or activity completion from the ground crew before the next equipment task.
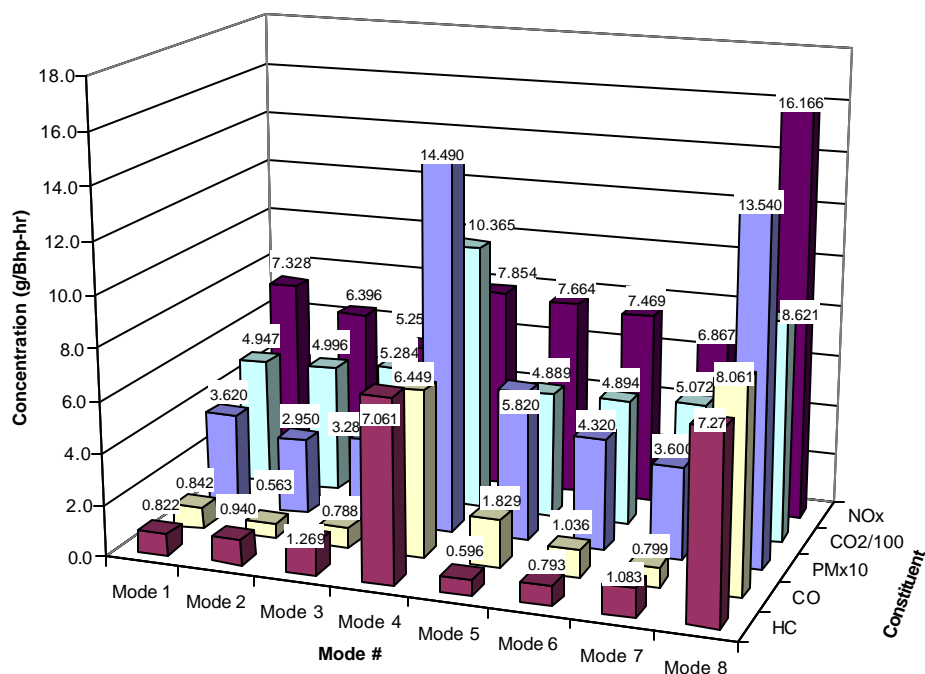
Figure 143 Average of 8-Mode Results for the Komatsu S6D 125-1 Engine (g/bhp-hr).
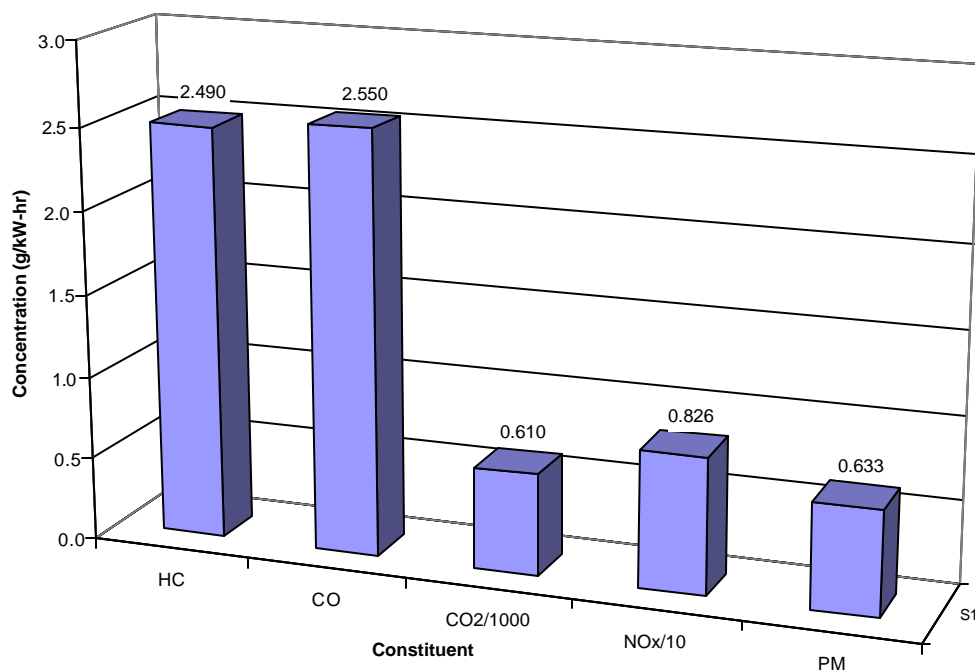
Figure 144 Average Weighted 8-Mode Emissions for the Komatsu S6D125-1 Engine (g/bhp-hr).

Table 33 Comparison of Weighted 8-Mode Results with Average Transient Test Results for the Komatsu S6D125-1 Excavator Engine (g/bhp-hr)

	Weighted 8-Mode Results	Transient Cycle 1 Results	Transient Cycle 2 Results	Transient Cycle 3 Results	% Diff Cycle1 to 8-Mode	% Diff Cycle 2 to 8-Mode	% Diff Cycle 3 to 8-Mode
HC	2.49	1.202	1.145	1.100	-51.7	-54.0	-55.8
CO	2.55	0.915	0.871	0.853	-64.1	-65.8	-66.5
CO$_2$	609.91	538.43	533.49	525.59	-11.7	-12.5	-13.8
NO$_x$	8.26	5.366	5.390	5.327	-35.0	-34.7	-35.5
PM	0.633	0.277	0.280	0.332	-56.2	-55.7	-47.5

It is notable that emissions produced during the transient test cycles are much lower in value than those of the weighted 8-Mode results (see Figure 144). This indicates that use of the 8-Mode test for emissions inventory purposes could provide misleading data.

3.6.4 Track-Type Tractor In-Field Emissions Tests Results

3.6.4.1 Vehicle Instrumentation

The testing of the D-11R CD Track-type Tractor was performed in early 2002. This vehicle was tested in-field only. Therefore, engine maps and engine speed and load-CO_2 matrices were not developed. The in-field testing of the track-type tractor with the objective of collecting laboratory grade emissions data was a monumental task that required many considerations. The vehicle operated in an environment that tested the reliability and durability of any equipment, for example the vehicle itself is designed to withstand 10 G vertical loadings. As the machine removed material, it dug through layers of sandstone that caused substantial amounts of vibration. High levels of dust became airborne as material was moved. The climate of the area was also very extreme with high winds, inclement weather, and extremely cold temperatures. The weather on the day of the test was windy with brief scattered rain showers and temperatures around 4° C (40° F).

Prior to testing, the oil, fuel, and air filters, as well as engine oil, were changed as part of routine maintenance. The exhaust stack caps were removed so that exhaust flow measurement devices could be affixed to the stack. The Caterpillar inlet air pre-filter system was disabled prior to testing the vehicle, due to its inherent entrainment of excess ambient air into the exhaust stream. This technique would have invalidated the PM concentrations that were sampled from a slip-stream, since an accurate account of exhaust dilution could not have been readily obtained. Due to proprietary issues, a Caterpillar representative was on site to collect engine speed and power data from the engine controller. The WVU MEMS is capable of interrogating engine control units that broadcast public information data streams, but this particular Caterpillar system did not operate according to industry-standard communication protocols. Therefore, the WVU system could not parse the collected data stream. WVU could have undertaken the task, but representatives from Caterpillar were unwilling to provide WVU with the requisite ECU interface tools for proprietary reasons. The information collected here would be

useful in calculating engine load and thus the duty cycle, and to provide a check on the emissions analyzers, so Caterpillar opted to send a representative to record this data and report it to WVU. Engine speed was recorded directly from a magnetic pickup. The signal was divided between the Caterpillar ECU interface, the MEMS gaseous emissions system, and the MARI RPM100. This common data stream provided for necessary time alignment information. The emissions testing equipment was securely mounted to the external surfaces of the track-type tractor, and thus exposed to environment and vibration. Vibration damping material was used to protect against vibration and shock loading, and strain-reliefs were applied in order to reduce the likelihood of component failure. Heated sample lines were used to transfer the exhaust sample to the analyzers. Vehicle information pertaining to identification numbers and overall vehicle condition was also collected via manual inspection. Once all emissions testing equipment was secured and operational, the testing procedure began.

3.6.4.2 Testing Procedure

The first test was a transport operation where the vehicle moved from the set-up site to the digging site. This operation was used as a "shakedown" exercise to verify system operation. Once at the digging site, the emissions measurement system was calibrated. This procedure was also repeated between each test. As the test commenced, there was a short idle period, then the vehicle moved into the area material was to be removed from. The digging operation consisted of pushing down from one side of a pit and pushing material across and piling it over the area where coal had been previously removed. When the operator reached a point where material had been sufficiently moved from the area, the vehicle reversed to the original starting point and pushed another load across the pit. This cycle repeats itself until the loose material is removed to the point where excavators and end loaders can finish the last removal of overburden and extract coal. During normal operation the vehicle will operate like this for 11 hours, after which time the vehicle is refueled, lubricated, and inspected. The machine is usually stopped for one hour while this process takes place. For the purposes of this testing, data collection was scheduled to coincide with operating cycles that were approximately 30 minutes in length. This test plan provided adequate cycle information, without risking the introduction of errors due to instrumentation drift, etc. In addition, it was anticipated that problems could be addressed without expending large amounts of time on voided tests. During the testing process, numerous problems were encountered that shortened the amount of data collected. Ultimately, a power generator failure, which was quickly rectified, and time scheduling constraints ended the in-field testing, but not before a sufficient amount of emissions data was collected.

3.6.4.3 Emissions Test Results

Due to engine size restrictions as well as reluctance of the vehicle's owner to modify the production exhaust system, the researchers had planned to measure the mass emissions of exhaust constituent emitted from the individual exhaust stacks. The Vee configuration and the exhaust system design, which incorporated an exhaust manifold equalization crossover, provided a means to independently measure the mass emissions from each stack. During the tests, each exhaust stack was outfitted with the short test sections in order to avoid significant backpressure differentials, and hence exhaust flow rates difference, between the two exhaust streams.

As mentioned in the previous section, due to proprietary issues, it was necessary to schedule the services of a Caterpillar representative to collect engine speed and power data from the engine controller. A Caterpillar data-link was installed by Mr. Pat Jones, from Caterpillar, and the unit was initialized to log the necessary engine speed and load information that is paramount to providing brake-specific mass emissions results. At the test-site it was indicated that the data collected using the data-link had been truncated. Apparently the system malfunctioned in recording the data during the digging tests. After further consultation during the week following the in-field tests, the researchers learned that Caterpillar would only be able to provide WVU with a limited amount of information that was recorded during the transportation of the tractor from the instrumentation set-up/tractor storage location to the actual mining test-site as the data from the other tests was not recorded due to this malfunction. It was originally decided that this operation would be used as a "shakedown" exercise; therefore no exhaust emissions data was collected. However, the data collected by Caterpillar is included in Figure 146. Since no engine loading information was provided by Caterpillar for the remaining tests, the researchers attempted to retrieve detailed brake-specific fuel consumption data from Caterpillar, but, again, due to its proprietary nature this data was not provided by Caterpillar. As a result, the emissions data presented herein for the in-field testing of the D11R CD are in a mass-per-unit-time (g/s) basis. An engine lug curve was recorded by Caterpillar from the ECU memory and is shown in Figure 145.
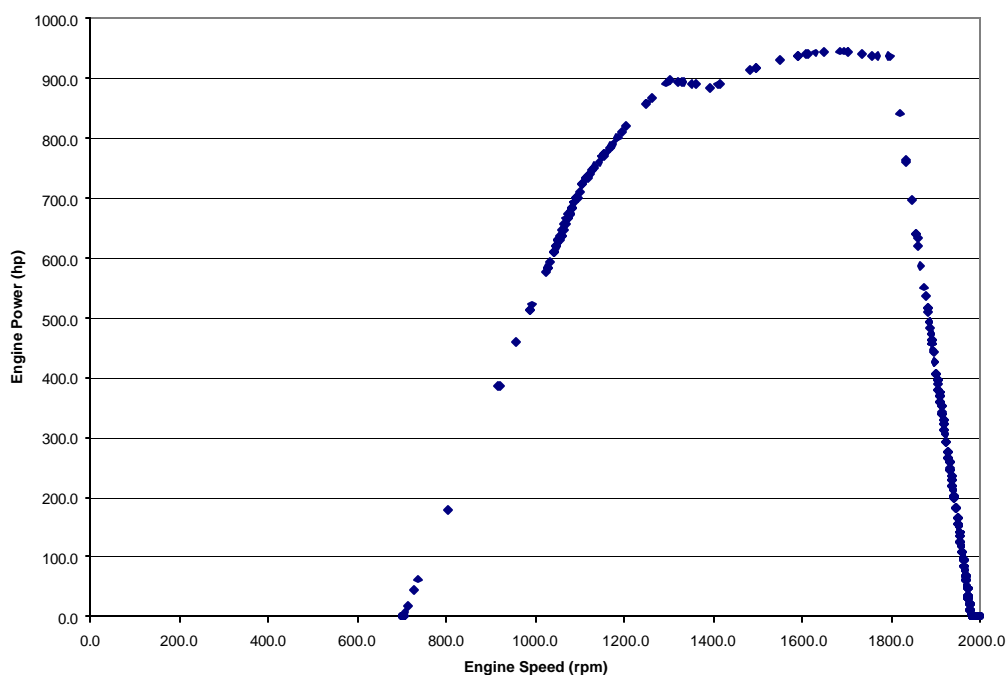
Figure 145 Caterpillar D-11R CD Track-type Tractor 3508 Engine Lug Curve

3.6.4.3.1 Gaseous Emissions Results

The results presented herein were collected during the in-field testing of the D-11R CD Track-type Tractor. Due to a data acquisition problem encountered during the

first digging test, PM data was only collected for a portion of the full test. The gaseous results of this test have been presented in two formats. First the data is shown for the length of the test that PM data was collected such that integrated gaseous results can be compared to PM results. Secondly, the full gaseous test results are reported in their entirety. Figure 147 shows the full engine speed and raw CO_2 data recorded by the MEMS during the first digging test, whereas Figure 148 illustrates the shortened results of the first digging test that coincide with the PM data collected during this test. Similarly, Figure 149 shows the full engine speed and NO_x data as recorded by the MEMS during the first digging cycle, whereas Figure 150 illustrates the shortened version of these results that provide for comparison with PM results. The second test (a repeat of the operations from the first test) was performed after a zero/span verification of the emissions testing equipment. Figure 152 presents the continuous engine speed and CO_2 results recorded by the MEMS during this second digging test, while Figure 153 shows the NO_x results from this test.

3.6.4.3.2 Particulate Matter Emissions Results

Gravimetric PM data was collected during the tractor in-field operation, and PM data is presented for a portion of the first test. In order to provide for more information, the gaseous emissions test results were shortened to yield integrated results that would coincide with PM data. The full test results have also been included in order to present CARB with additional in-field emissions information.

The test cycle over which the PM mass results were integrated was 360s in length. The operation consisted of approximately 260s of idle data, with the remainder of the test being comprised of transport and digging. Figure 151 presents the NO_x mass rate (g/s) and PM concentration (mg/m^3) for the test cycle. As stated earlier, since Caterpillar was unable to provide the necessary engine speed and load data, the data for the in-field tests are presented on a mass rate basis. As Figure 151 indicates, the integrated PM mass emissions for the test cycle (360 seconds long) were 0.349g.
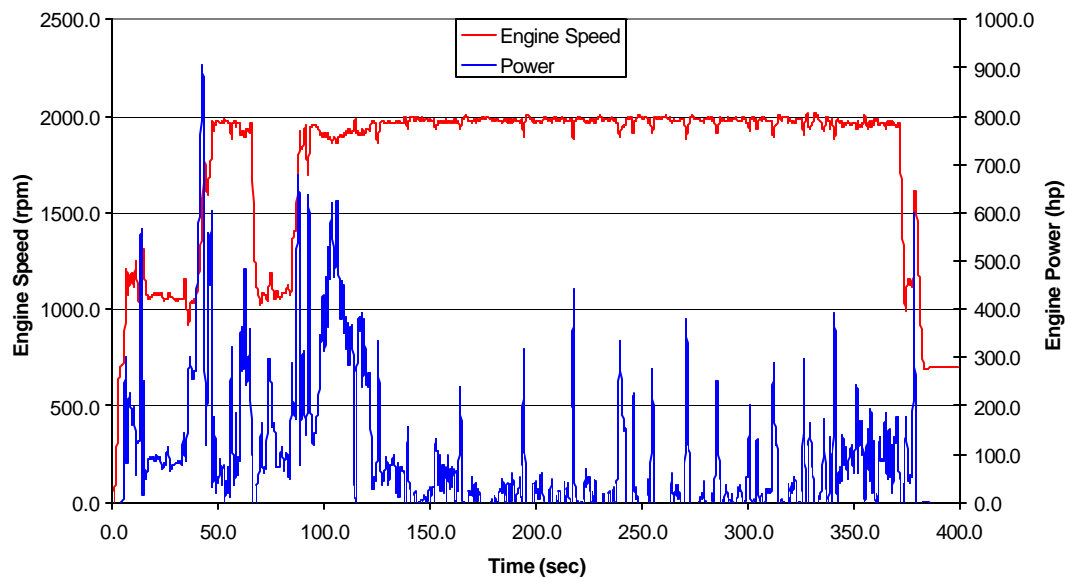
Figure 146 Engine Speed and Power Data Collected by Caterpillar during Track-type Tractor Transport.

This figure shows the characteristics of transport mode. The engine operates at high idle and the loading is relatively low. The large spike at the 50 second mark indicates the point at which the blade was lifted. The smaller peaks along the test cycle are most likely the result of steering loads imposed as the dozer locks one track while the other continues motion. The cycle involved moving along a relatively level plane until about 125 seconds at which point the dozer started traveling down a grade into the mine pit. The engine seems also to idle at a higher rate when it is not warm as indicated by the engine idle speeds at the beginning and end of the test cycle.
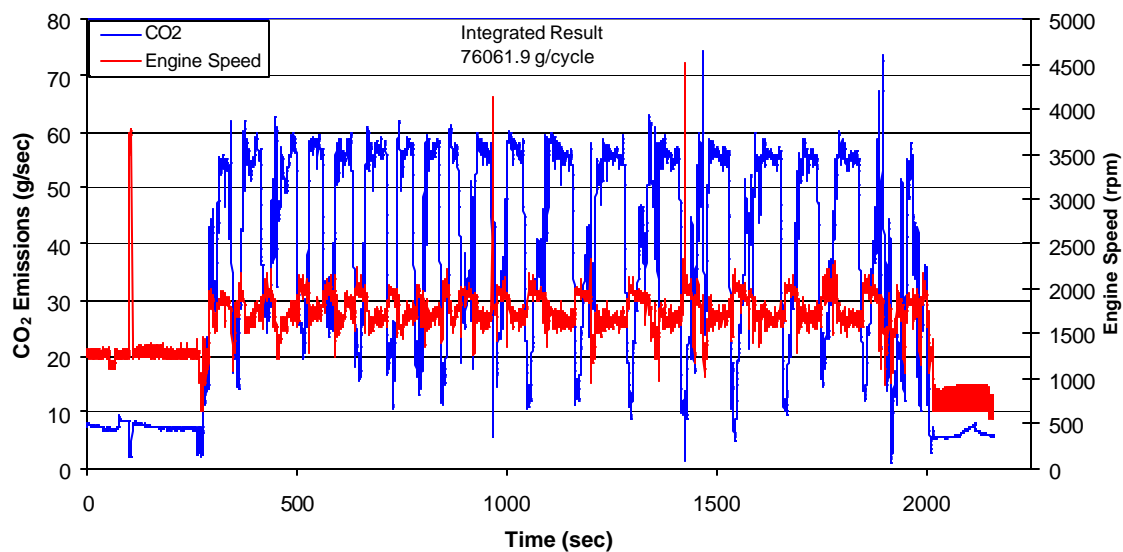
Figure 147 CO₂ Mass vs. Time for the First Track-type Tractor Digging Test (Full Cycle)
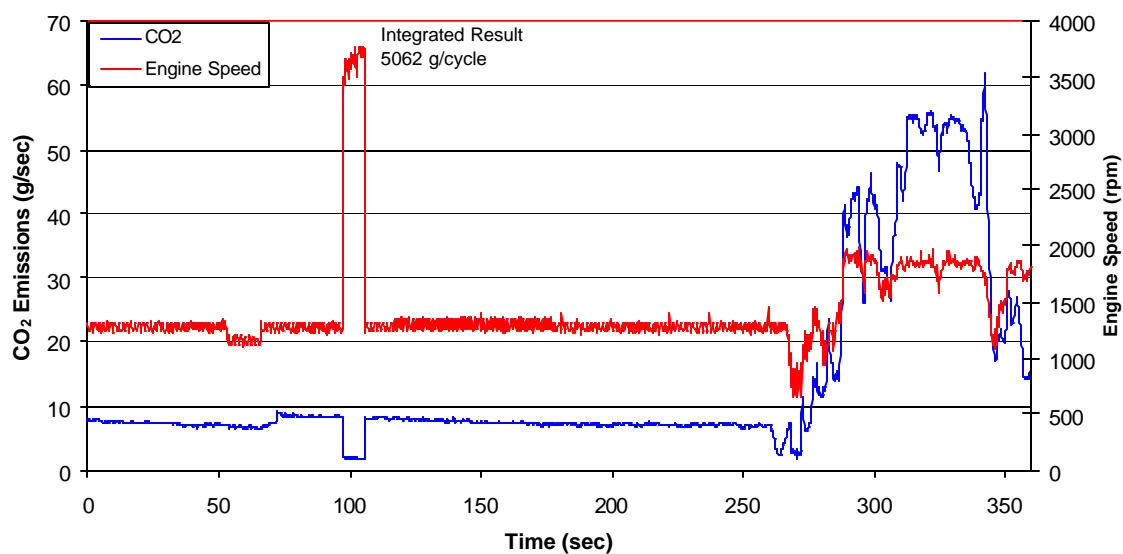
Figure 148 CO₂ Mass vs. Time for the First Track-type Tractor Digging Test (Cycle Shortened to Coincide with PM Data)
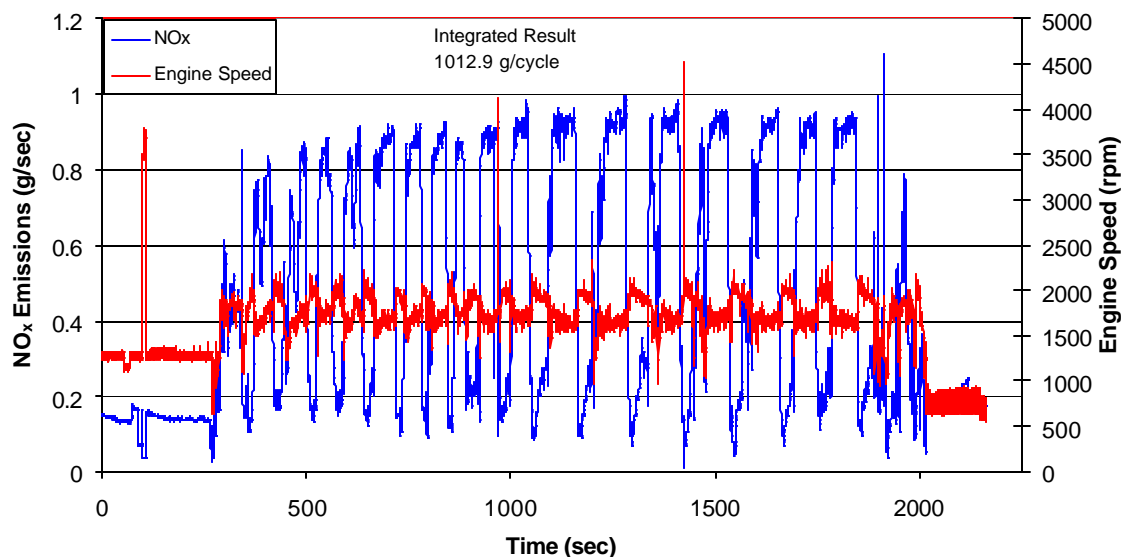
Figure 149 NO$_x$ Mass vs. Time for the First Track-type Tractor Digging Test (Full Cycle)
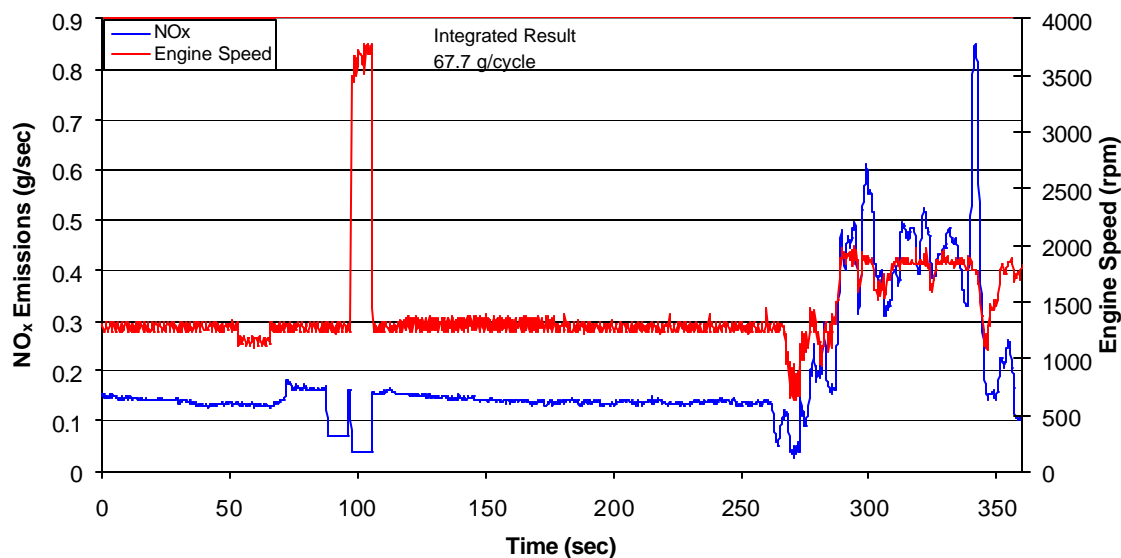
Figure 150 NO$_x$ Mass vs. Time for the First Track-type Tractor Digging Test (Cycle Shortened to Coincide with PM Data)

The periods of high engine speed indicate the transport of the tractor to the starting point, and the lower speed and higher emission peaks indicate the production run of the machine as it moves material across the pit. These figures illustrate that the duty cycle of the engine is very repeatable in nature. The initial cycle peak from idle, which occurs near 250 seconds, is the result of a transport up a steep grade over loose material

as the tractor was moved into position to begin the first digging cycle. At the end of the test, the tractor was moved back down this grade to a point where the test equipment could be serviced and calibrated.
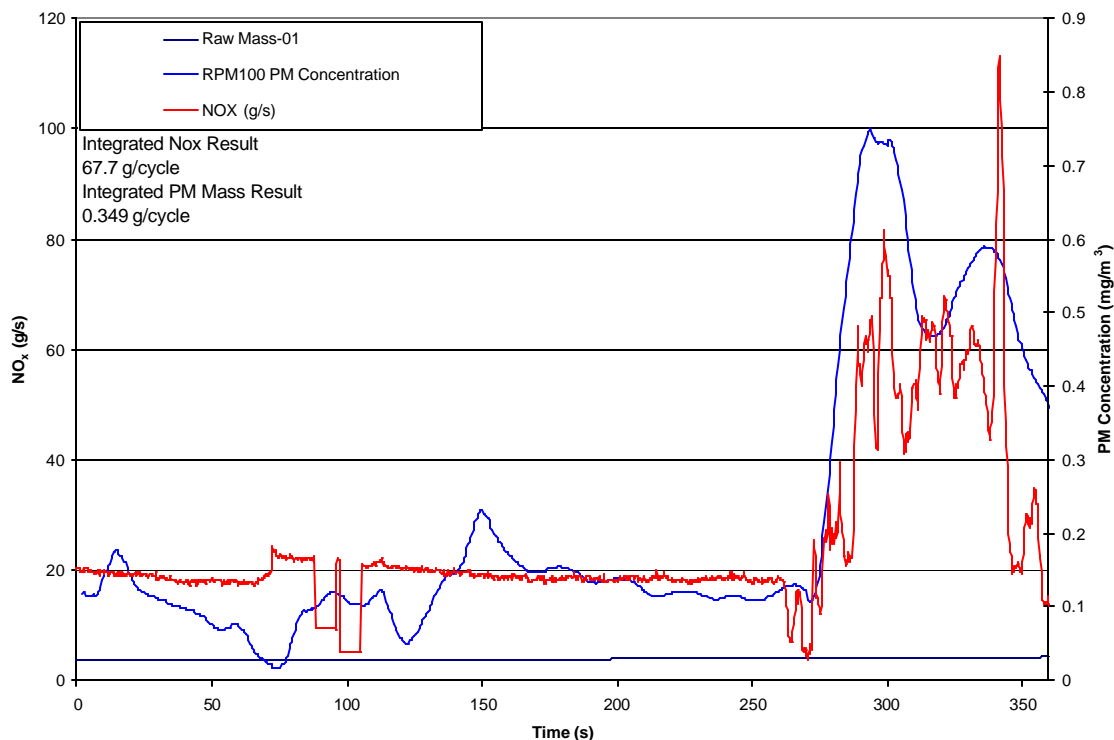
Figure 151 NOx and PM Concentration Data for the First Track-type Tractor Digging Test.

The continuous PM concentration data is shown in Figure 151, the data of most interest starts at 250 seconds. The trend here shows a smooth increase in PM concentration with increasing engine speed and load, which is expected. The reasons that this curve appears smooth relative to the NO_x data could be in the speed of data recording, or it may be due to the continuous adjustments made by the RPM 100 to the sample, which dampen instantaneous effects. Over the entire cycle, the tractor produced 0.349 grams of PM that was recorded by the RPM 100.

After the first digging test, it was observed by the Caterpillar representative that the ECU data had not been recorded. During the time between tests, an attempt was made to find and fix the problem. This process continued through the first part of test two, which is visible in the following figures as the speed of the engine changes near the 300 second mark. This is due to the changing of engine speed to determine if Caterpillar's data logging equipment was functioning properly. The test was

shortened by an equipment failure, but it is evident that the engine duty cycle is very repeatable in nature.
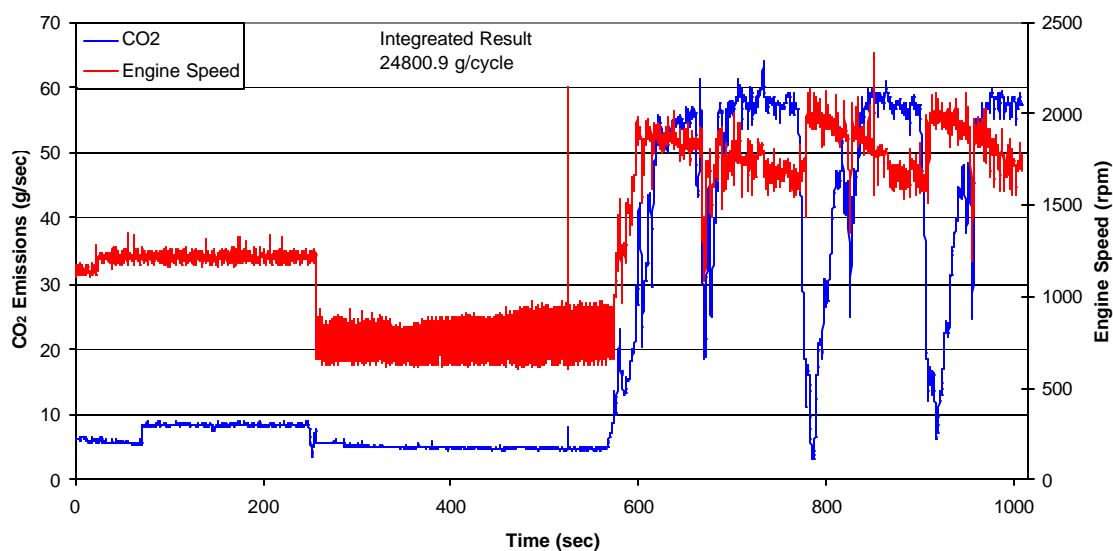
Figure 152 CO$_2$ Mass vs. Time for the Second Track-type Tractor Digging Test

Again noise spikes can be observed in the data, which is most likely the result of vibration. The engine at full load tends to produce nearly 60 grams of CO$_2$ per second, as recorded from one stack, which agrees with the data from the first digging test. Figure 153 shows that the full load continuous production of NO$_x$ was recorded as nearly 0.9 grams per second from one stack, which is also in agreement with data from the first test.
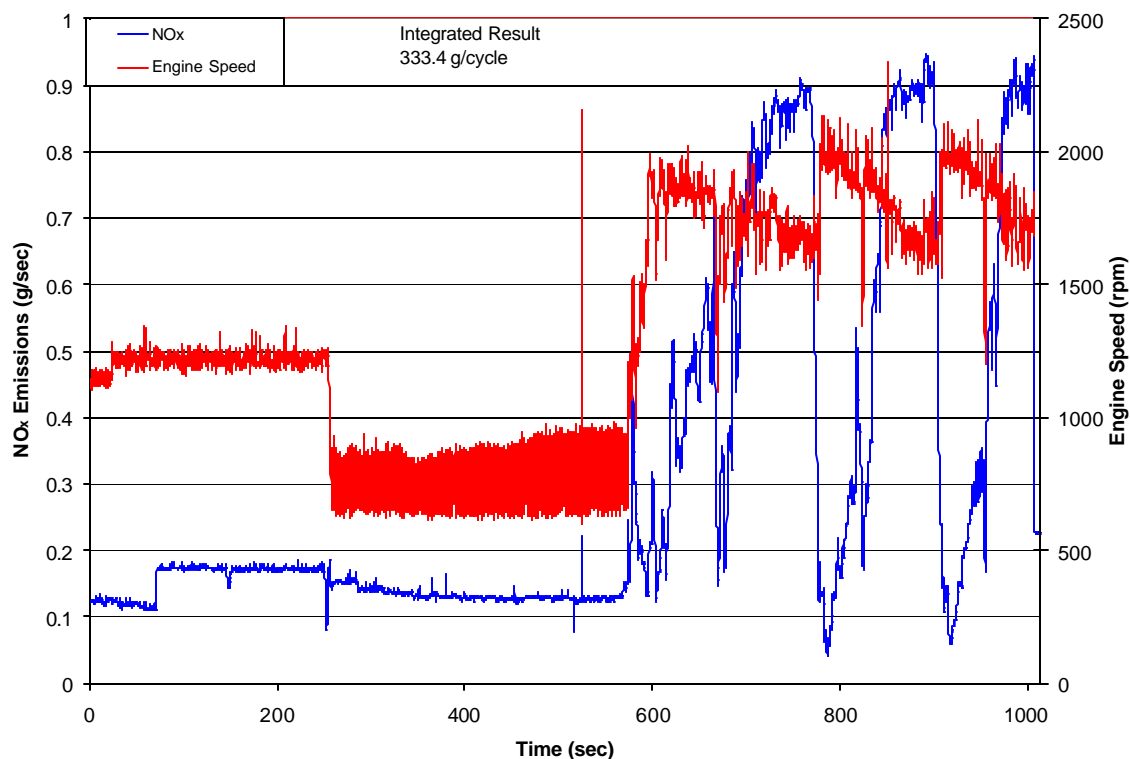
Figure 153 NO$_x$ Mass vs. Time for the Second Track-type Tractor Digging Test

The limited amount of data collected from the testing of this machine makes it difficult to draw meaningful conclusions relative to emissions production rates from these vehicles. For comparative measures, the EPA crawler tractor cycle and the laboratory cycle used to test emissions measurement equipment for this study have also been characterized. Figure 154 displays the speed ranges observed during the track-type tractor transport test. The data for this cycle was recorded by Caterpillar from the ECU. The most significant speed range is 1900 rpm-2000 rpm. This is due to the fact that transport is conducted at higher engine speeds for higher vehicle speeds so as to reduce operation of the machine that is considered to be non-productive. Figure 155 shows the loading characterization for the 1900 rpm -2000 rpm speed range.
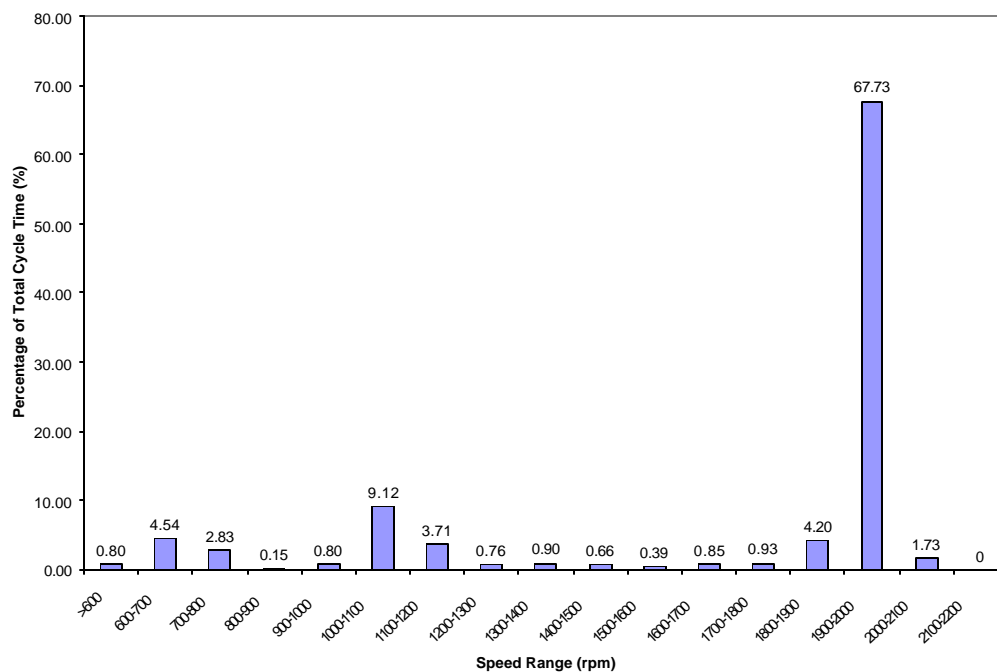
Figure 154 Speed Range Characterization for Track-type Tractor Transport Test
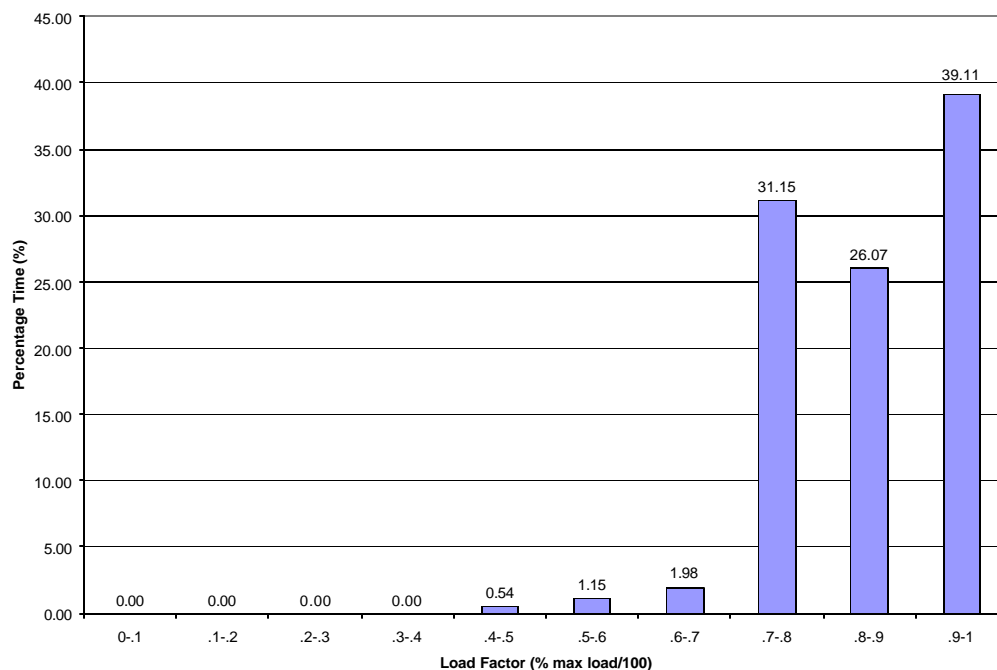
Figure 155 Load Factor Characterization for Track-type Tractor Transport Test in

1900-2000 rpm Speed Range

This figure indicates that the transport cycle was performed near maximum engine loading for this speed range. This again is due to the fact that maximum vehicle speed is desired for non-productive operation. This speed range is slightly past peak power production and seems to be operating in the area where maximum speed is achieved while still having enough power to move such a large machine.

Figure 156 displays the speed characterization for the first in-field track-type tractor digging test. This data was recorded by MEMS test equipment. The data in the figure indicates that the operating range for the engine as the tractor moves material varies from 1600 rpm -1900 rpm. The operator attempts to keep the engine speed as close to rated speed as possible during normal operation. The 1900 rpm -2000 rpm speed range is larger than any other range because the transport to the starting point is a steady constant operation, so the amount of time in transport would fall under this column, as can be witnessed in Figure 154.
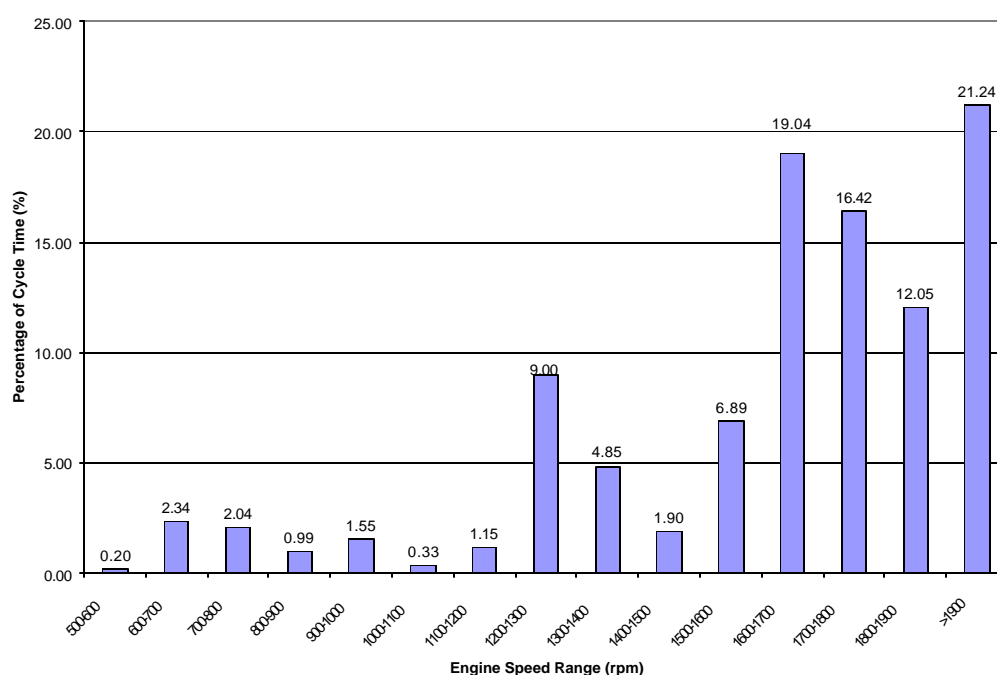
Figure 156 Engine Speed Characterization for In-field Digging Transient Test Cycle

#1

Figure 157 shows the engine speed characterization for the second track-type tractor in-field digging test cycle. This cycle was shortened by equipment failure, and there was a long idle period at the beginning of the test, therefore the characterization does not exactly match the trends shown in Figure 156. Upon close evaluation of the characteristics of this test, one can see that the speed ranges for digging and transport here lie in the same areas as for digging test 1. Both Figure 156 and Figure 157 display

operation in the 1200 rpm speed range. This is where the engine tends to idle until it has reached a designed operating temperature.
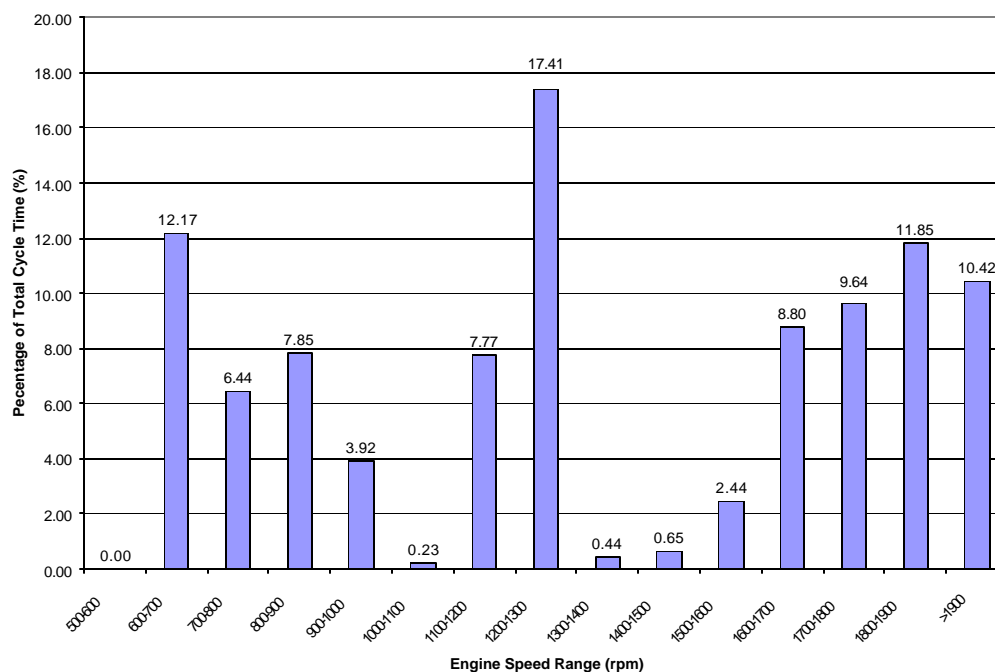
Figure 157 Engine Speed Characterization for Track-type Tractor In-field Digging

Transient Test #2

For comparative purposes, two other test cycles have been characterized. One is the EPA cycle designed for crawler tractors, which was adjusted to the engine specifications of the Caterpillar 3508 engine, and the other is the laboratory test cycle used to qualify test equipment for the in-field testing of the track-type tractor. Figure 158 shows the speed range characterization for the EPA cycle. This cycle spends significant amounts of time at idle and in the 1300-1600 rpm speed ranges. The cycle is published in percentage speed and load. It was adjusted to the Caterpillar 3508 engine by multiplying the percent speeds by governed central speed as determined from the engine lug curve provided by Caterpillar. Many factors may be causes of differences between cycle trends shown in the transient cycles recorded during in-field testing of the track-type tractor and the EPA crawler tractor test cycle. It is witness to the paramount issue of problems that will be encountered if an attempt is made to develop standardized transient testing procedures for off-highway engines.
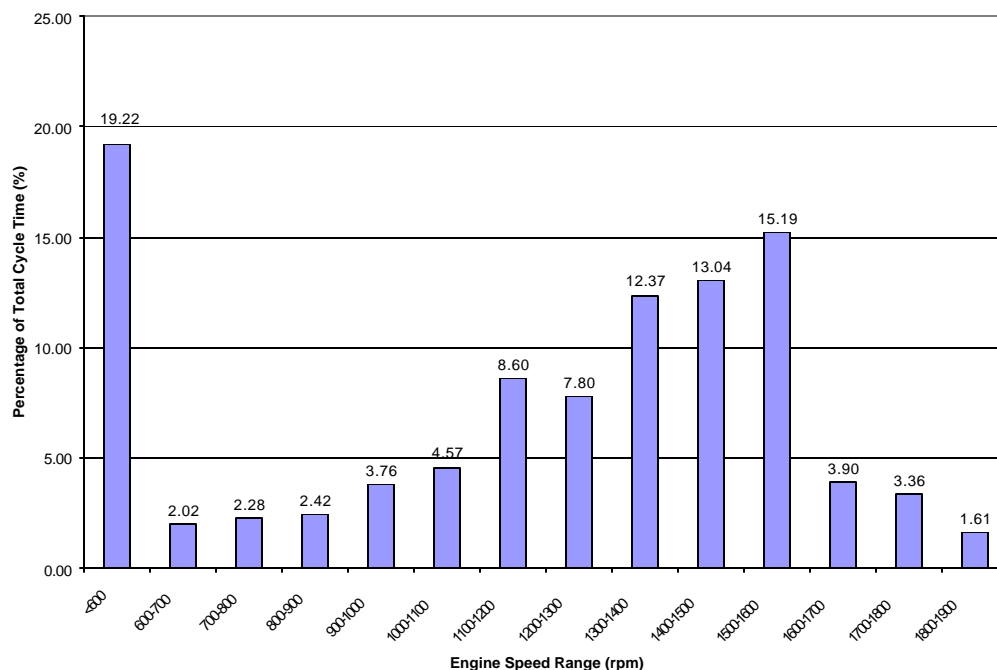
Figure 158 Speed Range Characterization for EPA Crawler Tractor Cycle

Figure 159 shows the load factors for the 1300 rpm-1600 rpm speed range from the EPA crawler tractor cycle. This indicates that the characteristic operation of this cycle is in the fully loaded state, which logically follows as the design of this type vehicle is to move the maximum amount of material possible in the most efficient least time consuming manner.

A cycle was developed from estimations of the types of loading that would be encountered during field testing of the track-type tractor, and it was used to qualify test equipment. The cycle was very simple and repetitive in nature, and its characteristics were moving material, then transport, and then moving material again. The speed range characterization for this cycle is shown in Figure 160.
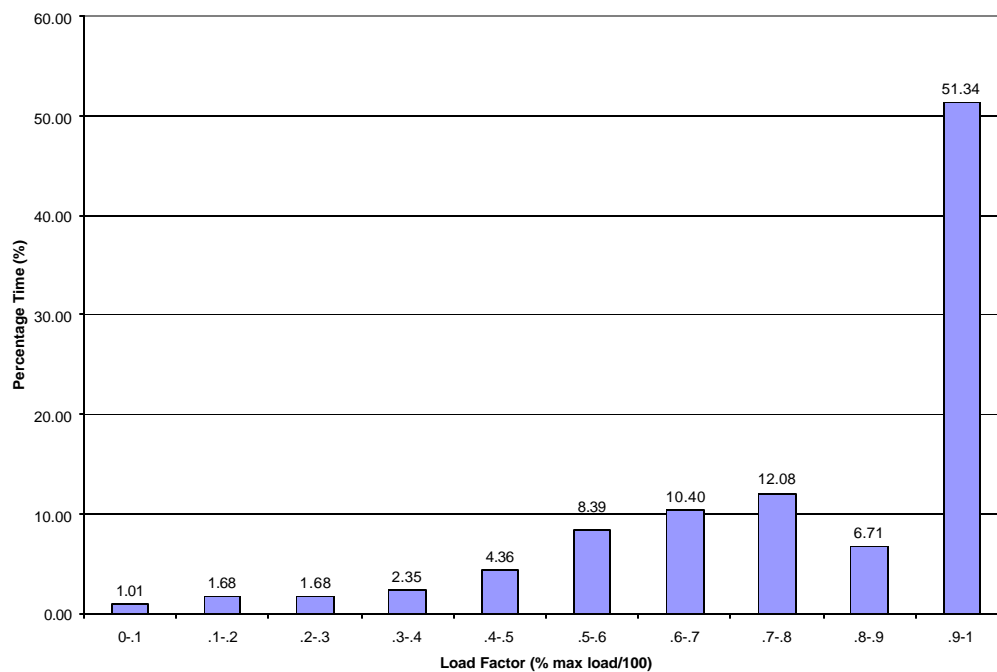
Figure 159 Load Factor Characterization for EPA Crawler Tractor Cycle 1300-1600 rpm Speed Range
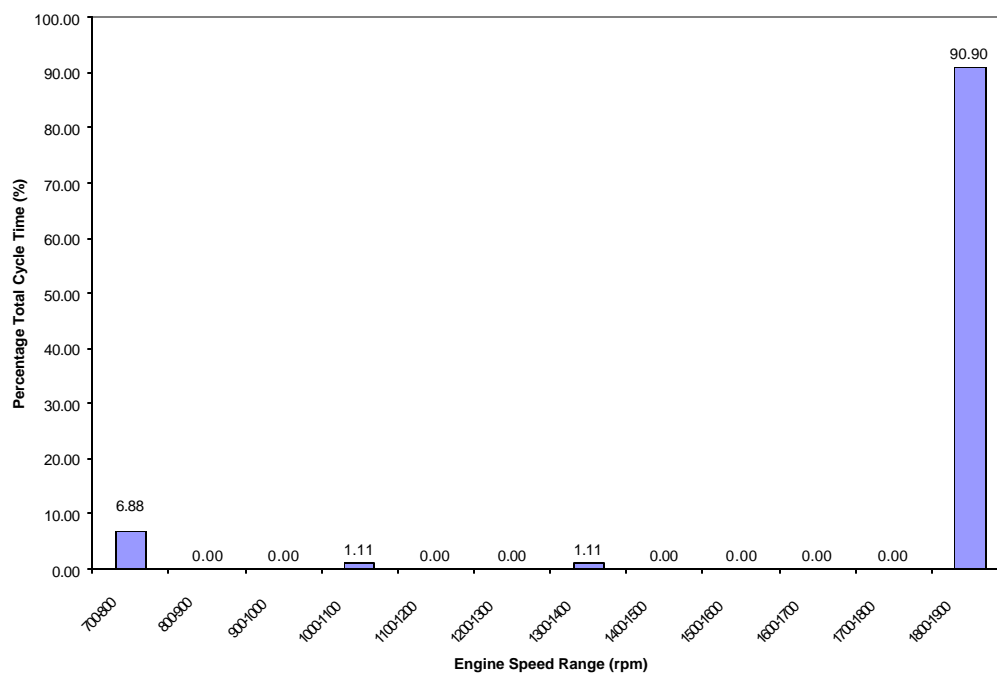
Figure 160 Laboratory Qualification Test Cycle Speed Range Characterization

The laboratory test cycle was set to maintain a constant speed (1800-1900 rpm, rated) and the torque was varied to simulate the loading that would be encountered in-field.
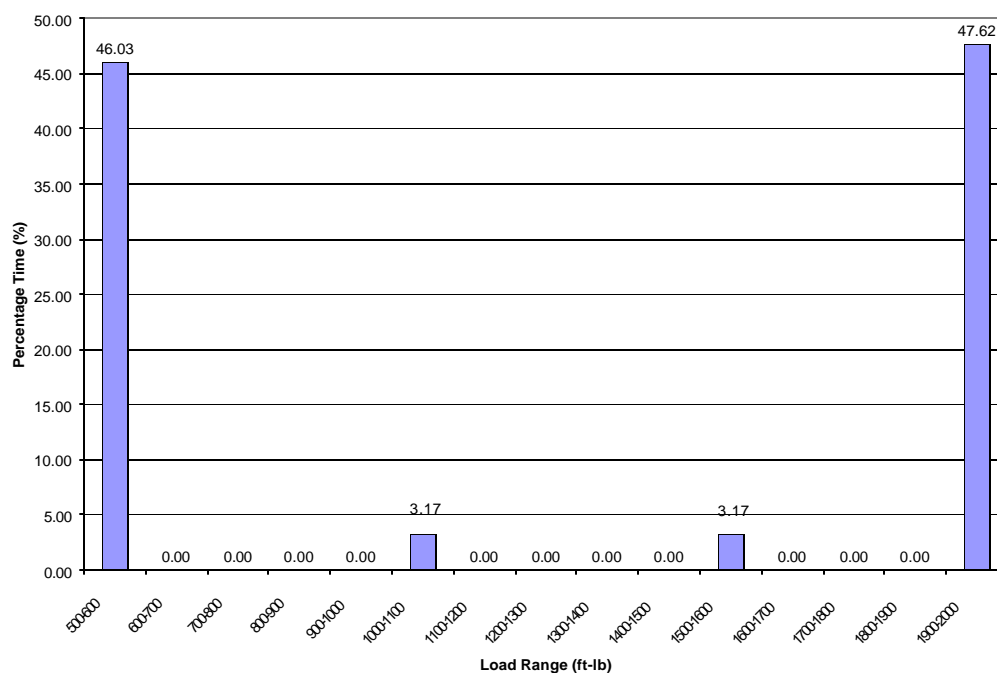
Figure 161 Load Range Characterization for Laboratory Qualification Testing

Cycle

Figure 161 displays the load ranges for this cycle. The 1900-2000 ft-lb range was used as the loading portion to simulate moving material, and the 500-600 ft-lb range was used to simulate transport. The loading values were slightly exaggerated in order to avoid problems with fueling control such that the rack position would go to 100% as the engine tried to reach a loading value greater than 100% of its max power at the speed it was operating.

While it is difficult to draw conclusions based on limited data, the trends of the cycles performed by this vehicle seem to be operation near full load at rated speed and transport at high idle speed. More extensive testing of track-type tractors in different environments would be a more thorough approach to understanding the emissions production of this vehicle class.

4 Discussion

The objective of this study was to determine the emissions produced from four diesel-powered off-road engines that were operated under "real-world" conditions. This information could then be used to formulate conclusions regarding the effect of engine type and use on exhaust emissions produced by off-road engines and to provide additional information for the development of air inventory models. The engines from three of the targeted test vehicles were exercised on an engine dynamometer according to the current ISO-8178 Cycle C1 Federal 8-mode steady-state test cycle as well as a transient cycle developed from activity information logged while these vehicles were operated in the field. As these engines were operated according to these test schedules, mass emission rates of particulate matter, oxides of nitrogen, carbon monoxide, total hydrocarbons and carbon dioxide were measured. In addition, total particulate matter as well as size selective particulate matter (PM_{10} and $PM_{2.5}$) gravimetric measurements were made. Size distribution and concentrations of ultrafine and nanoparticles in the diesel exhaust were also investigated, since there exists a potential health hazard that is associated with such particles. It should be noted that based upon CARB directives, size-distribution measurements were not part of the deliverables. For the fourth vehicle (track-type tractor) the exhaust mass emissions were measured on-board the vehicle as it operated in-field. WVU's Mobile Emissions Measurement System, which is a portable, on-board unit capable of providing measurements of mass emissions of NO_x and CO_2, was integrated with the MARI RPM 100, which provides real-time gravimetric particulate matter results, to provide these in-use results.

In the past, exhaust emissions testing for off-road diesel engines has been performed predominantly on an engine dynamometer test bed, with only a limited amount of off-road vehicles being evaluated using chassis dynamometers. Engine dynamometer tests are time consuming and labor intensive, and the emissions results obtained through such tests are quite specific of engine, test cycle, test condition, etc. The steady-state tests and associated weighting factors were intended to provide an integrated summary that could be used to represent a wide range of engines and applications. Although these test cycles effectively serve as a benchmark for engine certification, they do not provide an accurate prediction of emissions from all types of off-road vehicles. Chassis dynamometer testing provides a more realistic test of the integrated engine-vehicle system, but is also associated with unique problems, such as driver error, which can have a significant impact on emissions production. More importantly, off-road vehicle designs generally prohibit a chassis dynamometer configuration from properly loading the test vehicle, since hydraulic systems and specialized drive attachments are often integrated into off-road vehicles. To accurately test these vehicles, chassis dynamometer test beds would have to be customized for each vehicle. Even if the hydraulic and unique power attachments could be accommodated, the fact remains there are no widely accepted, representative chassis cycles available.

The lack of available representative transient test cycles for off-road vehicles makes the accurate estimation of their contributions to air inventories impossible. Off-road vehicles are currently certified using steady-state cycles and an associated set of weighting factors meant to estimate in-field emissions from a wide range of vehicle applications. In order to more accurately predict the influence of emissions contributed

by off-road diesel engines, research directed toward the development of transient test cycles and quantification of real-world mass emissions rates from off-road vehicles will be necessary. A significant source of estimation error attributed to air inventory model is resultant of the insufficient real-world activity data in the current emissions databases. The currently-used steady-state engine certification test cycles could provide a poor indication of the actual emissions contributed by off-road diesel vehicles. Although these cycles provide a universally accepted method of testing off-road diesel engines, the cycles do not adequately represent actual in-field operation – thus making it difficult to use such test results for the development of accurate emissions inventories. In order to investigate this matter a study was initiated to collect real-world activity data from four off-road vehicles that were targeted to be representative of the major off-road diesel emissions contributors in California. In-field vehicle activity data from these vehicles was collected and the engines from three of these vehicles (street sweeper, rubber-tired front-end loader, and track-excavator) were removed and installed on dynamometer test beds. From the collected in-field data, transient dynamometer test cycles were generated, and the engines were operated according to the derived transient cycles while engine exhaust emissions were recorded. For the emissions testing, measurements of currently regulated exhaust species were made as well as exhaust particulate matter size distributions and concentrations. For comparative purposes, the standard certification test cycle, the ISO 8178 steady-state 8-mode cycle, was also used to exercise the engines from three of the vehicles (street sweeper, rubber-tired front-end loader, and track-excavator). The mass emissions from the fourth vehicle, a Caterpillar D-11R CD track-type tractor, were measured using WVU's on-board mobile emissions measurement system (MEMS) while the vehicle operated in the field.

To develop standardized test cycles would be a daunting task indeed, and the validity of such cycles could only be evaluated by comparing them with actual in-field emissions production. It is very difficult to accurately mimic the real-world operating conditions of the test engine in a laboratory; moreover there is a lack of truly representative test cycles for off-road diesel-powered engines that were developed from actual in-field continuous engine speed and load data. A considerable amount of the diesel engine emissions research involving on-highway vehicles has been directed toward the development of standardized transient testing cycles that accurately represent real-world operating conditions for these vehicles. Such cycle development provides a performance benchmark to assist in the development of standardized emissions regulations and an evolutionary approach to cleaner, more efficient engine designs. With increasing attention being focused on the reduction of emissions from off-road sources, the development of representative testing cycles for these vehicles is of utmost importance. Similarly, the protocols regarding the manner by which emissions from off-road diesel engines are measured need further development. Since the off-road sector encompasses a multitude of applications in which the diesel engine is implemented, a better understanding of the correlation, or lack thereof, between the current certification engine tests and actual in-field operating conditions needs to be afforded.

In order to create a dynamometer test cycle for an off-road vehicle it is necessary to log pertinent engine operating parameters while the engine is operating in its working environment. Tertiary measurements such as intake boost pressures, intake charge temperature, and exhaust temperature are easily managed, as is continuous engine speed.

However, the determination of on-board engine torque can be much more difficult. Few methods have been previously employed to quantify engine torque in the field, including driveshaft-mounted strain gauges that broadcast results via radio transmitter collars, and fuel consumption estimates inferred from injection rack position measurements made with linear position sensors.

Though devices are currently available for the direct measurement of torque, they are generally complex and prohibitively expensive. These devices are placed in the driveline and measure the torque transmitted through the drive shaft. The intrusive nature of the devices often makes their use infeasible – either due to design constraints or the refusal of the equipment owner. Drive shafts used in off-road equipment are generally enclosed and very difficult to access, which compounds the problem. More importantly, on a large number of off-road vehicles there is no exposed driveshaft that can be replaced or outfitted.

Since there are inherent problems associated with the direct measurement of engine torque, indirect torque inferences must often be implemented. Common approaches to quantification of engine torque have generally relied on the measurement of the engine-fueling rate. To accomplish this, the displacement of the rack in the injection pump determines the amount of fuel that is injected in a given engine cycle, which has traditionally been monitored by means of linear position sensors. This approach has several associated problems, including measurement inaccuracies, difficulties involving the instrumentation of the injector pump, and vibration-induced sensor problems. Quite often the use of linear position sensors to determine rack position necessitates the disassembly and modification of the injection pump, which is labor intensive and often not permitted by the owner of the test vehicle. For modern electronically controlled engines, a more direct approach can be implemented by using algorithms to estimate the torque output through fueling data. An interface can be used to retrieve desired fueling rate commanded by the ECU (Engine Control Unit), which is calculated based upon fuel pressure and injector pulse-width. Component degradation as well as inherent algorithm inaccuracies are identified shortcomings of this inference method. Yet in laboratory tests with properly operating systems, results with this method have been reported to be accurate to within 10% of actual torque output. For the off-road arena, the implementation of electronically controlled fuel injection systems for diesel engines has lagged behind that of the on-highway sector, with the vast majority of units introduced in the past two years. With the current majority of off-road equipment being mechanically injected, the aforementioned method is not globally feasible as a torque prediction method. However, as the current inventory of equipment is replaced by more modern electronically injected machinery, this could become the most desirable method for power prediction inferred from engine fueling rates.

Closely related to the on-board determination of engine activity data, and even more useful in terms of accurately assessing contributions to emissions inventories, would be direct on-board emissions measurements that were made while these off-road vehicles were operated in the field. For such testing, engine exhaust emissions could be measured on a continuous basis, or integrated exhaust gas samples can also be collected in special Tedlar bags and analyzed as a post-test process. While the integrated bag approach provides for the simplification of the on-board measurement component of the

system, it can only be used to determine an average of the emissions produced during a particular operation or cycle. Use of the bags makes it very difficult for the researcher to determine the effects of transient conditions on emission rates and makes cycle development work nearly impossible. Conversely, a continuous on-board emissions measurement system provides detailed information on transient vehicle response, and data that is crucial for the accurate recreation of representative engine dynamometer test cycles. In order to facilitate such measurements, it is imperative to develop on-board emissions measurement systems and test protocols.

Portable, relatively compact on-board emissions testing equipment is currently available that can be integrated to make raw exhaust gas sampling possible during actual in-field operation of the equipment being studied. Engine speed can be readily determined from the alternator or inductive-pickup devices, such as Hall-effect sensors. Intake and exhaust temperatures can easily be measured with thermocouples and pressure data can be obtained with miniaturized pressure transducers. The determination of engine torque would still be an issue, particularly for mechanically controlled diesel engines. However, engine load estimates would only be required if the emissions results were to be reported in a brake-specific format. While this normalization process provides for a more direct emissions comparison from engines with different power output levels, it unnecessarily complicates on-board emissions measurements by requiring a very accurate determination of engine work. Although emissions test data has typically been reported on a brake-specific mass emissions basis, an obviously equal method would be the representation of mass emissions data in a fuel-specific manner. Although data presentation standards have typically favored the brake-specific format, a fuel-specific approach lends itself quite nicely to the on-board testing arena, since it does not require the often problematic determination of engine output torque.

Considering the above discussion, the method used to infer in-field engine torque output in this study was to measure raw CO_2 concentrations in the raw exhaust stream, along with engine speed, while the vehicle was operating in-field. Once the engine was removed, brake-specific CO_2 performance maps were then developed under quasi-steady-state operation and the engine loads from the recorded in-field cycle were inferred using linear interpolation between engine speed, raw exhaust CO_2 concentrations, and applied dynamometer load.

Prior to initiating the in-field testing of the first off-road vehicle, WVU decided to evaluate the feasibility of inferring torque using such an approach. A Cummins ISM 370, 10.8L inline six-cylinder diesel engine, was exercised over a series of steady-state operating conditions that spanned the engines operating range while continuous raw CO_2 emissions were recorded with a Sensors AMB-II solid-state non-dispersive infrared (NDIR) analyzer. All testing was performed with the engine operating on a DC dynamometer test bed. Raw CO_2 emissions data was first collected during the running of a series of load maps at predetermined engine speed ranges to determine how the raw CO_2 emissions rates related to engine horsepower output. The ISM 370 was then exercised according to a step input cycle while raw CO_2 emissions data were collected. The previously collected CO_2 vs. engine speed/load data was then used to estimate the engine load encountered during the running of the step input cycle. The engine was then operated through a series of mapping exercises at motored, 0%, 25%, 50%, 75%, and

100% load conditions while raw exhaust CO_2 concentrations were again recorded using the Sensors analyzer. This data was then used to develop correlation curves for the various engine speeds that were measured from the arbitrary test cycle. These figures show that the relationship between CO_2 emissions and engine torque produced is very close to linear, as expected. Results showed that this surrogate method of horsepower estimation was capable of providing results that were within 5% of actual measured values for steady-state engine operating points.

Following the favorable results obtained from the preliminary laboratory evaluation of the proposed torque inference methodology, the next step was to attempt to derive engine load figures from a vehicle operating under real-world conditions. Engine speed and raw exhaust emissions data were recorded as the vehicles were operated in-field under real-world conditions, then the engines were removed and installed on engine dynamometer test beds. In order to provide a starting point for the development of the cycle, the engine was exercised according to a step input cycle (30-second speed/load setpoints at discretized speed ranges throughout the engine operating map) while raw CO_2 emissions data were collected with the same raw CO_2 exhaust concentration measurement system that was used during the in-field testing. The resultant data was used to develop CO_2 vs. engine output power performance maps that could be used to infer engine power from raw exhaust CO_2 concentration and engine speed measurements. Simple linear interpolation of engine load was accomplished through comparison of in-field engine speed and CO_2 versus time traces with a raw CO_2 versus engine speed matrix. The engine was loaded according to the torque estimates generated by this program and the raw CO_2 concentrations and engine speed were recorded with the same acquisition system that was used for in-field testing – this produced the first iteration of the transient cycle. The accuracy of the process was further improved by comparing the in-laboratory transient cycle raw CO_2 traces from this first iteration with the in-field raw CO_2 exhaust concentration data. The dynamometer cycle set-points could then be adjusted in an iterative fashion until satisfactory correlation existed between the in-field raw exhaust CO_2/engine speed traces and the raw exhaust CO_2/engine speed traces measured in the laboratory. The converged test cycle setpoints were then used to exercise the engine so that exhaust mass emissions measurements could be made – thus providing an estimate of the actual in-field, in-use mass emissions produced by the off-road test vehicle. The effect of cycle recreation accuracy upon emissions results was also investigated by comparing the engine emissions results from different stages in the iteration process.

The acquired data from the derived transient cycles provides for emissions results that are more representative of actual "in-use" emissions. The results indicate that the current steady-state, ISO 8178, 8-mode test cycles are not very representative of the actual emissions produced by off-road, diesel-powered equipment during day-to-day operations. Furthermore, the exhaust emissions produced by a vehicle are very vehicle- and task-specific. The research reported herein suggests that the inference of in-field torque through raw exhaust CO_2 measurements is a feasible means of determining the engine load information of off-road vehicles. These cycles can then be used to develop standardized off-road cycles that can be used for emissions certification as well as emissions inventory purposes. The current certification standard, based upon the ISO 8178, steady-state 8-mode test cycle, does provide a universally accepted method of

testing these engines, but the mass emissions rates may not be representative of actual in-field emissions production from off-road diesel engine-powered vehicles. Furthermore, the results presented from the in-field-derived transient test cycles suggest that the exhaust emissions produced by off-road vehicles are very vehicle- and task-specific in nature.

4.1 Comparison of Test Cycle Emissions Results: WVU Off-Road Transient Cycle vs. EPA Off-Road Transient Cycle

In order to provide comparative insight into the accuracy of the methods used for the development of the transient dynamometer test cycles for this project, a review of relevant, published engine test cycles was conducted. A test cycle was developed using information from prior research performed by the EPA. These tests were 30 minutes in length and encompassed a range of operations normally performed by this class of engine. The results from this testing are listed below as well as compared to the final cycles developed from field data.
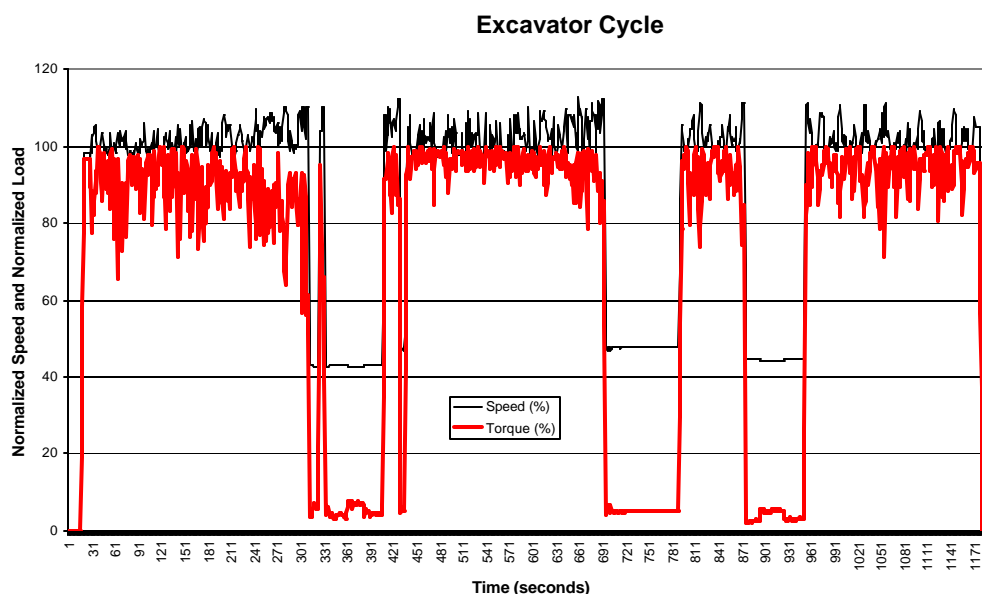
Figure 162 WVU Excavator Cycle Percentage Load Setpoints

Epa Cycle Set-point File
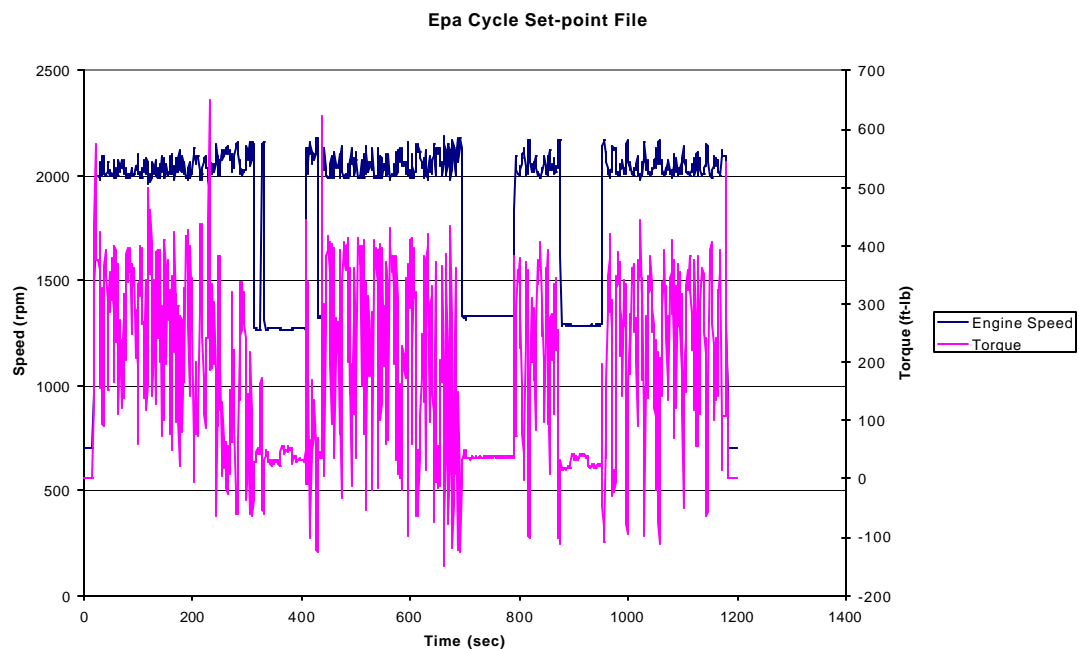
Figure 163 Set-point Torque and Speed for EPA Cycle
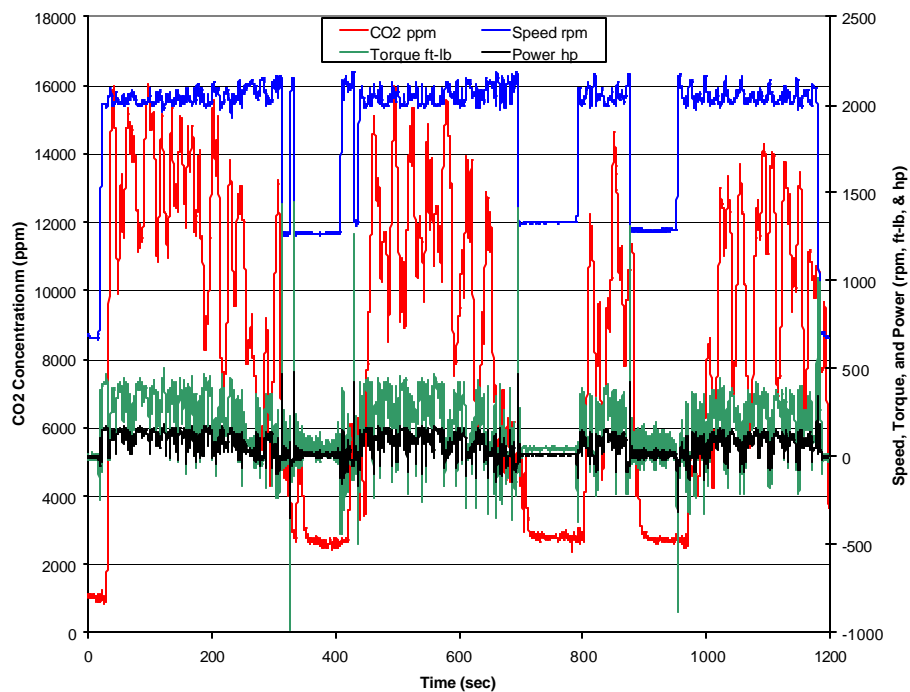
Figure 164 EPA Cycle Final Laboratory Results

Table 34 Emissions Results for the Komatsu S6D125-1 Excavator Engine Operating According to the EPA Excavator Test Cycle (g/bhp-hr).

	EPA Cycle Test 1**	EPA Cycle Test 2	EPA Cycle Test 3	Test 2-3 Average
HC	2.127	2.085	2.016	2.05
CO	1.891	1.942	1.865	1.903
CO$_2$	631.08	628.53	636.03	632.28
NO$_x$	4.879	4.907	4.838	4.873
PM	1.027	0.586	0.418	0.502

Table 35 Comparison of Emissions Results for the Komatsu S6D125-1 Excavator Engine Operating According to the WVU Excavator Test Cycles and the EPA Excavator Test Cycle (g/bhp-hr).

	Cycle 1 Average	Cycle 2 Average	Cycle 3 Average	EPA Cycle
HC	1.202	1.145	1.100	2.05
CO	0.915	0.871	0.853	1.903
CO$_2$	538.43	533.49	525.59	632.28
NO$_x$	5.366	5.390	5.327	4.873
PM	0.277	0.280	0.332	0.502

This table compared to the other cycle results shows that the brake specific emissions will vary significantly with engine duty cycle. Therefore extensive testing would be required among different operators and machinery to find a realistic representation of the emissions produced by off-road machinery.

The EPA transient test designed for excavators was performed for a comparative measure. The results of this test varied widely from the tests derived from in-field test data recorded under this study. The following figures may provide some answers as to why, and what differences in these test cycles may be the root for varying emissions levels.
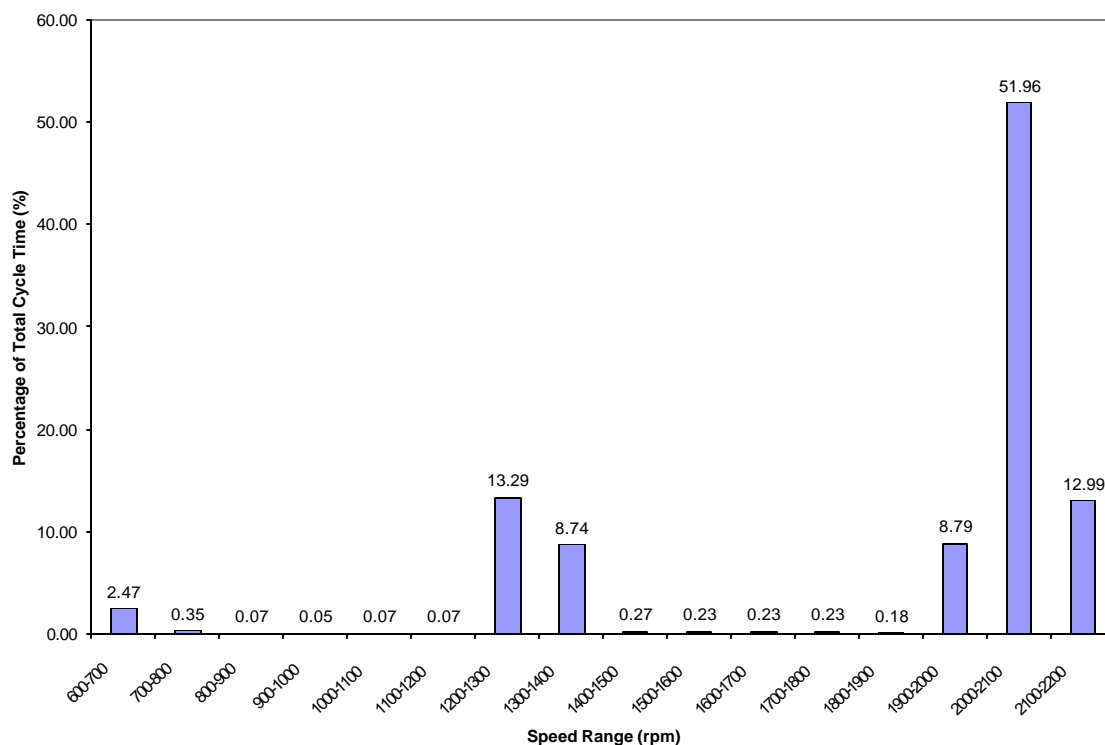
Figure 165 Speed Range Characterization for EPA Transient Excavator Test Cycle

Figure 165 indicates that there is a significant amount of time spent near the intermediate speed of the excavator engine. This is not the case in the 3 cycles derived from in-field data. This may be due largely in part to the effort to make this cycle more applicable to a wide range of equipment designs. The excavator tested during this study was driven completely by hydraulic systems. The cycle characteristics seen by this engine would vary widely with a machine that may also have direct mechanical drive systems in addition to the hydraulic systems, thus this may be a source of difference between the EPA test cycle and the 3 cycles developed under this study. It is rather illogical and unscientific however, to draw conclusions relative to a variety of machines from the testing of only one. The significant speed ranges for this cycle are 1200 rpm-1400 rpm and 2000 rpm -2100 rpm.
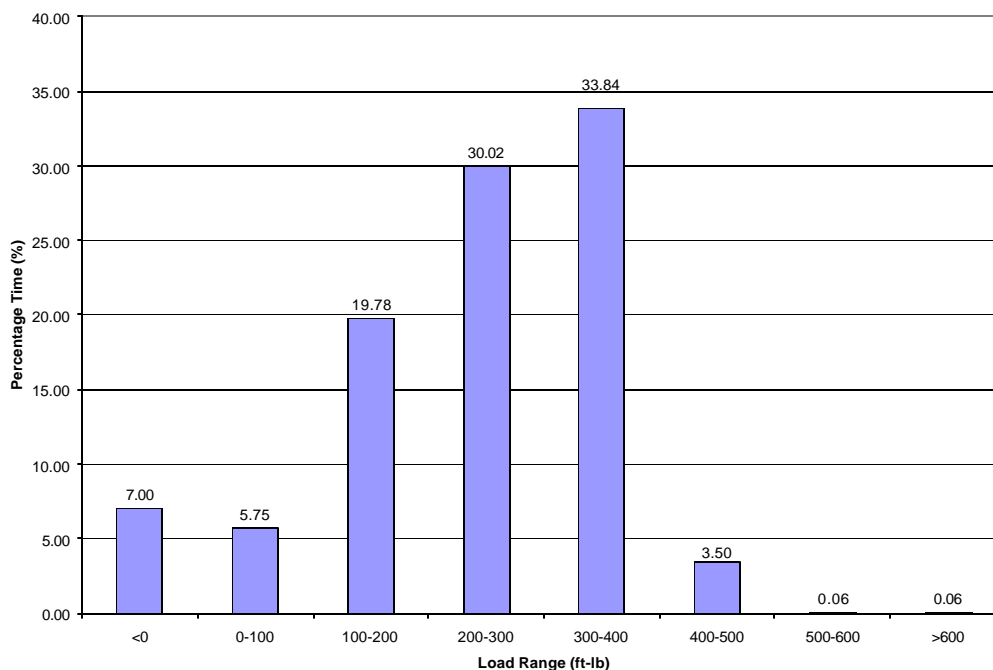
Figure 166 Load Range Characterization for 2000-2100 rpm Speed Range for EPA Excavator Cycle

Figure 166 displays the load ranges for the 2000 rpm -2100 rpm speed range for the EPA transient excavator test cycle. This shows some similarity to the other 3 excavator transient test cycles as a large amount of the time spent in this speed range is at or near 100% loading for the engine. This may be skewed however as the 2000 rpm -2100 rpm range is the most significant speed range in the EPA cycle and the 1900 rpm -2000 rpm range is the most significant in the other 3 transient cycles. Due to any number of reasons, the calculation of engine speeds from governed central speed may have slightly missed their mark on the intended operating range, and if the cycle spent most of it's time in the 1900 rpm -2000 rpm range it is possible that the emissions results from this test would have more closely matched those of the other 3 transient test cycles. A trend identified in the EPA cycle that is not shown in the other cycles is the time spent near intermediate speed.
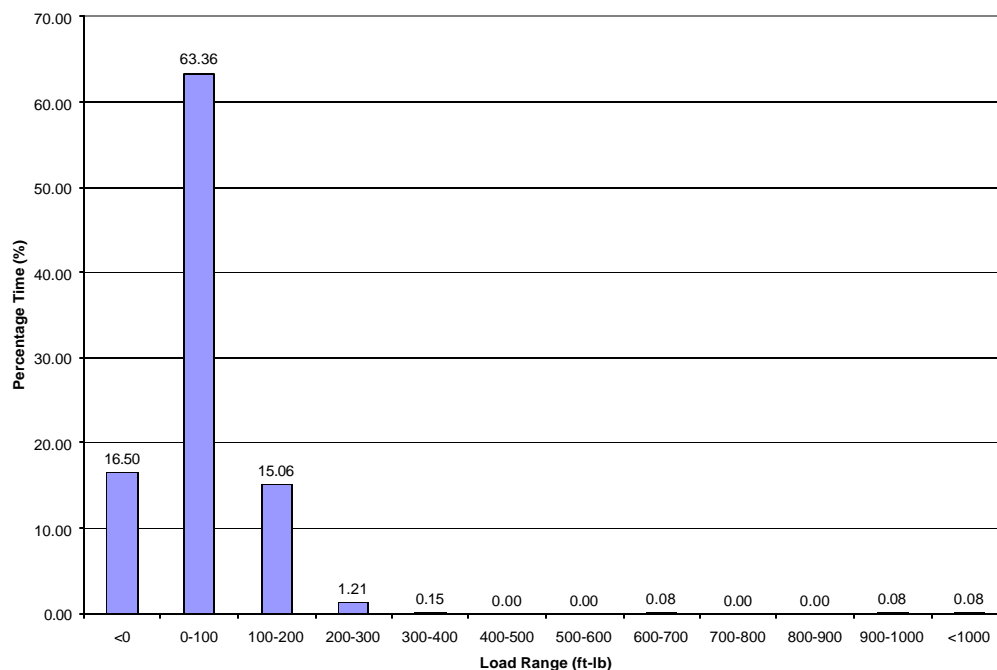
Figure 167 Load Range Characterization for 1200-1400 rpm Speed Range for EPA

Excavator Cycle

Figure 167 shows the amount of time spent in different load ranges during the 1200 rpm -1400 rpm speed range operation of the EPA excavator cycle. Loads are most often in the area of 100 ft-lb, which is nearly 0-10% of the max load at this speed range. When coupled with the information from the 2000 rpm -2100 rpm speed range, this data seems to indicate that the engine speed range characteristics of a cycle may be a very significant factor relative to emissions production.

4.2 Operation of the John Deere 4039T Street Sweeper Engine According to the Transient Cycle Developed for the Rubber-Tired, Front-End Loader Engine

The 4039T street sweeper engine was operated according to a normalized cycle developed previously for the rubber-tired loader. This test was performed to determine the feasibility of using the same cycle to test engines of different displacements but similar power levels and to determine the dependence of emissions levels on the specific cycles used. Since the turbocharged 4039T street sweeper engine produced a similar amount of peak power, the results from this test could be indicative of the differences in mass emissions rates associated with an engine family could produce due solely to the specific vehicle application.

It can be seen from the data of Table 25 and Figure 111 of Section 3.6.2.3 that the nature of the cycle followed during testing had a dramatic effect on emission levels. In comparison with the Sweeper-on-Sweeper Cycle test, the Sweeper-on-Loader Cycle test

yielded substantially higher CO (92.61%) and PM (51.19%) levels coupled with lower CO_2 (-10.26%) levels, which is an indication of less thorough combustion of the fuel consumed. This result can be explained in terms of the number of transient events encountered in the running of each cycle. The more steady-state nature of the sweeper cycle exhibited itself in the form of more complete combustion, and lower mass emissions. In contrast, the aggressive engine speed changes and load transients of the loader cycle combined to produce increased levels of CO and PM emissions. These results illustrate the need to create cycles that accurately represent the "real world" operating conditions of the vehicle in the field. In terms of the immediate cycle development procedures, the results of the study indicate that the specific test cycle activity plays a much larger role in determining emissions results than does the accurate recreation of the in-field cycle. While the laborious and time-consuming process of cycle iteration changed the street sweeper cycle averaged CO_2 results by only 0.68%, running the street sweeper on the unrepresentative loader cycle changed cycle averaged CO_2 results by –10.26% on a brake-specific basis.

5 Summary and Conclusions

5.1   Overview

Additional means to provide a more detailed view of contributors to air inventories are in demand due to increasingly more stringent air quality standards. The need to develop test cycles that accurately represent real "in-use" conditions for off-road vehicles has fueled research and development of many portable emissions testing systems capable of logging data in the field. Though off-road vehicles are known to be major contributors to air inventories, the diverse range of application of diesel engines in off-road equipment has made individual test cycle development a tremendous undertaking. New methods are being explored that provide pathways for development of testing guidelines and protocols for the evaluation of these off-road vehicles.

The results of this study have focused on only four of the vast number of diesel-powered off-road vehicles in use today. Care must be taken when attempting to apply data presented in this document to other off-road equipment, regardless of engine size, power output, etc. Testing has shown that the nature of the test cycle has the largest effect on the emissions levels emitted, and that different testing cycles are needed for each type of equipment (loader, scraper, street sweeper, dozer, etc.) being evaluated to obtain an accurate assessment of their contributions to air quality issues in the future.

5.2   Summary

In summary, four off-highway diesel powered vehicles have been tested to determine in-use emissions. The engines from three of these vehicles were removed and installed on a dynamometer test bed where they were exercised over transient test cycles designed to recreate the cycles performed in-field, and according to the ISO 8178 8-Mode test cycle. Table 36 shows the emission factors for the loader, street sweeper, excavator, and the track-type tractor as determined by CARB's OFFROAD model, based upon total hours and model year of each vehicle. Data presented in Table 36 was provided by CARB.

Table 36 Emission Factors for Test Vehicles

Vehicle	Loader	Street Sweeper	Excavator	Track-type Tractor
Model Year	<1995	1995+	1987	2001
Total Hours	2756	6841	3263	2750
HC (g/hp-hr)	1.12	1.30	1.01	0.35
CO (g/hp-hr)	3.74	4.12	4.56	0.97
NOx (g/hp-hr)	9.31	10.13	11.83	6.54
PM (g/hp-hr)	0.83	1.03	0.68	0.17

Table 37 shows the brake specific results of these tests for the three laboratory tested vehicles, and the integrated mass results from the field testing of the fourth vehicle.

Table 37 Summary of Emissions from all Tests (g/bhp-hr Unless Otherwise Noted)

John Deere 444 Wheel Loader with 107 hp 6059 D Engine	Transient Test Results	8 – Mode Results (by mode and weighted average)								
		1	2	3	4	5	6	7	8	Wtd Avg
HC	0.74	0.33	0.48	0.99	9.74	0.48	0.40	0.73	22.48	4.77
CO	2.17	2.02	2.86	3.18	18.48	4.17	0.30	1.09	35.32	8.91
CO_2	546.4	483.7	497.3	556.0	1236	471.3	334.6	483.0	4235	1118.0
NO_x	8.10	11.72	10.32	7.90	9.21	20.78	13.03	16.64	107.1	26.51
PM	0.181	0.188	0.367	0.347	0.849	0.172	0.083	0.094	1.641	0.502

Elgin Street-Sweeper with 110 hp John Deere 4039 T Engine	Transient Tests		8 – Mode Results (by mode and weighted average)								
	Sweeper Trans Cycle	Sweeper on Loader	1	2	3	4	5	6	7	8	Wtd Avg
HC	0.50	0.37	0.13	0.16	0.27	2.17	0.04	0.20	0.23	9.82	1.95
CO	1.85	3.57	1.60	0.59	0.53	4.96	11.31	2.04	0.34	16.29	5.65
CO_2	626.0	561.8	508.4	514.3	545.2	974.7	527.4	516.4	521.6	3297.0	1111.0
NO_x	5.59	7.36	9.33	8.29	5.49	4.51	8.37	9.78	7.54	24.49	11.67
PM	0.245	0.370	0.181	0.134	0.143	0.228	0.882	0.269	0.117	1.207	0.474

Komatsu Excavator with 266 hp S6D125-1 Engine	Transient Tests				8 – Mode Results (by mode and weighted avg)								
	Cycle 1	Cycle 2	Cycle 3	EPA	1	2	3	4	5	6	7	8	Wtd Avg
HC	1.202	1.145	1.100	2.05	0.82	0.94	1.26	7.06	0.59	0.79	1.08	7.27	2.49
CO	0.915	0.871	0.853	1.903	0.84	0.56	0.78	6.44	1.82	1.03	0.79	8.06	2.55
CO_2	538.4	533.4	525.5	632.28	494	499	528	1036	488	489	507	862	610
NO_x	5.366	5.390	5.327	4.873	7.32	6.39	5.25	7.85	7.66	7.46	6.86	16.1	8.26
PM	0.277	0.280	0.332	0.502	0.36	0.29	0.32	1.44	0.58	0.43	0.36	1.35	0.633

Caterpillar D-11R CD Track-Type Tractor with 950 hp Model 3508 Engine	Integrated Results (g/test)		
	Digging Test 1		Digging Test 2
	Full Test	Coinciding with PM	
CO_2	76061.9	5062	24800.9
NO_x	1012.9	67.7	333.4
PM	-	0.349	-

An analysis of the laboratory produced test cycles was performed for all vehicles tested under this study to determine the average engine load and speed factors. To determine the load factor, the cycle was normalized against the engine map, using a program developed by WVU, to determine the percent load at each data point. This data set was then processed in order to produce the average cycle load factor. Engine speed data from the cycle was normalized against governed central speed (GCS, the speed at

which the engine produces ½ the maximum power once it has passed the maximum power point on the engine map). The following equation was used for normalization is:

$$(Engine\ Speed - Idle\ Speed)/(GCS - Idle\ Speed) * 100$$

Equation 15.

The results of this analysis are shown in the following figures. The engine load data for the track-type tractor was furnished by Caterpillar.
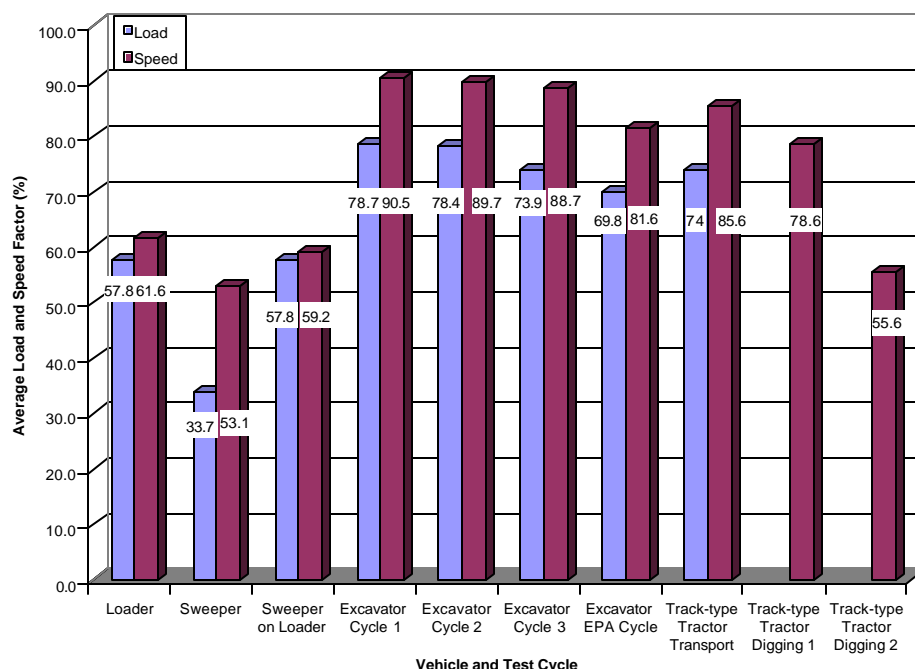
Figure 168 Average Load and Speed Factors for All Vehicles and Test Cycles

Figure 168 displays the averaged load and speed factors for each vehicle and test cycle evaluated under this study. Note that since the loader cycle was normalized for use on the sweeper, the load factors of the two cycles are identical. The load factor for the track-type tractor was derived directly from data that was received from Caterpillar. The speed factors for the track-type tractor are derived from the MEMS speed data files, and the Caterpillar supplied loading data was used for the determination of governed central speed. The following figures illustrate the normalized load and speed curves for cycles listed above.
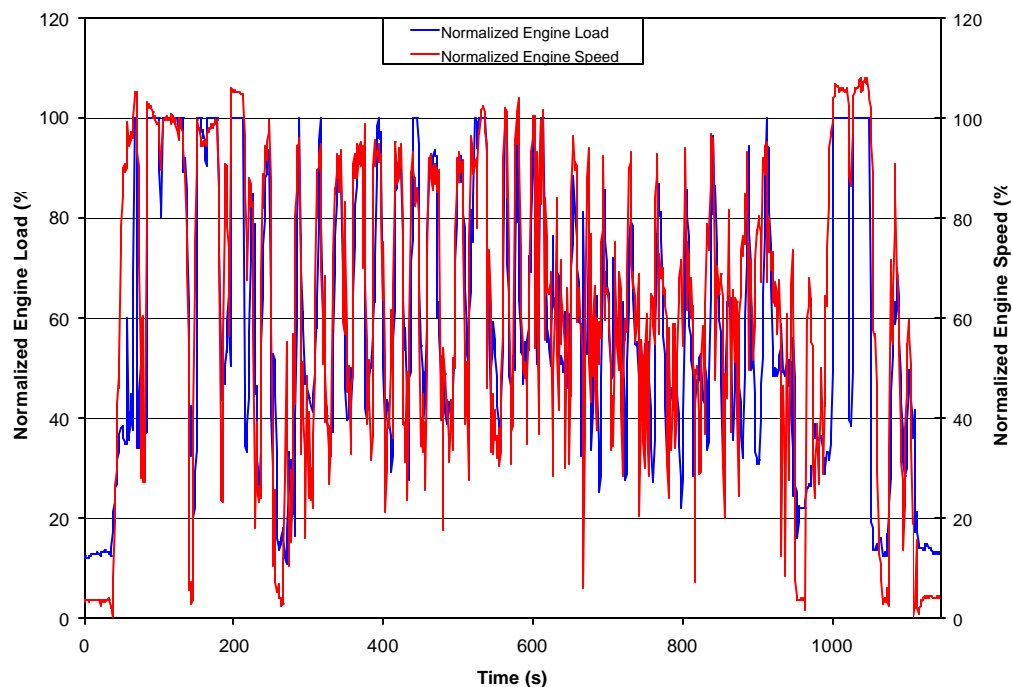
Figure 169 Normalized Load and Speed Curve for the WVU Loader Cycle

Figure 169 shows the normalized speed and load curve from the loader transient cycle that was developed by WVU as described earlier in this report. Values are shown in percentages. Note that since the speed curve was normalized to governed central speed, the curve occasionally exceeds 100% as the engine does occasionally operate above GCS.
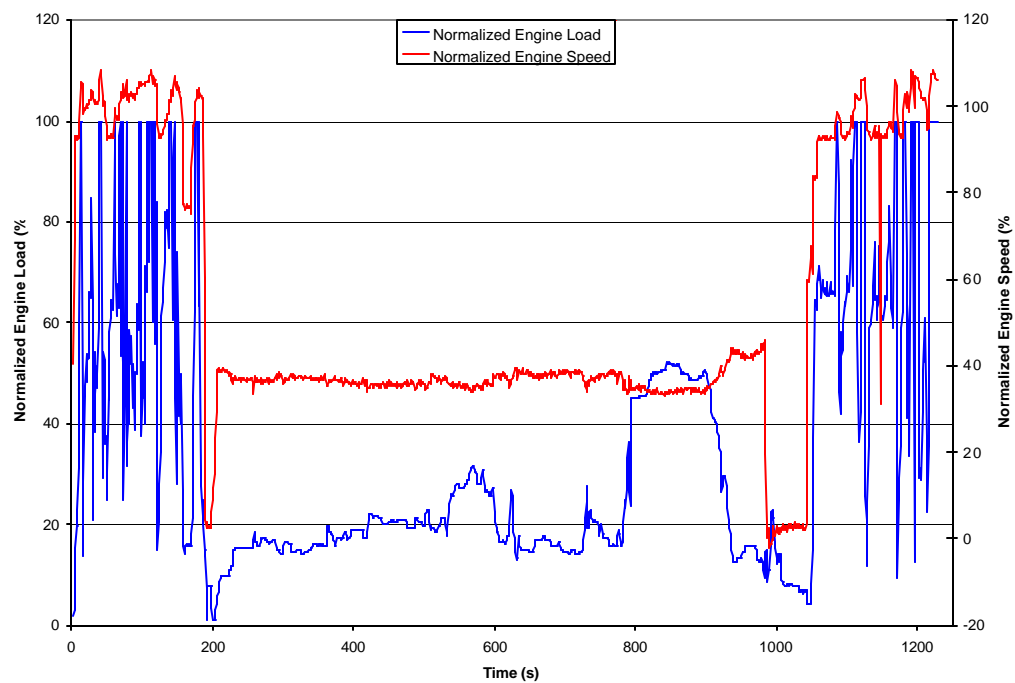
Figure 170 Normalized Load and Speed Curve for the WVU Street Sweeper Cycle
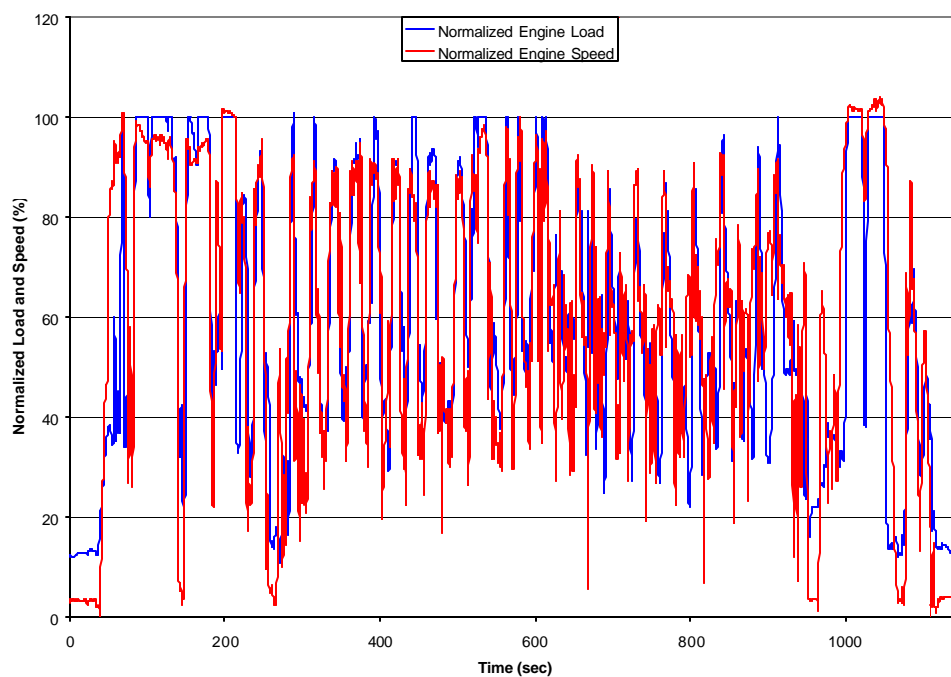
Figure 171 Normalized Load and Speed for the Street Sweeper on Loader Cycle

Figure 170 displays the normalized load and speed curve from the street sweeper transient cycle that was developed by WVU from the in-field data collected during this study. The figure shows that the characteristic cycle for this engine does not encounter high loading or high engine speed except during transport operation. In this case the vehicle normally operates on-highway, which leads to the genesis of a classification problem by which some off-highway vehicles do operate on-highway for a considerable period, and thus may be considered subject to on-highway diesel engine emissions standards. Figure 171 shows the normalized load and speed curve for the loader cycle applied to the street sweeper engine. Note that the normalized load curves for this cycle and the loader cycle are identical. Differences in the normalized speed curves are accounted for by the difference in governed central speeds between the two engines.
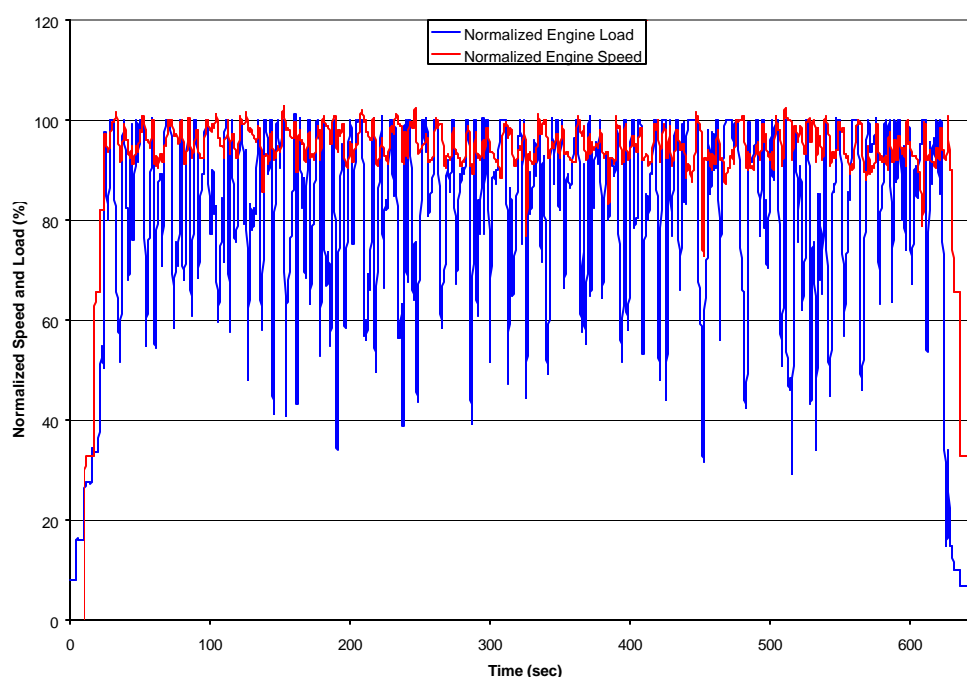
Figure 172 Normalized Load and Speed Curve for the WVU Excavator Cycle 1

Figure 172 shows the normalized load and speed curve for the excavator digging cycle (cycle 1) developed by WVU from in-field data. This shows a higher characteristic-loading curve than the first two vehicles tested under this study largely due to the manner in which the vehicle was operated. The excavator remained in one spot and continuously moved material with the engine operating at high speed, while the other vehicles spent more time in transit, moving material and had more variance in engine speed.
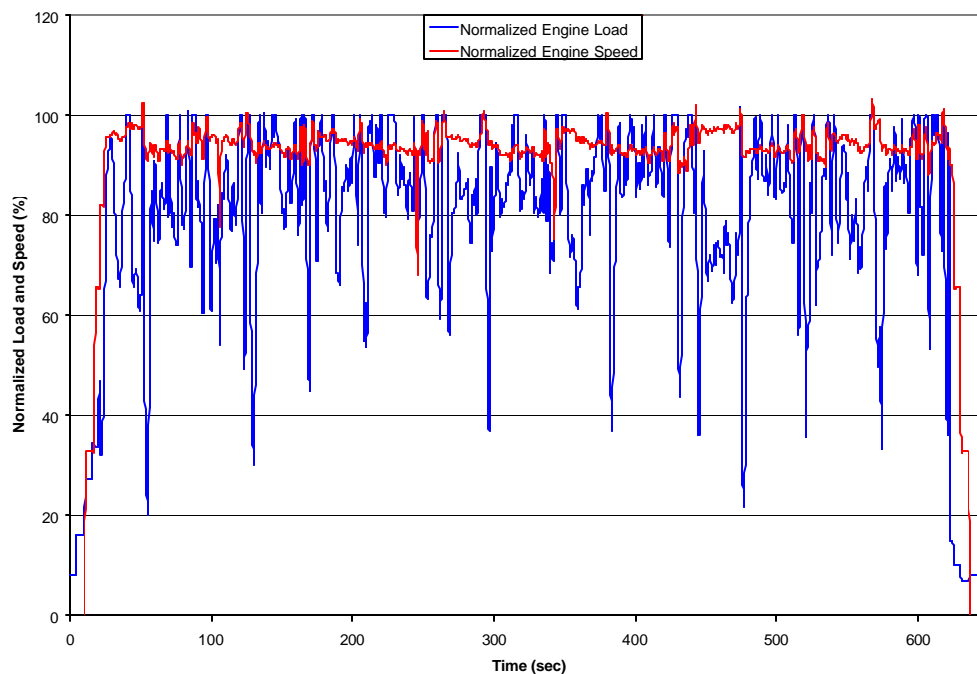
Figure 173 Normalized Load and Speed Curve for the WVU Excavator Cycle 2

Figure 173 shows the normalized engine load and speed curve for the excavator hauling cycle (cycle 2), which was developed by WVU from in-field data. This figure again displays that the excavator tended to operate at higher speed and load factors than the other vehicles.
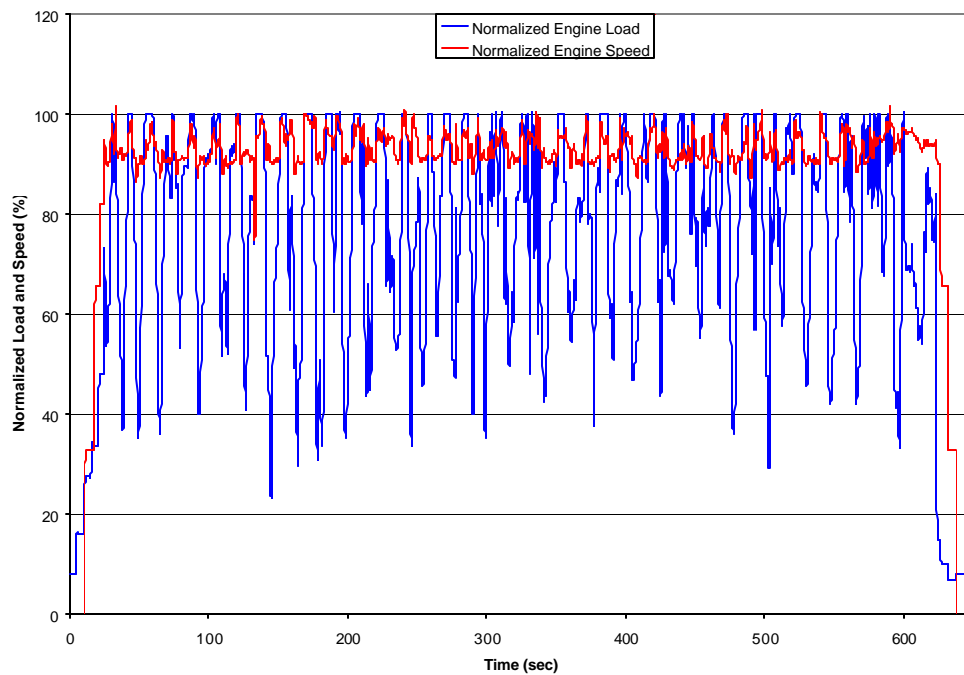
Figure 174 Normalized Load and Speed Curve for the WVU Excavator Cycle 3

Figure 174 shows the normalized engine load and speed curve for the excavator trenching cycle (cycle 3), which was developed by WVU from in-field operation data. The cycle averaged load factors for the three excavator cycles are relatively close, but review of the continuous curves reveals the different characteristics of each cycle.
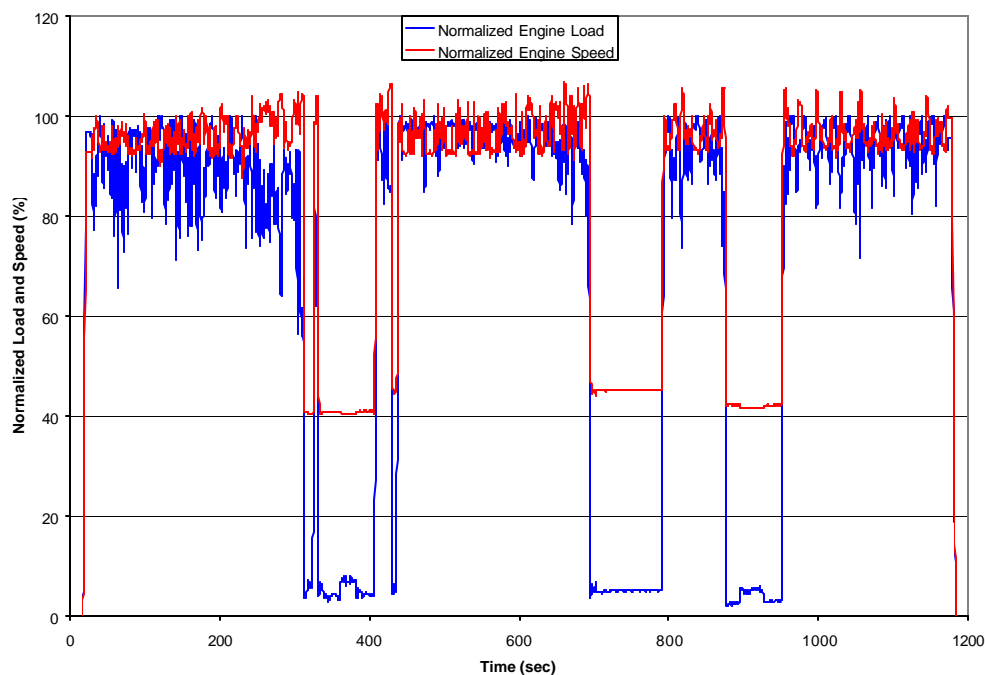
Figure 175 Normalized Load and Speed Curve for the EPA Excavator Cycle

Figure 175 displays the normalized engine load and speed curve for the EPA excavator cycle as tested by WVU. This cycle has lower average load and speed factors than the WVU developed cycles, and a simple review of the continuous curves reveals that this is because of the lengthy low-load, low-speed sections in the EPA cycle.

Table 38 shows the load factors and cycle lengths for each laboratory dynamometer cycle performed for this study.

Table 38 Load Factor and Cycle Length Data

Cycle	Loader	Sweeper	Sweeper on Loader	Excavator 1	Excavator 2	Excavator 3	Excavator EPA
Load Factor	57.8	33.7	57.8	78.7	78.4	73.9	74
Cycle Length (s)	1144	1226	1144	650	645	646	1198
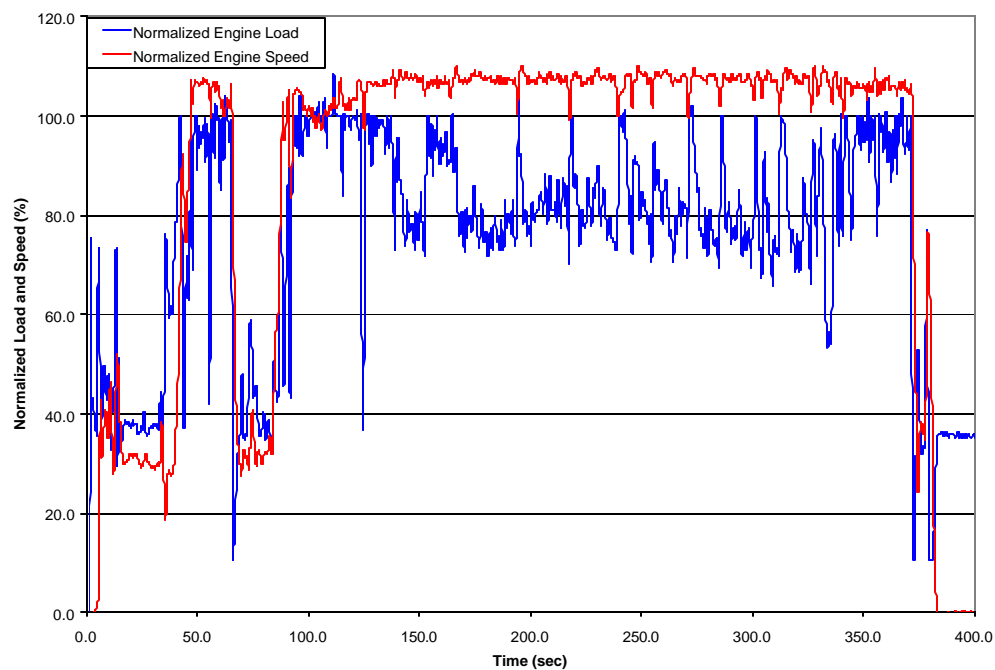
Figure 176 Normalized Load and Speed Curve for the Track-type Tractor Transport Test

Figure 176 shows the continuous engine load and speed data that was provided to WVU by Caterpillar. The cycle exhibits a high engine speed with moderate loading.
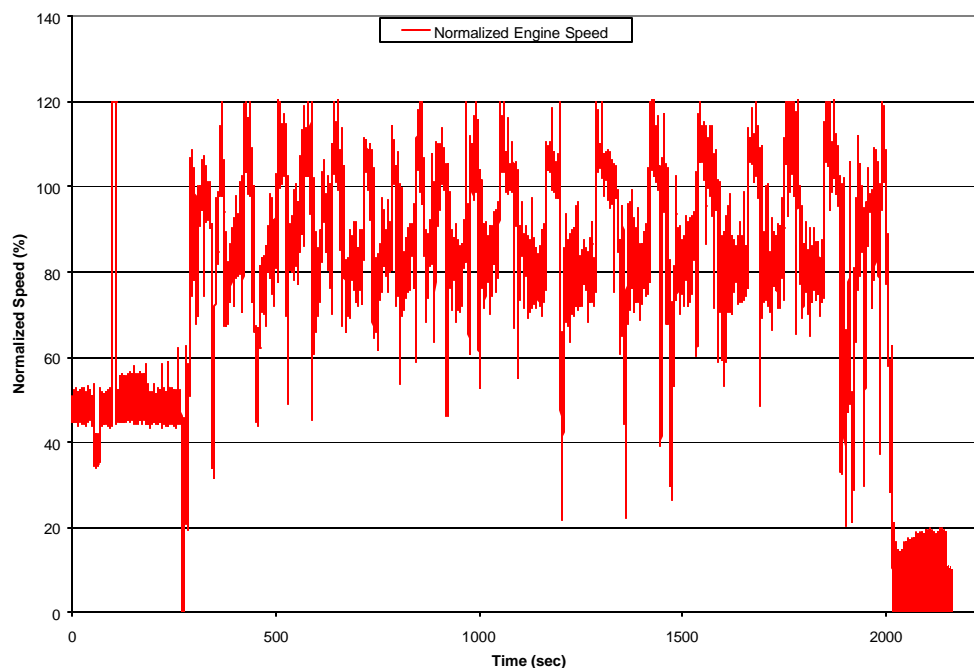
Figure 177 Normalized Engine Speed Data for Track-type Tractor Digging Cycle 1

Figure 177 displays the normalized speed data collected by the MEMS from the first digging test performed with the track type tractor. This figure indicates that the tractor operated at high speed and low load for a significant period, which was due to the transport of the vehicle to the digging start point after a digging cycle had been completed.
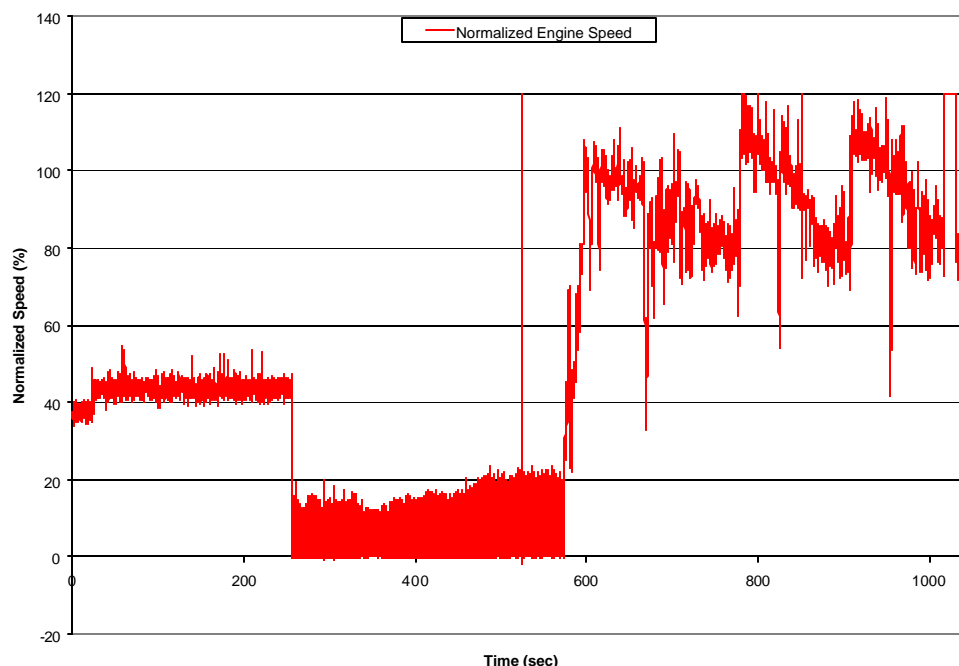
Figure 178 Normalized Engine Speed Data from Track-type Tractor Second Digging Test

Figure 178 shows approximately 1000 seconds of normalized engine speed data from the second track-type tractor digging test. This test exhibits the same characteristics as observed in Test 1.

The information presented herein provides further evidence that the operating cycles of off-highway equipment are very task and machine specific. When coupled with the results of emissions testing, the evidence leads to the conclusion that in order to understand the emissions produced by off-highway vehicles, each vehicle type will need separate consideration regardless of the given vehicles' engine power rating.

5.3 Conclusions

The emissions testing and cycle development work performed for this study provides additional information needed for the development of testing protocols for diesel-powered off-road equipment. The data produced through this research could be used to promulgate and develop requirements and standards for the testing of diesel-powered off-road vehicles and equipment.

Steady-state data was collected during this study with the ISO-8178 Type C 8-Mode Cycle. Weighted 8-Mode emissions (in g/bhp-hr) for the John Deere 6059 rubber-tired loader engine were 4.765 for HC, 8.910 for CO, 1118.0 for CO_2, 26.51 for NO_x, and 0.5015 for PM. For the John Deere 4039T street sweeper engine, weighted emissions

results were 1.954 for HC, 5.649 for CO, 1111.0 for CO_2, 11.67 for NO_x, and 0.4739 for PM.

Table 39 Comparison of Steady-State Dynamometer Test Results with the Current Off-Road Diesel Emissions Standards.

	PM (g/bhp-hr)	CO (g/bhp-hr)	HC (g/bhp-hr)	NO_x (g/bhp-hr)
1996 Std.	0.40	8.5	1.0	6.9
Street Sweeper	0.47	5.65	1.95	11.67
Loader	0.50	8.91	4.77	26.51
Excavator	0.63	2.55	2.50	8.26

It can be seen in Table 39 that the loader did not meet any of the current emissions standards and the street sweeper passed only the current CO standard, but its manufacture date precludes it from complying with these emissions standards.

The ISO-8178 Type C 8-Mode Cycle is the standard test used for the emissions evaluation of off-road diesel-powered equipment today. It is evident that the "real world" brake-specific emissions collected from the engine operating according to the transient test cycles differed significantly from the weighted brake-specific emissions collected during the running of the 8-Mode cycle. All brake-specific emissions levels were reported much higher by the 8-Mode tests than by the transient tests. For the John Deere 6059 engine, the transient test result for HC was 544.6% lower, CO was 310.6% lower, CO_2 was 104.6% lower, NO_x was 227.3% lower, and PM was 177.3% lower than the weighted brake-specific results collected during the 8-mode testing. For the John Deere 4039T street sweeper engine, the transient test result for HC was 290.0% less, CO was 295.4% less, CO_2 was 77.5% less, NO_x was 108.8% less, and PM was 93.5% less than the weighted brake-specific results collected during 8-mode testing. These characteristically large differences indicate that the testing of off-road equipment with a steady-state cycle may drastically over-estimate the contributions to air inventories by these vehicles.

Data were collected during the transient test cycle operation that was performed in the laboratory on the dynamometer test bed. Full-flow dilution tunnel exhaust emissions data were collected in the laboratory using the final transient cycle iterations. Cycle-averaged results for the John Deere 6059 Loader engine (in g/bhp-hr) were 546.4 for CO_2, 0.742 for HC, 2.168 for CO, 8.096 for NO_x, and 0.170 for PM. Results (g/bhp-hr) for the John Deere 4039T street sweeper engine were 561.8 for CO_2, 0.367 for HC, 3.569 for CO, 7.359 for NO_x, and 0.370 for PM. The comparable brake-specific average CO_2 results indicate that similar work was performed in each cycle. For comparative purposes, full-flow data was also collected on the street sweeper during the running of the first transient cycle iteration to investigate the impact that the accuracy of in-field cycle recreation had on emissions results. Street sweeper testing showed that the very labor

intensive and time consuming process of cycle iteration changed cycle-averaged CO_2 emissions by only -0.68%, HC by 1.83%, CO by -4.83%, NO_x by -1.51%, and PM by -7.53% between the first and final cycle iterations. Clearly, this is not a large change in the data for the amount of effort that was put into the accurate recreation of the in-field cycle. Therefore, it may be concluded that in-field CO_2 continuous data and manufacturer-supplied brake-specific fuel consumption versus load information may be sufficient to produce accurate cycle approximations, as is explained in Section 5.3.1.

A test was performed during this study to determine the effect that cycle suitability has on emissions levels. Running the street sweeper engine on the cycle developed for the rubber-tired loader illustrated the important role that an appropriate vehicle-specific cycle has on emissions. When the street sweeper engine was exercised according to the rubber-tired loader cycle, CO_2 emissions decreased by 10.26%, HC decreased by 26.54%, CO increased by 92.61%, NO_x increased by 31.60%, and PM increased by 51.19%. This illustrates the need for a representative cycle to be derived for each type of equipment being tested to get an accurate estimation of emissions contributions.

5.4 Recommendations

In the future, continued testing of off-road diesel-powered equipment will escalate as air quality standards become ever more stringent. The evolution of testing procedures and standards for off-road diesels will continue to accelerate in the years to come. Additional research will add to the already expanding database of testing procedures for the off-road arena. The future efforts suggested by the results of this study focus on additional labor saving techniques that would greatly reduce the amount of effort required for the recreation of the in-field cycle. A section is also devoted to refinements that could be made to test procedures followed in this study.

5.4.1   Future Research

It has been shown that the laborious process of cycle iteration did not produce a large difference in cycle averaged emissions results. The close accuracy of the laboratory transient cycle continuous CO_2 traces to the in-field cycle traces did not make a significant difference in the overall cycle-averaged emissions levels. However, with second-by-second data some factors such as rate of acceleration/deceleration could be significantly different. The elimination of the cycle iteration process would dramatically reduce the amount of time spent in the development of new transient emissions test cycles for off-road diesel engines

A method that should be explored in future test cycle creation work is to utilize manufacturer-supplied brake-specific fuel consumption (BSFC) data to directly estimate engine torque based on the gaseous emissions. The procedure for the estimation of fuel consumed from the measured exhaust emissions is outlined in the CFR 40, Part 89 [1].

To obtain brake-specific mass emissions from a mechanically injected diesel engine it is necessary to infer the work done by the engine over a cycle from BSFC data supplied by the engine manufacturer. A procedure would have to be implemented to

obtain the mass flow rate of engine exhaust. The simplest method would be to measure the intake air flow rate with a laminar flow element or equivalent flow device and measure the mass flow rate of the fuel with a metering device. Of course, techniques proven by WVU, such as Annubar^{TM} and V-cone^{TM}, could be used for exhaust flow rate measurement. Temperatures could be recorded to determine densities of the intake air and fuel during testing to allow the determination of mass flow rates. The process used to infer total cycle work would involve the following steps: 1) Measure the raw concentration of CO_2 and the exhaust flow rate over the cycle period. 2) Integrate the continuous raw CO_2 concentration data to arrive at an average concentration over the cycle period. A Tedlar bag sample could also be used to determine the cycle-averaged CO_2 concentration using laboratory-grade instruments. Calculate the BSFC of the engine from the average CO_2 concentration with the manufacturer-supplied information. Determine the mass of HC, CO, and CO_2 emitted from the raw exhaust concentration and the exhaust mass flow rate. Calculate the mass of fuel consumed with the following equation:

$$M = \frac{G_s}{R_2},$$

Equation 16.

where

$$G_s = R_2 \cdot HC_{mass} + 0.429 \cdot CO_{mass} + 0.273 \cdot CO_{2\,mass}$$

Equation 17.

and

$$R_2 = \frac{12.011}{12.011 + 1.008 \cdot a}$$

Equation 18.

Where,

$$\alpha \quad = \quad \text{The Hydrogen to Carbon Ratio of the Fuel}$$

The integrated work over the cycle can be inferred as:

$$Work = \frac{M}{BSFC}$$

Equation 19.

The resulting brake-specific mass emission is obtained by dividing the calculated integrated mass by the calculated work:

$$BSCO_2 = \frac{CO_{2mass}}{Work}$$

Equation 20.

The above method could also be used to directly estimate continuous cycle torque based on the calculated BSFC of the engine. Manufacturer-supplied BSFC vs. dry CO_2 (%) data could be cross-referenced to determine the continuous torque trace derived solely from the CO_2 continuous emissions data. This method would be much less time consuming, as it would eliminate the laborious cycle iteration process performed for this study. The accuracy of the manufacturer-supplied data would ultimately determine the accuracy that could be achieved for the recreation of the cycle for any future testing in a laboratory setting. Results of this study have shown that emissions data obtained during the running of the recreated cycle are not largely affected by very accurate recreation but, rather, by the basic transient nature of the test cycle itself.

To reiterate and break the previous method into basic steps, the first thing needed would be manufacturer-supplied BSFC plots based upon engine speed and some engine torque parameter (MEP, torque, power, raw CO_2 in %vol or ppm, etc.). The engine speed, raw CO_2 concentration, and the exhaust flow rate would all have to be measured and recorded in the field. From the recorded in-field data, the BSFC could be determined with the manufacturer-supplied data. The CO_2 mass could then be calculated from the exhaust flow rate and the raw CO_2 data. The next step is to perform a carbon balance of the CO_2 in the exhaust (neglecting HC and CO contributions) to determine the amount of fuel consumed. From the fuel consumed, the amount of engine power produced can be determined from manufacturer-supplied data. The torque can then be determined based on the calculated horsepower and the measured engine speed. The major obstacle encountered when utilizing this method for transient torque estimation is the problem of time aligning all of the measured parameters. The method is more suitable for steady-state testing where the parameters can be averaged and "smoothed" over a longer period of time.

6 References

1. Baumgard, K.J. (1995), "Effect of Fuel and Engine Design on Diesel Exhaust Particle Size Distributions", Ph.D. Dissertation, Michigan Technological University, Houghton, MI.

2. Baumgard, K.J. and Johnson, J.H. (1996), "The Effect of Fuel and Engine Design on Diesel Exhaust Particle Size Distributions", Society of Automotive Engineers, SAE Paper No. 960131.

3. Bentz, A. P., "Final Summary Report on Project 3310, Marine Diesel Exhaust Emissions (Alternative Fuels)," United States Department of Transportation United States Coast Guard Systems, Report No. CG-D-08-98, 1997.

4. Bentz, A. P. and Weaver, E., "Marine Diesel Exhaust Emissions Measured by Portable Instruments," SAE Technical Paper No. 941784, 1994.

5. Booker, D.R., Gautam, M., Carder, D.K., Gautam, S., (2001), ETH Nanoparticle Conference, August 6-8, 2001, Zurich.

6. Brockmann, J.E., Liu, B.Y.H and McMurry, P.H., "A Sample Extraction Diluter for Ultrafine Aerosol Sampling"., Aerosol Science & Technology, 441-451 (1984).

7. Butler, J. W., Gierczac, C. A., Jesion, G., Stedman, D. H., and Lesko, J. M., "On-Road NO_x Emissions Intercomparison of On-Board Measurement and Remote Sensing," Final Report, Coordinating Research Council, Inc., Atlanta, GA, CRC Report No. VE-11-6, 1994.

8. Butler, J. W., Korniski, T. J., Reading, A. R., and Kotenko, T. L., "Dynamometer Quality Data On-Board Vehicles for Real-World Emission Measurements," Proceedings of the Ninth CRC On-Road Vehicle Workshop, April 19-21, San Diego, CA, 1999.

9. Carder, D. K., "Performance Evaluation of Exhaust Aftertreatment Devices Used for Emissions Control On Diesel Engines Employed in Underground Coal Mines," M.S. Thesis, Department of Mechanical and Aerospace Engineering, West Virginia University, Morgantown, WV, 1999.

10. Cirillo, E.,"Development of a Micro-Dilution Tunnel System for In-Use, On-Board Heavy Duty Vehicle Particulate Matter Emission Measurement," M.S. Thesis, Department of Mechanical and Aerospace Engineering, West Virginia University, Morgantown, WV, 2001.

11. "Code of Federal Regulations," CFR 40 Parts 86 to 99, Washington, D.C., 1994

12. Comments on EPA's NPRM for the *Control of Emissions of Air Pollution from Nonroad Diesel Engines*

13. Doyle, G.J. (1961), "Self-nucleation in the Sulfuric Acid-Water System", Journal of Chemical Physics, Vol. 35, No. 3, pp. 795-799, September 1961.

14. Emissions Standards: USA-Heavy Duty Truck and Bus Engines/Off-Road Diesel Engines. www.dieselnet.com., EcoPoint Inc., April 2000.

15. Gierczac, C. A., Jesion, G., Piatak, J. W., and Butler, J. W., "On-Board Vehicle Emissions Measurement Program," Final Report, Coordinating Research Council, Inc., Atlanta, GA, CRC Report No. VE-11-1, 1994.

16. Heist, R.H. and Reiss, H., (1974), "Hydrates in Supersaturated Binary Sulfuric Acid-Water Vapor, Journal of Chemical Physics, Vol. 61, No. 2,

17. Hinds, W., Aerosol Technology. John Wiley & Sons, New York, New York, 1982.

18. Howes, P., "Final Report for the City of Houston Concerning the Municipal Waste Truck running on PuriNO$_x$ Fuel,"Environmental Research and Measurement Division, Gloucester, Ontario, 2000.

19. Human, D. M. and Ullman, T. L., "Development of an I/M Short Emissions Test for Buses," SAE Technical Paper No. 920727, 1992.

20. Karcher, B., Peter, Th., and Ottmann, R., (1995), Contrail Formation: Homogeneous Nucleation of H2SO4 /H2O Droplets, J., Geophys. Res. Lett. 22: pp 1501-1504.

21. Kelly, N.A. and Groblicki, P. J., "Real-world emissions from a modern production vehicle driven in Los Angeles," *Journal of Air and Waste Management Association*, Vol. 43, No. 10, 1993.

22. Kulmala, M., Laaksonen, A., and Pirjola, L., (1998), Parameterizations for sulfuric acid/water nucleation rates, J. Geophysical Research, V. 103, No. D7, pp 8301-8307.

23. Lammel, G. and Novakov, T., (1995), Water Nucleation Properties of Carbon Black and Diesel Soot Particles, J. Atmos. Environ. 29: pp 813-823.

24. Mackay, G. I., Nadler, S. D., Karecki, D. R., Schiff, H. I., Butler, J. W., Gierczac, C. A., and Jesion, G., "Dynamometer Intercomparison of Automobile Exhaust Gas CO/CO$_2$ Ratios and Temperature Between On-Board Measurements and a Remote Sensing Near Infrared Diode Laser System, "Phase 1b Report to the Coordinating Council and National Renewable Energy Laboratory, 1994.

25. Mackay, G. I., Nadler, S. D., Karecki, D. R., Schiff, H. I., Butler, J. W., Gierczac, C. A., and Jesion, G., "Dynamometer Intercomparison of Automobile Exhaust Gas

CO/CO_2 Ratios and Temperature Between On-Board Measurements and a Remote Sensing Near Infrared Diode Laser System, "Phase 1c Report to the Coordinating Council and National Renewable Energy Laboratory, 1994.

26. Niessner, R., Daeumer, B., and Klockow, D., (1990), "Investigation of Surface Properties of Ultrafine Particles by Application of a Multi-step Condensation Nucleus Counter", J. Aerosol Sci. Techno., 12: pp 953-963.

27. Pei, Y., "Development of Software for the Heavy-Duty Engine Testing at Engine Research Center, West Virginia University," M.S. Thesis, Department of Mechanical and Aerospace Engineering, West Virginia University, Morgantown, WV, 1993.

28. Petzold, A. and Shroeder, F. P., (1998), "Jet Engine Exhaust Aerosol Characterization", Aerosol Sci. and Techno., 28: pp 62-76, 1998

29. Reschke, G. D., "Optimization of a Flame Ionization Detector for the Determination of Hydrocarbon in Diluted Automotive Exhausts." SAE 770141, 1977.

30. Roedel, W., (1979), "Measurement of Sulfuric Acid Saturation Vapor Pressure: Implications for Aerosol Formation by Heteromolecular Nucleation", Journal of Aerosol Science, Vol. 10, pp.375-386.

31. Schlicting, "Boundary Layer Theory", McGraw-Hill, New York, 1955.

32. Shade, B. C., " A Performance Evaluation of the MEMS – An On-Road Emissions Measurement System Study," M.S. Thesis, Department of Mechanical and Aerospace Engineering, West Virginia University, Morgantown, WV, 2000.

33. Summary Report: "Construction Equipment Retrofit Project,"Northeast States for Coordinated Air Use Management, Boston, Mass., 1997.

34. Technical Report: "Selection Criteria for Diesel Particulate Trap Systems: Vert Experience". www.dieselnet.com, Ecopoint Inc., December 1998.

35. Technical Report: "VERT: Curtailing Emissions of Diesel Engines in Tunnel Sites". www.dieselnet.com., EcoPoint Inc., April 1998.

36. Vojtisek-Lom, M. and Cobb, Jr., J. T., "On-Road Light-Duty Vehicle Mass Emission Measurements Using a Novel Inexpensive On-Board Portable System,"Proceedings of the Eighth CRC On-Road Vehicle Workshop, San Diego, CA, April 20-22, 1998.

37. Wysloouzil, B. E., Carleton, K. L., Sonnenfroh, D. M., Rawlins, W. T., and Arnold, S., (1994), Observation of Hydration of Single, Modified Carbon Aerosols, J. Geophys. Res. Lett. 21: pp 2107-2110.

7 Glossary of Terms, Abbreviations, and Symbols

AC	Alternating Current
BSFC	Brake-Specific Fuel Consumption
CARB	California Air Resources Board
CFR	Code of Federal Regulations
CFV	Critical Flow Venturi
CO	Carbon Monoxide
CO_2	Carbon Dioxide
CVS	Constant Volume Sample
DC	Direct Current
ECU	Engine Control Unit
EERL	Engine and Emissions Research Laboratory
EGS	Electrochemical Gas Sensor
EPA	Environmental Protection Agency
GPS	Global Positioning System
HC	Hydrocarbon
HFID	Heated Flame Ionization Detector
IR	Infrared
LFE	Laminar Flow Element
MARI	Mid-Atlantic Research Institute, LLC.
MEMS	Mobile Emissions Measurement System
NDIR	Non-dispersive Infrared
NDUV	Non-dispersive Ultraviolet
NESCAUM	Northeast States for Coordinated Air Use Management
NIST	National Institute of Standards and Technology
NMHC	Non-Methane Hydrocarbons
NO	Nitric Oxide
NO_2	Nitrogen Dioxide
NO_x	Oxides of Nitrogen
O_2	Oxygen
O_3	Ozone
OBE	On-Board Emissions

PM	Particulate Matter
PPM	Parts per million
PREVIEW	Portable Real-Time Emission Vehicular Integrated Engineering Workstation
QC/QA	Quality Control/Quality Assurance
ROVER	Real-time On-Road Vehicle Emissions Recorder
RPM 100	Real-time Particulate Mass Monitor
RTD	Resistive Temperature Device
Scfm	Standard Cubic Feet per Minute
SO_2	Sulfur Dioxide
SOF	Soluble Organic Fraction
TTL	Transistor-Transistor Logic
UDDS	Urban Dynamometer Driving Schedule
VEOM	Vito on-the Road Emission and Energy Measurement
VOC	Volatile Organic Compounds
WVU	West Virginia University
FTP	Federal Test Procedure
PID	Proportional Integral Derivative

Appendix A -Additional Data for the John Deere 6059 Loader Engine.
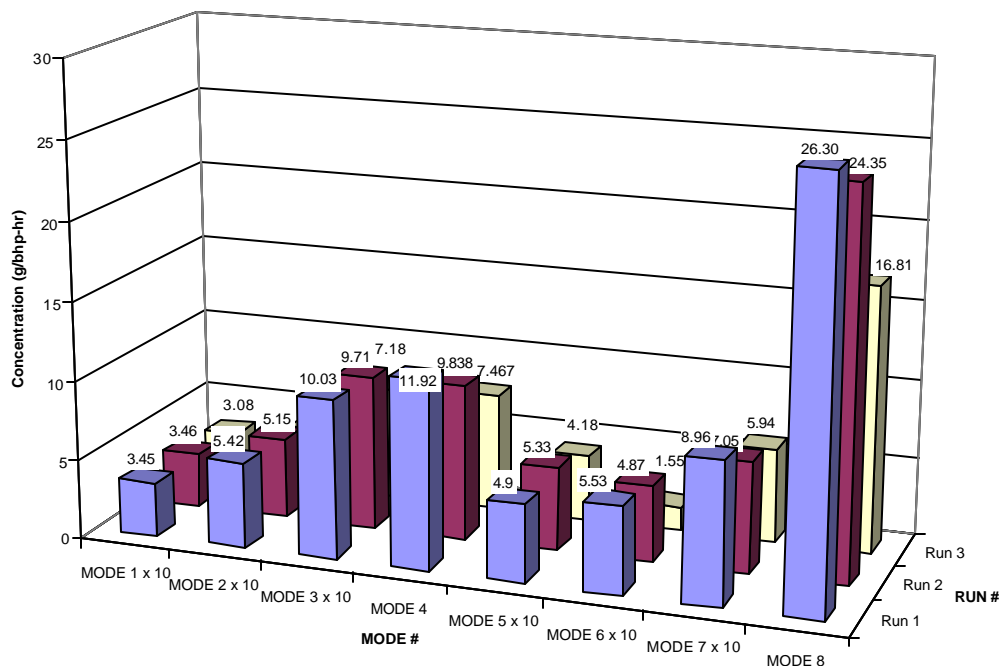
Figure A.179 HC 8-Mode Results for the John Deere 6059 (g/bhp-hr).
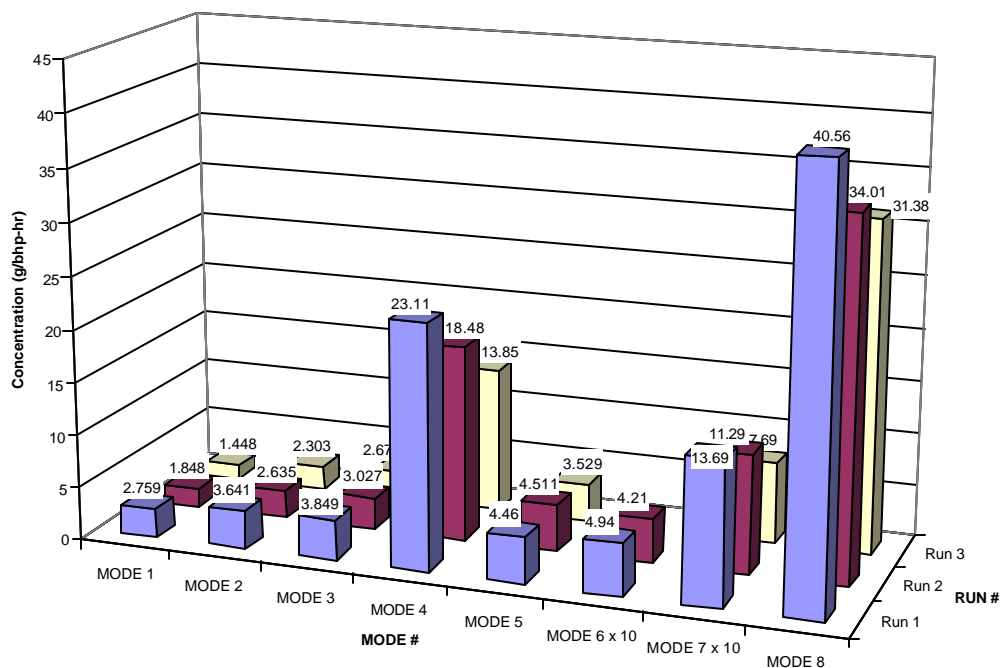
Figure A.180 CO 8-Mode Results for the John Deere 6059 (g/bhp-hr).
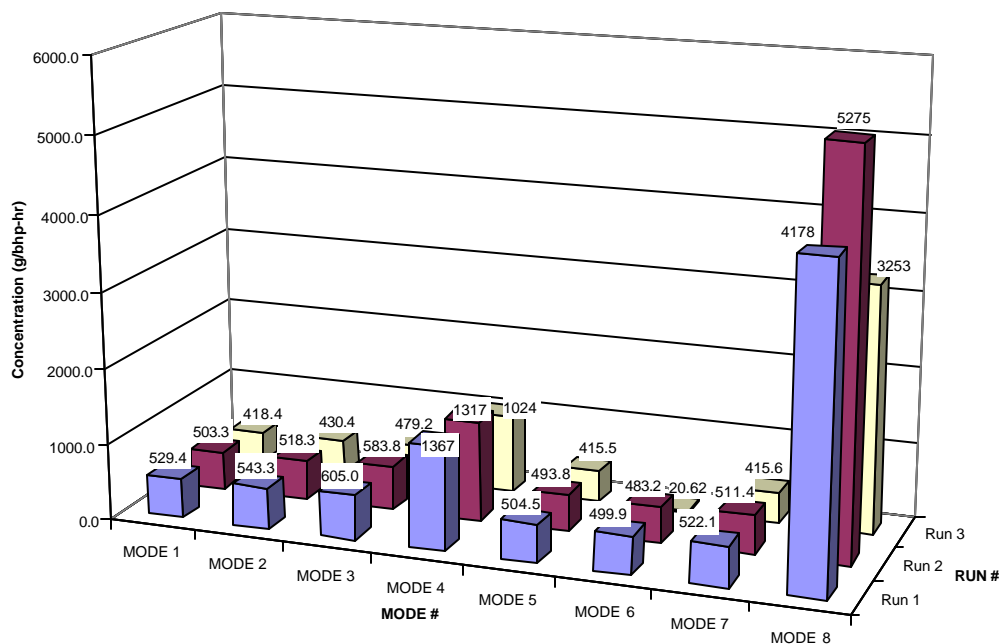
Figure A.181 CO$_2$ 8-Mode Results for the John Deere 6059 (g/bhp-hr).
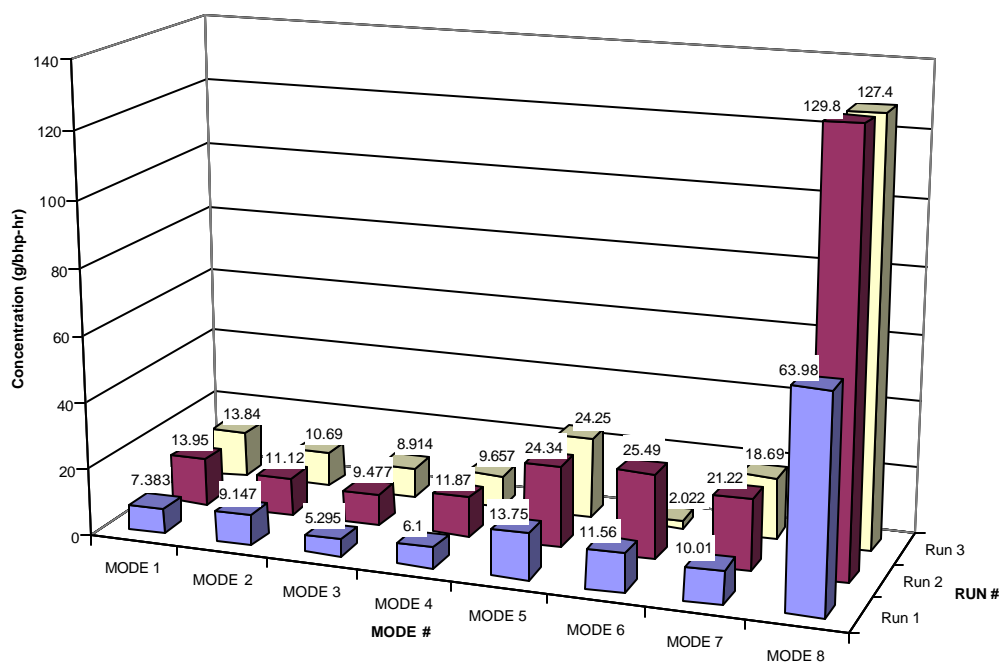
Figure A.182 NO$_x$ 8-Mode Results for the John Deere 6059 (g/bhp-hr).
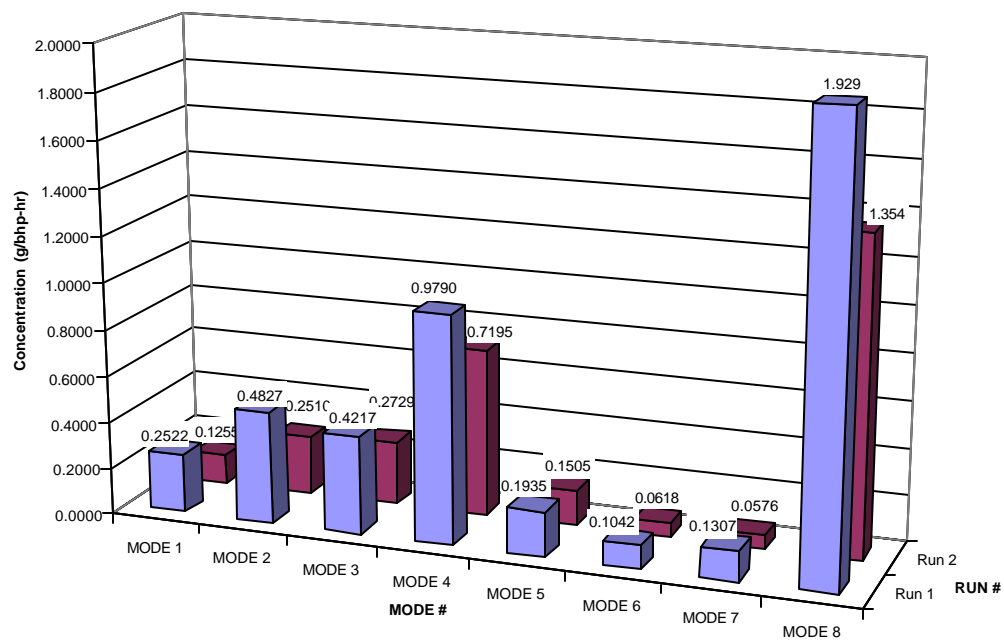
Figure A.183 PM 8-Mode Results for the John Deere 6059 (g/bhp-hr).

Appendix B -Additional Data for the John Deere 4039T Street sweeper Engine.
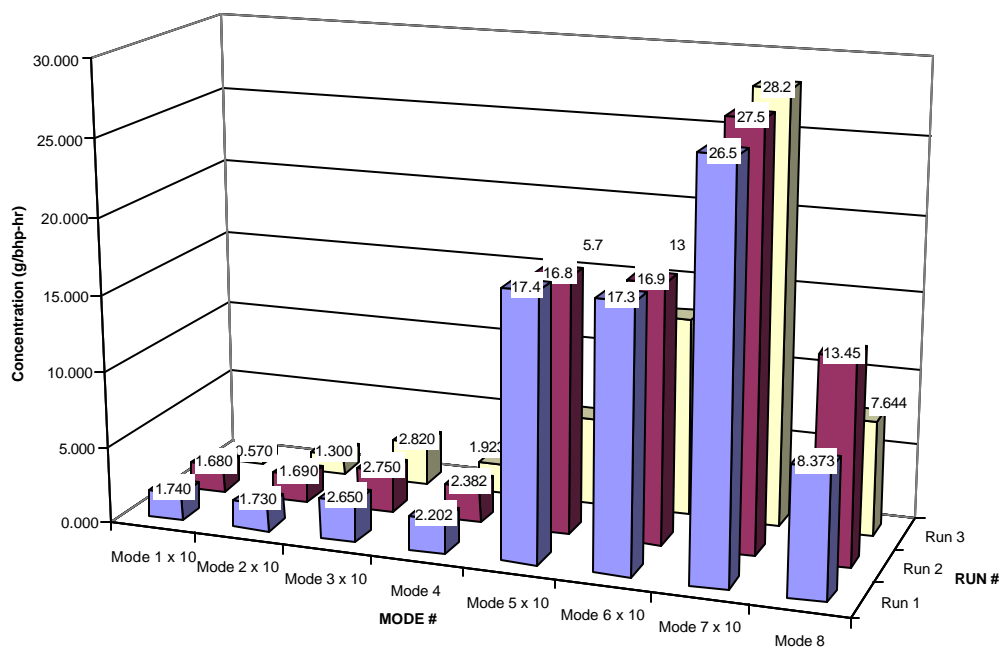
Figure B.184 HC 8-Mode Results for the John Deere 4039T (g/bhp-hr).
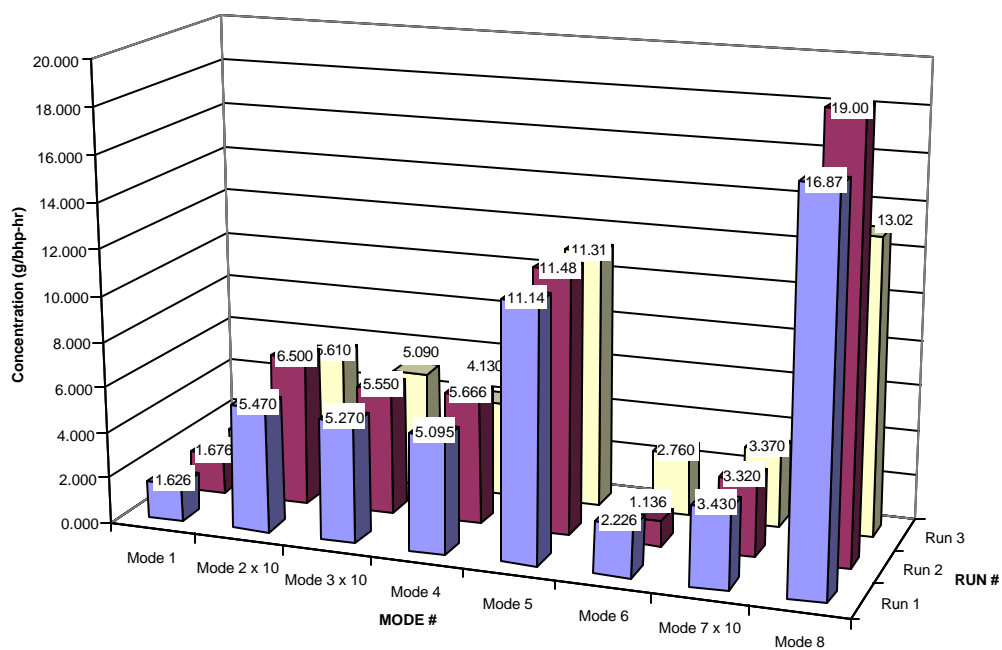
Figure B.185 CO 8-Mode Results for the John Deere 4039T (g/bhp-hr).
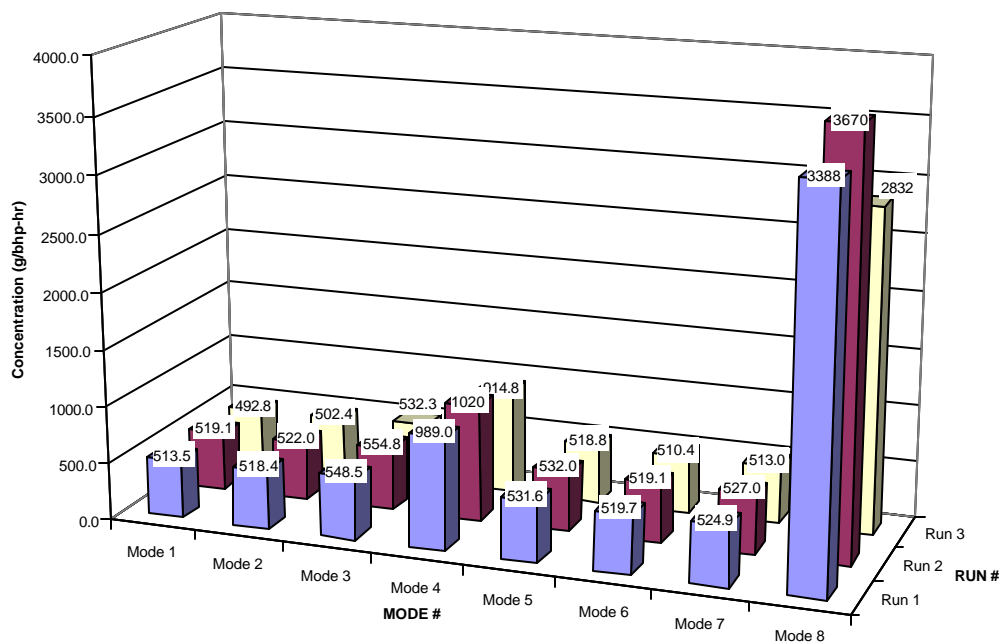
Figure B.186 CO$_2$ 8-Mode Results for the John Deere 4039T (g/bhp-hr).
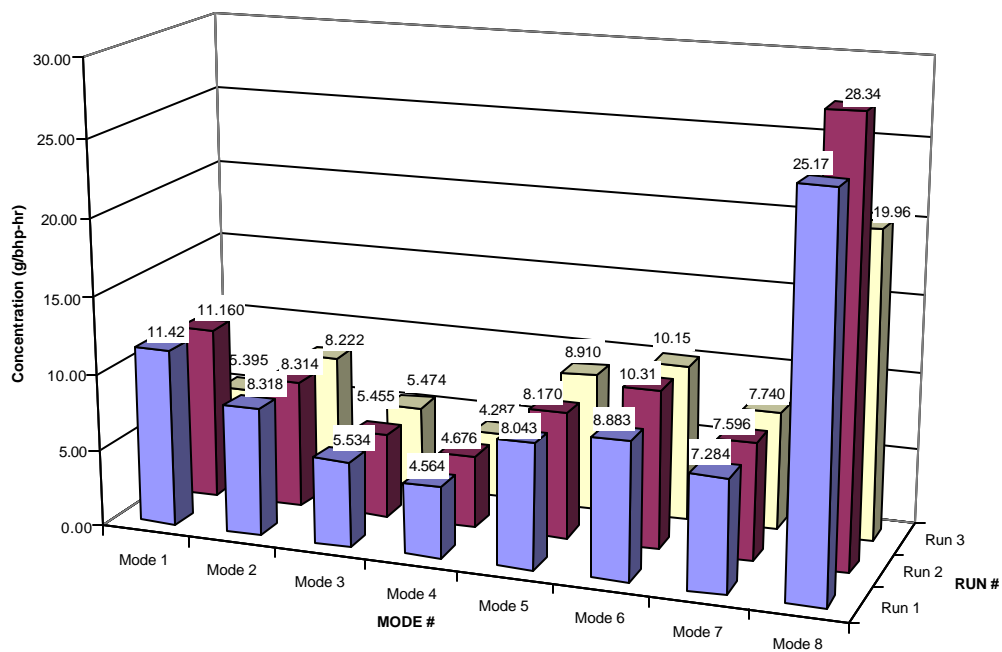
Figure B.187 NO$_x$ 8-Mode Results for the John Deere 4039T (g/bhp-hr).
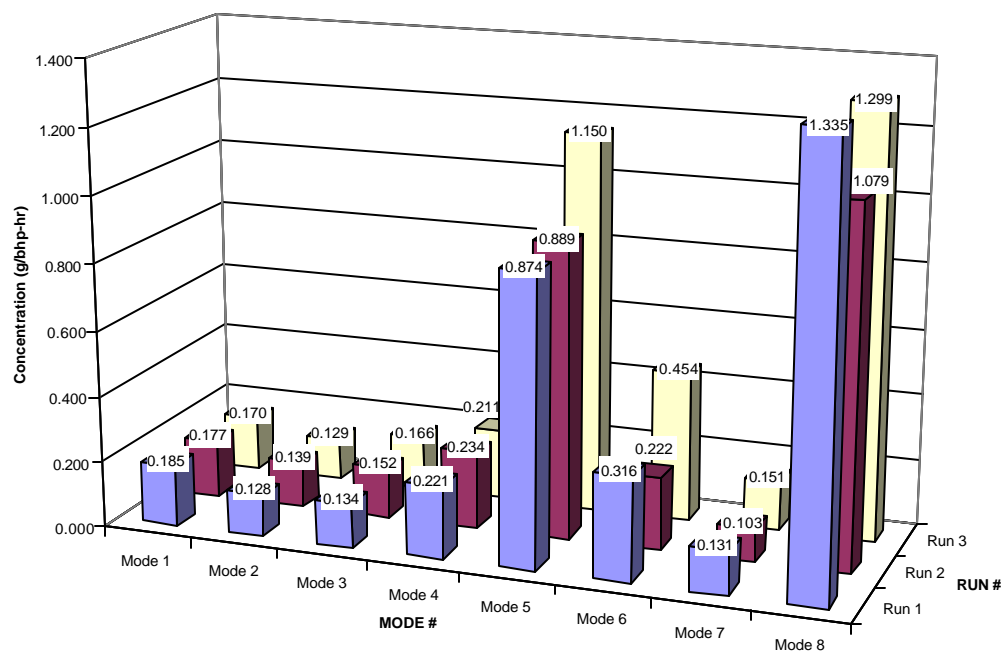
Figure B.188 PM 8-Mode Results for the John Deere 4039T (g/bhp-hr).

Appendix C -Additional Data for the Komatsu S6D125-1 Excavator Engine.
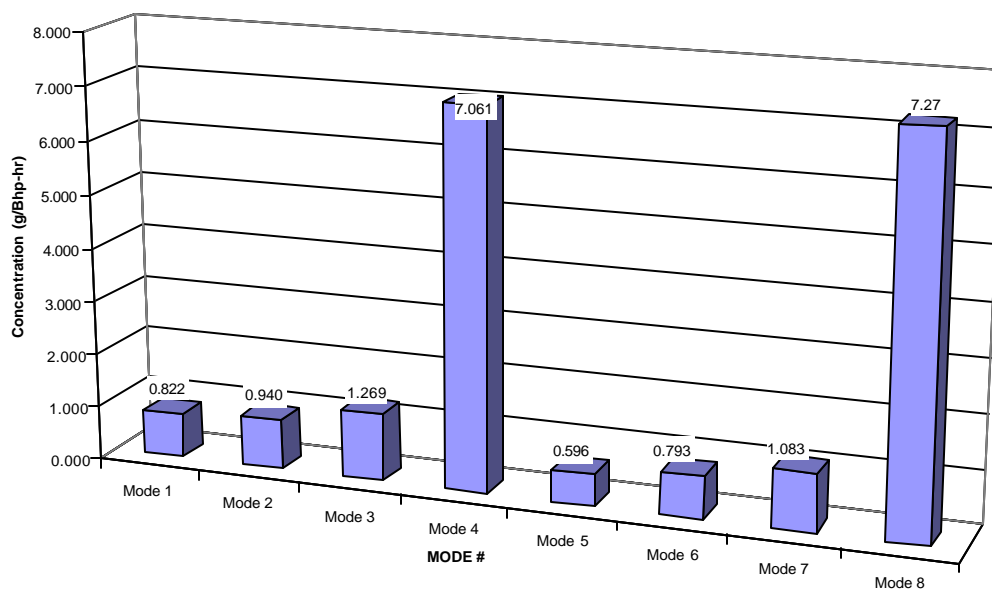
Figure C.189 HC 8-Mode Results for the Komatsu S6D125-1 (g/bhp-hr).
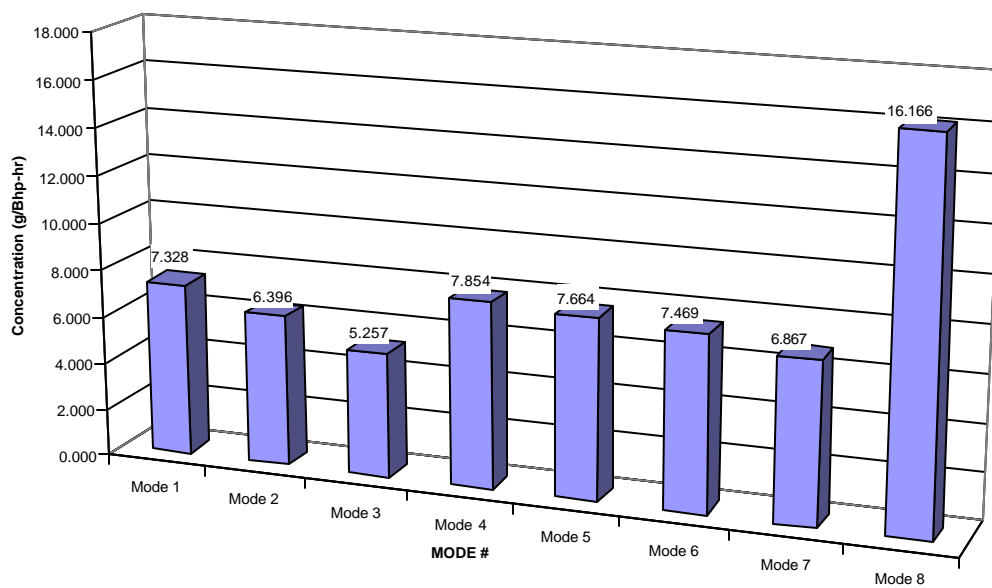
Figure C.190 NO$_x$ 8-Mode Results for the Komatsu S6D125-1 (g/bhp-hr).
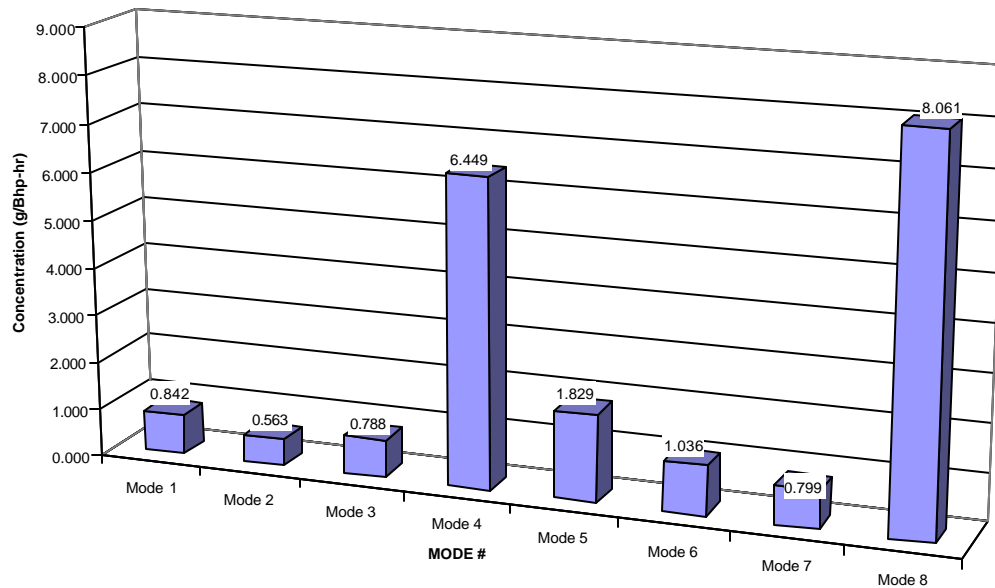
Figure C.191 CO 8-Mode Results for the Komatsu S6D125-1 (g/bhp-hr).
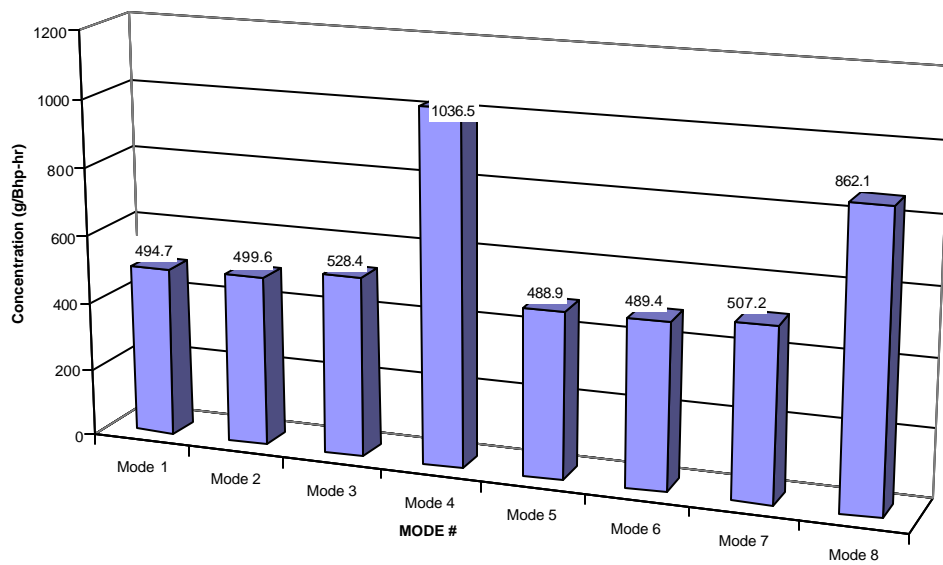
Figure C.192 CO$_2$ 8-Mode Results for the Komatsu S6D125-1 (g/bhp-hr).
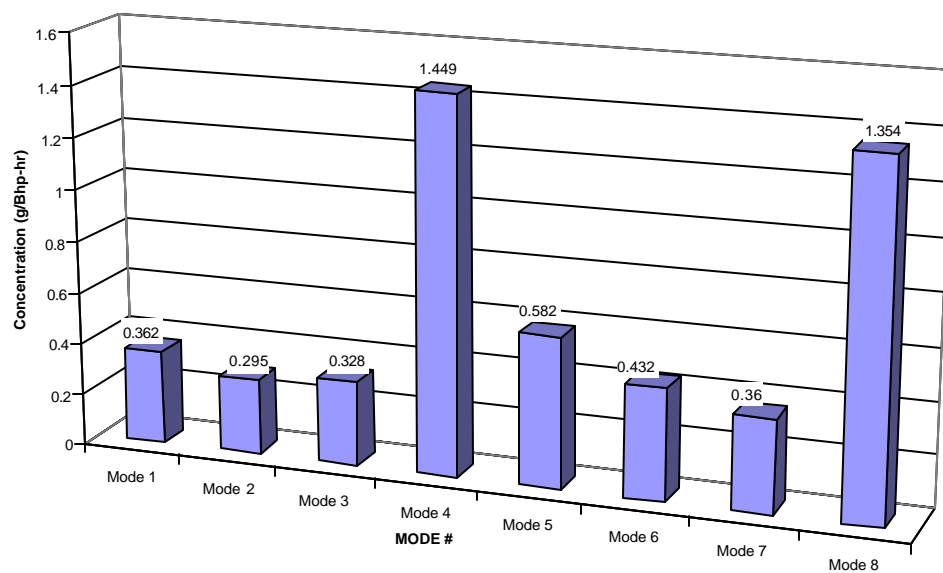
Figure C.193 PM 8-Mode Results for the Komatsu S6D125-1 (g/bhp-hr).

Appendix D -Completed Diesel Equipment Questionnaires.

DIESEL EQUIPMENT QUESTIONNAIRE

Company: WVU PHYSICAL PLANT

Address: WVU

Contact: BILL MYERS
Telephone: (304) 293-8942
Fax: (304) 293-3887
Email: bmyers@wvu.edu

(Note – If you require additional space for your responses, please use the back or add sheets as needed.)

General Information

Vehicle Type	Manufacturer	Model	Model Year	Type of Usage
1. STREET	ELGIN	Series P	Post 1996	Street
2. SWEEPER	PELICAN			Cleaning
3.				on
4.		ENGINE		WVU
5.		John Deere		Campus
6.				
7.		4039		
8.		Turbocharged		
9.				
10.				

Equipment Fueling Practices

1. Please list the diesel fuel types (by manufacturer) used in your equipment:_____
    _____ #2 _____

2. Please indicate the types of fuel additives and/or stabilizers used in your equipment during the last five years:_____ N/A _____

3. Please estimate you total yearly diesel fuel usage:___ All equipment → 1400 gallons mo.

4. Have there been any noticeable increases in the fueling requirements for any of the equipment listed above? If so please estimate the percentage increase in fuel usage for the equipment:_____ No _____

Equipment Usage

5.   Please indicate the total run-time (to the nearest half-hour) for the vehicle(s) during the following possible operating periods.

	Vehicle Type	Daytime Weekday Operation	Nighttime Weekday Operation	Daytime Weekend Operation	Nighttime Weekend Operation
1.	*Sweeper*	*15-20 hours/week*			
2.					
3.					
4.					
5.					
6.					
7.					

6.   For each vehicle listed above, please list common areas of operation, vehicle usage, and the subsequent run-time (hours).

	Vehicle Type	Locations of Operation	Vehicle Usage (Local, Short-haul; Long-haul)	Total Run Time
1.	*Sweeper*	*WVU Campus Streets*	*Short distance*	*15-20 hours/week* *2756 hr.*
2.				
3.				
4.				
5.				
6.				
7.				

Maintenance History

7.   Do you have a regularly scheduled vehicle maintenance plan?   *Yes*
Daily - Routine greasing etc.

8.   Please indicate the frequency of the following maintenance procedures.

Vehicle Type	Oil Change	Correction or Measurement of Fueling Rates	Exhaust Opacity Measurement
1. *Sweeper*	*100 hours*	*N/A*	*N/A*
2.			
3.			
4.			
5.			
6.			
7.			

9.   Please list any other maintenance that has been performed on the equipment during the last two years.

Equipment Type   Maintenance Procedure and Frequency

1. *Sweeper*   *Mechanical - Hydraulic pump work on the hopper.*

2. _____   _____

3. _____   _____

4. _____   _____

5. _____   _____

6. _____   _____

7. _____   _____

DIESEL EQUIPMENT QUESTIONNAIRE

Company: _WVU_
Address: _PHYSICAL PLANT_

Contact: _BILL MYERS_
Telephone: _(304) 293-8942_
Fax: _(304) 293-3887_
Email: _bmyers@wvu.edu_

(Note – If you require additional space for your responses, please use the back or add sheets as needed.)

General Information

Vehicle Type	Manufacturer	Model	Model Year	Type of Usage
1. FRONT END	JOHN DEERE	JD 444	1980	Moving
2. loader		S.N. A350454		equipment
3.				material
4.		Engine:		
5.				
6.		JD 6059 D		
7.		S.N. T06059D33094		
8.				
9.			1990	
10.				

Equipment Fueling Practices

1. Please list the diesel fuel types (by manufacturer) used in your equipment:_____
    #2 (Federal on-highway diesel)

2. Please indicate the types of fuel additives and/or stabilizers used in your equipment during the last five years:_____NONE_____

3. Please estimate you total yearly diesel fuel usage: _1400 gallons/month for all vehicles in the division (≈ 30-35 vehicles)_

4. Have there been any noticeable increases in the fueling requirements for any of the equipment listed above? If so please estimate the percentage increase in fuel usage for the equipment:_____
    _No ._

Equipment Usage

5.   Please indicate the total run-time (to the nearest half-hour) for the vehicle(s) during the following possible operating periods.

Vehicle Type	Daytime Weekday Operation	Nighttime Weekday Operation	Daytime Weekend Operation	Nighttime Weekend Operation
1. FRONT END LOADER	20 hours/week			
2. (ALL DAYTIME)				
3.				
4.				
5.				
6.				
7.				

6.   For each vehicle listed above, please list common areas of operation, vehicle usage, and the subsequent run-time (hours).

Vehicle Type	Locations of Operation	Vehicle Usage (Local, Short-haul; Long-haul)	Total Run Time
1. Loader	@ WW	local	20 hours/week 6841 hr
2.			
3.			
4.			
5.			
6.			
7.			

Maintenance History

7.   Do you have a regularly scheduled vehicle maintenance plan?   *Yes. Every 100 hour* *Minac*

8.   Please indicate the frequency of the following maintenance procedures.

Vehicle Type	Oil Change	Correction or Measurement of Fueling Rates	Exhaust Opacity Measurement
1. *loader*	*1000 hours*	*N/A*	*N/A*
2.			
3.			
4.			
5.			
6.			
7.			

9.   Please list any other maintenance that has been performed on the equipment during the last two years.

Equipment Type

1. *loader*

2.

3.

4.

5.

6.

7.

Maintenance Procedure and Frequency

Water pump.

DIESEL EQUIPMENT QUESTIONNAIRE

Company: Richard Construction Inc.
Address: _____   Contact: Mr. Bill Bland
     Dellslow, WV   Telephone: _____
     _____   Fax: _____
     _____   Email: _____

(Note – If you require additional space for your responses, please use the back or add sheets as needed.)

General Information

Equipment Type	Manufacturer	Model	Model Year
1. Excavator	Komatsu	PC400LC-3	1997
2.			
3.		Engine Model	
4.			
5.		S6D 125-1	
6.			
7.			
8.			
9.			
10.			

Equipment Fueling Practices

1. Please list the diesel fuel types (by manufacturer) used in your equipment:_____
    Federal Diesel No. 2
    _____.

2. Please indicate the types of fuel additives and/or stabilizers used in your equipment during the last five years:___None_____
    _____
    _____.

3. Please estimate you total yearly diesel fuel usage:___500 gallons___.

4. Have there been any noticeable increases in the fueling requirements for any of the equipment listed above? If so please estimate the percentage increase in fuel usage for the equipment:___No_____
    _____
    _____.

Equipment Usage

5. Please indicate the total run-time (to the nearest half-hour) for the equipment during the following possible operating periods.

|	Equipment Type	Daytime Weekday Operation	Nighttime Weekday Operation	Daytime Weekend Operation	Nighttime Weekend Operation
1.	Excavator	Variable	—	—	—
2.		0-10 hr			
3.					
4.					
5.					
6.					
7.					
8.					
9.					
10.					

6. For each piece of equipment listed above, please list common locations of operation and the subsequent yearly run-time at each location (in hours).

Equipment Type	Locations of Operation	Total Run Time
1. Excavator	Star City, WV	~~~
		3263 hr
2.		
3.		
4.		
5.		
6.		

8.			
9.			
10.			

Maintenance History

7. Do you have a regularly scheduled equipment maintenance plan? _Yes_ .

8. Please indicate the frequency of the following maintenance procedures.

Equipment Type	Oil Change	Correction or Measurement of Fueling Rates	Exhaust Opacity Measurement
1. ~~Excavator~~ Excavator	6 months or 100 hr		
2.			
3.			
4.			
5.			
6.			
7.			
8.			
9.			
10.			

9. Please list any other maintenance that has been performed on the equipment during the last two years.

Equipment Type

1. _Excavator_

2. _____

3. _____

Maintenance Procedure and Frequency

Repair Turbo Flange, Replace Oil Pan Gasket → Prior to Lab Testing .

DIESEL EQUIPMENT QUESTIONNAIRE

Company: Buffalo Coal Corp

Address: _____   Contact: Mr. John Geroski

Mt. Storm, WV   Telephone: _____

_____   Fax: _____

_____   Email: _____

(Note – If you require additional space for your responses, please use the back or add sheets as needed.)

General Information

Equipment Type	Manufacturer	Model	Model Year
1. Track-type Tractor	Caterpillar	D-11R CD	2001
2.			
3.		Engine Model	
4.		3308 BTA	
5.			
6.			
7.			
8.			
9.			
10.			

Equipment Fueling Practices

1.   Please list the diesel fuel types (by manufacturer) used in your equipment:_____
     Federal No. 2 _____ .

2.   Please indicate the types of fuel additives and/or stabilizers used in your
     equipment during the last five years:_____ None _____

     _____

     _____ .

3.   Please estimate you total yearly diesel fuel usage: 150,000 Gallons .

4.   Have there been any noticeable increases in the fueling requirements for any of
     the equipment listed above? If so please estimate the percentage increase in fuel
     usage for the equipment: No _____

     _____

     _____ .

Equipment Usage

5. Please indicate the total run-time (to the nearest half-hour) for the equipment during the following possible operating periods.

Equipment Type	Daytime Weekday Operation	Nighttime Weekday Operation	Daytime Weekend Operation	Nighttime Weekend Operation
1. D-11	11 hr	11 hr	0-11 hr	0-11 hr
2.				
3.				
4.				
5.				
6.				
7.				
8.				
9.				
10.				

6. For each piece of equipment listed above, please list common locations of operation and the subsequent yearly run-time at each location (in hours).

Equipment Type	Locations of Operation	Total Run Time
1. D-11	Mt. Storm, WV Strip Mine	~~—~~ 2750 hr
2.		
3.		
4.		
5.		
6.		

8.			
9.			
10.			

Maintenance History

7. Do you have a regularly scheduled equipment maintenance plan? _Yes_.

8. Please indicate the frequency of the following maintenance procedures.

Equipment Type	Oil Change	Correction or Measurement of Fueling Rates	Exhaust Opacity Measurement
1. D-11R CD	250-300 hrs	ECU –Continuous	———
2.			
3.			
4.			
5.			
6.			
7.			
8.			
9.			
10.			

9. Please list any other maintenance that has been performed on the equipment during the last two years.

Equipment Type   Maintenance Procedure and Frequency

1. __D-11R CD__   __Replace Exhaust Stacks w/Stainless Stacks__

_____   _____
                                _____.

2._____   _____
                                _____
                                _____.

3._____   _____
                                _____

Addendum - Brake Specific Fuel Consumption

Brake Specific Fuel Consumption

Transient Cycles (Developed by WVU)

1.   Street Sweeper Engine   206.8 g/bhp-hr (0.456 lb/bhp-hr)
      John Deere 4039T

2.   Rubber-tired Front-end Loader   173.3 g/bhp-hr (0.382 lb/bhp-hr)
      John Deere 6059

3.   Excavator
      Komatsu S6D125-1

            Cycle # 1 (Loading):   166.5 g/bhp-hr (0.367 lb/bhp-hr)

            Cycle # 2 (Transport):   164.6 g/bhp-hr (0.363 lb/bhp-hr)

            Cycle # 3 (Trenching):   164.6 g/bhp-hr (0.363 lb/bhp-hr)

            EPA Excavator Cycle: 197.9 g/bhp-hr (0.436 lb/bhp-hr)
             (Not engine specific)

Steady-State 8-Mode Cycle

	Mode 1 (g/bhp-hr)	Mode 2 (g/bhp-hr)	Mode 3 (g/bhp-hr)	Mode 4 (g/bhp-hr)	Mode 5 (g/bhp-hr)	Mode 6 (g/bhp-hr)	Mode 7 (g/bhp-hr)	Mode 8 (g/bhp-hr)	Weighted Results (g/bhp-hr)
John Deere 4039T Street Sweeper Engine	161.8	170.7	173.2	320.2	170.9	166.9	167.5	1161.6	332.7
John Deere 6059 Rubber-Tired Front-End Loader Engine	162.5	167.7	187.8	430.4	159.7	154.2	162.1	1444.0	384.9
Komatsu S6D125-1 Excavator Engine	159.3	161.8	172.5	349.6	157.9	157.2	163.4	335.6	207.2